Fibration symmetries uncover the building blocks of biological networks

Flaviano Morone[a,b,1], Ian Leifer[a,b,1], and Hernán A. Makse[a,b,1,2]

[a]Levich Institute, City College of New York, New York, NY 10031; and [b]Physics Department, City College of New York, New York, NY 10031

Edited by Terrence J. Sejnowski, Salk Institute for Biological Studies, La Jolla, CA, and approved February 18, 2020 (received for review August 22, 2019)

A major ambition of systems science is to uncover the building blocks of any biological network to decipher how cellular function emerges from their interactions. Here, we introduce a graph representation of the information flow in these networks as a set of input trees, one for each node, which contains all pathways along which information can be transmitted in the network. In this representation, we find remarkable symmetries in the input trees that deconstruct the network into functional building blocks called fibers. Nodes in a fiber have isomorphic input trees and thus process equivalent dynamics and synchronize their activity. Each fiber can then be collapsed into a single representative base node through an information-preserving transformation called "symmetry fibration," introduced by Grothendieck in the context of algebraic geometry. We exemplify the symmetry fibrations in gene regulatory networks and then show that they universally apply across species and domains from biology to social and infrastructure networks. The building blocks are classified into topological classes of input trees characterized by integer branching ratios and fractal golden ratios of Fibonacci sequences representing cycles of information. Thus, symmetry fibrations describe how complex networks are built from the bottom up to process information through the synchronization of their constitutive building blocks.

complex networks | fibration symmetry | statistical mechanics | biological networks

A central theme in systems science is to break down the system into its fundamental building blocks to then uncover the principles by which complex collective behavior emerges from their interactions (1–3). In number theory, every natural number can be represented by a unique product of primes. Thus, prime numbers are the building blocks of natural numbers. This mathematical notion of building blocks is extended to the more abstract notion of group theory since finite groups can also be factored into simple subgroups (4). The latter example, entirely abstract as it may be, has important implications for natural systems due to the fundamental relationship between group theory and the notion of symmetry that has led to the discovery of the fundamental building blocks of matter, such as quarks and leptons (3, 5). Here we ask whether similar principles of symmetry can uncover the fundamental building blocks of biological networks (1, 2, 6, 7). Primary examples of these networks are gene regulatory networks that control gene expression in cells (2, 8–10); as well as metabolic networks, cellular processes and pathways, neural networks, and ecosystems; and, beyond biology, other information-processing networks like social and infrastructure networks (7). Previous studies have identified building blocks or "network motifs" (2, 6, 8) by looking for patterns in the network that appear more often than they would by pure chance. The crux of the matter is to test whether the building blocks of these networks obey a predictive principle that explains how the cell functions and whether such a principle can be expressed in the language of symmetries.

We introduce the use of symmetries in biological networks by analyzing the transcriptional regulatory network of bacterium *Escherichia coli* (11), since this is a well-characterized network. We find that this network exhibits fibration symmetries (12–14), first introduced by Grothendieck (12) in the context of algebraic geometry.

Symmetry fibrations are morphisms between networks that identify clusters of synchronized genes (called fibers) with isomorphic input trees. Genes in a fiber are collapsed by a symmetry fibration into a single representative gene called the base. The fibers are then the synchronized building blocks of the genetic network and symmetry fibrations are transformations that preserve the dynamics of information flow in the network. We use this symmetry principle to classify the building blocks into topological classes of input trees characterized by integer branching ratios and complex topologies with golden ratios of Fibonacci sequences representing cycles in the network. We then show that symmetry fibrations explain synchronization patterns of gene coexpression in cells and universally apply to a range of complex networks across different species and domains beyond biology.

Results

We search for symmetries in the *E. coli* transcriptional regulatory network [most updated compilation at RegulonDB (11)] where nodes are genes and a directed link represents a transcriptional regulation (*SI Appendix*, section III).

A directed link from a source gene i to a target gene j in a transcriptional regulatory network represents a direct interaction

Significance

The success of symmetries in explaining the physical world, from general relativity to the standard model of particle physics and all phases of matter, raises the question of why the same concept could not be equally applied to explain emergent properties of biological systems. In other words, we ask—if life is an emergent property of physics—why the same symmetry principles that explain physics could not explain the organizing principle of life. Here we show that a particular form of symmetry, called symmetry fibration, explains the building blocks of biological networks and other social and infrastructure networks. This result opens the way to understand how information-processing networks are assembled from the bottom up.

Author contributions: F.M., I.L., and H.A.M. designed research, performed research, analyzed data, and wrote the paper.

The authors declare no competing interest.

This article is a PNAS Direct Submission.

Data deposition: Full details of each network and results can be accessed on GitHub at https://github.com/makselab/fibrationData/blob/master/datasets.xlsx. The codes to reproduce this analysis are on GitHub at https://github.com/makselab (*SI Appendix*, section V). The full datasets are on GitHub at https://github.com/makselab/fibrationData/blob/master/rawData.zip.

[1]F.M., I.L., and H.A.M. contributed equally to this work.

[2]To whom correspondence may be addressed. Email: hmakse@ccny.cuny.edu.

This article contains supporting information online at https://www.pnas.org/lookup/suppl/doi:10.1073/pnas.1914628117/-/DCSupplemental.

First published March 31, 2020.

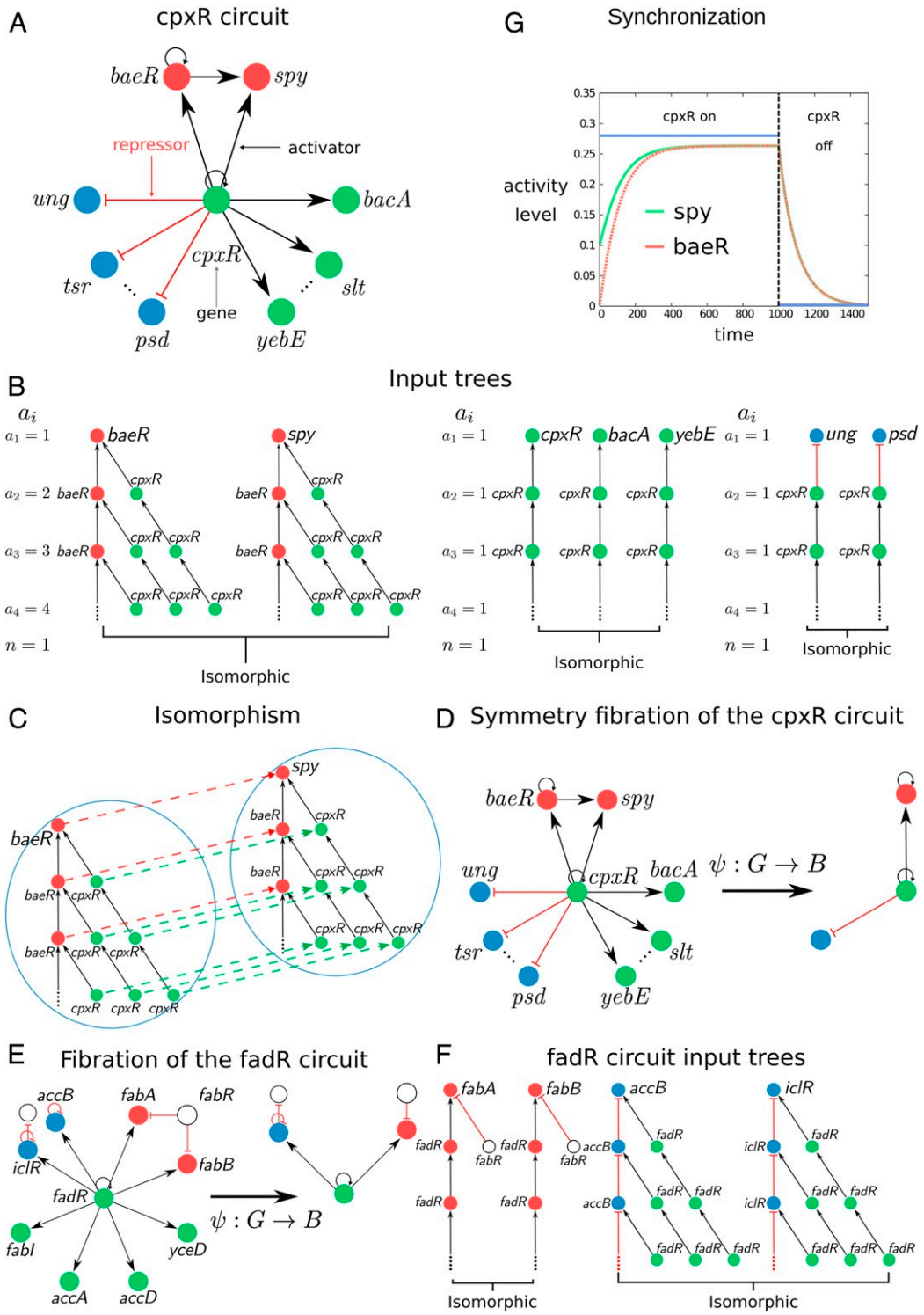

Fig. 1. Definition of input tree, symmetry fibration, fiber, and base. (*A*) The circuit controlled by the *cpxR* gene regulates a series of fibers as shown by the different-colored genes. The circuit regulates more genes represented by the dotted lines which are not displayed for simplicity. The full lists of genes and operons in this circuit are in *SI Appendix*, Table VI, ID nos. 27, 28, and 54. (*B*) The input tree of representative genes involved in the *cpxR* circuit showing the isomorphisms that define the fibers. For each fiber, we show the number of paths of length $i-1$ at every layer of the input tree, a_i, and its branching ratio n. (*C*) Isomorphism between the input trees of *baeR* and *spy*. The input trees are composed of an infinite number of layers due to the autoregulation loop at *baeR* and *cpxR*. How does one prove the equivalence of two input trees when they have an infinite number of levels? A theorem proved by Norris (26) demonstrates that it suffices to find an isomorphism up to $N-1$ levels, where N is the number of nodes in the circuit. Thus, in this case, two levels are sufficient to prove the isomorphism. (*D*) Symmetry fibration ψ transforms the *cpxR* circuit G into its base B by collapsing the genes in the fibers into one. (*E* and *F*) Symmetry fibration of the *fadR* circuit (*E*) and its isomorphic input trees (*F*). Full list of genes in this circuit appears in *SI Appendix*, Table VI, ID nos. 3, 4, and 58. (*G*) Symmetric genes in the fiber synchronize their activity to produce the same activity levels. We use the mathematical model of gene regulatory kinetics from ref. 8 (sigmoidal interactions lead to qualitatively similar results) to show the synchronization inside the fiber *baeR-spy* when the fiber is activated by its regulator *cpxR*. Note that *cpxR* does not synchronize with the fiber.

where gene i encodes for a transcription factor that binds to the binding site of gene j to regulate (activate or repress) its expression. Such a link represents a regulatory "message" sent by the source to the target gene using the transcription factor as a "messenger." This process defines the "information flow" in the system which is not restricted to two interacting genes, but it is transferred to different regions within the network that are accessible through the connecting pathways. The information arriving to a gene contains the entire history transmitted through all pathways that reach this gene. We formalize this process of communication between genes with the notion of "input tree" of the gene. In a network $G=(N_G, E_G)$ with N_G nodes and E_G directed edges, for every gene $i \in N_G$ there is a corresponding input tree, denoted as T_i, which is the tree of all pathways of G ending at i. More precisely, T_i is a rooted tree with a selected node i at the root, such that every other node j in the tree represents the initial node of a path in the network ending at i.

Next, we analyze the input trees in the *E. coli* subcircuit shown in Fig. 1*A* regulated by gene *cpxR* which regulates its own expression (via an autoregulation activator loop) and also regulates other genes as shown in Fig. 1*A*. Gene *cpxR* is not regulated by any other transcription factor in the network, so we say that this gene forms its own "strongly connected component"; see below. Therefore, it is an ideal simple circuit to explain the concept of fibration.

Input Tree Representation. In practice, the input tree of a gene is constructed as follows (*SI Appendix*, section IV.A). Consider the circuit in Fig. 1*A*. The input tree of gene *spy* depicted in Fig. 1*B* starts with *spy* at the root (first layer). Since this gene is upregulated by *baeR* and *cpxR*, then the second layer of the input tree contains these two pathways of length 1 starting at both genes. Gene *baeR* is further upregulated by *cpxR* and by itself through the autoregulation loop and *cpxR* is also autoregulated. Thus, the input tree continues to the third layer taking into account these three possible pathways of length 2 from the source gene to the *spy* gene. The procedure now continues, and since there are loops in the circuit, the input tree has an infinite number of layers.

The input tree formalism is a powerful framework to search for symmetries in information-processing networks, in that it replaces the canonical notion of a single trajectory with the set of all possible "histories" from an initial to a final state of the network, and this makes, in practice, it reasonably straightforward to "guess" a type of symmetry which is not apparent in the classical network framework. Based on results from refs. 13–16, we show in *Symmetry Fibration Leads to Synchronization* that if two input trees have the same "shape," then the genes at the root of the input trees synchronize their activity (17–23), even though their input trees are made of different genes. This informal notion of equivalence is formalized by isomorphisms. An isomorphism between two input trees is a bijective map that preserves the topology of the input trees including the type of links. Specifically, a map $\tau: T \to T'$ is an isomorphism if and only if for any pair of nodes a and b of T connected by a link, the pair of nodes $\tau(a)$ and $\tau(b)$ of T' is connected by the same type of link (*SI Appendix*, section IV.B). In practice, this means that isomorphic input trees are "the same" except for the labeling of the nodes. Genes with isomorphic input trees are symmetric and synchronous. We quantify this result, next, by introducing the concept of symmetry fibration (13).

Symmetry Fibration of a Network. The set of all input tree isomorphisms defines the symmetries of the network, which can be described by a "Grothendieck fibration" (12). The original Grothendieck definition of fibration is between categories (12), so the passage to a definition of fibration between graphs requires one to associate a category with a graph and rephrase Grothendieck's definition in elementary terms. Different categories may be associated with a graph, giving rise to different notions of fibrations between graphs. The notion of fibration that we use henceforth has been introduced in computer science as a "surjective minimal graph fibration" (13, 15).

In general, a graph fibration $G=(N_G, E_G)$ is any morphism

$$\psi: G \to B \qquad [1]$$

that maps G to a graph $B=(N_B, E_B)$ (with N_B nodes and E_B edges) called the "base" of the graph fibration ψ (*SI Appendix*, section IV.C). In this work we consider a surjective minimal graph fibration (13) which is a graph fibration ψ that maps all nodes with isomorphic input trees, comprising a "fiber," to a single node in B, thus producing the minimal base of the network. In this case, the base B consists of a graph where all genes in a fiber have been collapsed into one representative node by the minimal fibration. Thus, a surjective minimal graph fibration, hereafter called symmetry fibration for the sake of lexical convenience, leads to a dimensional reduction of the network into its irreducible components. Crucially, a symmetry fibration is a dimensional reduction that preserves the dynamics in the network as we show next.

Symmetry Fibration Leads to Synchronization. Next, we explain the connection between fibration and synchrony in a generality that is needed to justify our results following refs. 15 and 16. To describe the dynamical state of each gene in the transcriptional regulatory network, we first attach a phase space to each node in $G=(N_G, E_G)$ by considering a map $P: N_G \to M$ that assigns each node $i \in N_G$ to the phase space of the node denoted by the manifold M. For example, in a transcriptional regulatory network we assign to each gene $i \in N_G$ the phase space of real numbers $M=\mathbb{R}$. Then, the state of each gene is described by $x_i(t) \in \mathbb{R}$, representing the expression level of the gene i at time t, which is typically measured by mRNA concentration of gene product. We then obtain the total phase space of G as the product $PG=\prod_{i \in N_G} P(i)$.

The fibers partition the graph G into unique and nonoverlapping sets $\Pi=\{\Pi_1, \ldots, \Pi_r\}$, such that $\Pi_1 \cup \cdots \cup \Pi_r = G$ and $\Pi_k \cap \Pi_l = \emptyset$ if $k \neq l$ (24). We denote $i \sim_\Pi j$ when the input trees of i and j are isomorphic and belong to the same fiber Π_k. That is, $\exists k \mid i, j \in \Pi_k$ and there exists a symmetry fibration that sends both nodes to the same node in the base, $\psi(i)=\psi(j)$. DeVille and Lerman (15) showed that symmetry fibrations induce robust synchronization in the system (theorem 4.3.1 in ref. 15). In particular, it was shown that if ψ is a symmetry fibration, then—by proposition 2.1.12 in ref. 15—there exists a map $\mathbb{P}_\psi: PB \to PG$ that maps the total phase space of the base B, named PB, to the total phase space of the graph G. This map creates a polysynchronous subspace of synchronized solutions in fibers: $\Delta_\Pi = \{x \in PG \mid x_i(t)=x_j(t) \text{ whenever } \psi(i)=\psi(j)\}$, where each set of synchronous components of this subspace corresponds to a fiber in Π (lemma 5.1.1 in ref. 15; see also ref. 16). In other words, Δ_Π is a polysynchronous subspace of PG, such that components $x_i, x_j \in x$ synchronize (i.e., $x_i(t)=x_j(t)$) whenever the symmetry fibration ψ sends them to the same node in B.

According to these results, we interpret synchronous genes to process the same information received through isomorphic pathways in the network, and, accordingly, we interpret a symmetry fibration as a transformation that preserves the dynamics of information flow since it collapses synchronous nodes in fibers (redundant from the point of view of dynamics) into a common base with identical dynamics to those of the fiber.

Synchronous nodes in a fiber induced by symmetry fibration correspond to the "minimal balanced coloring" in ref. 14. A balanced coloring assigns two nodes the same color only if their inputs, self-consistently, receive the same content of colored nodes, whence the term "balanced." Thus, the flow of

information arriving to genes in a fiber is analogous to a process of assigning a color to each gene such that each gene "receives" the colors from adjacent genes via incoming links and "sends" its color to the adjacent genes via its outgoing links. The nodes in a fiber have the same color symbolizing the fact that they synchronize. The nodes with the same color in the balanced coloring partition (14) correspond to fibers induced by symmetry fibrations (15). We use the minimal balanced coloring algorithm proposed in ref. 25 for the computation of minimal bases (24) to find fibers (*SI Appendix*, section V).

Strongly Connected Components of the *E. coli* Network. The input trees in the *E. coli cpxR* circuit are displayed in Fig. 1*B*. The input trees of *baeR* and *spy* are isomorphic and define the *baeR-spy* fiber (Fig. 1*C*). We call this circuit a feedforward fiber (FFF). The input tree of *cpxR* is not isomorphic to either *baeR* or *spy*, and therefore *cpxR* is not symmetric with these genes, but it is isomorphic to *bacA*, *slt*, and *yebE* forming another fiber. Likewise, genes *ung*, *tsr*, and *psd* are all isomorphic, composing another fiber (Fig. 1*B*). Fig. 1*D* shows the symmetry fibration $\psi : G \to B$ that collapses the genes in the fibers to the base B. Fig. 1*E* shows another example (of many) of a single connected component, *fadR*, and its corresponding isomorphic input trees (Fig. 1*F*), fibers, and base.

The dynamical state of a gene is encoded in the topology of the input tree. In turn, this topology is encoded by a sequence, a_i, defined as the number of genes in each ith layer of the input tree (Fig. 1*B*). The sequence a_i represents the number of paths of length $i-1$ that reach the gene at the root. This sequence is characterized by the branching ratio n of the input tree defined as $a_{i+1}/a_i \xrightarrow[i\to\infty]{} n$, which represents the multiplicative growth of the number of paths across the network reaching the gene at the root. For instance, the input trees of genes *baeR-spy* (Fig. 1*B*) encode a sequence $a_i = i$ with branching ratio $n = 1$ representing the single ($n = 1$) autoregulation loop inside the fiber.

Beyond several single-gene strongly connected components like those shown in Fig. 1, we find that the *E. coli* network has other strongly connected components (in a strongly connected component, each gene is reachable from every other gene; *SI Appendix*, section VI), three in total, which regulate more involved topologies of fibers. We find 1) a two-gene strongly connected component composed of master regulators *crp-fis* involved in a myriad of functions like carbon utilization (Fig. 2 *A*, *Top*), 2) a five-gene strongly connected component involved in the stress response system (*SI Appendix*, Fig. S7), and 3) the largest strongly connected

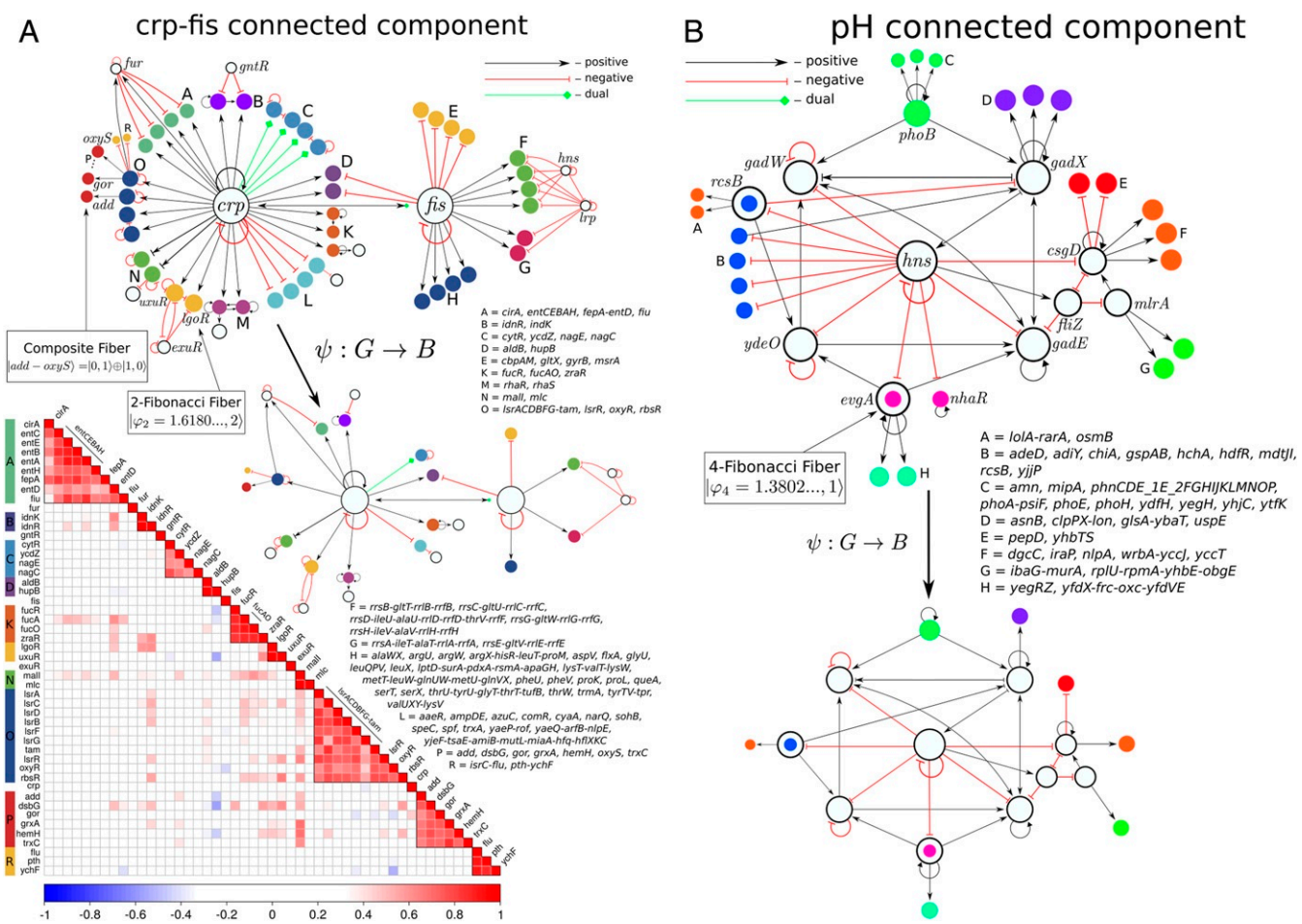

Fig. 2. Strongly connected components of the genetic network and synchronization of gene coexpression in the fibers in *E. coli*. (*A*, *Top*) Two-gene connected component of *crp-fis*. This component controls a rich set of fibers as shown. We also show the symmetry fibration collapsing the graph to the base. We highlight the fiber *uxuR-lgoR* which sends information to its regulator *exuR* and forms a 2-Fibonacci fiber $|\varphi_2 = 1.6180.., \ell = 2\rangle$, as well as the double-layer composite $|add - oxyS\rangle = |0, 1\rangle \oplus |1, 1\rangle$. (*A*, *Bottom*) Coexpression correlation matrix calculated from the Pearson coefficient between the expression levels of each pair of genes in *A*, *Top*. Synchronization of the genes in the respective fibers is corroborated as the block structure of the matrix. (*B*) The core of the *E. coli* network is the strongly connected component formed by genes involved in the pH system as shown. This component supports two Fibonacci fibers: 3-FF and 4-FF and fibers as shown. Open colored circles indicate genes that are in fibers and also belong to the pH component.

component at the core of the network which is composed of genes involved in the pH system that regulate hydrogen concentration (Fig. 2*B*). Each of these three components regulates a rich variety of fiber topologies which are collapsed into the base by the symmetry fibration $\psi: G \to B$, as shown in Fig. 2*B*.

Fiber Building Blocks. We find that the transcriptional regulatory network of *E. coli* is organized in 91 different fibers. The complete list of fibers in *E. coli* is shown in *SI Appendix*, section VII and Table VI and the statistics are shown in *SI Appendix*, Table I. Plots of each fiber are shown in Dataset S1. We find a rich variety of topologies of the input trees. Despite this diversity, the input trees present common topological features that allow us to classify all fibers into concise classes of fundamental "fiber building blocks" (Fig. 3 *A* and *B*). We associate a building block to a fiber by considering the genes in the fiber plus the external incoming regulators of the fiber plus the minimal number of their regulators in turn that are needed to establish the isomorphism in the fiber. When the fiber is connected to any external regulator, either via a direct link or through a path in the strongly connected component forming a cycle, then the genes in this cycle are considered part of the building block of the fiber, since such a cycle is crucial to establish the dynamical synchronization state (when there is more than one cycle, the shortest cycle is considered).

We find that the most basic input tree topologies can be classified by integer "fiber numbers" $|n, \ell\rangle$ reflecting two features: 1) infinite n-ary trees with branching ratio n representing the infinite pathways going through n loops inside the base of the fiber and 2) finite trees representing finite pathways starting at ℓ external regulators of the fiber. The most basic fibers in *E. coli* have three values of $n = 0, 1, 2$ (Fig. 3*A*): 1) fibers with $n = 0$ loops, called star fibers (SF); 2) fibers with $n = 1$ loop, called chain fibers (CF); and 3) fibers with $n = 2$ loops, called binary-tree fibers (BTF). This classification does not take into account the types of repressor or activator links in the building blocks, which lead to further subclasses of fibers that determine the type

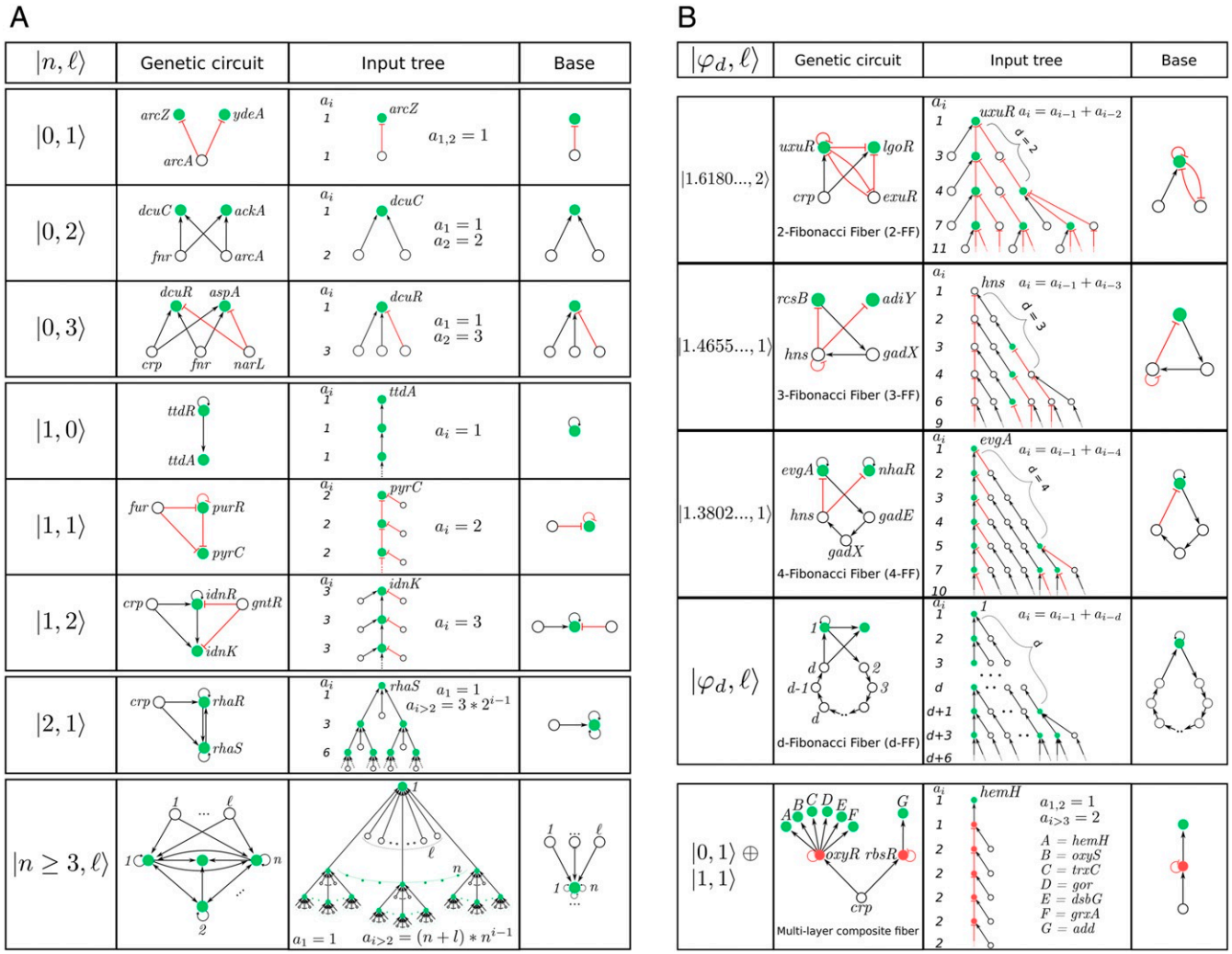

Fig. 3. Classification of building blocks in *E. coli*. (*A*) Basic fiber building blocks. These building blocks are characterized by a fiber that does not send back information to its regulator. They are characterized by two integer fiber numbers: $|n, \ell\rangle$. We show selected examples of circuits and input trees and bases. The full list of fibers appears in *SI Appendix*, Table VI and Dataset S1. The statistical count of every class is in *SI Appendix*, Table I. *Bottom* example shows a generic building block for a general *n*-ary tree $|n, \ell\rangle$ with ℓ regulators. (*B*) Complex Fibonacci and multilayer building blocks. These building blocks are more complex and characterized by an autoregulated fiber that sends back information to its regulator. This creates a fractal input tree that encodes a Fibonacci sequence with golden branching ratio in the number of paths a_i versus path length, $i - 1$. When the information is sent to the connected component that includes the regulator, then a cycle of length *d* is formed and the topology is a generalized Fibonacci block with golden ratio φ_d as indicated. We find three such building blocks: 2-FF, 3-FF, and 4-FF. *Bottom* panel shows a multilayer composite fiber with a feedforward structure.

of synchronization (fixed point, limit cycles, etc.) and thus the functionality of the fibers.

Fig. 3*A* shows a sample of dissimilar circuits that can be concisely classified by $|n, \ell\rangle$ (full list in Dataset S1). For instance, the $n=0$ SF class includes dissimilar circuits like $|arcZ-ydeA\rangle = |0,1\rangle$, $|dcuC-ackA\rangle = |0,2\rangle$, which is a bifan network motif (2), and generalizations with $\ell=3$ regulators like $|dcuR-aspA\rangle = |0,3\rangle$ (Fig. 3 *A*, *Top*). The main feature of these building blocks is that they do not contain loops and therefore the input trees are finite. The CF class contains $n=1$ loop in the fiber and therefore an infinite chain in the input tree, like the autoregulated loop in the fiber $|ttdR\rangle = |1,0\rangle$. We note that while the input tree is infinite, the topological class is characterized by a single number $n=1$ concisely represented in the base. Furthermore, a theorem proved by Norris (26) demonstrates that it suffices to test N_G-1 layers of the input trees to prove isomorphism, even though the input tree may contain an infinite number of layers. Adding one external regulator ($\ell=1$) to this circuit converts it to the purine fiber $|purR\rangle = |1,1\rangle$ which is an example of a FFF, like the *baeR* circuit in Fig. 1*A*. This circuit resembles a feedforward loop motif (2), but it differs in the crucial addition of the autoregulator loop at *purR* that allows genes *purR* and *pyrC* to synchronize. When another external regulator is added, we find the idonate fiber $|idnR\rangle = |1,2\rangle$. More elaborated circuits contain two autoregulated loops and feedback loops featuring trees with branching ratio $n=2$.

Fibonacci Fibers. So far we have analyzed building blocks that receive information from the external regulators in their respective strongly connected components, but do not send back information to the external regulators. These topologies are characterized by integer branching ratios, $n=0,1,2$, as shown in Fig. 3*A*. We find, however, more interesting building blocks that also send information back to their regulators. These circuits contain additional cycles in the building blocks that transform the input trees into fractal trees characterized by noninteger fractal branching ratios. Notably, the building block of the fiber *uxuR-lgoR* that is regulated by the connected component *crp-fis* (Fig. 2) forms an intricate input tree (Fig. 3 *B*, *Top*) where the number of paths of length $i-1$ is encoded in a Fibonacci sequence $a_i=$ 1, 3, 4, 7, 11, 18, 29, ... characterized by the Fibonacci recurring relation $a_1=1$, $a_2=3$, and $a_i=a_{i-1}+a_{i-2}$ for $i>2$. This sequence leads to the noninteger branching ratio known as the golden ratio: $a_{i+1}/a_i \xrightarrow[i\to\infty]{} \varphi=(1+\sqrt{5})/2=1.6180...$

This topology arises in the genetic network due to the combination of two cycles of information flow. First, the autoregulation loop inside the fiber at *uxuR* creates a cycle of length $d=1$ which contributes to the input tree with an infinite chain with branching ratio $n=1$. This sequence is reflected in the Fibonacci series by the term $a_i=a_{i-1}$. The important addition to the building block is a second cycle of length $d=2$ between *uxuR* in the fiber and its regulator *exuR*: *uxuR* → *exuR* → *uxuR*. This cycle sends information from the fiber to the regulator and back to the fiber by traversing a path of length $d=2$ that creates a "delay" of $d=2$ steps in the information that arrives back to the fiber (Fig. 3 *B*, *Top*). This short-term "memory" effect is captured by the second term $a_i=a_{i-2}$ in the Fibonacci sequence leading to $a_i=a_{i-1}+a_{i-2}$ and the golden ratio. We call this topology a Fibonacci fiber (FF).

This argument implies that an autoregulated fiber that further regulates itself by connecting to its connected component via a cycle of length d encodes a generalized Fibonacci sequence of order d defined as $a_i=a_{i-1}+a_{i-d}$ with generalized golden ratio φ_d (Fig. 3 *B*, *Top*, fourth row). We find such a Fibonacci sequence in the *evgA-nhaR* fiber building block linked to the pH strongly connected components shown in Fig. 2*B*. This fiber contains an autoregulation cycle inside the fiber and also an external cycle of length $d=4$ through the pH strongly connected component: *evgA* → *gad E* → *gadX* → *hns* → *evgA* (Fig. 3 *B*, *Top*, third row). This topology forms a fractal input tree with sequence $a_i=a_{i-1}+a_{i-4}$ (sequence A003269 in ref. 27) and branching golden ratio $\varphi_4=1.38028...$ We call this topology 4-Fibonacci fiber, 4-FF. Generalized Fibonaccis appear inside strongly connected components, like the *rcsB-adiY* 3-FF in the pH system (Fig. 3 *B*, *Top*, second row). Likewise, if the network contains many cycles of varying length up to a maximum d, the Fibonacci sequence generalizes to $a_i=a_{i-1}+a_{i-2}+\cdots+a_{i-1-d}+a_{i-d}$, and the branching ratio satisfies $d=-\frac{\log(2-\varphi_d)}{\log\varphi_d}$ (28).

Multilayer Composite Fibers. Building blocks can also be combined to make composite fibers, like prime numbers or quarks can be combined to form natural numbers or composite particles like protons and neutrons, respectively. The ability to assemble fiber building blocks to make larger composites is important in that it helps to understand systematically higher-order functions of biological systems composed of many genetic elements. We discover a particular type of composite made up of two elementary building blocks that we name multilayer composite fiber. For instance, the double-layer *add-oxyS* fiber in the *crp-fis* connected component (Figs. 2*A* and 3 *B*, *Bottom* and ID 7 in *SI Appendix*, Table VI and Dataset S1) is a composite $|add-oxyS\rangle = |0,1\rangle \oplus |1,1\rangle$ made of a series of genes composing a single fiber of type $|0,1\rangle = |add, dsbG, gor, grxA, hemH, oxyS, trxC\rangle$ that are regulated by two different transcription factors *rbsR* and *oxyR* that form another fiber of type $|1,1\rangle = |rbsR, oxyR\rangle$. This composite is of importance since it allows for information to be shared between two genes, for instance *add* and *oxyS*, which are not directly connected (in this case, separated by a distance in the network of length 2 from *crp*).

Composite fibers satisfy a simple engineering "sum rule": elementary fibers are composed in series of fibers in a predefined order where the first layer is represented by an entry fiber (carrying transcription factors), and the last layer is formed by a terminator fiber of output genes (encoding enzymes), as shown in Fig. 3 *B*, *Bottom*. This multilayer composite fiber is biologically significant because genes in the output layer synchronize a genetic module that implements the same function even though the genes in the module are not directly connected and, indeed, can be at far distances in the network. Such functionally related modules could not be identified by modularity algorithms (29) which cluster nodes in modules of highly connected nodes.

We find that composite fibers are dominant in eukaryotes (yeast, mice, humans; see *Fibration Landscape across Biological Networks, Species, and System Domains*). They resemble the building blocks of multilayered deep neural networks where each subsequent gene in the layer synchronizes despite the fact that nodes can be distant in the network. More generally, composite fibers with multiple layers streamline the construction of larger aggregates of fibration building blocks, performing more complex function in a coordinated fashion. These composite topologies complete the classification of input trees.

Fibration Landscape across Biological Networks, Species, and System Domains. To study the applicability of fibration symmetries across domains of complex networks we have analyzed 373 publicly available datasets (*SI Appendix*, section VIII). Full details of each network and results can be accessed on GitHub at https://github.com/makselab/fibrationData/blob/master/datasets.xlsx. The codes to reproduce this analysis are on GitHub at https://github.com/makselab (*SI Appendix*, section V). The full datasets are on GitHub at https://github.com/makselab/fibrationData/blob/master/rawData.zip. We analyze biological networks spanning from transcriptional regulatory networks, metabolic networks, cellular processes networks and signaling

pathways, disease networks, and neural networks. We span different species ranging from *Arabidopsis thaliana*, *E. coli*, *Bacillus subtilis*, *Salmonella enterica*, *Mycobacterium tuberculosis*, *Drosophila melanogaster*, *Saccharomyces cerevisiae* (yeast), and *Mus musculus* (mouse) to *Homo sapiens* (human). The topological fiber numbers $|n, \ell\rangle$ allow us to systematically classify fibers across the different domains in a unifying way. We find that fibration symmetries are found across all biological processes and domains. The fiber distributions for each type of biological network calculated by summing over the studied species are displayed in Fig. 4*A* and the fiber distributions for each species calculated over the type of biological networks are shown in Fig. 4*B*. Our analysis allows us to investigate the specific attributes and commonalities of the fiber building blocks inside and across biological domains. We find a varied set of fibers that characterize the biological landscape. Certain features of the fiber number distribution are visible in the transcriptional networks in Fig. 4*A*. For instance, a tail with ℓ is seen in the $n=0$ class as well as in the $n=1$ class. Across species (Fig. 4*B*), bacteria like *E. coli* or *B. subtilus* display a majority of $n=0$ building blocks, while higher-level organisms like yeast, mice, and humans display a majority of more complex building blocks like multilayers and Fibonaccis.

To test the existence of symmetry fibrations across other domains we extend our studies to complex networks beyond biology ranging from social, infrastructure, internet, software, and economic networks to ecosystems (details of datasets in *SI Appendix*, section VIII). Fig. 4*C* shows the obtained fiber distributions for each domain. A normalized comparison across domains is visualized in Fig. 4*D*, showing the cumulative number of fibers over all domains and species per network size of 10^4 nodes. The results support the applicability of the concept of symmetry fibration beyond biology to describe the building blocks of networks across all domains.

Gene Coexpression and Synchronization via Symmetry Fibration. We have shown in *Symmetry Fibration Leads to Synchronization* that fibers in networks determine cluster synchronization in the dynamical system. In a gene regulatory network, symmetric genes in a fiber synchronize their activity to produce gene coexpression levels that sustain cellular functions. We corroborate this result numerically in Fig. 1*G* in the particular example of the *baeR-spy*

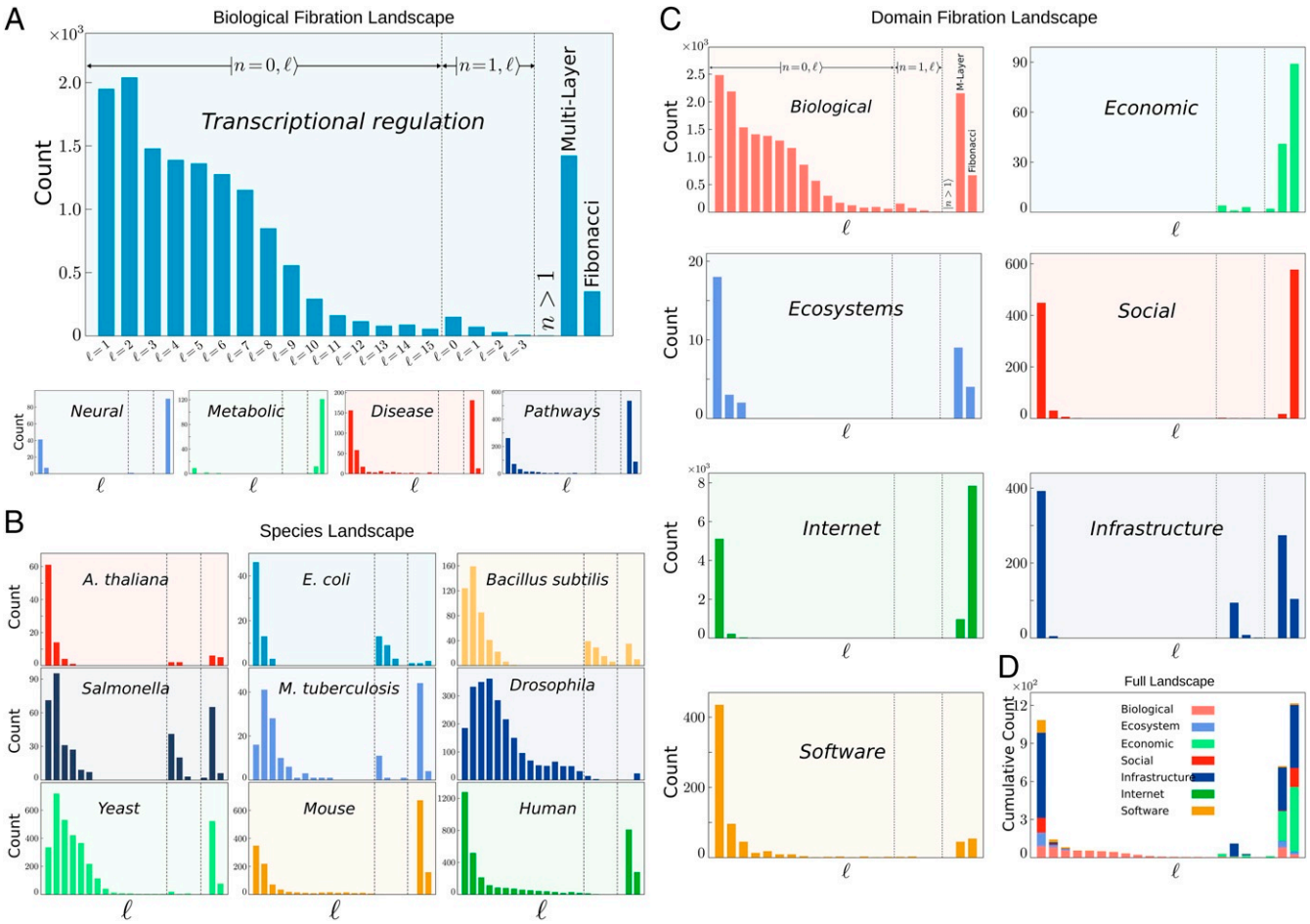

Fig. 4. Fibration landscape across domains and species. (*A*) Fibration landscape for biological networks. Shown is the total number of fiber building blocks across five types of biological networks analyzed in the present work. The count includes the total number of fibers in the networks of each biological type considering all species analyzed for each type (*SI Appendix*, Table IV). (*B*) Fibration landscape across species. Shown is the count of fibers across each analyzed species. Each panel shows the count over the different types of biological networks (*E. coli* contains only the transcriptional network; see *SI Appendix*, Table IV). (*C*) Fibration landscape across domains. Shown is the count of fibers across the major domains studied. The biological domain panel is calculated over all networks and species in *A* and *B*. (*D*) Global fibration landscape. Shown is the cumulative count of fibers in all domains in *C*. The cumulative count represents the total number of fibers per network of 10^4 nodes. Specifically, the quantity is calculated as the total number of fibers divided by the total number of nodes in all networks per domain multiplied by 10^4.

FFF in *E. coli*, and this result applies to all fibers, irrespective of the dynamical system law.

To exemplify the synchronization in fibers, we consider the dynamics in the composite fiber $|add - oxyS\rangle = |0,1\rangle \oplus |1,1\rangle$ depicted in Figs. 2*A* and 3 *B*, *Bottom*, which is composed of autoregulator $1 = crp$, and two layers of fibers: $2 = rbsR$, $3 = oxyR$ and $4 = add$, $5 = oxyS$ (we consider here a reduced fiber for simplicity, and we add the autoregulator to *crp* to the building block for completeness). Graph $G = \{N_G, E_G\}$ consists of $N_G = \{1,2,3,4,5\}$, $E_G = \{1 \to 1, 1 \to 2, 1 \to 3, 2 \dashv 2, 3 \dashv 3, 2 \to 4, 3 \to 5\}$ ($\dashv$ refers to repressor and $\to$ to activation), and a five-dimensional total phase space $PG = \mathbb{R}^5$ with state vector $X(t) = \{x_1(t), x_2(t), x_3(t), x_4(t), x_5(t)\}$ describing the expression levels of each gene's product (e.g., mRNA concentration).

The symmetry fibration $\psi : G \to B$ collapses the graph G into the base $B = \{N_B, G_B\}$, where $N_B = \{a, b, c\}$ and $E_B = \{a \to a, a \to b, b \dashv b, b \to c\}$. The symmetry fibration acts on the nodes $\psi(1) = a$, $\psi(2) = \psi(3) = b$, and $\psi(4) = \psi(5) = c$ and on the edges $\psi(1 \to 1) = a \to a$, $\psi(1 \to 2) = \psi(1 \to 3) = a \to b$, $\psi(2 \dashv 2) = \psi(3 \dashv 3) = b \dashv b$, and $\psi(2 \to 4) = \psi(3 \to 5) = b \to c$. Thus, the fibers partition the graph G as $\Pi = \{\Pi_a, \Pi_b, \Pi_c\}$, where $\Pi_a = \{1\}$, $\Pi_b = \{2,3\}$, and $\Pi_c = \{4,5\}$.

We represent the dynamics by two functions $k(x)$ and $g(x)$ modeling degradation and synthesis of gene product, respectively (9, 10). For example, $k(x)$ can be modeled as a linear degradation term and $g_i(x)$ as a Hill function ($i = A, R$, activation or repression) (9). We consider that multiple inputs are combined by multiplying functions $g(x)$, but any other way of combining inputs can be used. Then, the dynamics of the expression levels of the genes in the circuit are described by ref. 14:

$$\begin{cases} \frac{dx_1}{dt} = -k(x_1) + g_A(x_1) \\ \frac{dx_2}{dt} = -k(x_2) + g_A(x_1) * g_R(x_2) \\ \frac{dx_3}{dt} = -k(x_3) + g_A(x_1) * g_R(x_3) \\ \frac{dx_4}{dt} = -k(x_4) + g_A(x_2) \\ \frac{dx_5}{dt} = -k(x_5) + g_A(x_3). \end{cases} \quad [2]$$

The dynamics of the base are described by the state vector of the base: $(y_a(t), y_b(t), y_c(t))$ with dynamical equations (16):

$$\begin{cases} \frac{dy_a}{dt} = -k(y_a) + g_A(y_a) \\ \frac{dy_b}{dt} = -k(y_b) + g_A(y_a) * g_R(y_b) \\ \frac{dy_c}{dt} = -k(y_c) + g_A(y_b). \end{cases} \quad [3]$$

If $(y_a(t), y_b(t), y_c(t))$ is a solution for the base Eq. **3**, then the map $\mathbb{P}_\psi$ sends the phase space of this base to the phase space of the solutions in the graph G (16):

$$\begin{aligned} &(x_1(t), x_2(t), x_3(t), x_4(t), x_5(t)) \\ &\quad = \mathbb{P}_\psi\,[y_a(t), y_b(t), y_c(t)] = (y_a(t), y_b(t), y_b(t), y_c(t), y_c(t)). \end{aligned} \quad [4]$$

Therefore, the graph G sustains a polysynchronous subspace (see for instance motivating example 1.4 in ref. 15):

$$\begin{aligned} \Delta_\Pi = \{&(x_1, x_2, x_3, x_4, x_5) \in \mathbb{R}^5 \mid x_1(t), x_2(t) = x_3(t), x_4(t) \\ &= x_5(t)\}. \end{aligned} \quad [5]$$

This result can be corroborated by simply plugging $(x_1(t), x_2(t), x_3(t) = x_2(t), x_4(t), x_5(t) = x_4(t))$ into Eq. **2** to obtain a solution of the dynamics, implying the synchrony $x_2(t) = x_3(t)$ in fiber Π_b and $x_4(t) = x_5(t)$ in fiber Π_c. We note that the concept of sheaves and stacks might be useful to generalize the symmetry fibration framework to multiplex networks.

We test this gene synchronization with publicly available transcription profile experiments available from the literature. We use gene expression data profiles in *E. coli* compiled at Ecomics: http://prokaryomics.com (30). This portal collects microarray and RNA-seq experiments from different sources such as the NCBI Gene Expression Omnibus (GEO) public database (31) and ArrayExpress (32) under different experimental growth conditions. The data are also compiled at the Colombos web portal (33). The database contains transcriptome experiments measuring the expression level of 4,096 genes in *E. coli* strains over 3,579 experimental conditions which are described as strain, medium, stress, and perturbation. Raw data are preprocessed to obtain expression levels by using noise reduction and bias correction to normalize data across different platforms (30).

E. coli can adapt its growth to the different conditions that it finds in the medium. This adaptation is made by sensing extra and intracellular molecules and using them as effectors to activate or repress transcription factors. This implies that the different fibers are activated by specific experimental conditions. The Ecomics portal allows one to obtain those experimental conditions where a set of genes has been significantly expressed under a particular set of conditions. We perform standard gene expression analysis (http://colombos.net and ref. 33) of the expression levels in *E. coli* obtained under these conditions.

For a given set of genes in a fiber, we find the experimental conditions for which the genes have been significantly expressed by comparing the expression samples over the 1,576 different WT growth conditions. Following ref. 33, the experimental conditions are ranked with the inverse coefficient of variation (ICV) defined as $\mathrm{ICV}_k = |\mu_k|/\sigma_k$, where μ_k is the average expression level of the genes in the condition k and σ_k is the SD. Following ref. 33, we select those conditions with $\mathrm{ICV}_k > \langle\, \mathrm{ICV}_k \rangle$, i.e., where the average expression levels in the particular condition k are significantly higher than the SD. This score reflects the fact that, in a relevant condition, the genes show an increment of their expression above the individual variations caused by random noise. Details on the expression analysis can be found in ref. 33 and https://doi.org/10.1371/journal.pone.0020938.s001. Thus, we obtain expression levels organized by the relevant experimental conditions which are labeled according to the GEO database (31). From these data, we calculate the coexpression matrix using the Pearson correlation coefficient between the expression levels of two genes i and j in the relevant conditions for genes in a fiber. For off-diagonal correlations between genes in different fibers, we use the combined sets of conditions of both genes.

Results for the correlation matrix are shown in Fig. 2 *A*, *Bottom* for fibers regulated by the *crp-fis* strongly connected component. Gene expression is obtained for every gene, so we plot the correlation matrix calculated over each pair of genes. Genes that belong to the same operon are transcribed as a single unit by the same mRNA molecule, so these genes are expected to trivially synchronize (variations exist due to attenuators inside the operon). Thus, we group together these genes as operons in Fig. 2*A* to indicate this trivial synchronization. To test the existence of fiber synchronization we compare gene coexpression belonging to different operons. Fig. 2 *A*, *Bottom* shows that expression levels of the genes that belong to a fiber are highly correlated as predicted by the symmetry fibration. Genes that belong to different fibers show no significant correlations among them. In particular, there is no significant correlation between the expression of genes in a given fiber and the two master regulators *crp* and *fis*. This result is consistent with the fibration symmetry and occurs despite the fact that both *crp* and *fis* directly regulate all genes in the studied fibers. We find some off-diagonal weak correlations between fibers (e.g., *malI*), probably indicating missing links or missing regulatory processes that produce extra synchronizations. Some genes present weak correlations inside fibers (e.g., *cirA*), indicating weak symmetry

breaking probably from asymmetries in the strength of binding rate of transcription factors or input functions, effects that are not considered in the topological view of the input trees and can lead to desynchronization inside the fiber.

Discussion

Fibration symmetries make sure that genes are turned on and off at the right amount to ensure the synchronization of expression levels in the fiber needed to execute cellular functions. In the fibration framework, network function can be pictured as an orchestra in which each instrument is a gene in the network. When the instruments play coherently, with structured temporal patterns, the network is functional. Here we have concentrated on the simplest temporal organization, one in which some units (instruments) act synchronously in time, a ubiquitous pattern observed in all biological networks. Our findings identify the symmetries that predict this synchronization and give rise to functionally related genes from the fibrations of the genetic network.

Unlike network motifs which are identified by statistical overrepresentation (2), fibers in biology arise from principles of symmetries following the tradition of how the building blocks of elementary particles have being discovered in physics and geometry (5). Our first principle approach to identify building blocks is based on the circuit's theoretical and practical (rather than statistical) significance to serve minimal forms of coherent function and logic computation.

Further results shown in ref. 34 indicate that symmetries also describe the structure of neural connectomes and these symmetries factorize according to function. Thus, symmetries can be used to systematically organize biological diversity into building blocks using invariances in the information flow encoded in the topologies of the input trees. Genes related by symmetries are coexpressed, thus providing a functional rationale for the biological existence of these symmetries.

ACKNOWLEDGMENTS. Research was sponsored by Grants NIH-National Institute of General Medical Sciences R01EB022720, NIH-National Cancer Institute U54CA137788/U54CA132378, NSF-Information and Intelligent Systems 1515022, and NSF-Division of Materials Research 1308235. We thank L. Parra, W. Liebermeister, C. Ishida, M. Sánchez, and J. D. Farmer for discussions.

1. L. H. Hartwell, J. J. Hopfield, S. Leibler, A. W. Murray, From molecular to modular cell biology. *Nature* **402**, C47–C52 (1999).
2. U. Alon, *An Introduction to Systems Biology: Design Principles of Biological Circuits* (CRC Press, Boca Raton, FL, 2006).
3. M. Gell-Mann, *The Quark and the Jaguar* (Holt Paperbacks, New York, NY, 1994).
4. J. D. Dixon, B. Mortimer, "Permutation groups" in *Graduate Texts in Mathematics*, S. Axler, K. Ribet, Eds. (Springer-Verlag, New York, NY, 1996), vol. 163.
5. S. Weinberg, *The Quantum Theory of Fields* (Cambridge University Press, Cambridge, UK, 2005).
6. R. Milo *et al.*, Network motifs: Simple building blocks of complex networks. *Science* **298**, 824–827 (2002).
7. M. Buchanan, G. Caldarelli, P. De Los Rios, F. Rao, M. Vendruscolo, Eds., *Networks in Cell Biology* (Cambridge University Press, Cambridge, UK, 2010).
8. S. S. Shen-Orr, R. Milo, S. Mangan, U. Alon, Network motifs in the transcriptional regulation network of *Escherichia coli*. *Nat. Genet.* **31**, 64–68 (2002).
9. G. Karlebach, R. Shamir, Modeling and analysis of gene regulatory networks. *Nat. Rev. Mol. Cell Biol.* **9**, 770–780 (2008).
10. E. Klipp, W. Liebermeister, C. Wierling, A. Kowald, *Systems Biology* (Wiley-VCH, Weinheim, Germany, 2016).
11. S. Gama-Castro *et al.*, RegulonDB version 9.0: High-level integration of gene regulation, coexpression, motif clustering and beyond. *Nucleic Acids Res.* **44**, D133–D143 (2016).
12. A. Grothendieck, Technique de descente et théorémes d'existence en géométrie algébrique, I. Généralités. Descente par morphismes fidélement plats. *Séminaire N. Bourbaki* **5**, 299–327 (1958–1960).
13. P. Boldi, S. Vigna, Fibrations of graphs. *Discrete Math.* **243**, 21–66 (2001).
14. M. Golubitsky, I. Stewart, Nonlinear dynamics of networks: The groupoid formalism. *Bull. Am. Math. Soc.* **43**, 305–364 (2006).
15. L. DeVille, E. Lerman, Modular dynamical systems on networks. *J. Eur. Math. Soc.* **17**, 2977–3013 (2015).
16. E. Nijholt, B. Rink, J. Sanders, Graph fibrations and symmetries of network dynamics. *J. Differ. Equ.* **261**, 4861–4896 (2016).
17. D. M. Abrams, L. M. Pecora, A. E. Motter, Focus issue: Patterns of network synchronization. *Chaos* **26**, 094601 (2016).
18. L. M. Pecora, F. Sorrentino, A. M. Hagerstrom, T. E. Murphy, R. Roy, Cluster synchronization and isolated desynchronization in complex networks with symmetries. *Nat. Commun.* **5**, 4079 (2014).
19. F. Sorrentino, L. M. Pecora, A. M. Hagerstrom, T. E. Murphy, R. Roy, Complete characterization of the stability of cluster synchronization in complex dynamical networks. *Sci. Adv.* **2**, e1501737 (2016).
20. I. Stewart, M. Golubitsky, M. Pivato, Symmetry groupoids and patterns of synchrony in coupled cell networks. *SIAM J. Appl. Dyn. Syst.* **2**, 609–646 (2003).
21. A. Arenas, J. K. A. Díaz-Guilera, Y. Moreno, C. Zhou, Synchronization in complex networks. *Phys. Rep.* **469**, 93–153 (2008).
22. F. A. Rodrigues, T. K. Peron, P. Ji, J. Kurths, The Kuramoto model in complex networks. *Phys. Rep.* **610**, 1–98 (2016).
23. S. Strogatz, *Nonlinear Dynamics and Chaos: With Applications to Physics, Biology, Chemistry, and Engineering* (Westview Press, Boulder, CO, 2000).
24. A. Cardon, M. Crochemore, Partitioning a graph in $O(|A| \log_2 |V|)$. *Theor. Comput. Sci.* **19**, 85–98 (1982).
25. H. Kamei, P. J. A. Cock, Computational of balanced relations and their lattice for a coupled cell network. *SIAM J. Appl. Dyn. Syst.* **12**, 352–382 (2013).
26. N. Norris, Universal covers of graphs: Isomorphism to depth n - 1 implies isomorphism to all depths. *Discrete Appl. Math.* **56**, 61–74 (1995).
27. OEIS Foundation Inc. (2020), The On-Line Encyclopedia of Integer Sequences. http://oeis.org/A003269. Accessed 6 March 2020.
28. M. Gardner, *The Scientific American Book of Mathematical Puzzles and Diversions* (Simon & Schuster, 1961), vol. II, p. 101.
29. M. Girvan, M. E. J. Newman, Community structure in social and biological networks. *Proc. Natl. Acad. Sci. U.S.A.* **99**, 7821–7826 (2002).
30. M. Kim *et al.*, Multi-omics integration accurately predicts cellular state in unexplored conditions for Escherichia coli. *Nat. Commun.* **7**, 13090 (2016).
31. T. Barrett *et al.*, NCBI GEO: Archive for functional genomics data sets– update. *Nucleic Acids Res.* **41**, D991–D995 (2016).
32. N. Kolesnikov *et al.*, ArrayExpress update: Simplifying data submissions. *Nucleic Acids Res.* **43**, D1113–D1116 (2015).
33. M. Moretto *et al.*, COLOMBOS v3.0: Leveraging gene expression compendia for cross-species analyses. *Nucleic Acids Res.* **44**, D620–D623 (2016).
34. F. Morone, H. A. Makse, Symmetry group factorization reveals the structure-function relation in the neural connectome of *Caenorhabditis elegans*. *Nat. Commun.* **10**, 4961 (2019).

Supplementary Information

Fibration symmetries uncover the building blocks of biological networks

Flaviano Morone, Ian Leifer, Hernán A. Makse

Contents

www.pnas.org/cgi/doi/10.1073/pnas.1914628117

III. TRANSCRIPTIONAL REGULATORY NETWORK OF *E. COLI*

To define the transcriptional regulatory network (TRN) we use the transcription factor-gene target bi-partite network of *Escherichia coli* K-12 obtained from the RegulonDB data source (`http://regulondb.ccg.unam.mx`). RegulonDB manually curates all transcriptional regulations from literature searches [11]. We download all transcriptional regulatory interactions catalogued in RegulonDB version 9.0 from `http://regulondb.ccg.unam.mx/menu/download/datasets/files/network_tf_gene.txt`, last accessed September 15, 2018.

The database downloaded from RegulonDB is composed of a bipartite transcription factor - gene target network. In this bi-partite dataset, a directed link between a source transcription factor (TF) and a target gene means that the TF binds to the DNA sequence at the binding site of the target gene to regulate its rate of transcription. In *E. coli*, each gene expresses a single TF (this is not the case in eukaryotic genes that contains introns and splicing of protein-coding RNA can produce many proteins from a single gene). Therefore, a gene-gene regulatory network can be constructed from the bipartite transcription factor-gene target network by associating each TF to the gene that expresses the TF. Then, a directed link in the TRN from gene $i \rightarrow$ gene j implies that gene i encodes for a TF that controls the rate of transcription of gene j. Thus, a directed link encodes the combined processes of transcription, translation and TF binding to a target gene. We denote genes in bacteria in italics, e.g., *gadX* and its protein as GadX. Thus, we say that gene i sends a genetic 'message' to gene j and the 'messenger' is the TF. The history of all messages passing in the network defines the information flow in the network. A TF can either be an activator, repressor or can have a dual function. For the purpose of calculating isomorphisms between input trees, the dual interactions are treated as distinct interactions. Thus, these three interactions are treated as three different types.

For the purpose of building the TRN it is important to distinguish the gene's products between genes encoding for TFs and the rest of the genes encoding for the rest of the proteins (enzymes, kinases, transport proteins, etc). A TF is a regulatory protein that regulates a gene by binding, and therefore will always have an out-going link in the network. There are other regulatory proteins (like kinases, histones, coactivators, etc) that regulate gene expression but they do not have a DNA-binding domain and they regulate gene expression without binding. In our TRN, genes that encode for a protein that is not a TF do not have

out-going links in the network. They only have in-going links and therefore are dangling ends in the network. In *E. coli* most of these proteins are enzymes that catalyze biochemical reactions in the metabolic network. Other proteins are involved in transport and signaling processes (kinase) in the cell.

TF are also activated by effector molecules (metabolites) that bind non-covalently to an allosteric site of the TF to alter the conformation of the TF to activate it or deactivated by controlling the binding/unbinding of the TF to DNA. Effectors can also produce covalent activation of the TF like for instance during phosphorylation mediated by kinases in the two component TFs.

We treat these effector activities as external parameters, determined by the growth conditions in the surrounding system (the cell in its changing environment) or by the metabolic network, which is considered external to the TRN. These external perturbations are considered as the external growth conditions when we analyze the co-expression profiles in Section II. In the present study, the metabolic network is considered external to the TRN, so we do not consider feedback loops from the TRN to the metabolic network and back to the TRN mediated by effector metabolites. This extended network is treated in a follow up.

In *E. coli*, genes are also grouped by operons. An operon is a set of contiguous genes that are transcribed as a single unit from the same mRNA molecule and the same promoter site upstream of all genes and a terminator downstream [11]. An operon can contain genes encoding for TF or non-TF proteins, and more than two TFs can be part of the operon. Since the operons are transcribed by the same RNA molecule, then we group these genes into a single node in the network. This is certainly the case when the operon has a single promoter transcribing the full operon. However, there is some ambiguity in the construction of the network using the definition of operon in RegulonDB when there are promoters in the middle of the operon and these promoters transcribe more than one TF in the operon, forming different transcription units. For instance, the operon in the gad system, *gadAXW* which is important in the pH strongly connected component in Fig. 2b. This operon expressed two TFs, GadX and GadW, and one enzyme GadA. Here, each gene has its own promoter and terminator and thus are different nodes in the network. Moreover, each TF is regulated by different TFs as well as each TF regulates different genes. As seen in Fig. 2b, for instance, GadX binds to *hns* but not GadW. Also, GadW is regulated by *ydeO* but *ydeO* does not regulate *gadX*. Thus, putting together these two genes in the same operon

gadAXW would miss all these links. Thus, when two TF with different promoters are part of the operon, we consider the TF as different genes. On the other hand, the non-TF genes in operons are always put together with other genes in the operon. For instance, the *gadAXW* operon from RegulonDB is considered as two nodes: *gadW* and *gadAX*. To simplify notation, when there is an operon that contains one TF and several non-TF proteins, then for simplicity, we call this operon by the name of the TF. For instance, *gadAX* is simply called *gadX* or the operon *rbsDACBKR* is called *rbsR* and therefore the TF *rsbR* represents the entire operon *rbsDACBKR*. Finally, when all the genes in the operon are non-TF, then we call the operon with all the genes names, as for instance, *lsrACDBFG-tam*.

In the RegulonDB database there are a total of 4690 genes. Out of these genes, Regulon DB provides a bipartite network consisting of 1843 genes with interactions from or to other genes, the remaining genes are not considered in the analysis. There are 192 genes that encode for TFs. We cluster the genes into 313 operons as explained above. Full names of operons and genes appear in SI Table VI. After grouping the genes into operons, the network is reduced to 879 nodes. There are 1835 directed edges with an average in-degree (or out-degree) of 2.1. In this network we find 91 different fibers that encompass 416 different nodes. We find that 28 nodes are involved in 7 strongly connected components of size larger than one node, and the rest are single node connected components.

IV. SYMMETRY FIBRATIONS

Below we provide formal definitions of the main concepts using in the paper: (a) input trees and isomorphisms, (b) from fibrations $\rightarrow$ surjective minimal graph fibrations called here symmetry fibrations, (c) fibers and minimal bases, and (d) minimal balance coloring algorithm. We start with a review of the literature (not exhaustive).

The literature on fibrations and groupoids crosses the fields of mathematics, computer science and dynamical systems theory. The notion of fibration was first introduced by Grothendieck as fibrations between categories in algebraic geometry [12]. The original paper of Grothendieck has been published as a part of the Séminaire N. Bourbaki in 1958 and can be found at `http://www.numdam.org/article/SB_1958-1960__5__299_0.pdf`. A mathematical account of Grothendieck fibrations in the context of category theory appears in `https://ncatlab.org/nlab/show/Grothendieck+fibration`. For a review of

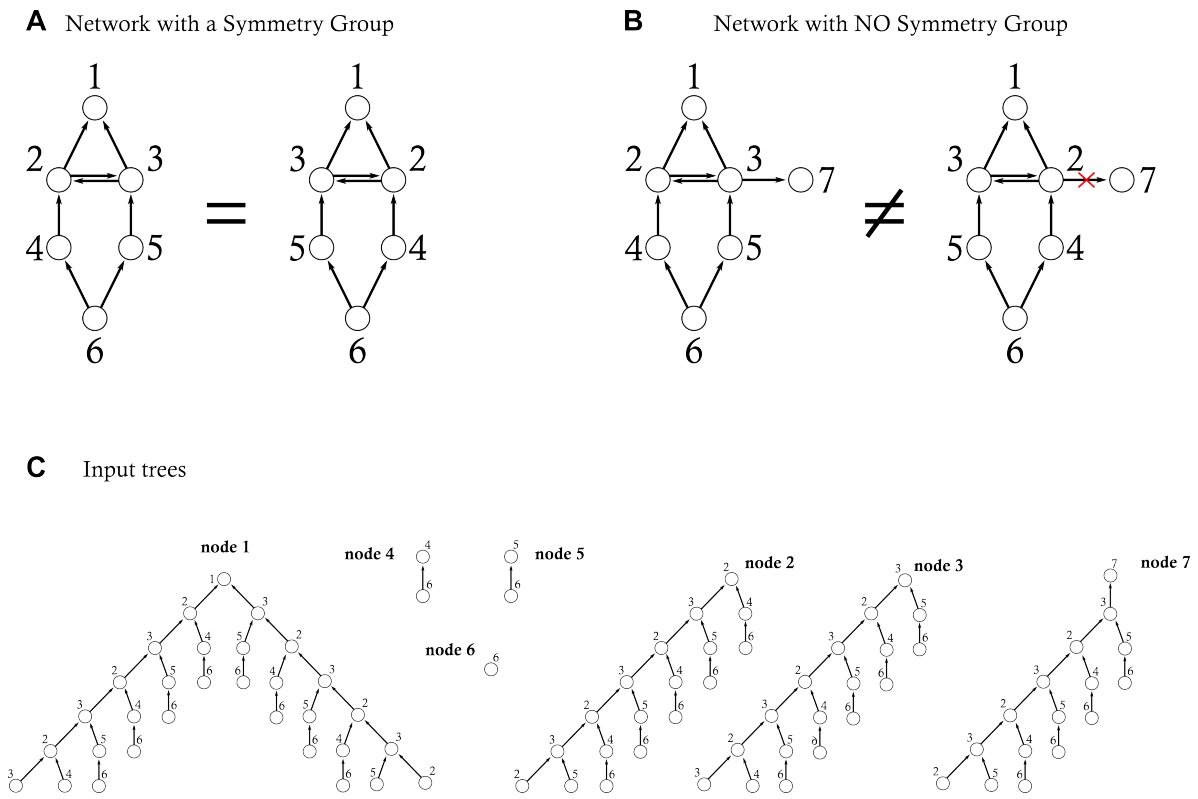

FIG. 5: **Group symmetries and fibrations with their input tree**. **a,** Example of a network with a symmetry group. The automorphism shown maps the network into another network leaving invariant the connectivity of every nodes in the network [4, 14, 17, 18]. **b,** A network without automorphisms but with a fibration. The addition of a single out-link from $3 \to 7$ breaks the whole group symmetry. However, since fibrations are defined according only to the input tree, then the network still have a symmetry, a fibration arising from the fact that the input trees of nodes 2 and 3 are isomorphic, as well as between the input trees of nodes 4 and 5 as shown in **(c).** There are no more isomorphisms as shown by the rest of the input trees. Therefore, nodes 2 and 3 form a fiber. Nodes 4 and 5 also form another fiber, yet independently of the other fiber. The fibration is a morphism that maps the network into a base which is formed by collapsing the isomorphic nodes into one, i.e., collapsing node 2 and 3 together, and node 4 and 5 together. The resulting base is also called a quotient graph.

the history of fibrations from Grothendieck to modern studies, see the blog of Vigna at `http://vigna.di.unimi.it/fibrations/`. The formulation of Grothendieck is highly abstract and differs from our present work which refers to the notion of surjective minimal graph fibration which is a fibration between graphs. The work of Boldi & Vigna

[13] and DeVille & Lerman [15] on graph fibrations are the closest to our formulation, see http://vigna.di.unimi.it/ftp/papers/FibrationsOfGraphs.pdf. Graph fibrations have been applied in computer science to understand PageRank [35], and the state of synchrony of processors in computing distributed systems [36, 37], where fibrations are the key concept in the computation of identical states in distributed system. The relation between surjective minimal graph fibrations and synchronous subspaces is elaborated in DeVille & Lerman [15] and Nijholt, Rink & Sanders [16]. It should be noted that all these works on fibrations pertain to a highly abstract mathematical level which, in turn, provides the concept of fibration with a quite broad applicability. For a more accessible reading on fibrations within the particular context application to biological networks, the reader is recommended to follow our paper and supplementary sections.

In parallel, the work of Golubitsky and Stewart [14, 20] and others in dynamical systems theory consider the equivalent formalism of symmetry groupoids, equitable partition of balanced colored nodes and its relation with synchronization [21–23]. A review of the groupoid formalism and its application to synchronization in dynamical systems appears in [14]. DeVille and Lerman [15] also discuss the relation between graph fibrations and the groupoid formalism.

Synchronization arises also as a consequence of permutation symmetries in the network, called automorphisms [4], which form symmetry groups and are different from symmetry fibrations and symmetry groupoids. There is a large literature in the dynamical system community dealing with cluster synchronization from automorphisms, since synchronization is an ubiquitous phenomenon across all sciences [21–23]. Reviews can be found in the work of Golubitsky and Stewart [14, 20] to recent work in [17–19] and references therein. Symmetry groups are the cornerstone of physical phenomena appearing in all physical systems [5].

Below, to elaborate on the definition of symmetry fibrations, we first compare fibrations to automorphisms which form symmetry groups [4, 14, 17–19] using the example networks of Figs. 5a and 5b. An automorphism is a transformation that preserves the full connectivity of the network. That is, an automorphism preserves not only the inputs but also the outputs of each node in the network, and therefore, it presents more stringent conditions on the connectivity than symmetry fibrations which preserve only the input trees. For example,

the network of Fig. 5a is invariant under the automorphism defined by the permutation:

$$\sigma = \begin{pmatrix} 1 & 2 & 3 & 4 & 5 & 6 \\ \downarrow & \downarrow & \downarrow & \downarrow & \downarrow & \downarrow \\ 1 & 3 & 2 & 5 & 4 & 6 \end{pmatrix} , \tag{6}$$

because the nodes are connected exactly to the same nodes before and after the application of the permutation σ, which is a global mirror symmetry.

Next, consider the slightly modified network depicted in Fig. 5b left, which differs from the network in Fig. 5a by one extra out-going link from node 3 to 7. In this network, the permutation of nodes $2 \leftrightarrow 3$ and $4 \leftrightarrow 5$, Eq. (6), is not an automorphism anymore, because it does not preserve the in and out connectivities of all nodes, e.g., node 3 is connected with 7 but loses this connection after the permutation (Fig. 5b right). It is interesting to see how fragile group symmetries are: if we connect just one extra node to the network as shown in Fig. 5b, the symmetry (i.e. the network automorphism group) is broken. This occurs because automorphisms require very strict arrangements of nodes and links to preserve, rigidly, the global structure of the network. Fibration symmetries, with their emphasis in the preservation of the input trees only, is less restrictive. This might explain why fibration symmetries emerged in living systems as opposed to the more restrictive automorphisms which describe all aspects of matter, from elementary particles to atoms, molecules and phases of matter.

This example raises the following question: are there extra symmetries in the network shown in Fig. 5b beyond its automorphisms? The answer to this question is, indeed, yes: there are extra symmetries in the network of Fig. 5b, the fibration symmetries [12, 13], which do not form a group [4] but groupoids [14]. A groupoid is a set of transformations satisfying the axioms of invertibility, identity and associativity but not the composition law (closure) [14], while in a group, transformations satisfy the four axioms. For this reason, groupoids are fundamentally different algebraic structures compared with traditional group symmetries.

A. Input tree

Roughly speaking, symmetry fibrations take into account only the input trees of the nodes, but not the output-trees (this is not true though when the input and output trees

are connected). Thus, node 3 in Fig. 5b is connected to node 7 via an out-going link, and this link destroys the symmetry group, but node 3 is still symmetric with 2 via a symmetry fibration, since the input trees of nodes 2 and 3 are isomorphic, even though node 3 is connected with 7. This is because the connection $3 \to 7$ is an out-going link of node 3 and, therefore, is not part of its input tree. Simply put, symmetry fibrations preserve input trees only, while automorphisms preserve both input and output-trees, since they preserve the full connectivity of the network, and thus, they represent more stringent symmetries than fibrations. We formalize this idea next after introducing some definitions.

The basic ingredient to define a new symmetry beyond automorphisms is the **input tree**, which contains the full information received by a given node through the totality of all the possible paths ending in that node and starting from every other node in the network. Thus, for every node i in the network G there is a corresponding input tree, called T_i, which is defined as a tree with a selected node r_i, called the root, and such that every other node is a path $\mathcal{P}_{j\to i}$ of G starting from j and ending in i [16]. A link from node $\mathcal{P}_{j\to i}$ to node $\mathcal{P}_{k\to i}$ exists if $\mathcal{P}_{j\to i} = e_{j\to k}\mathcal{P}_{k\to i} =$, where $e_{j\to k}$ is an edge of G.

The concept of input tree has appeared in the literature as the universal total space in traditional categorical or topological terminology [12], the universal total graph from [13], the view in the theory of distributed systems, or the unfolding of a nondeterministic automaton in concurrency theory [13].

For example, let us construct the input tree T_2 of node 2 in the network on the left of Fig. 5b. The root is the node r_2 at the uppermost level of the tree. Every other node of the input tree of node 2 is a path $\mathcal{P}_{j\to 2}$ ending in 2. There are two paths of length 1: $\mathcal{P}^{(1)}_{3\to 2}$ and $\mathcal{P}^{(1)}_{4\to 2}$; three paths of length 2: $\mathcal{P}^{(2)}_{2\to 2}$, $\mathcal{P}^{(2)}_{5\to 2}$, and $\mathcal{P}^{(2)}_{6\to 2}$; and so on. Since $\mathcal{P}^{(2)}_{2\to 2} = e_{2\to 3}\mathcal{P}^{(1)}_{3\to 2}$, we put a link in the input tree from $\mathcal{P}^{(2)}_{2\to 2}$ to $\mathcal{P}^{(1)}_{3\to 2}$ because $\mathcal{P}^{(2)}_{2\to 2} = e_{2\to 3}\mathcal{P}^{(1)}_{3\to 2}$. We then add all other links in the input tree using the same criterion. The resulting input tree T_2 is shown in Fig. 5c, together with the input trees of all other nodes in the network in Fig. 5b.

To simplify, we label each node of T_i using the starting point of the corresponding path $\mathcal{P}_{j\to i}$. For example, in T_2 nodes $\mathcal{P}^{(1)}_{3\to 2}$ and $\mathcal{P}^{(1)}_{4\to 2}$ are labeled 3 and 4 respectively, and the length of the path is equal to the depth of the node in the input tree.

Thus, in practice, we arrive at the following way to construct the input tree: we start with the node at the root, lets say node 2. We label every node $\mathcal{P}_{j\to 2}$ in the input tree by

node j where the path starts. The first layer of the input tree consists of all the nodes that are at a distance one from the root. In this case, nodes 3 and 4. Thus we add two links to 2 from 3 and 4 in the input tree.

The second layer of the input tree is obtained applying the same procedure to each node in the first layer, 3 and 4. For instance, node 3 receives a link from 2 and 5. Therefore the second layer of the input tree contains nodes 2 and 5 connected to node 3. We repeat the procedure with the other node in layer 2: node 4. Node 4 receives a link only from node 6, and node 6 from no one. So, we add a link from 6 to 4 and this path does not propagate further. The third layer of the input tree is obtained iteratively applying the same procedure, and so on.

We note that the input trees of nodes 1, 2, 3 and 7 are infinite since the network contains a cycle (or loop) between nodes $2 \rightleftarrows 3$. For instance, T_1 is infinite because there are paths crossing the loop infinite times. On the other hand, the input trees of nodes 4, 5 and 6 are finite since they do not cross the loop.

B. Isomorphic input trees

The input tree T_i at node i can be interpreted as the collection of all possible 'histories' starting at some node and ending in node i. As shown in Section I C, if two input trees T_i and T_j are isomorphic, then the corresponding nodes i and j in network G have the same dynamical state [15, 16]. This equivalence is understood in terms of a local in-isomorphism that maps nodes to nodes and links to links, so it formalizes the fact that the dynamical interactions represented by a directed link from gene to gene could be in principle different across genes, as long as the links are the same (or similar, in case that the produced synchronization is approximate) inside the fiber.

An isomorphism between T_i and T_j is defined as a bijective map $\tau : T_i \to T_j$, which maps one-to-one the nodes and edges of T_i to nodes and edges of T_j.

A minimal condition for the existence of an isomorphism between the input trees is that the two input trees have the same number of nodes (we could also add a condition of the same degree sequence). Thus, it is clear that there could be no isomorphism between the input trees of nodes 2 and 4, since the former contains an infinite number of nodes and the later just two. Thus, a minimal condition for an isomorphism to exist is that it should be a

mapping between two input trees with the same number of nodes, since the mapping needs to be bijective, i.e., with an inverse. By inspection it is then clear that there is an isomorphism between the input trees of nodes 4 and 5. This isomorphism is the map $\tau_{4\to 5} : T_4 \to T_5$, and it is written as a transformation following the notation:

$$\tau_{4\to 5} = \begin{pmatrix} 4: & 6 \\ \downarrow & \downarrow \\ 5: & 6 \end{pmatrix}, \qquad \text{(isomorphism between input trees of nodes 4 and 5).} \tag{7}$$

which maps the root of T_4 to the root of T_5 as $\tau_{4\to 5}(4) = 5$, and node $6 \in T_4$ to node $6 \in T_5$ as $\tau_{4\to 5}(6) = 6$. The notation starts with the root of the tree and then we write nodes in each level from top to bottom starting from left to right in each level. In this particular example the links are of the same type, so there is no need to specify the mapping between links in the isomorphism, but in general the local equivalence require that nodes are map to nodes and also links are mapped to the same type of link by the isomorphism.

The map in Eq. (7) is one of the simplest isomorphism since the input tree contains only one level. In this particular case, to see that nodes T_4 and T_5 are isomorphic, it is thus enough to see that both nodes 4 and 5 connect to one and the same node, which is node 6 in this case. That is, both input trees of nodes 4 and 5 are isomorphic because they are made up of just two nodes and one edge, and this isomorphism implies that 4 and 5 receive the same information. This is the simplest form of an isomorphism between input trees. In this case, we say that node 4 and 5 have the same *input-set*, which is an input tree of only one level, that is the set of incoming links. The input-set is used in the groupoid formalism in Ref. [14].

Next, we consider the input trees of nodes 2 and 3. By visual inspection, both input trees have the same 'shape'. However, these trees are infinite in the number of levels. How do we decide if two input trees are isomorphic when they have an infinite number of levels? Remarkably, to determine if two input trees are isomorphic, it suffices to check that they are isomorphic up to the $N-1$ level, thanks to a theorem by Norris [26], where N is the total number of nodes in the network G. This is an important result that allows us to avoid to check an infinite number of equivalences. Since G has $|N_G| = 7$, we use six levels in the input trees to determine that there is an isomorphism between T_2 and T_3 which corresponds

to the following map:

$$\tau_{2\to 3} = \begin{pmatrix} 2: & 3 & 4 & 2 & 5 & 6 & 3 & 4 & 6 & \dots \\ \downarrow & \downarrow & \downarrow & \downarrow & \downarrow & \downarrow & \downarrow & \downarrow & \downarrow & \downarrow \\ 3: & 2 & 5 & 3 & 4 & 6 & 2 & 5 & 6 & \dots \end{pmatrix}, \quad \text{(isomorphism between input trees of 2 and 3).} \tag{8}$$

There are no other isomorphism between the other input trees. Notice that T_7 is not isomorphic to T_3 and T_2 by just one link to the root.

The existence of an isomorphism τ from the input tree of node i to the input tree of node j implies the synchronization of x_i and x_j [15]. In the groupoid formalism of Golubitsky and Stewart, it is said that two nodes are synchronized if their input-set are synchronized, too [14]. Analogous work in dynamical systems shows that automorphisms in networks lead to synchronized nodes in orbits, see [17–20] and references therein. The orbit of a given node is obtained by applying all automorphisms of a network to the node and the nodes in the orbit are synchronous. The synchronized orbits obtained from automorphisms are analogous to the synchronized fibers obtained from symmetry fibrations. In general, every orbit is also a fiber, but the opposite is not true, since a fiber is not necessarily an orbit.

In our analysis of the *E. coli* network, we find some automorphisms. Some of the star fibers with $n = 0$ are also orbits of the networks since they are invariant under permutation symmetries of the symmetric group of order n, S_n. But this is only when the genes in the star have no out-going links. As shown in the example of Fig. 5, an out-going link in any of the star genes, will destroy the automorphism, but not the fiber. For this reason, automorphisms are somehow more prevalent in undirected networks. For instance, we have found that automorphisms describe the symmetries of the gap junction connectome of *C. elegans*, which is composed all of undirected links [34]. In the case of directed biological networks treated here, while automorphisms could be of use to discover some synchronized nodes, the majority of synchronization is due to symmetry fibrations, which are not described by automorphisms.

C. From fibrations to symmetry fibrations via isomorphic input trees and minimal bases

A fibration is any morphism from a network $G = (N_G, E_G)$ to a base $G = (N_G, E_G)$: $\psi : G \to B$ [12]. If a network $G = (N_G, E_G)$ has at least one pair of isomorphic input trees, then there exists a network $B = (N_B, E_B)$, called the **base** of G, such that G can be 'fibered' over B by the graph fibration. The base B is defined as follows:

- a node $I \in N_B$ is a representative of the set of nodes $\{i \in N_G\}$ whose input trees are isomorphic;
- an edge $e_{I\to J}$ where $I, J \in E_B$ is defined as $e_{I\to J} = \sum_{i\in I} e_{i\to j}$, where $e_{i\to j} \in E_G$.

Having defined the base network B, we say that G is fibered over B if there exists a surjective morphism $\psi : G \to B$, called surjective graph fibration [13], that maps nodes and edges of G to nodes and edges of B as: $\psi(i) = I$ for all $i \in N_G$, and $\psi(e_{i\to j}) = e_{I\to J}$. A surjective morphism is a map between two sets (the domain and codomain) where each element of the codomain (in this case B) is mapped to, at least, by one element of the domain (in this case G). The set of nodes $i \in N_G$ that are mapped to the same node $I \in N_B$, and denoted by $\psi^{-1}(I)$, is called the fiber of G over node I. We notice that all input trees of nodes which belong to the same fiber are pairwise isomorphic.

In general a surjective graph fibration ψ can map nodes with isomorphic input trees to different bases, thus, the number of fibers is not minimal.

A surjective graph fibration that maps all genes with isomorphic input trees to a single common node in B is called a surjective minimal graph fibration in the sense of [13]. Such a minimal fibration will generate then the minimal bases of the network and will produce the largest collapse of nodes in fibers. In this work we only deal with surjective minimal graph fibrations and we call them symmetry fibrations for short.

In practice, a symmetry fibration maps G to the minimal base B (analogous to the quotient), that consists of the following steps: *(i)* consider all the nodes in a fiber (which have isomorphic input trees) and choose one as the representative I, *(ii)* collapse the nodes in the fiber into one single node in B and call it by the name of the representative node I, *(iii)* for every link of a node j in G directed to the node I in G, add a link in B from j to I. If the node j belongs to the fiber, then the corresponding link in B is an autoregulation

loop in B, *(iv)* repeat for every fiber in G. When fibers belong to disjoint components of the network, then they are considered as distinct fibers.

V. ALGORITHM TO FIND FIBERS WITH MINIMAL BALANCE COLORING

The algorithm to partition the network into fibers is based on the 'minimal balanced coloring' algorithm developed by Cardon & Crochemore in Ref. [24]. Here we follow a version developed by Kamei & Cock [25] to construct a *minimal* balanced coloring of a network, namely a coloring that employs the least possible number of colors, which is associated with minimal graph fibrations. The algorithm's runtime scales as $O(|E_G| \log_2 |N_G|)$, which implies that it is essentially linear with the network size, specially for sparse networks, and can be applied to very large networks.

The theory of balance coloring is explained in Ref. [14]. A balance coloring creates a partition of nodes of G into disjoint sets (corresponding to synchronous fibers) such that each node in one set receives the same number of colors from nodes within other sets [14, 20]. A coloring of G with this property is the *balanced coloring* and represents an *equitable partition* of the network, see [14, 20]. The sets identified by a *minimal balanced coloring* partitions the network with minimal colors and corresponds to the fibers of G identified by minimal graph fibrations ψ [13–15].

Thus, we color nodes such that synchronous nodes in a fiber receive the same colors from their synchronous nodes. As example, the genes *baeR* and *spy* (Fig. 1a) have the same color and are in the same fiber since they receive the same colors from their neighbors: both *baeR* and *spy* receive one red color via the activator link from one red node (*baeR* from itself and *spy* from *baeR*) and one green activator link each from the green node *cpxR*.

The algorithm constructs a coloring of the nodes that is balanced. A coloring is balanced if two identically colored nodes are connected to identically colored nodes via their inbound links. Each balanced colored cluster is a fiber in the network. The fibers also corresponds to the orbits in a network when the symmetries are automorphisms rather than isomorphisms in the input trees. The flow of the algorithm is exemplified with the example network of Fig. 6.

- **Step 1** - We start by assigning the same color to all nodes. In Fig. 6a all nodes are initially colored in blue. In addition, we assign to each link the same color of the

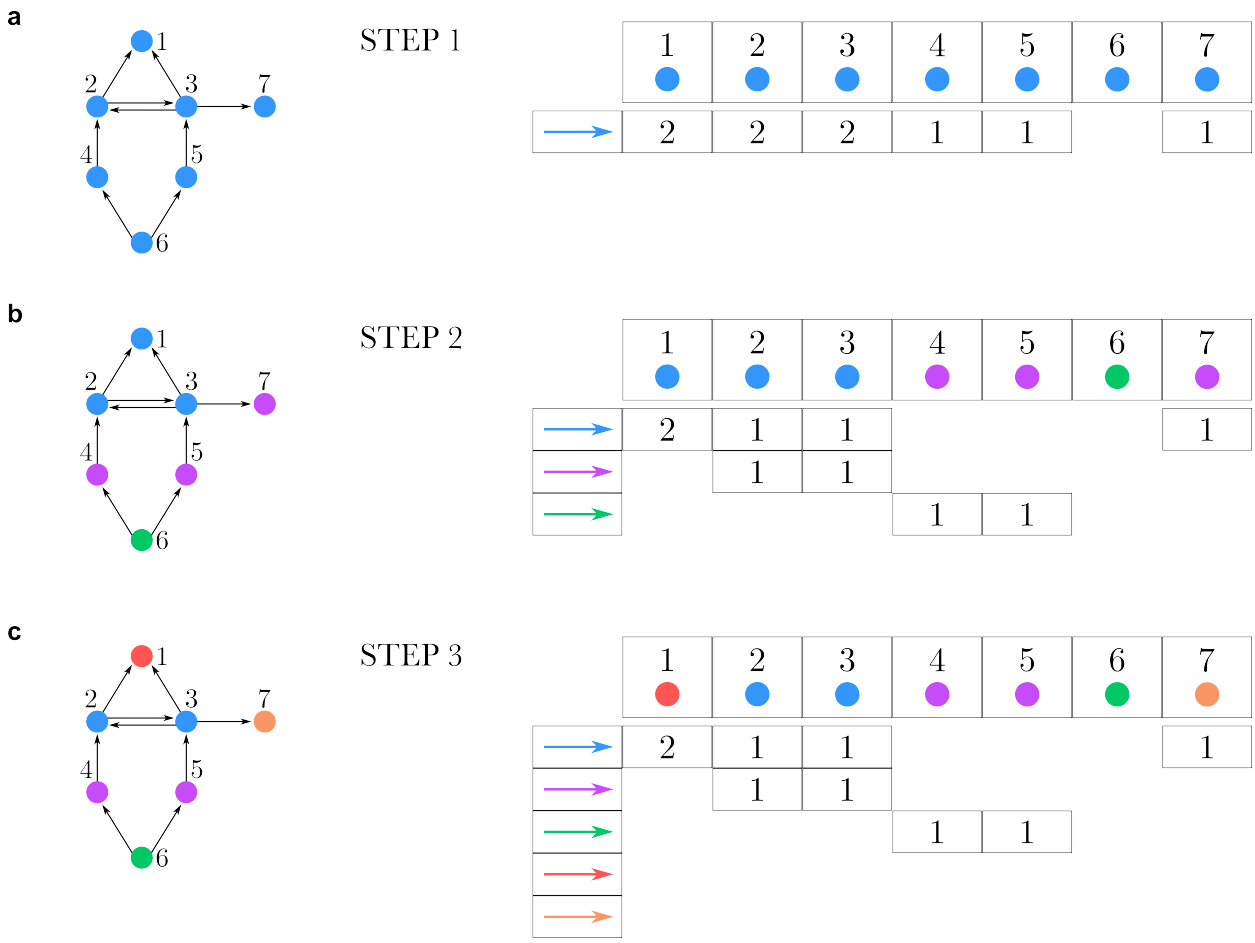

FIG. 6: **Algorithm to find the fibers of a network through a minimal balanced coloring.** The goal of the algorithm is to find a minimal balanced coloring of the network, so that two nodes have the same color only if they are connected to the same number of identically colored nodes via inbound links. The colors represent the fibers in the network.

node from where it emanates. To update the coloring (or, equivalently, to generate a new partition) of nodes, we construct the table shown in the right panel of Fig. 6a, as explained next. In the top row of this table we put the network nodes colored with their current color. In the leftmost column we put each type of colored link. In this initial stage of the algorithm we only have a blue link for all the nodes. Then, we fill the entries of the table with the number of colored links of this blue type that are received by the corresponding node. For example, node 1 receives two 2 blue links as well as nodes 2 and 3. Nodes 4, 5 and 7 receive one blue link each, and node 6 nothing. The structure of this table determines the new coloring as explained in the next step.

- **Step 2** - Using the table in Fig. 6a we update the coloring of nodes as follows. We assign the same color to all nodes that receive the same number of colored links of each type. Specifically, nodes 1, 2 and 3 receive two blue links, so we assign them the same (blue) color. Analogously, nodes 4, 5 and 7 receive one blue link, so we assign them the same color, but different from blue. We assign them a purple color. Similarly, we assign another color to node 6 (green). We then obtain the colored network in the left of Fig. 6b. Applying the counting of receiving coloring links to this network, we obtain the new coloring table shown in Fig. 6b, where each link has the color of the node from where it emanates. Thus, we update the table to generate the new coloring, as shown in the right panel of Fig. 6b.

- **Step 3** - Using the same criterion as in Step 2, we update the coloring of nodes, comprising now five different colors, and then we generate the new table, as shown in Fig. 6c. At this point the algorithm stops, because we do not need to introduce more colors, since each color is balanced. Each color corresponds to a fiber, and each node in each colored fiber receives the same colors from other fibers or from nodes in the same fiber. Therefore, the coloring shown in the network of Fig. 6c is the minimal balanced coloring of the network, and the colors indicate the fibers in the network.

As far as only minimal fibrations are considered, the algorithm will return always the same fibers containing the same nodes, for any initial condition and realization. Below we provide the pseudo-code to clarify the algorithm. More detailed instructions and methodology for obtaining fiber building blocks will be given in a follow-up paper. We start by assigning all nodes to the same fiber and then continue to refine the partition basing on the input set of the node until no further refinement can be obtained.

Algorithm 1 Finding fibers following Kamei & Cock Ref. [25]

Input: Graph $G = \{N_G, E_G\}$, where N_G are vertices and E_G are edges of the analyzed network

$\mid N_G \mid$ - number of vertices, $N_G = \{v_1 \dots v_{|N_G|}\}$

Output: $C = \{c_i\}$, where c_i - color of node i and $i = 1 \cdots \mid V \mid$

Notation: $I_i = \{I_i^1 \dots I_i^N\}$, where N = current number of colors

$N_0 = 1$
for $i = 1 \cdots \mid N_G \mid$ **do**
    $c_i = 1$
end for
$j = 0$
repeat
    for $i = 1 \cdots \mid N_G \mid$, $k = 1 ... N_j$ **do**
        I_i^k = number of nodes of color k in the input set of v_i
    end for
    H = set of all unique $\{I_i\}$
    // assign each unique vector a color and color the graph accordingly
    for $i = 1 \cdots \mid N_G \mid$ **do**
        c_i = index of I_i in H, e.g. if two nodes have the same I_i and $I_j \rightarrow c_i = c_j$
    end for
    $j = j + 1$
    $N_j = \mid H \mid$
until $N_j \neq N_{j-1}$
return $\{c_i\}$

VI. STRONGLY CONNECTED COMPONENT

In a directed network, the strongly connected component is composed of nodes that are reachable from every other node in the component. That is, there is a directed path from every node to any other node in the strongly connected component. A weakly connected component is obtained when we ignore the directionality of the links. Strongly connected components are relevant to genetic fibers since they contain loops that control the state of the genes. We find four types of strongly connected components. Single-gene components composed of autoregulator loops like *cpxR* and *fadR* in Figs. 1a and 1e. The other type of components are those in Fig. 2a and Fig. 2b and also a five-gene connected component shown in SI Fig. 7. We note that most of the fibers regulated by these components do not belong to the connected component. This is because they receive information but do not send information back to the connected component. These fibers are characterized by integer fiber numbers. When the fiber receives and sends back information, that is, when the fiber belongs to the strongly connected component, then it becomes a Fibonacci fiber. The largest strongly connected component in the *E. coli* network controls the pH system shown in Fig. 2b.

VII. STATISTICS OF FIBERS IN THE TRN OF *E. COLI*

A. Fibers statistics in *E. coli*

SI Table I shows the counts in the *E. coli* network of each building block. For instance the most abundant building blocks are the following:

$|n = 0, \ell = 1\rangle$: 45
$|n = 1, \ell = 0\rangle$: 13
$|n = 0, \ell = 2\rangle$: 13
$|n = 1, \ell = 1\rangle$: 8

The list is completed with the fractal building blocks of Fibonacci sequences which are less numerous but more complex in their structure:
$|\varphi_2 = 1.6180.., \ell = 2\rangle$: 1

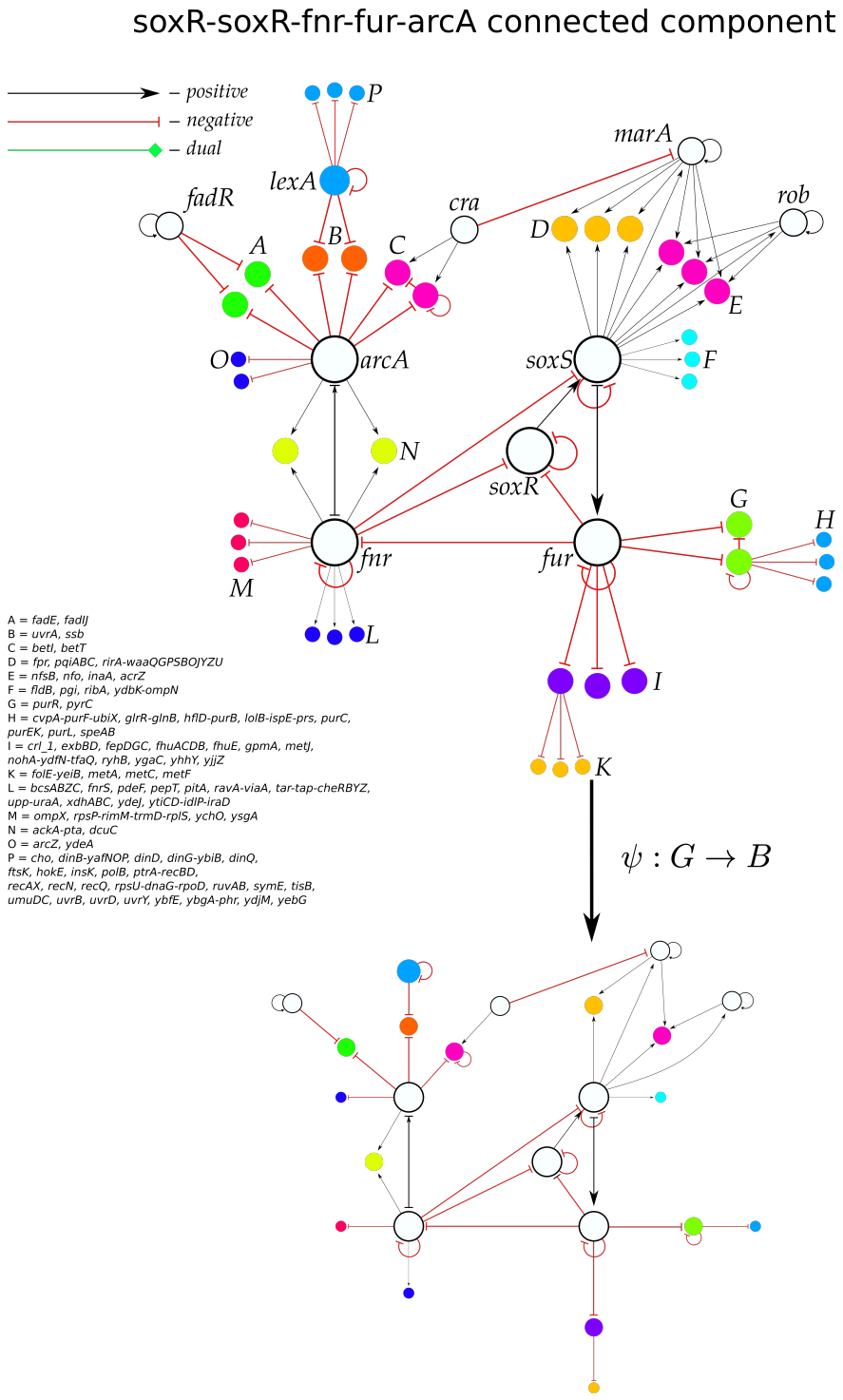

FIG. 7: A five-gene connected component of *soxR, soxS, fnr, fur,* and *arcA* with its regulated fibers.

$|\varphi_3 = 1.4655.., \ell = 1\rangle$: 1

$|\varphi_4 = 1.3802..., \ell = 1\rangle$: 1

Structure type	Amount in E-coli
$\|n = 0, l = 1\rangle$	45
$\|n = 0, l = 2\rangle$	13
$\|n = 0, l = 3\rangle$	3
$\|n = 1, l = 0\rangle$	13
$\|n = 1, l = 1\rangle$	8
$\|n = 1, l = 2\rangle$	3
$\|n = 2, l = 0\rangle$	1
$\|n = 2, l = 1\rangle$	1
$\|\varphi_d = 1.3802.., l = 1\rangle$	1
$\|\varphi_d = 1.4655.., l = 1\rangle$	1
$\|\varphi_d = 1.6180.., l = 2\rangle$	1
Composite Fiber	1
Total number of building blocks	91

TABLE I: Building block statistics. We show the count of every building block defined by the fiber numbers.

B. Full list of fibers in *E. coli*

SI Table VI shows the complete list of the 91 fibers building blocks found in the genetic network of *E. coli*. We list the genes in the fiber plus their external regulators. If a gene or operon is not in this list, for instance *lacZYA*, it means that the gene or operon is not in a fiber. Supplementary File 1 shows the plot of the circuit of every fiber and the fiber building block.

The first column in SI Table VI is the ID of the fiber. This ID refers to the plot of the fiber building block in Supplementary File 1. The second column lists the genes in the fiber, the third column lists the external regulators. The last column specifies the fiber number

associated with each fiber as $|n, \ell\rangle$ or $|\varphi_d, \ell\rangle$.

VIII. DATASETS OF BIOLOGICAL AND NON-BIOLOGICAL NETWORKS

To investigate the applicability of fibrations in a broader context, we performed an extensive analysis of different complex networks from diverse domains in systems science.

Full details of each network analyzed can be accessed at `https://docs.google.com/spreadsheets/d/1-RG5vR_EGNPqQcnJU8q3ky1OpWi3OjTh5Uo-XaOPjOc`. The codes to reproduce this analysis are at `github.com/makselab` and the full datasets appear at `kcorelab.org`. See also tables below with information about the networks.

We first show the symmetry fibrations in biological networks and species. See Section I H. We characterize biological networks spanning from:

- **Biological networks: transcriptional regulatory networks, metabolic networks, cellular processes networks and pathways, disease networks, neural networks.**

We study the following species:

- **Species: A. thaliana, E. coli, B. subtilis, S. enterica (salmonella), M. tuberculosis, D. melanogaster, S. cerevisiae (yeast), M. musculus (mouse), and H. sapiens (human).**

We then study non-biological networks in Section I H:

- **Social Networks: online social networks, Facebook, Twitter, Wikipedia, Youtube, email networks, communication networks, citation networks, collaboration networks, bloggers**
- **Internet: routers, autonomous systems, web graphs, hyperlinks, peer-to-peer**
- **Infrastructure Networks: power grid, airport, roads, flights**
- **Economic Networks**
- **Software Networks: Linux, jdk**
- **Ecosystems**

Network Domain	Total No. of nodes	Total No. of edges	No. of networks
Biological	287390	4211856	289
Economic	1752	108639	5
Ecosystems	1879	5378	14
Infrastructure	24511	82534	16
Internet	244634	835565	27
Social	104909	1261009	15
Software	43391	503645	3

TABLE II: Features of the networks across domains. We report the total numbers for each domain summed over all the networks in the domain.

Species	Total No. of nodes	Total No. of edges	No. networks
Yeast	55932	1392926	11
Arabidopsis Thaliana	790	1431	1
Bacillus subtilis	5602	11417	3
Drosophila	39549	321734	5
Escherichia coli	879	1835	1
Human	72587	1198712	248
Micobacterium Tuberculosis	1624	3212	1
Mouse	64709	987424	7
Salmonella	8293	15589	6

TABLE III: Number of networks per species.

	Arabidopsis Thaliana	Bacillus subtilis	Caenorhabditis elegans	Cat	Drosophila	Escherichia coli	Human	Micobacterium Tuberculosis	Mouse	Rat	Salmonella	Yeast
TF	1	2	2	0	4	1	4	1	4	0	2	11
Neuron	0	0	0	1	1	0	0	0	3	3	0	0
Metabolic	0	0	0	0	0	0	48	0	0	0	2	0
Disease	0	0	0	0	0	0	66	0	0	0	0	0
Kinase	0	0	0	0	0	0	2	0	0	0	0	0
Pathway	0	0	0	0	0	0	127	0	0	0	0	0
Protein	0	1	0	0	0	0	1	0	0	0	2	0

TABLE IV: Table with the count of networks per type of biological network and species. These networks are used to calculate the distributions of fiber across species and biological types in Figs. 4a, b, and c. For each type of biological network in Fig. 4a, b, we calculate the count over the total number of networks as indicates at the end of each row for each biological type. The same occurs with the number of networks at the end of each column for each species. Figure 4c shows the counts over all the network shown in the last row/column.

Network Subdomain	Total No. of nodes	Total No. of edges	No. of networks
Autonomous systems graphs	141842	481415	14
Bitcoin	9664	59777	2
Collaboration networks	50260	504897	4
Disease	4309	15254	66
Facebook	4039	88234	1
Youtube subscriptions	13723	76765	1
Internet peer-to-peer networks	31978	110154	4
Jazz	198	5484	1
Linux	30837	213954	1
Metabolic	4273	33829	50
Networks with ground-truth communities	1005	25571	1
Neural networks	3694	129812	8
Cellular processes and Pathways	9825	54712	127
Plant-Pollinator	1631	2719	11
Plant-Seed-Disperser	65	165	2
Power grid	4941	6594	1
Sentiment	99	278	2
Transcriptional regulatory	260258	3908769	32

TABLE V: Subtypes of networks belonging to the different domains.

Id	Fiber	Regulators	Fiber Number
1	aaeR, ampDE, azuC, comR, cyaA, narQ, sohB, speC, spf, trxA, yaeP-rof, yaeQ-arfB-nlpE, yjeF-tsaE-amiB-mutL-miaA-hfq-hflXKC	crp	$\|n = 0, l = 1\rangle$
2	aaeXAB, agp, cpdB, cstA, glgS, glpR, grpE, hofMNOP, ivbL-ilvBN-uhpABC, lacI, mcaS, mhpR, nadC, ompA, ppdD-hofBC, preTA, raiA, rmf, rpsF-priB-rpsR-rplI, sfsA-dksA-gluQ, sxy, ubiG, ychH, yeiP, yeiW, yfiP-patZ, yibN-grxC-secB-gpsA, ykgR	crp	$\|n = 0, l = 1\rangle$
3	accA, accD, fabI, fadR, yceD-rpmF-plsX-fabHDG-acpP-fabF		$\|n = 1, l = 0\rangle$
4	accB, iclR	fadR	$\|n = 1, l = 1\rangle$
5	ackA-pta, dcuC	arcA, fnr	$\|n = 0, l = 2\rangle$
6	acrZ, inaA, nfo, nfsB	marA, rob, soxS	$\|n = 0, l = 3\rangle$
7	add, dsbG, gor, grxA, hemH, oxyS, trxC	crp, oxyR, rbsR	$\|n = 0, l = 1\rangle \oplus \|n = 1, l = 1\rangle$
8	adeD, adiY, chiA, gspAB, hchA, hdfR, mdtJI, rcsB, yjjP	hns	$\|\varphi_d = 1.4655.., l = 1\rangle$
9	agaR, agaS-kbaY-agaBCDI		$\|n = 1, l = 0\rangle$
10	alaA-yfbR, avtA, leuE, livJ, livKHMGF, lysU, sdaA	lrp	$\|n = 0, l = 1\rangle$
11	alaE, kbl-tdh, yojI	lrp	$\|n = 0, l = 1\rangle$
12	alaWX, argU, argW, argX-hisR-leuT-proM, aspV, flxA, glyU, leuQPV, leuX, lptD-surA-pdxA-rsmA-apaGH, lysT-valT-lysW, metT-leuW-glnUW-metU-glnVX, pheU, pheV, proK, proL, queA, serT, serX, thrU-tyrU-glyT-thrT-tufB, thrW, trmA, tyrTV-tpr, valUXY-lysV	fis	$\|n = 0, l = 1\rangle$
13	aldB, hupB	crp, fis	$\|n = 0, l = 2\rangle$
14	allA, allS, gcl-hyi-glxR-ybbW-allB-ybbY-glxK	allR	$\|n = 0, l = 1\rangle$
15	alsR, rpiB		$\|n = 1, l = 0\rangle$
16	amiA-hemF, cmk-rpsA-ihfB, uspB	IHF	$\|n = 0, l = 1\rangle$

17	amn, mipA, phnCDE_1E_2FGHIJKLMNOP, phoA-psiF, phoB, phoE, phoH, ydfH, yegH, yhjC, ytfK		$\|n = 1, l = 0\rangle$
18	ampC, dacC	bolA	$\|n = 0, l = 1\rangle$
19	araE-ygeA, araFGH	araC, crp	$\|n = 0, l = 2\rangle$
20	arcZ, ydeA	arcA	$\|n = 0, l = 1\rangle$
21	argA, argCBH, argE, argF, argI, argR, artJ, artPIQM, lysO		$\|n = 1, l = 0\rangle$
22	argO, lysP	argP, lrp	$\|n = 0, l = 2\rangle$
23	aroF-tyrA, tyrB	tyrR	$\|n = 0, l = 1\rangle$
24	aroH, trpLEDCBA, trpR		$\|n = 1, l = 0\rangle$
25	asnB, clpPX-lon, glsA-ybaT, uspE	gadX	$\|n = 0, l = 1\rangle$
26	aspA-dcuA, dcuR	crp, fnr, narL	$\|n = 0, l = 3\rangle$
27	bacA, cpxPQ, cpxR, ftnB, ldtC, ldtD, ppiD, sbmA-yaiW, slt, srkA-dsbA, xerD-dsbC-recJ-prfB-lysS, yccA, yebE, yidQ, yqaE-kbp, yqjA-mzrA		$\|n = 1, l = 0\rangle$
28	baeR, spy	cpxR	$\|n = 1, l = 1\rangle$
29	bcsABZC, fnrS, pdeF, pepT, pitA, ravA-viaA, tar-tap-cheRBYZ, upp-uraA, xdhABC, ydeJ, ytiCD-idlP-iraD	fnr	$\|n = 0, l = 1\rangle$
30	bdcA, dkgB, grxD, mepH, mhpT, pgpC-tadA, rfe-wzzE-wecBC-rffGHC-wecE-wzxE-rffT-wzyE-rffM, rybB, tehAB, tsgA, ydbD, yeaE	nsrR	$\|n = 0, l = 1\rangle$
31	betI, betT	arcA, cra	$\|n = 1, l = 2\rangle$
32	bioA, bioBFCD	birA	$\|n = 0, l = 1\rangle$
33	bluF, ydeI	rcdA	$\|n = 0, l = 1\rangle$
34	borD, envY-ompT, mgrB, mgrR, mgtLA, mgtS, pagP, rstA, ybjG	phoP	$\|n = 0, l = 1\rangle$
35	cbpAM, gltX, gyrB, msrA	fis	$\|n = 0, l = 1\rangle$
36	cdaR, garD, gudPXD		$\|n = 1, l = 0\rangle$

37	cho, dinB-yafNOP, dinD, ding-ybib, dinQ, ftsK, hokE, insK, lexA, polB, ptrA-recBD, recAX, recN, recQ, rpsU-dnaG-rpoD, ruvAB, symE, tisB, umuDC, uvrB, uvrD, uvrY, ybfE, ybgA-phr, ydjM, yebG		$\|n = 1, l = 0\rangle$
38	cirA, entCEBAH, fepA-entD, fiu	crp, fur	$\|n = 0, l = 2\rangle$
39	copA, cueO	cueR	$\|n = 0, l = 1\rangle$
40	cra, pitB, sbcDC	phoB	$\|n = 0, l = 1\rangle$
41	crl_1, exbBD, fepDGC, fhuACDB, fhuE, gpmA, metJ, nohA-ydfN-tfaQ, ryhB, ygaC, yhhY, yjjZ	fur	$\|n = 0, l = 1\rangle$
42	cusCFBA, cusR, yedX	hprR, phoB	$\|n = 1, l = 2\rangle$
43	cvpA-purF-ubiX, glrR-glnB, hflD-purB, lolB-ispE-prs, purC, purEK, purL, speAB	purR	$\|n = 0, l = 1\rangle$
44	cysDNC, cysK, tcyP, yciW, ygeH, yoaC	cysB	$\|n = 0, l = 1\rangle$
45	cytR, nagC, nagE, ycdZ	crp	$\|n = 1, l = 1\rangle$
46	dapB, lysC	argP	$\|n = 0, l = 1\rangle$
47	ddpXABCDF, patA, potFGHI, yeaGH, yhdWXYZ	ntrC	$\|n = 0, l = 1\rangle$
48	decR, mlaFEDCB, yncE	marA	$\|n = 0, l = 1\rangle$
49	dgcC, iraP, nlpA, wrbA-yccJ, yccT	csgD	$\|n = 0, l = 1\rangle$
50	dicB-ydfDE-insD-7-intQ, dicC-ydfXW	dicA	$\|n = 0, l = 1\rangle$
51	dsdC, norR	nsrR	$\|n = 1, l = 1\rangle$
52	dtpA, omrA, omrB	ompR	$\|n = 0, l = 1\rangle$
53	ecpA, ecpR	matA	$\|n = 0, l = 1\rangle$
54	efeU_1U_2, motAB-cheAW, psd-mscM, tsr, ung	cpxR	$\|n = 0, l = 1\rangle$
55	epd-pgk-fbaA, gapA-yeaD, mpl	cra, crp	$\|n = 0, l = 2\rangle$
56	erpA, iscR, rnlAB		$\|n = 1, l = 0\rangle$
57	evgA, nhaR	hns	$\|\varphi_d = 1.3802.., l = 1\rangle$
58	fabA, fabB	fabR, fadR	$\|n = 0, l = 2\rangle$
59	fadE, fadIJ	arcA, fadR	$\|n = 0, l = 2\rangle$
60	fbaB, fruBKA, glk, gpmM-envC-yibQ, pfkA, ppc, pykF, pyrG-eno, tpiA	cra	$\|n = 0, l = 1\rangle$

61	fldB, pgi, ribA, ydbK-ompN	soxS	$\|n = 0, l = 1\rangle$
62	folE-yeiB, metA, metC, metF	metJ	$\|n = 0, l = 1\rangle$
63	fpr, pqiABC, rirA-waaQGPSBOJYZU	marA, soxS	$\|n = 0, l = 2\rangle$
64	fucAO, fucR, zraR	crp	$\|n = 1, l = 1\rangle$
65	gfcA, ybhL, yfiR-dgcN-yfiB, ymiA-yciX	yjjQ	$\|n = 0, l = 1\rangle$
66	hupA, trg	crp, fis	$\|n = 0, l = 2\rangle$
67	ibaG-murA, rplU-rpmA-yhbE-obgE	mlrA	$\|n = 0, l = 1\rangle$
68	ibpAB, yadV-htrE	IHF	$\|n = 0, l = 1\rangle$
69	idnK, idnR	crp, gntR	$\|n = 1, l = 2\rangle$
70	isrC-flu, pth-ychF	oxyR	$\|n = 0, l = 1\rangle$
71	lgoR, uxuR	crp, exuR	$\|\varphi_d = 1.6180.., l = 2\rangle$
72	lolA-rarA, osmB	rcsB	$\|n = 0, l = 1\rangle$
73	lsrACDBFG-tam, lsrR, oxyR, rbsR	crp	$\|n = 1, l = 1\rangle$
74	malI, mlc	crp	$\|n = 1, l = 1\rangle$
75	manA, yhfA	crp	$\|n = 0, l = 1\rangle$
76	mngAB, mngR		$\|n = 1, l = 0\rangle$
77	nadA-pnuC, nadB	nadR	$\|n = 0, l = 1\rangle$
78	nimR, nimT		$\|n = 1, l = 0\rangle$
79	ompX, rpsP-rimM-trmD-rplS, ychO, ysgA	fnr	$\|n = 0, l = 1\rangle$
80	pepD, yhbTS	csgD	$\|n = 0, l = 1\rangle$
81	phoP, slyB		$\|n = 2, l = 0\rangle$
82	pspABCDE, pspG	IHF, pspF	$\|n = 0, l = 2\rangle$
83	purR, pyrC	fur	$\|n = 1, l = 1\rangle$
84	rhaR, rhaS	crp	$\|n = 2, l = 1\rangle$
85	rrsA-ileT-alaT-rrlA-rrfA, rrsE-gltV-rrlE-rrfE	fis, lrp	$\|n = 0, l = 2\rangle$
86	rrsB-gltT-rrlB-rrfB, rrsC-gltU-rrlC-rrfC, rrsD-ileU-alaU-rrlD-rrfD-thrV-rrfF, rrsG-gltW-rrlG-rrfG, rrsH-ileV-alaV-rrlH-rrfH	fis, hns, lrp	$\|n = 0, l = 3\rangle$
87	ssb, uvrA	arcA, lexA	$\|n = 0, l = 2\rangle$
88	ttdABT, ttdR		$\|n = 1, l = 0\rangle$

89	ycjG, ycjY-ymjDC-mpaA	pgrR	$\|n = 0, l = 1\rangle$
90	yegRZ, yfdX-frc-oxc-yfdVE	evgA	$\|n = 0, l = 1\rangle$
91	ykgMO, znuA, znuCB	zur	$\|n = 0, l = 1\rangle$

TABLE VI: List of fiber building blocks with ID, genes in the fiber, external regulators of the fiber and fiber numbers. We provide Supplementary File 1 which plots every building block using the same IDs.

$\mathrm{Id} = 1$

$|n = 0, \ell = 1\rangle$

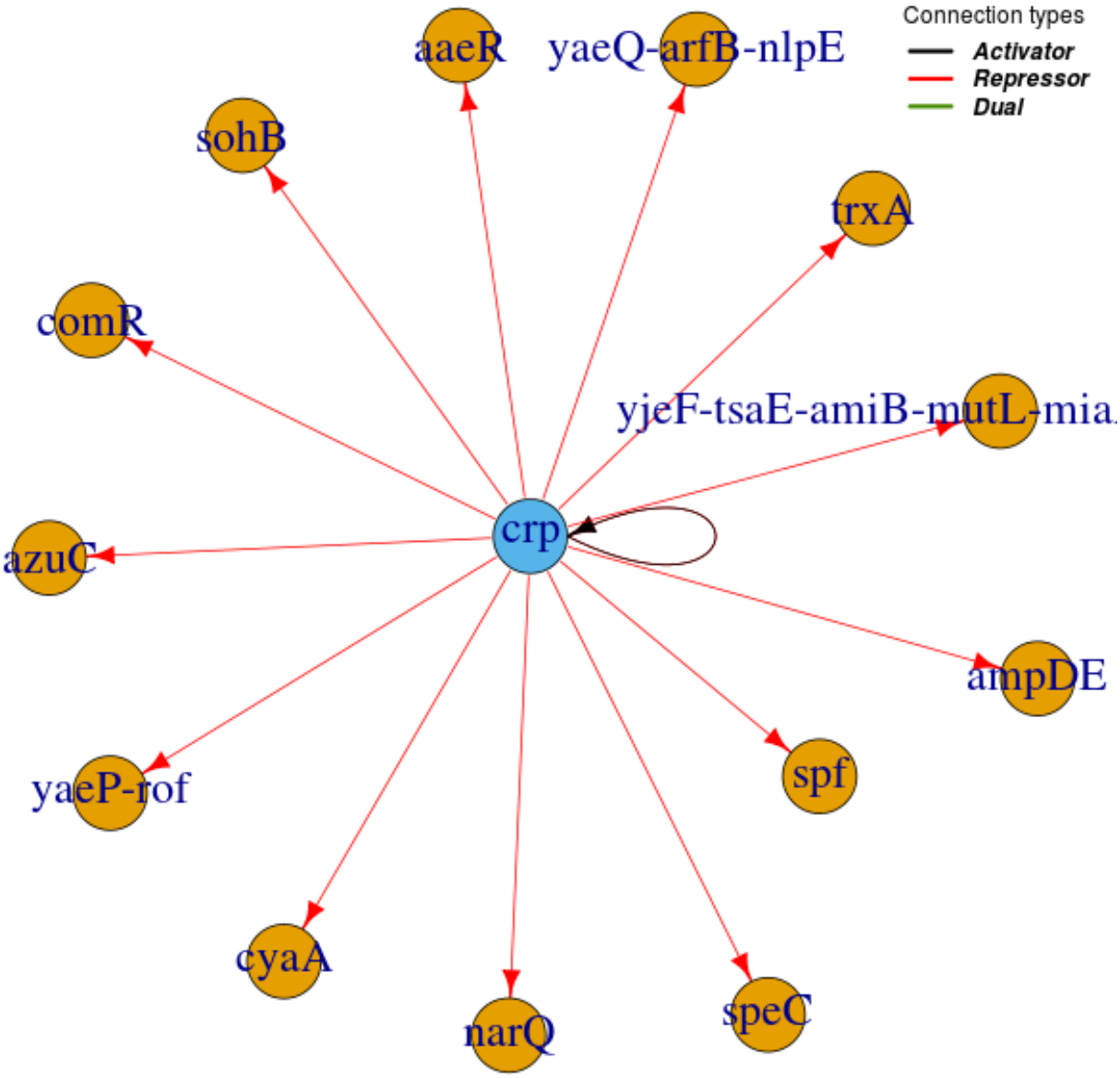

$\mathrm{Id} = 2$

$|n = 0, \ell = 1\rangle$

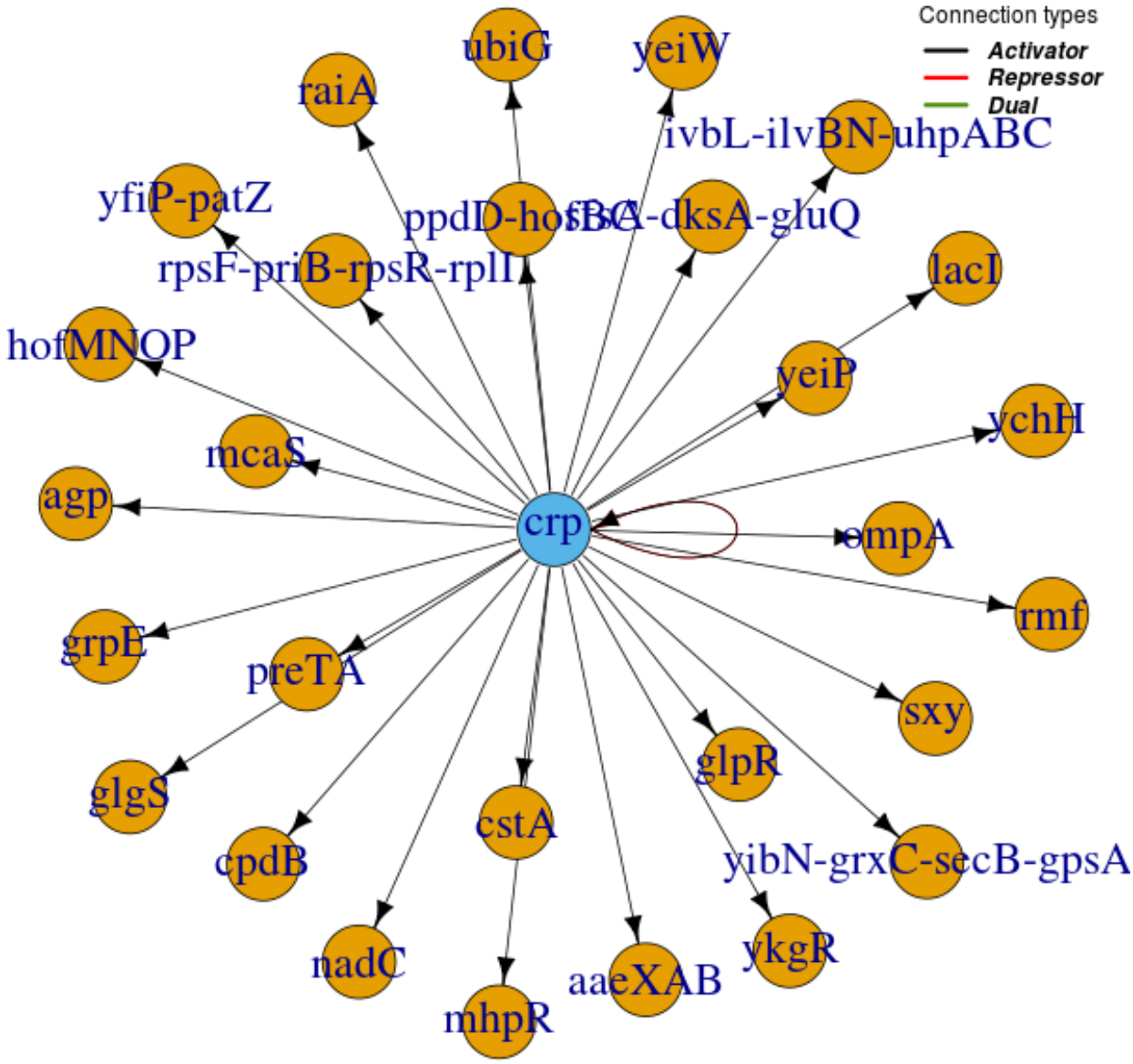

Id = 3

$|n = 1, \ell = 0\rangle$

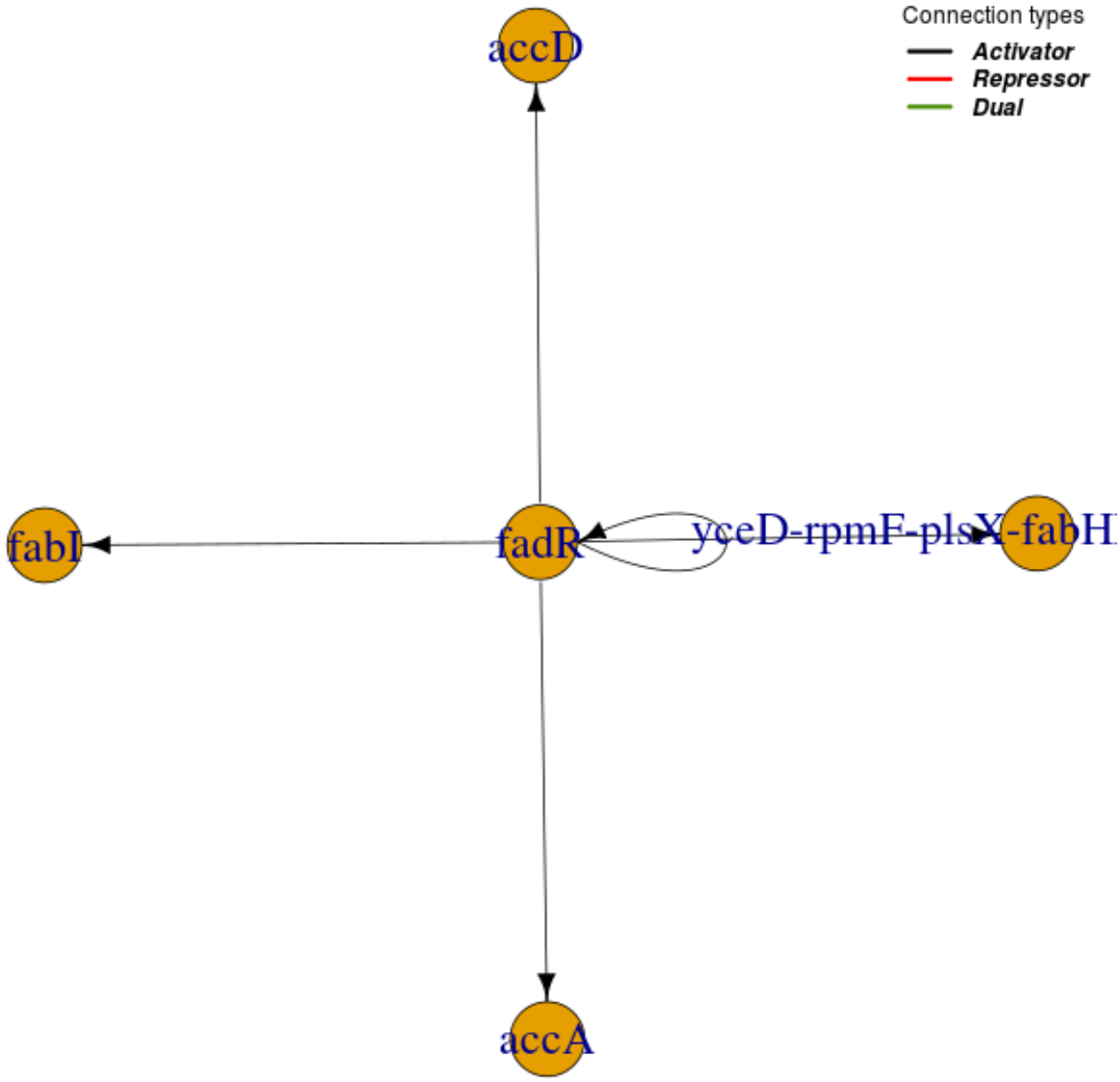

$\mathrm{Id} = 4$

$|n = 1, \ell = 1\rangle$

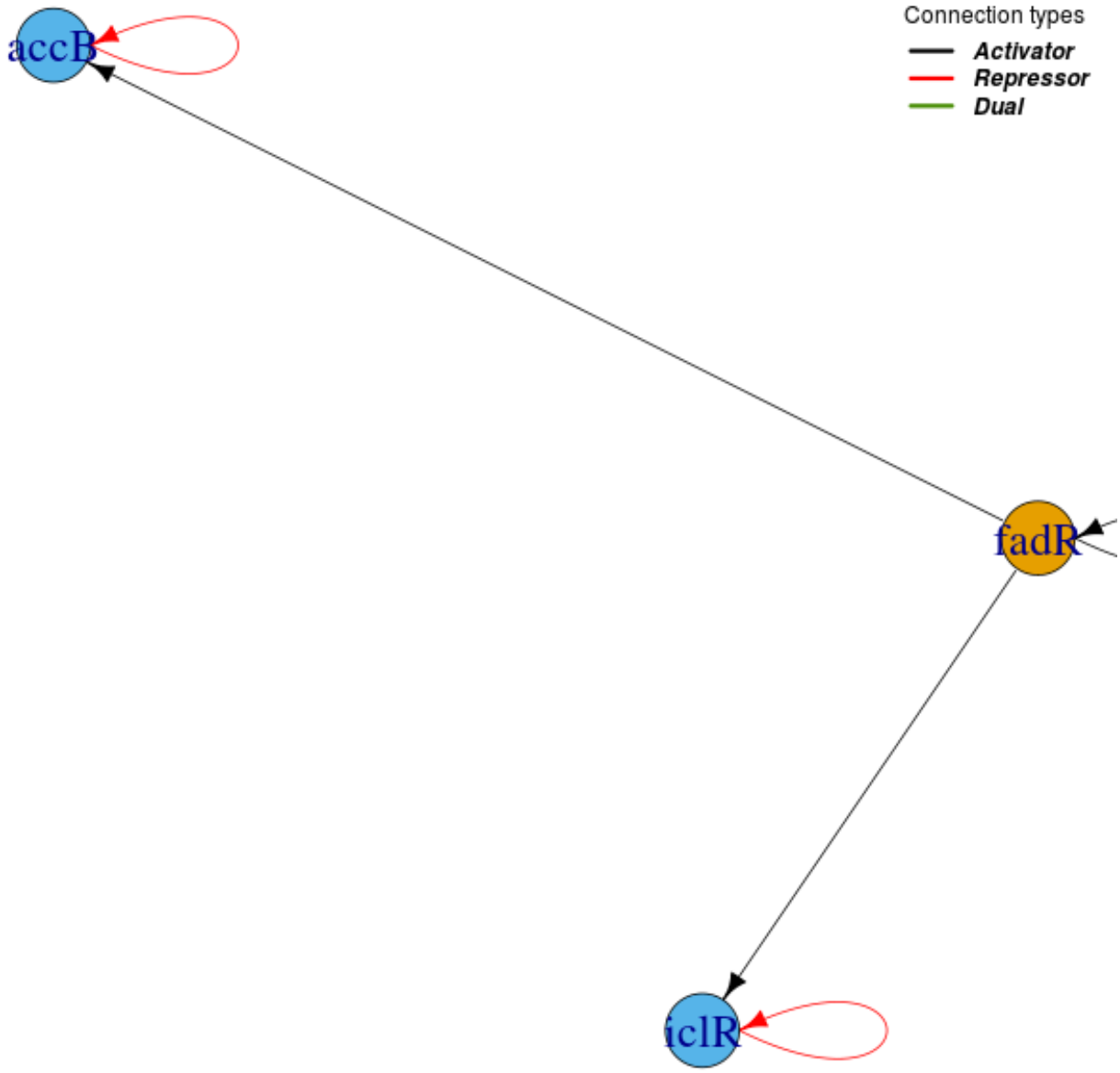

$\mathrm{Id} = 5$

$|n = 0, \ell = 2\rangle$

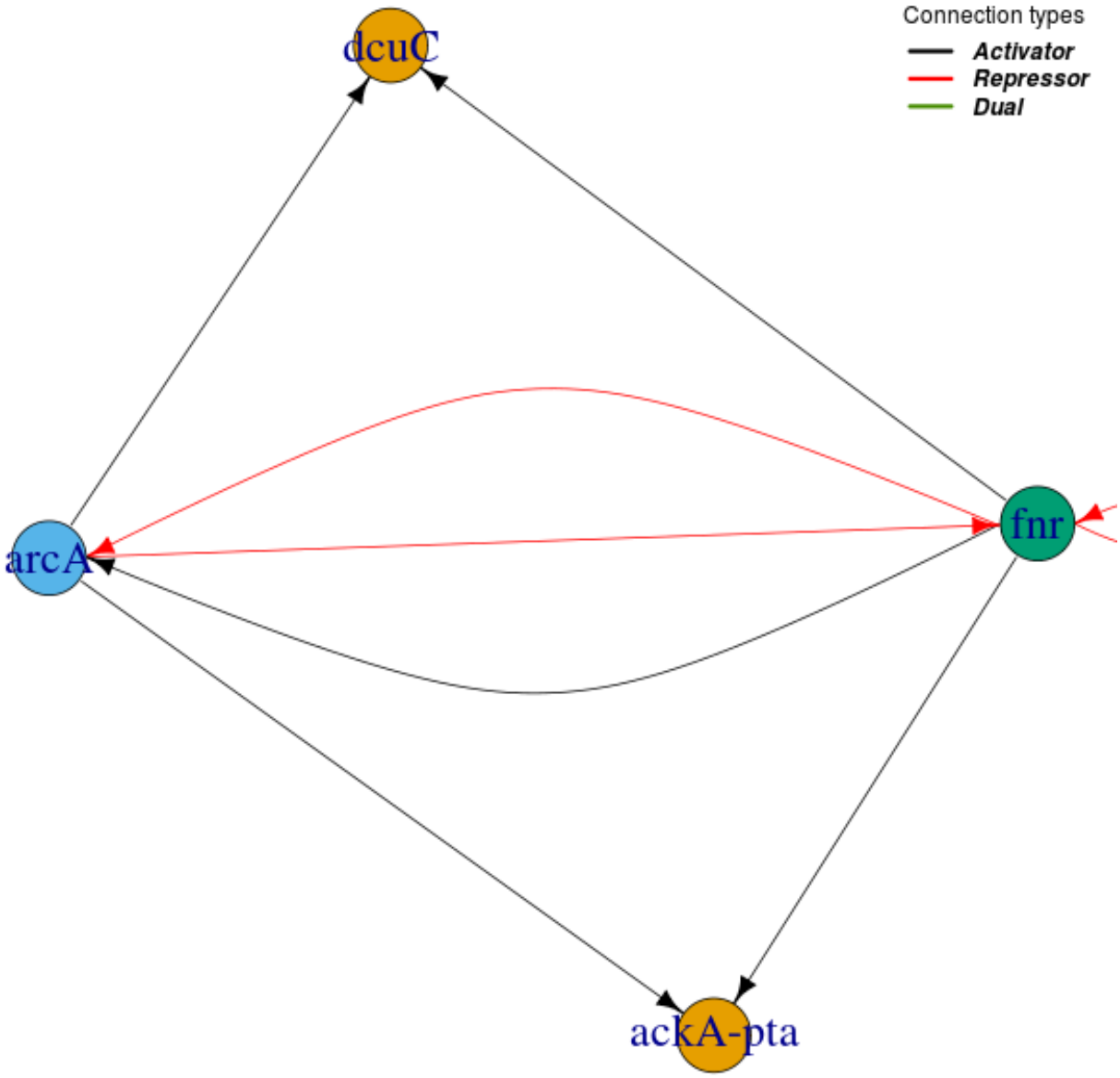

Id = 6

$|n = 0, \ell = 3\rangle$

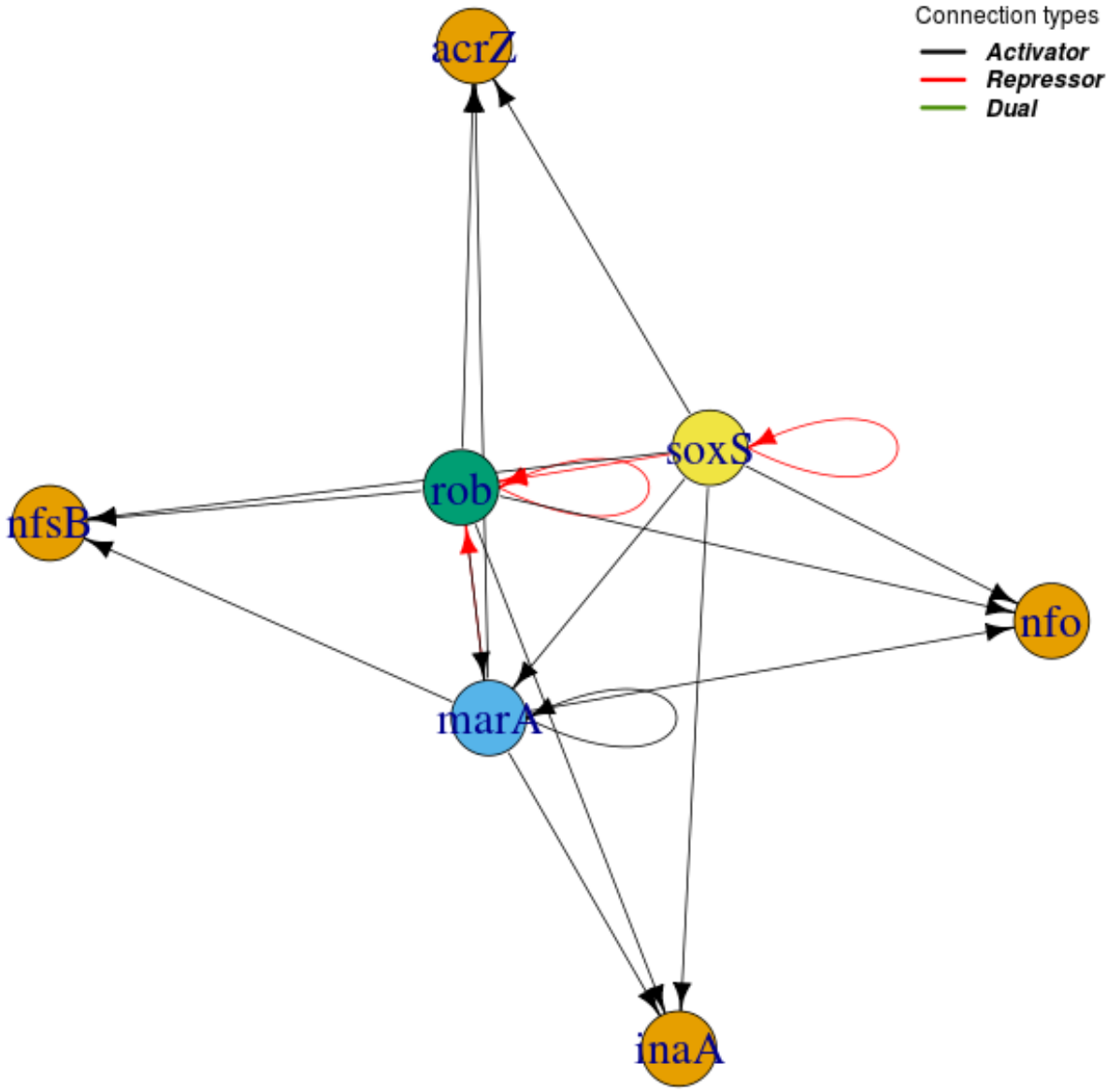

Id = 7

$|n = 0, l = 1\rangle \oplus |n = 1, l = 1\rangle$

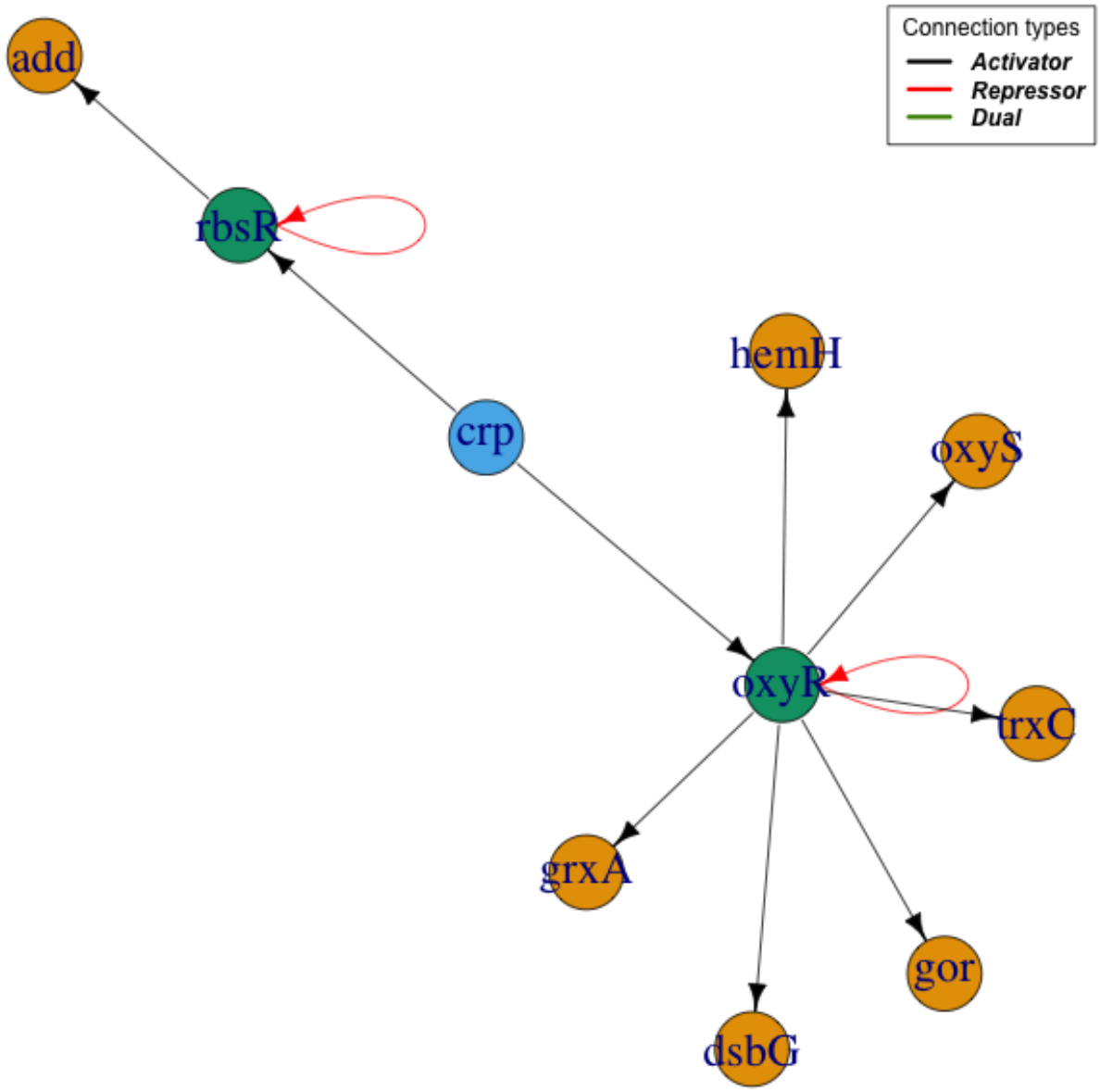

Id = 8

$|\varphi_d = 1.4655..., \ell = 1\rangle$

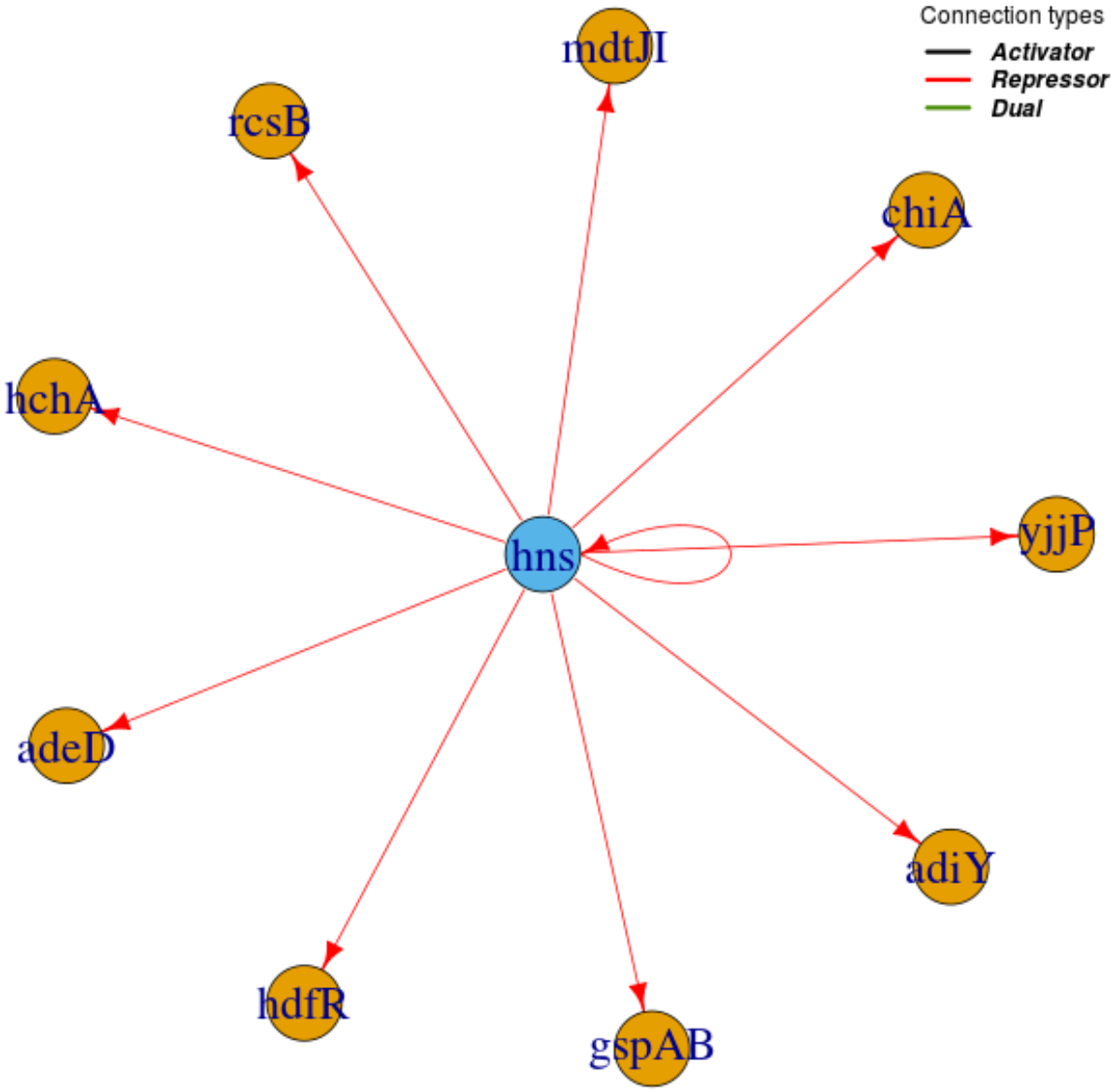

$\mathrm{Id} = 9$

$|n = 1, \ell = 0\rangle$

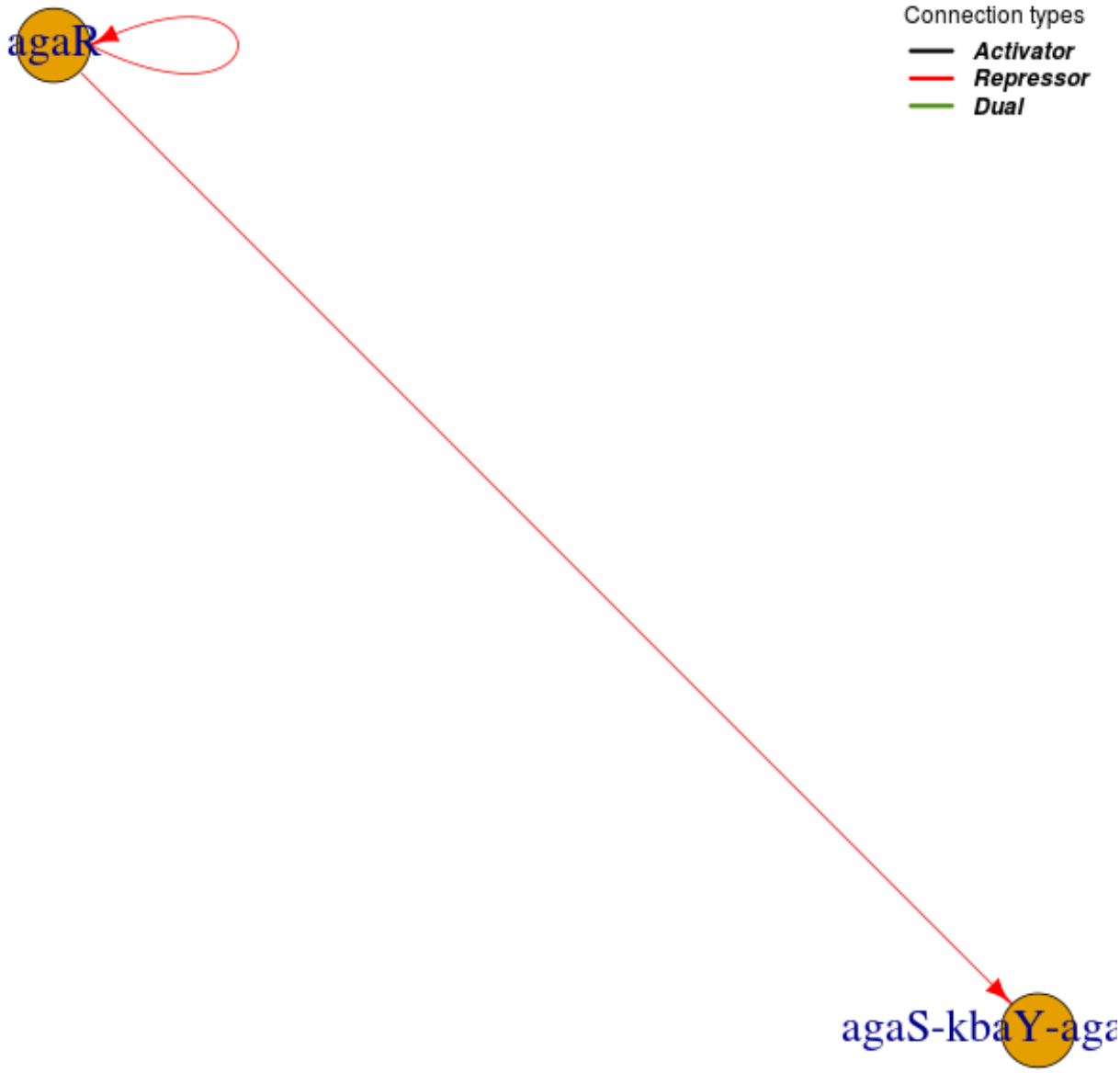

Id = 10

$|n = 0, \ell = 1\rangle$

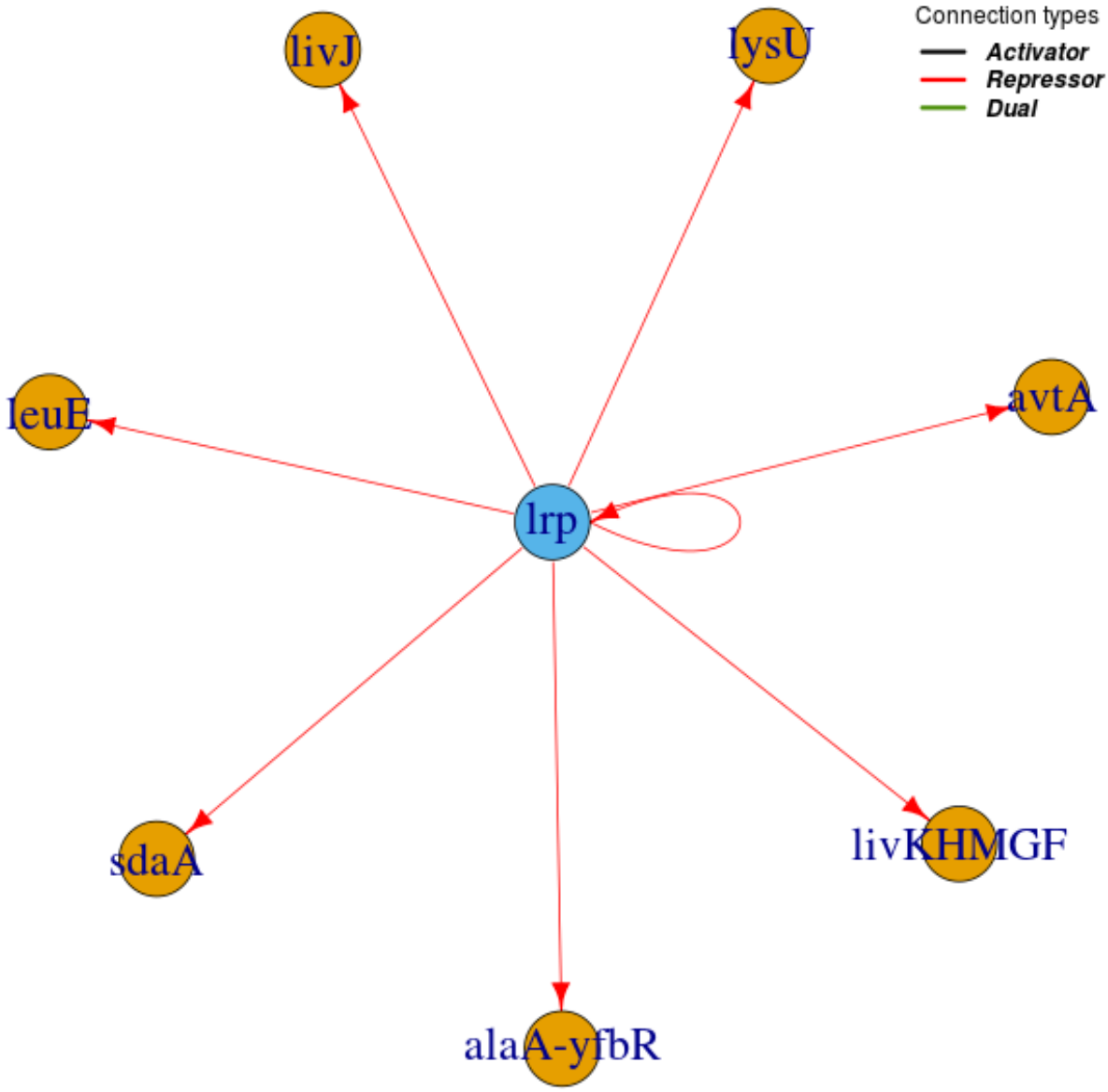

Id = 11

$|n = 0, \ell = 1\rangle$

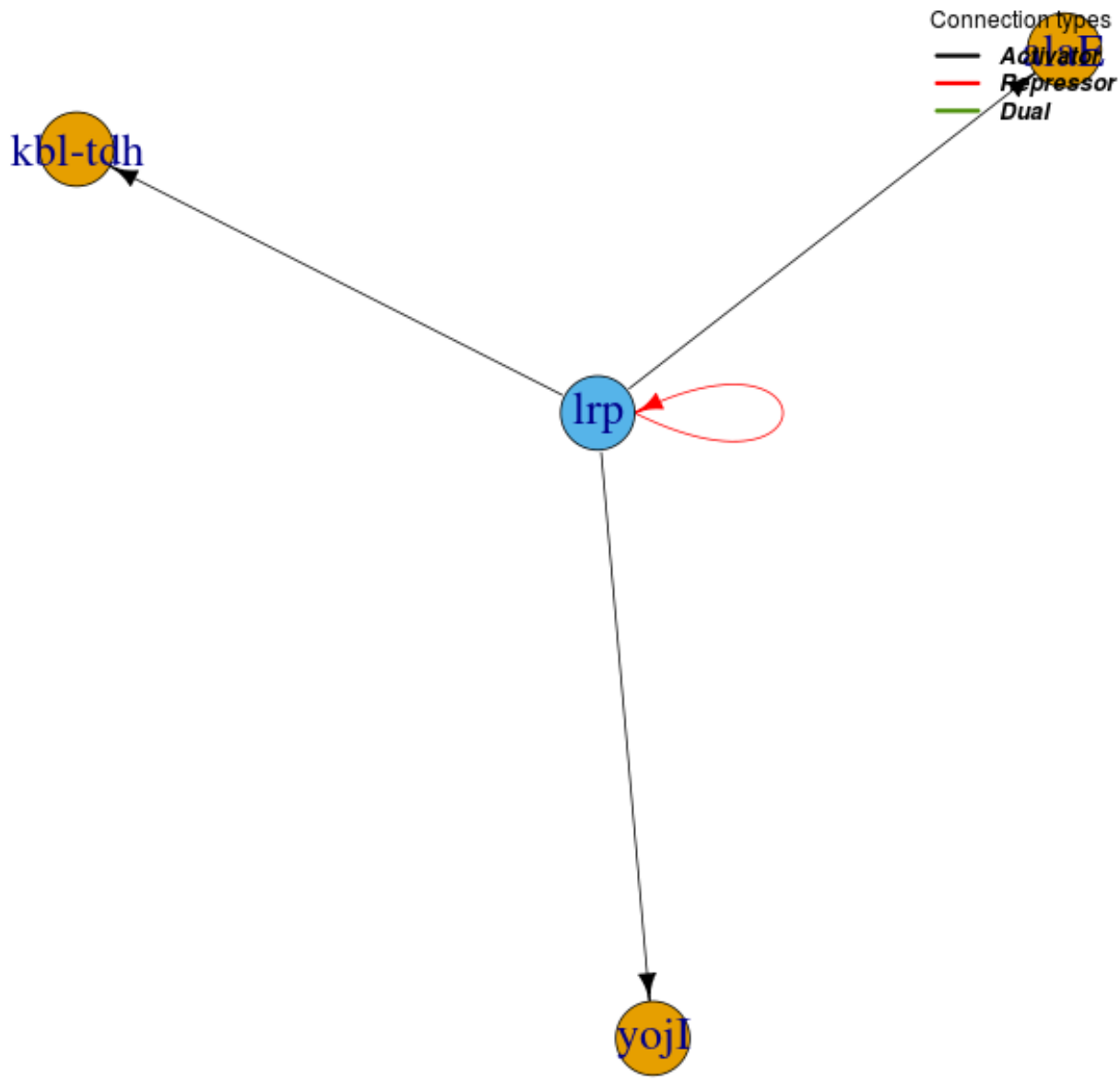

Id = 12

$|n = 0, \ell = 1\rangle$

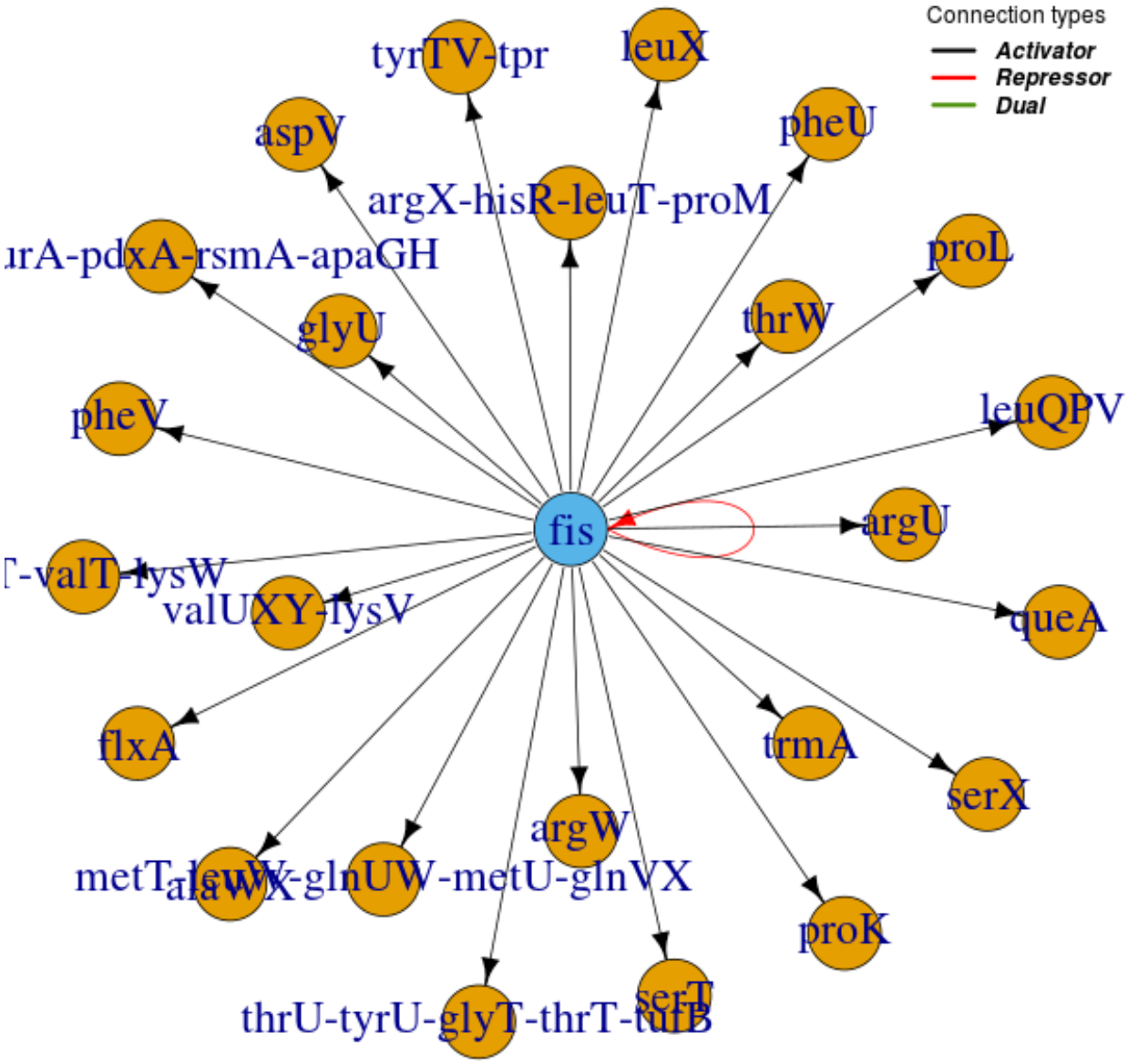

Id = 13

$|n = 0, \ell = 2\rangle$

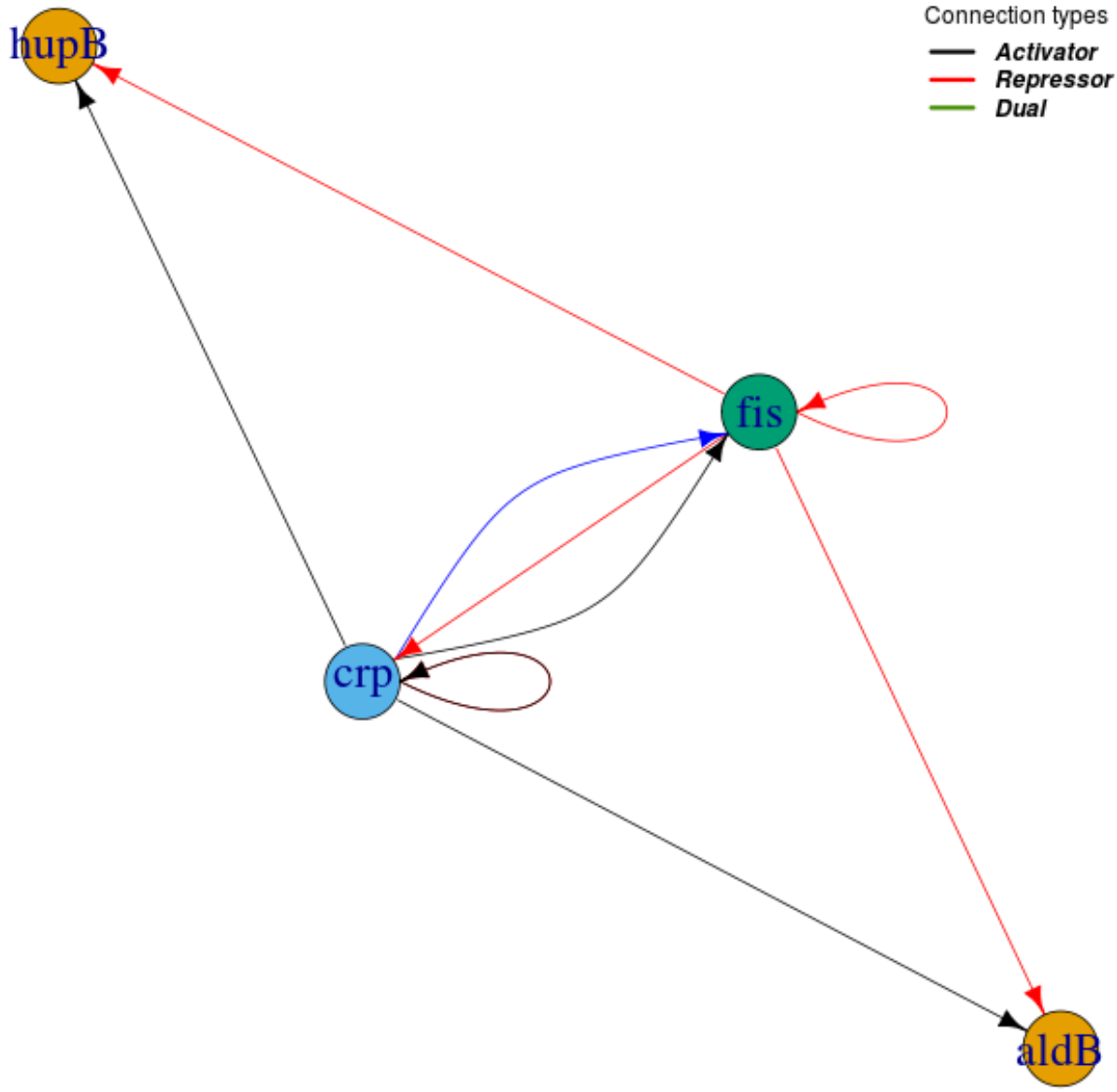

Id = 14

$|n = 0, \ell = 1\rangle$

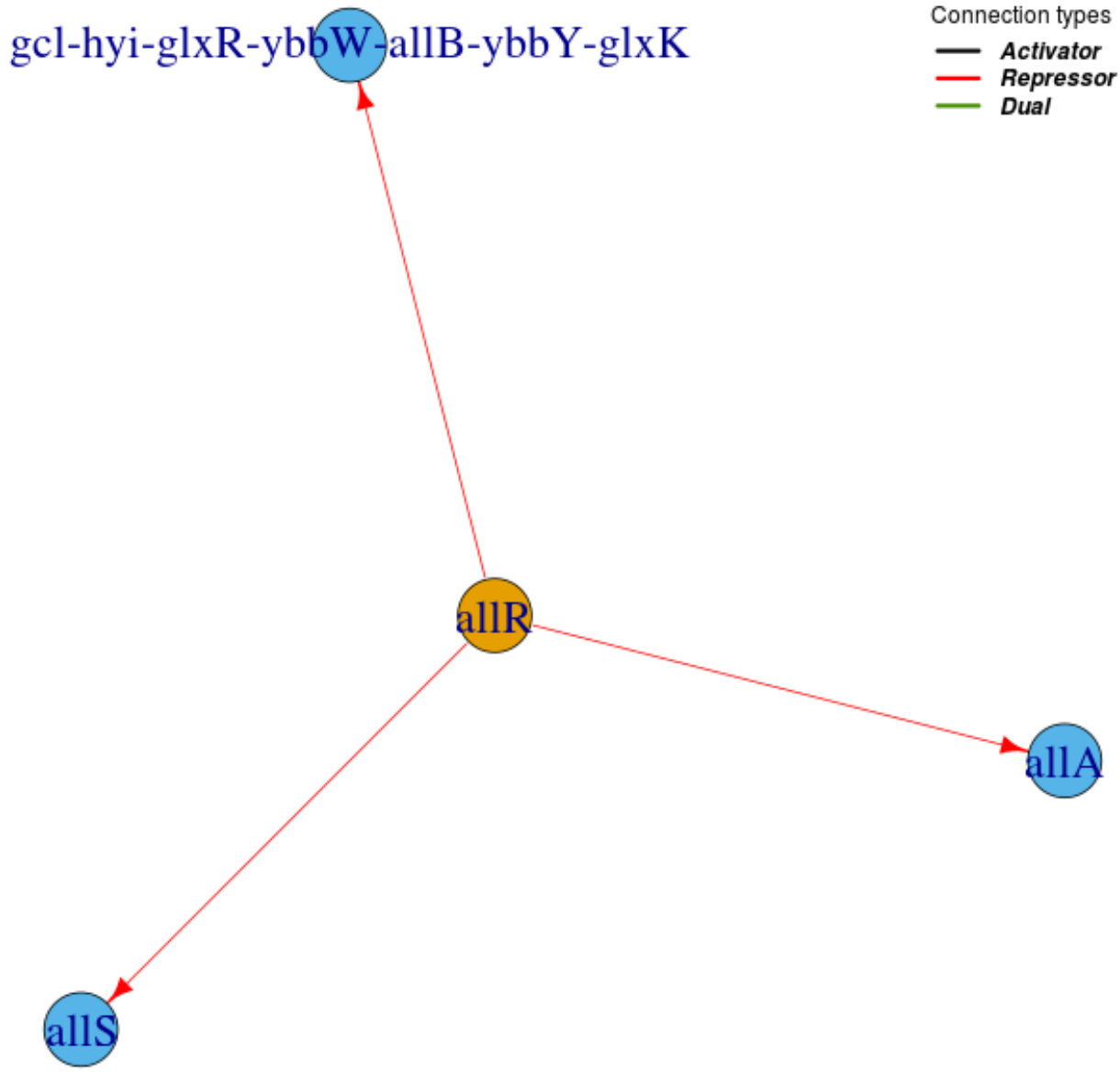

Id = 15

$|n = 1, \ell = 0\rangle$

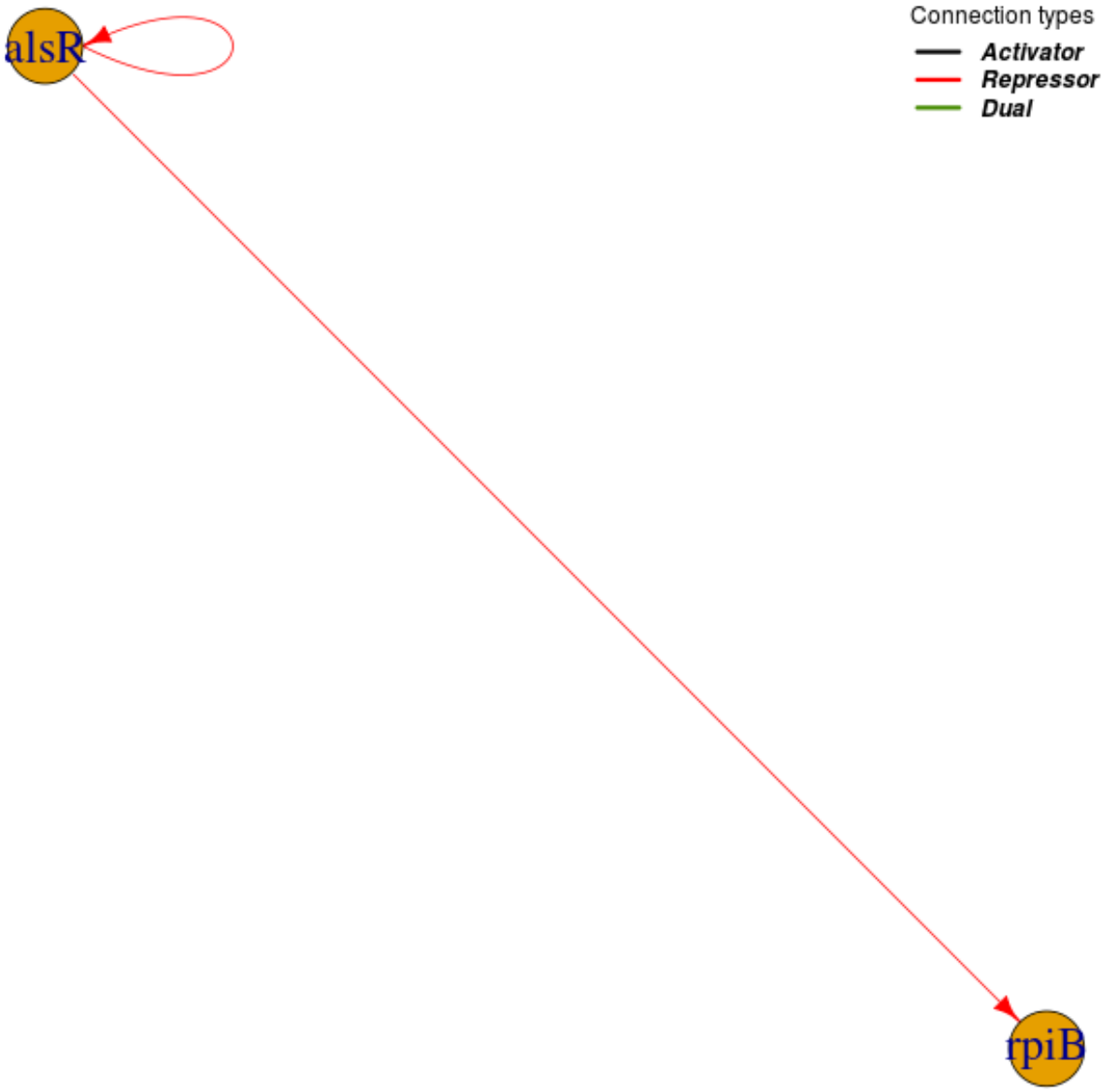

Id = 16

$|n = 0, \ell = 1\rangle$

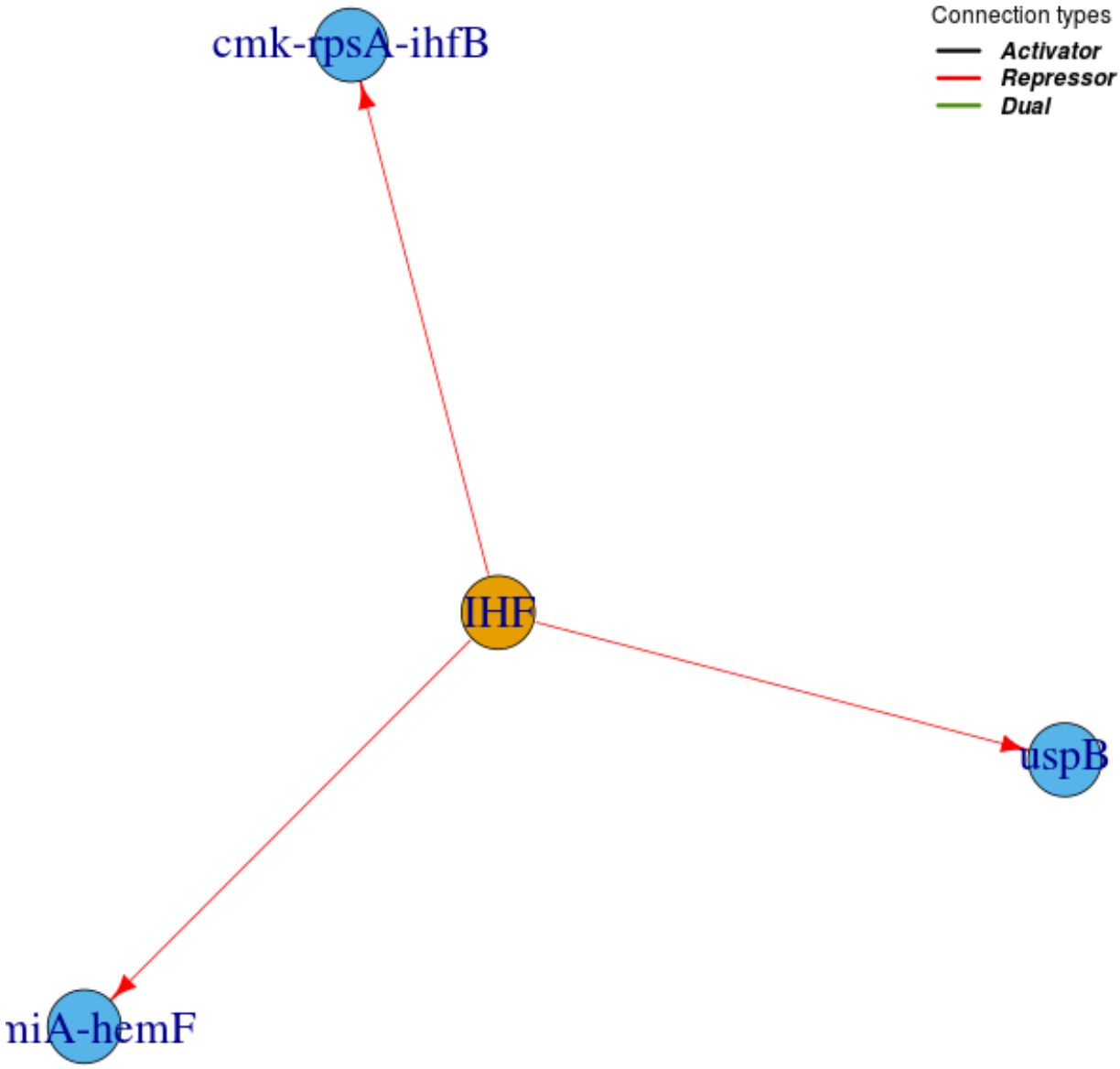

Id = 17

$|n = 1, \ell = 0\rangle$

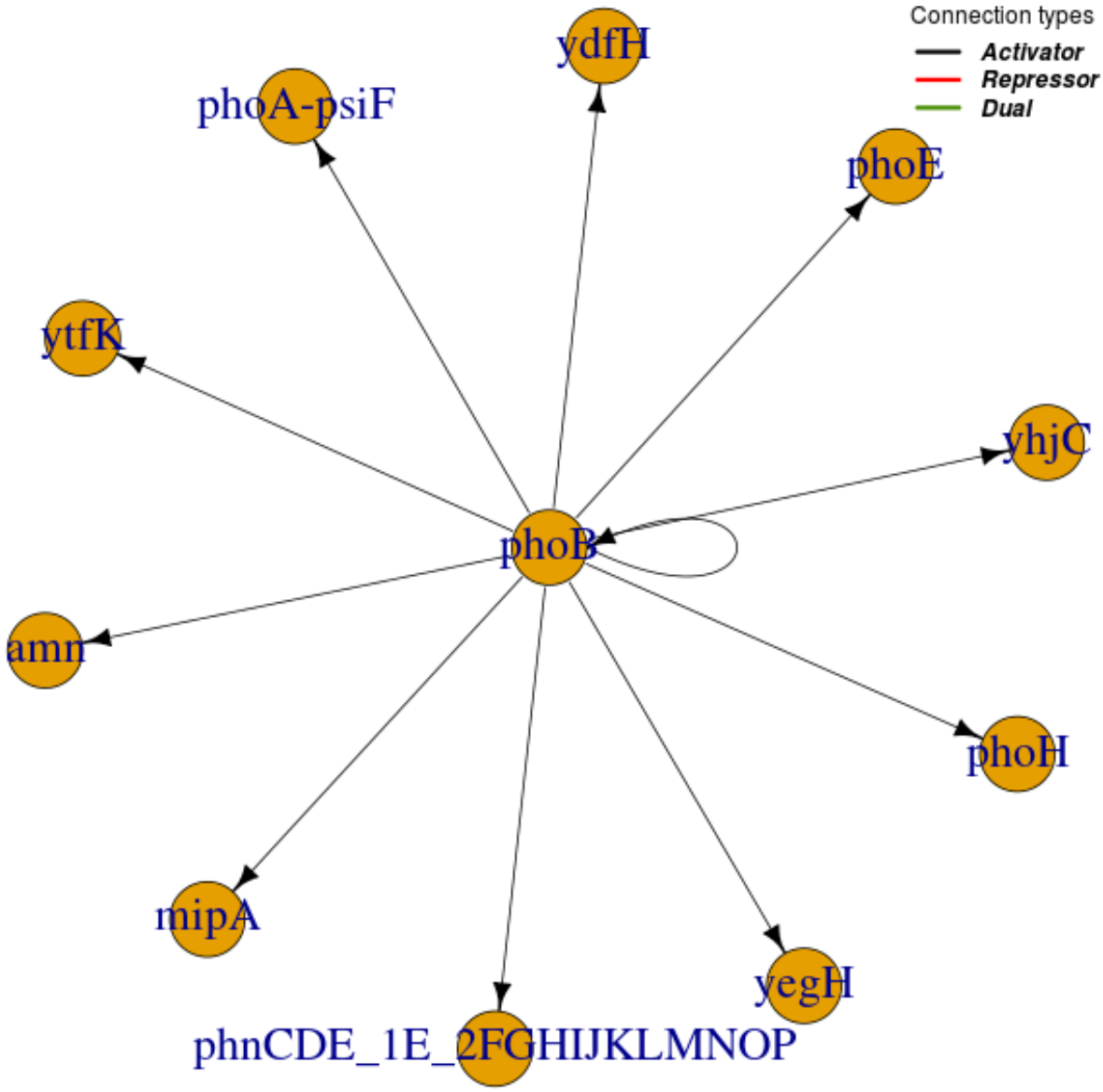

$\mathrm{Id} = 18$

$|n = 0, \ell = 1\rangle$

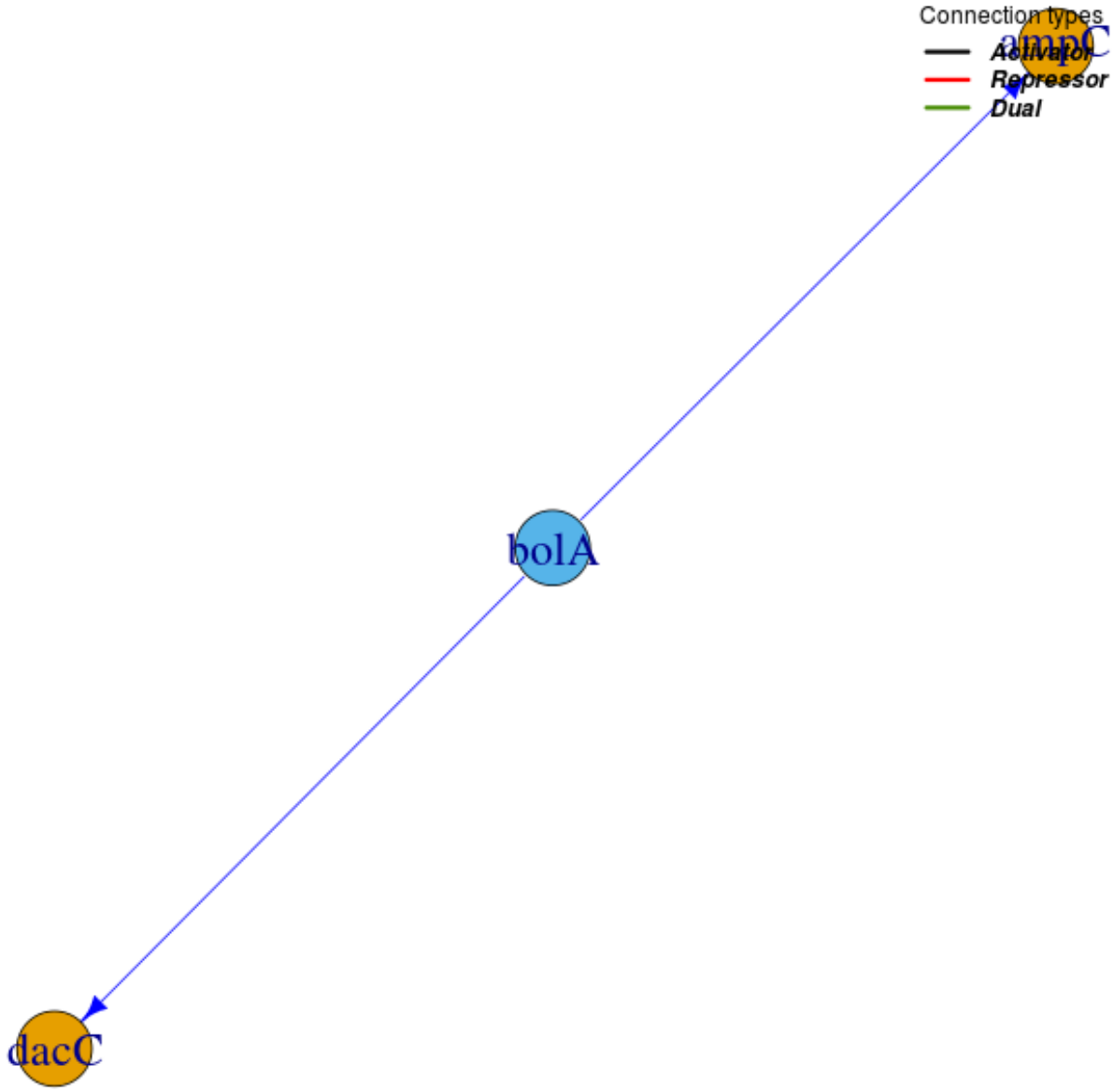

Id = 19

$|n = 0, \ell = 2\rangle$

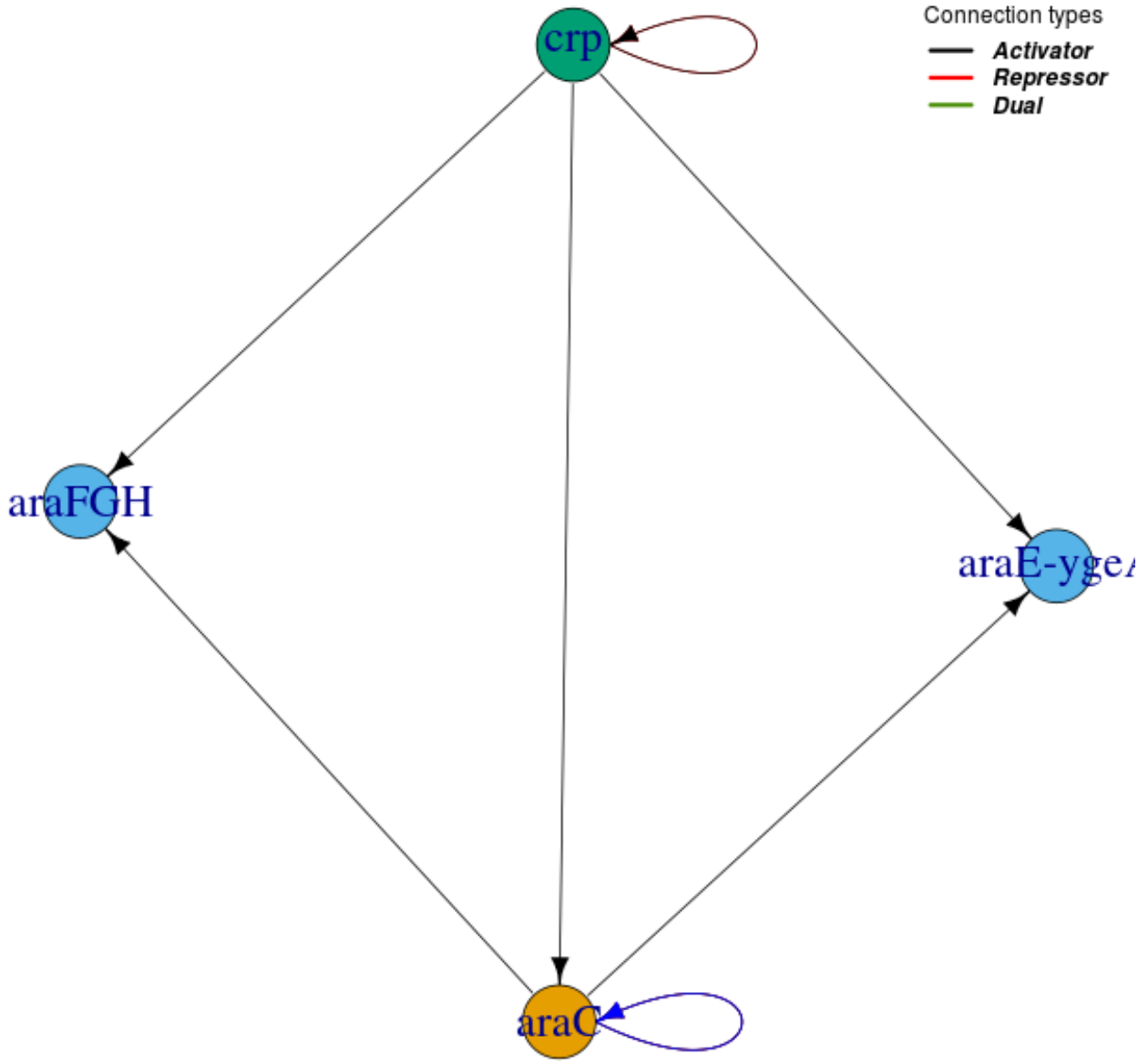

$\mathrm{Id} = 20$

$|n = 0, \ell = 1\rangle$

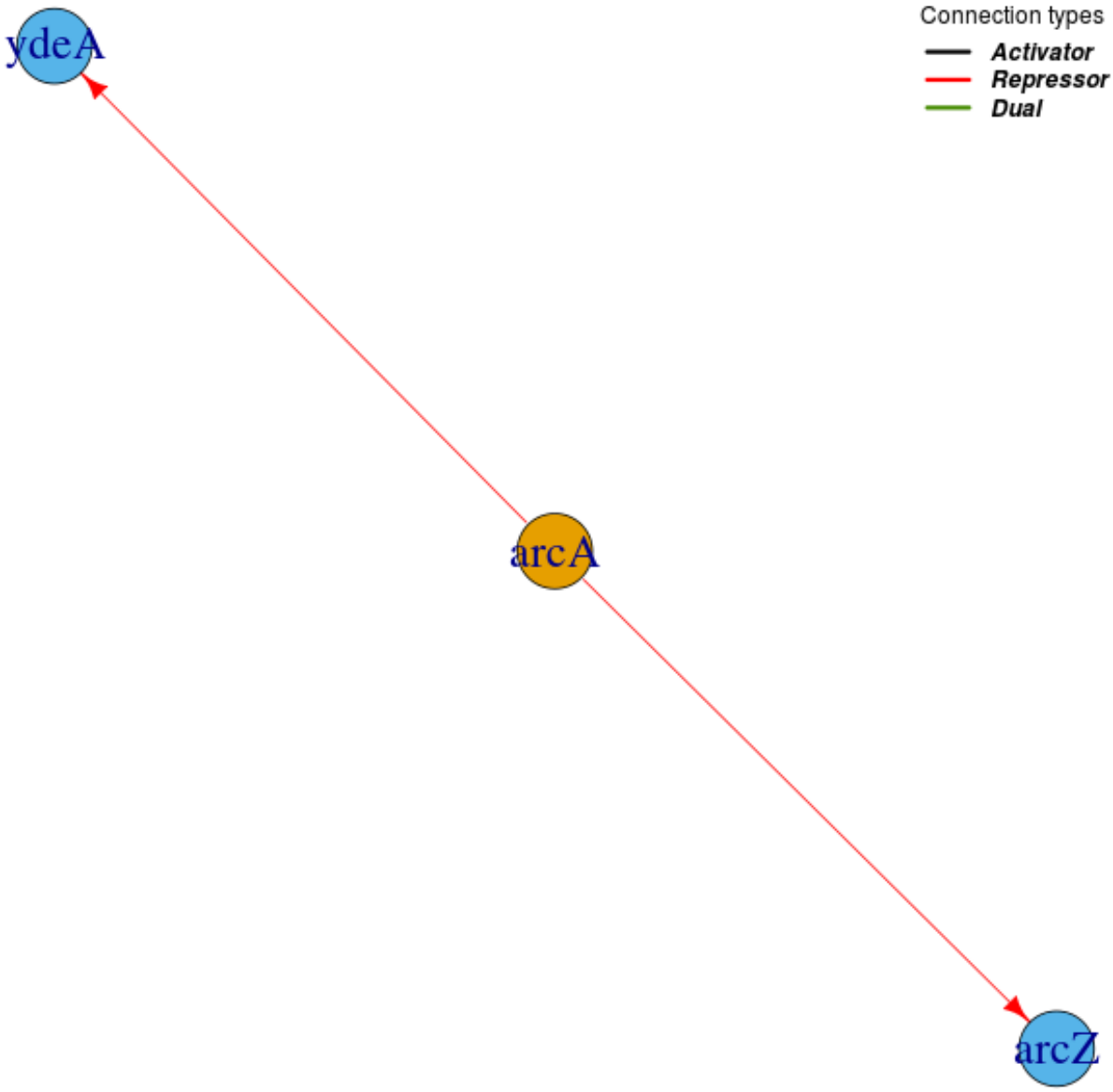

Id = 21

$|n = 1, \ell = 0\rangle$

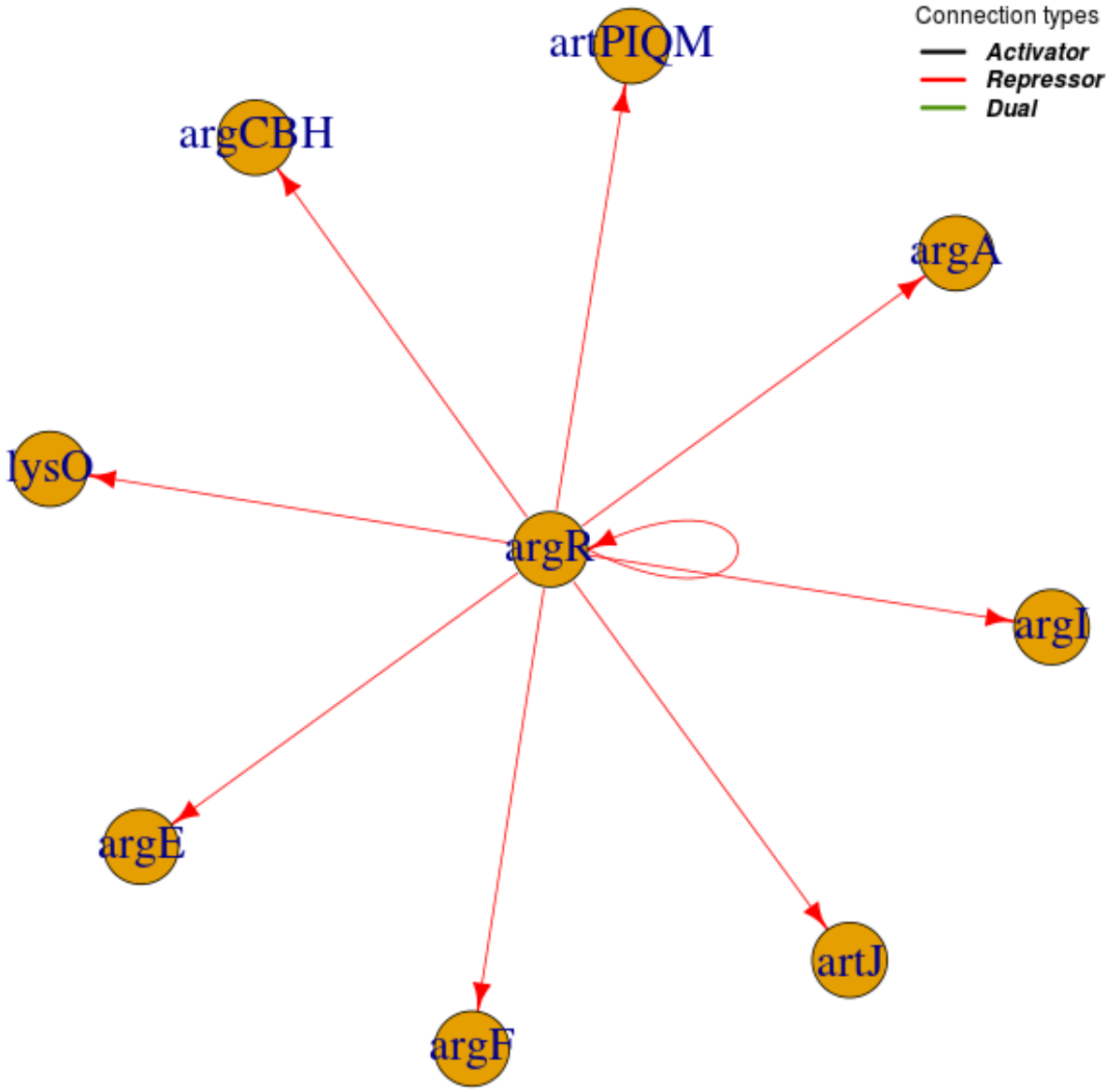

Id = 22

$|n = 0, \ell = 2\rangle$

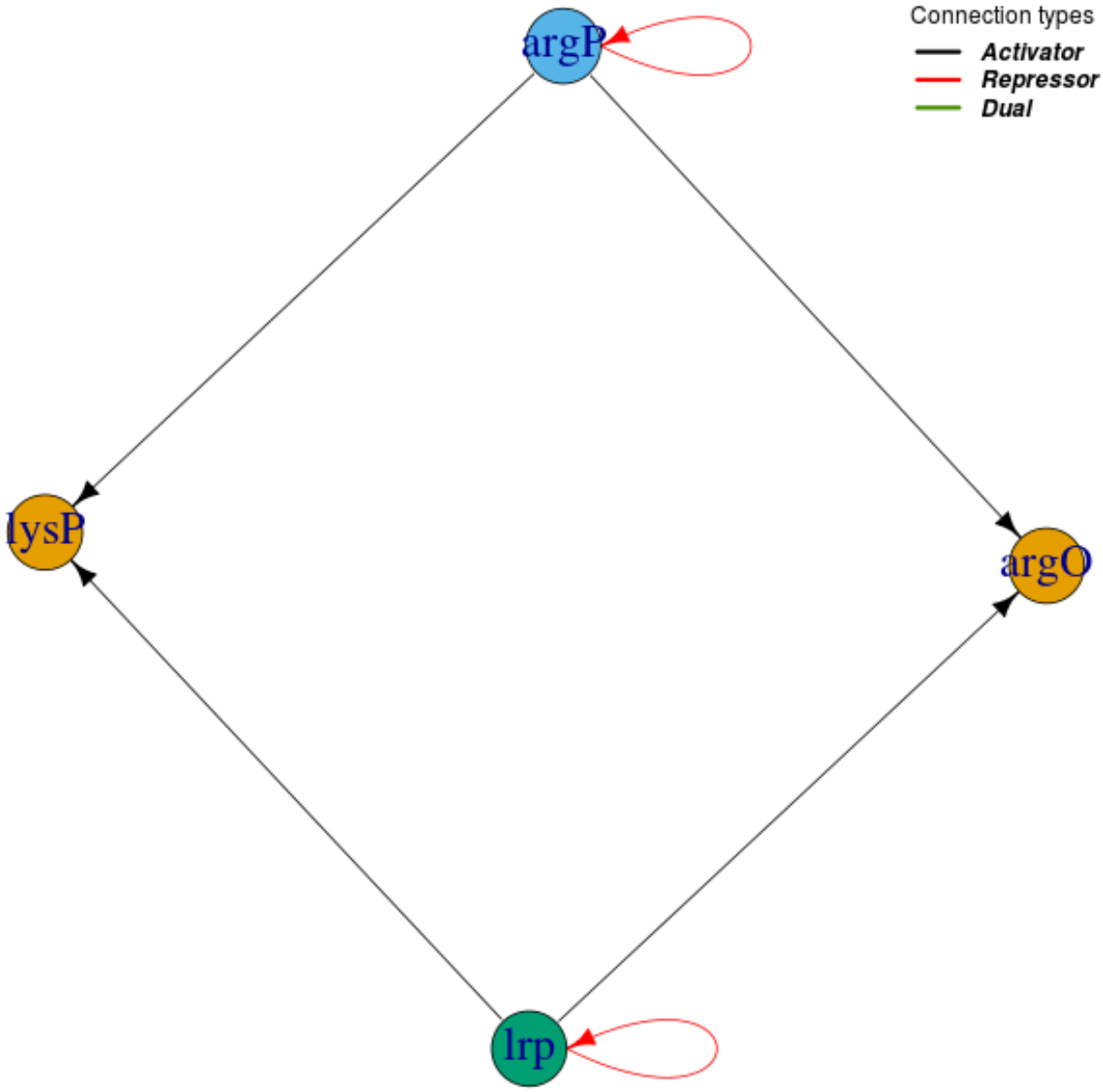

Id = 23

$|n = 0, \ell = 1\rangle$

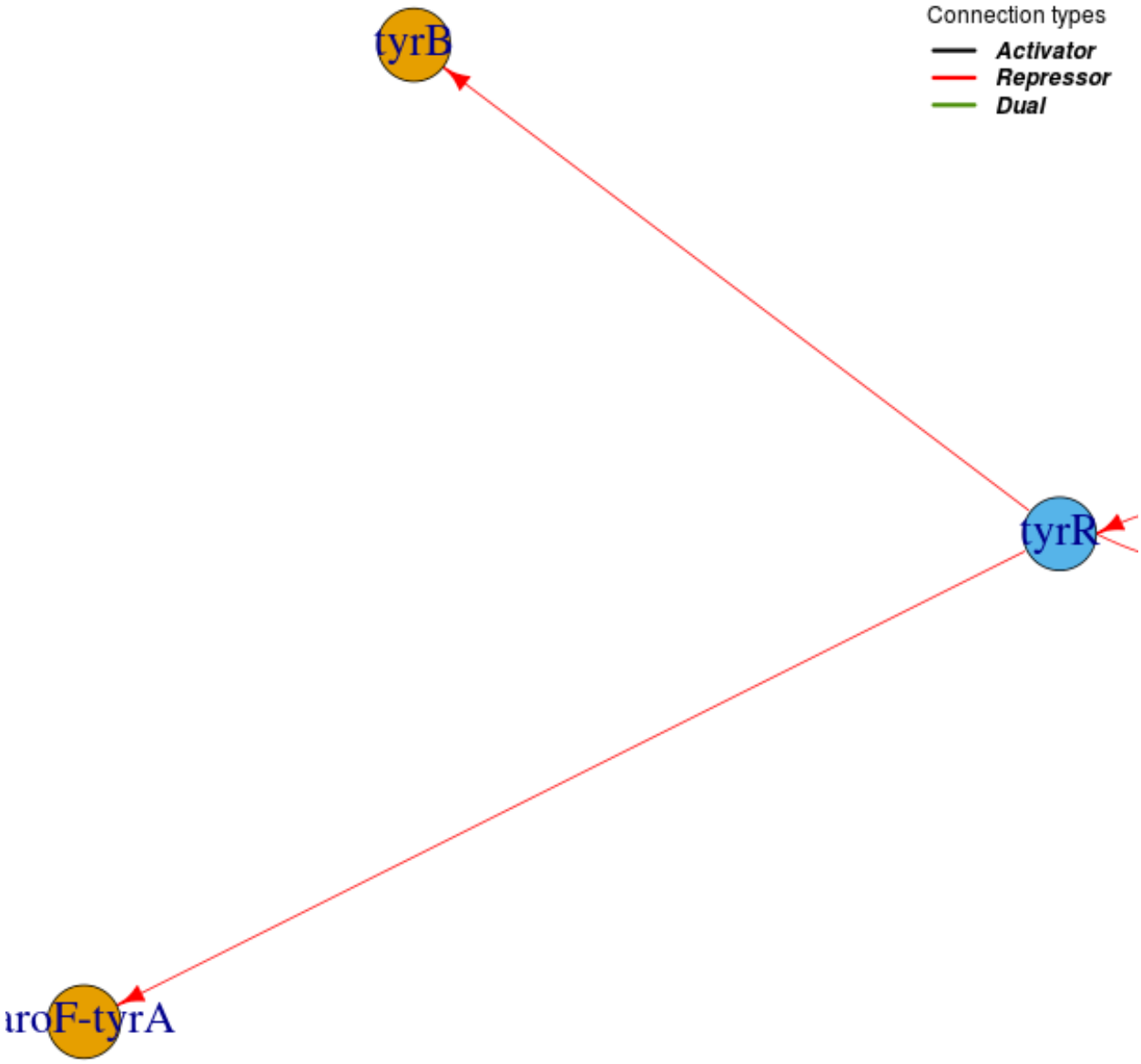

Id = 24

$|n = 1, \ell = 0\rangle$

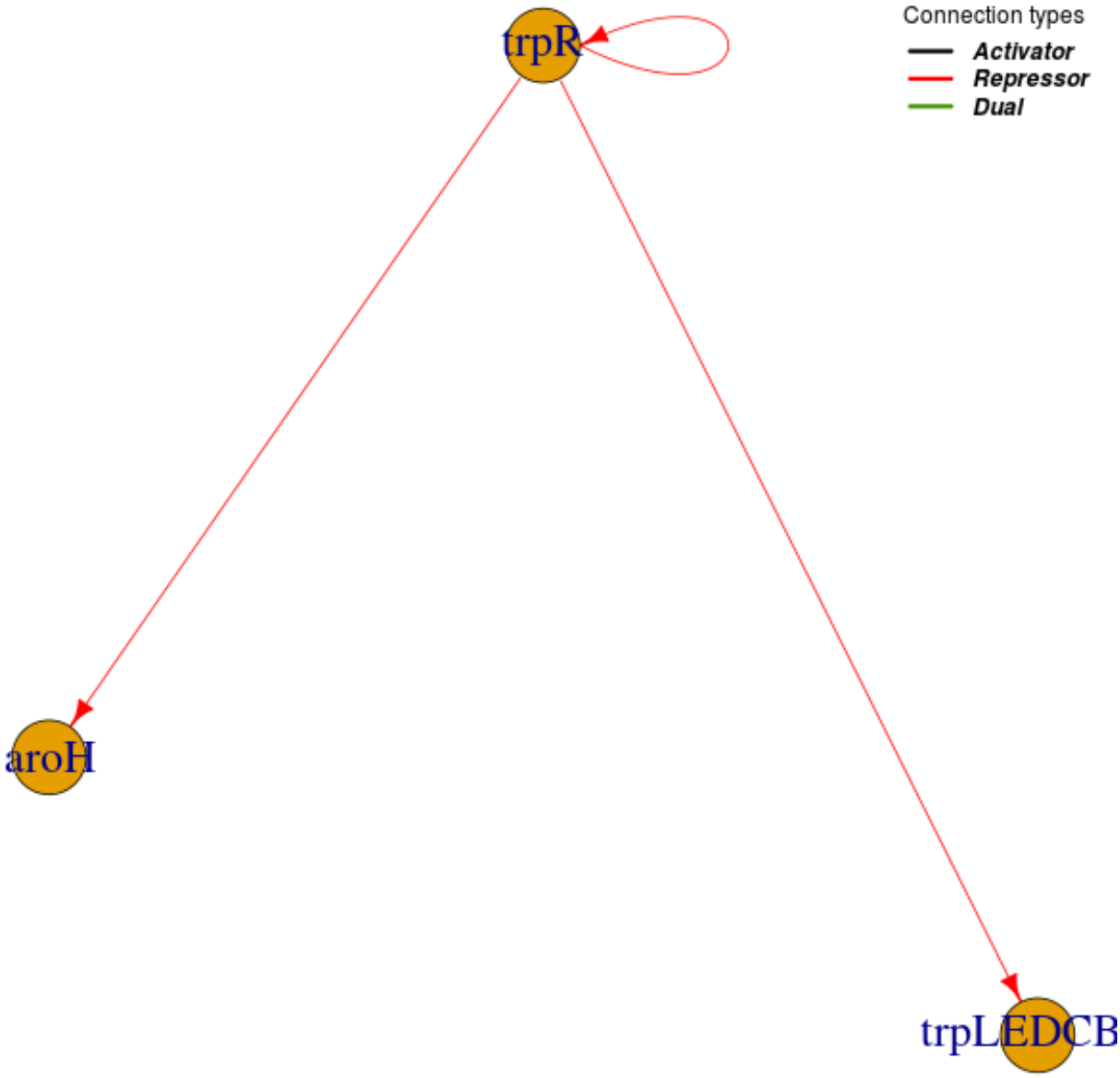

Id = 25

$|n = 0, \ell = 1\rangle$

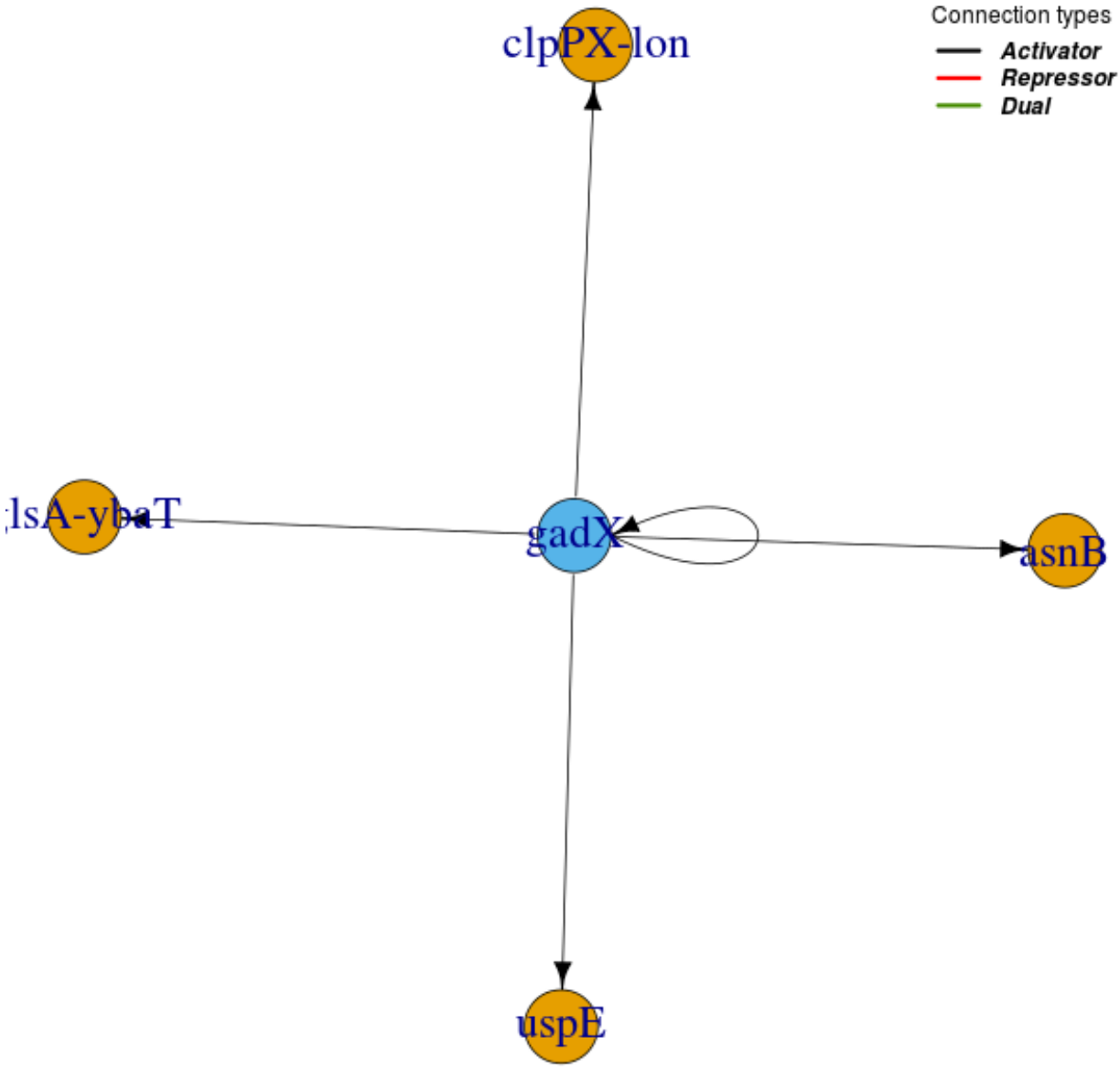

Id = 26

$|n = 0, \ell = 3\rangle$

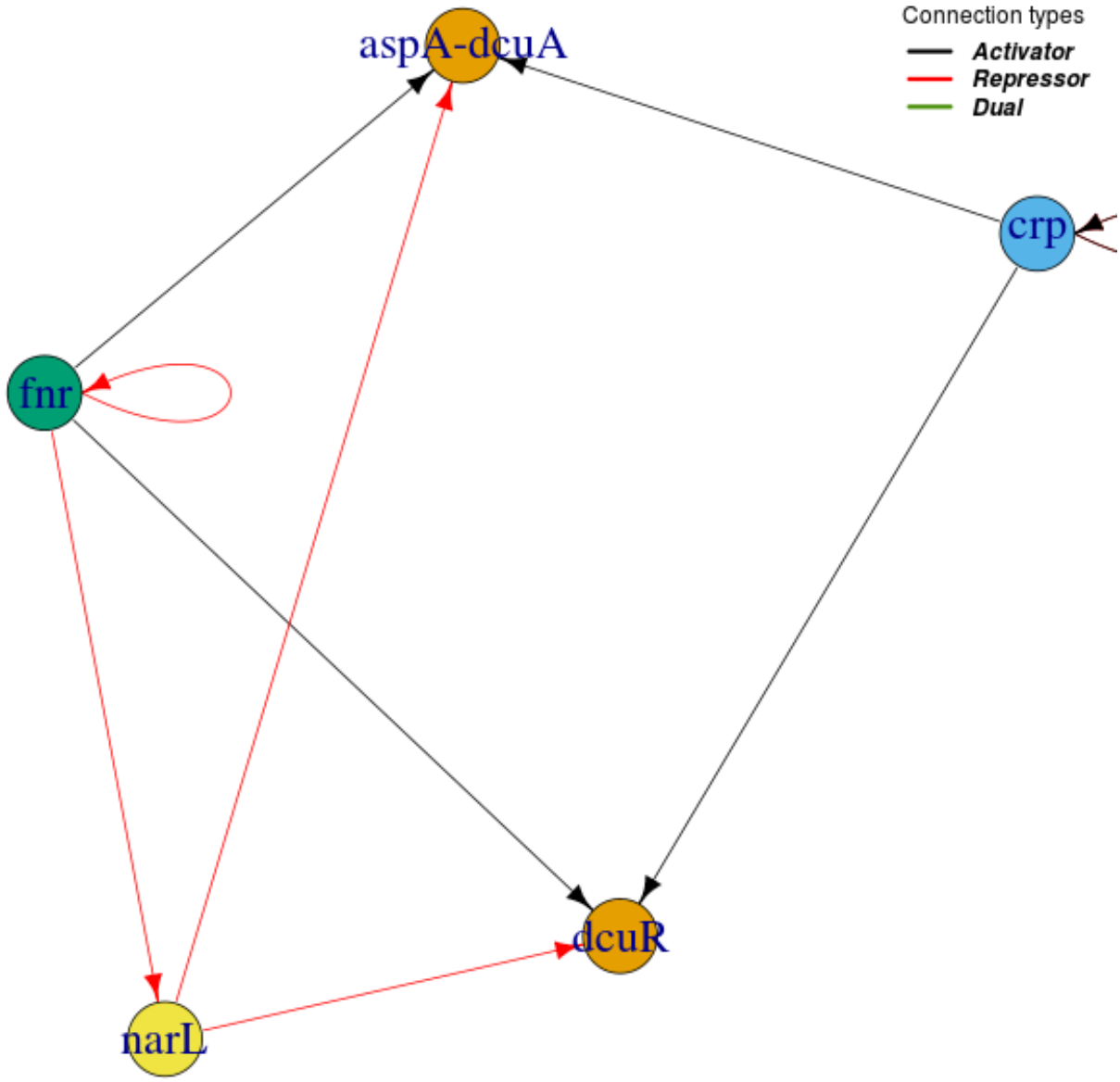

Id = 27

$|n = 1, \ell = 0\rangle$

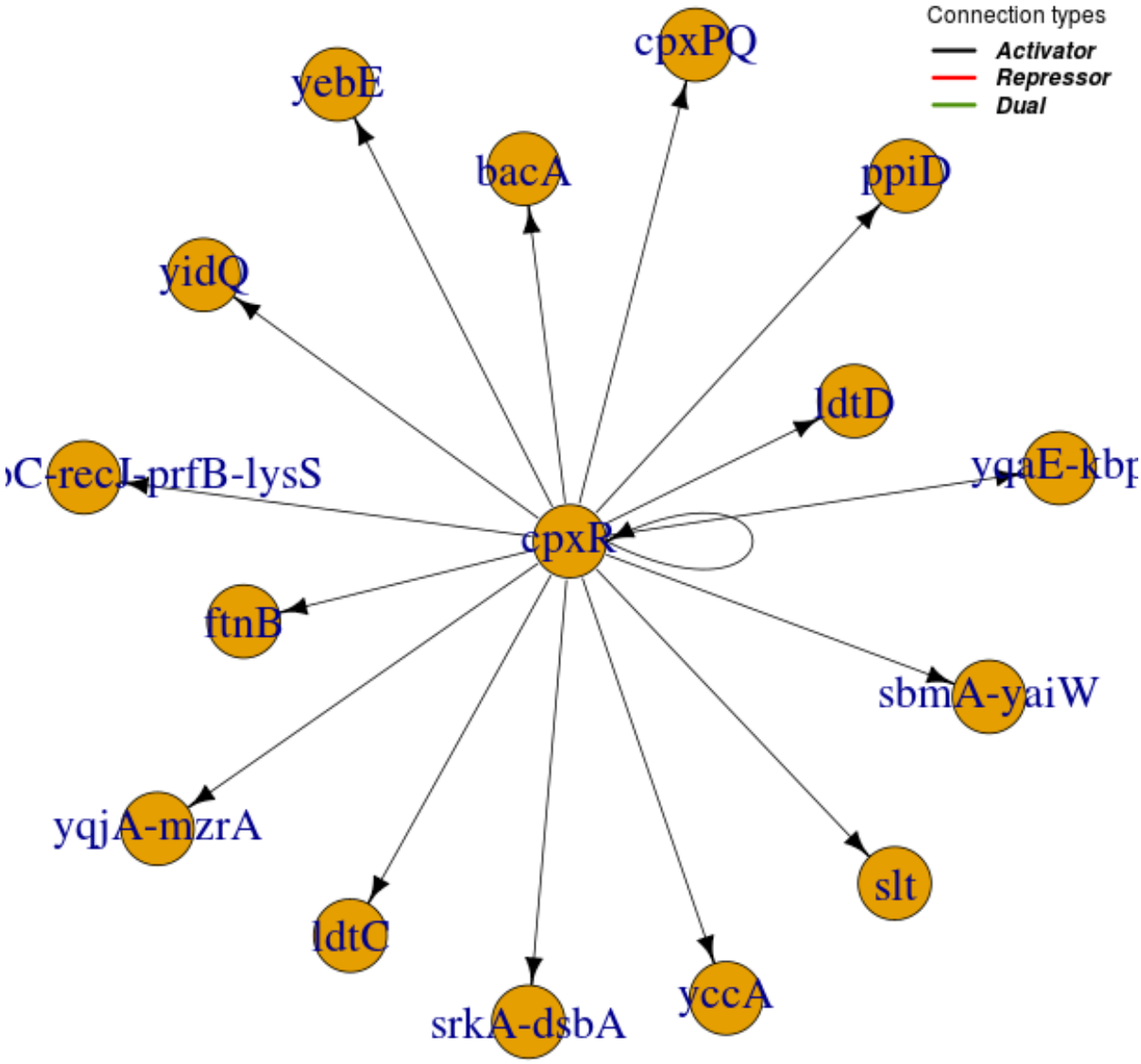

Id = 28

$|n = 1, \ell = 1\rangle$

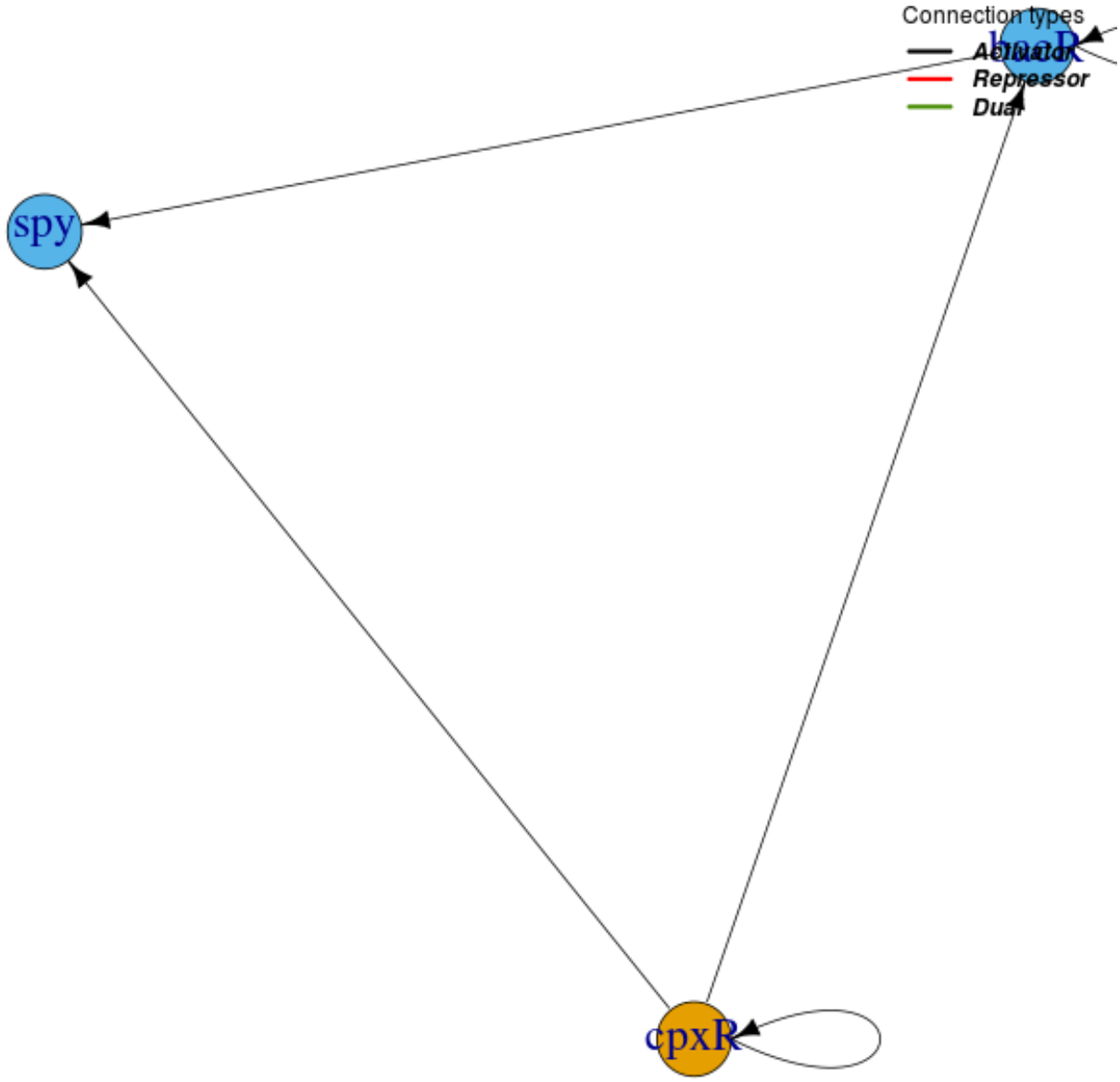

Id = 29

$|n = 0, \ell = 1\rangle$

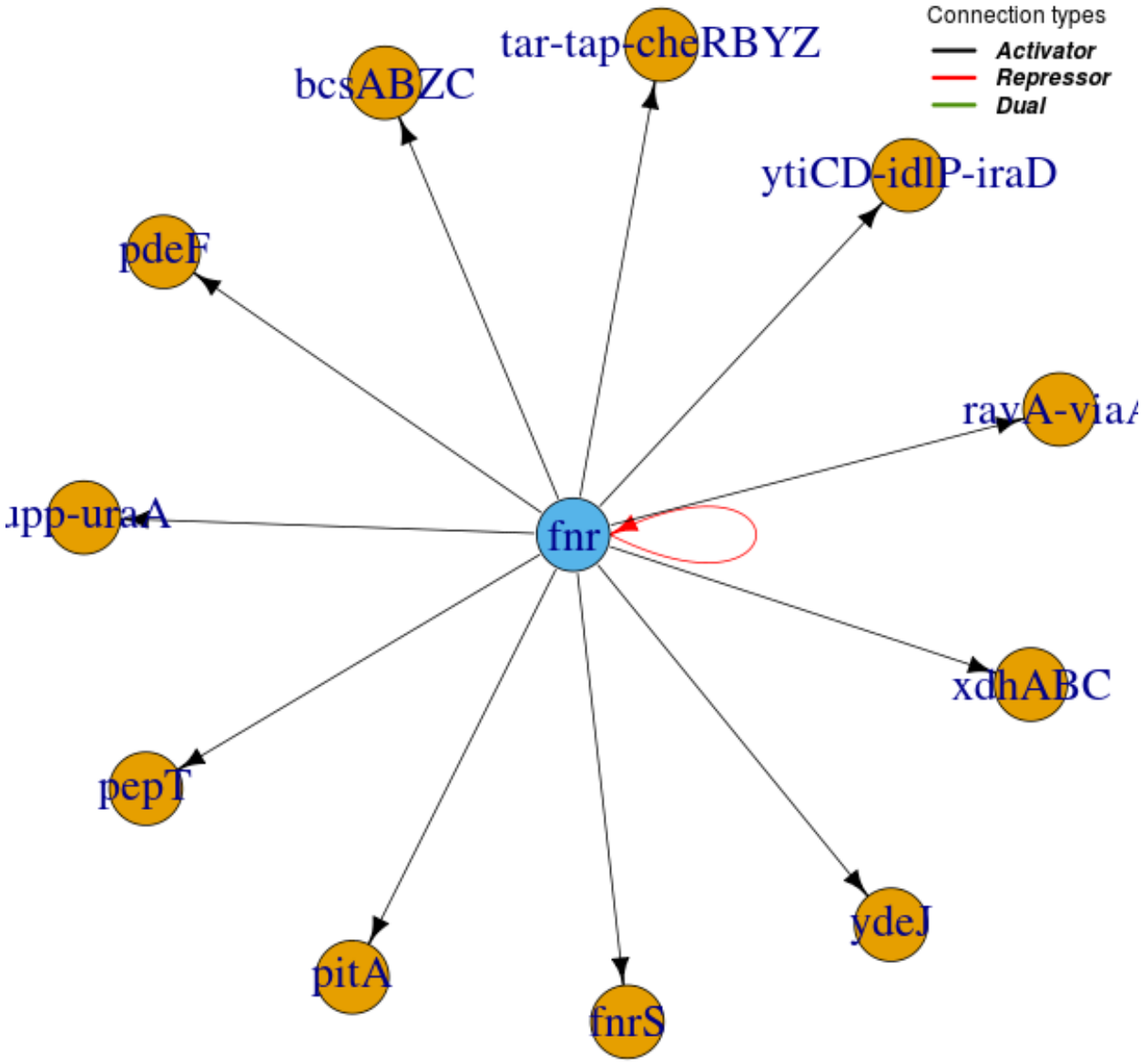

Id = 30

$|n = 0, \ell = 1\rangle$

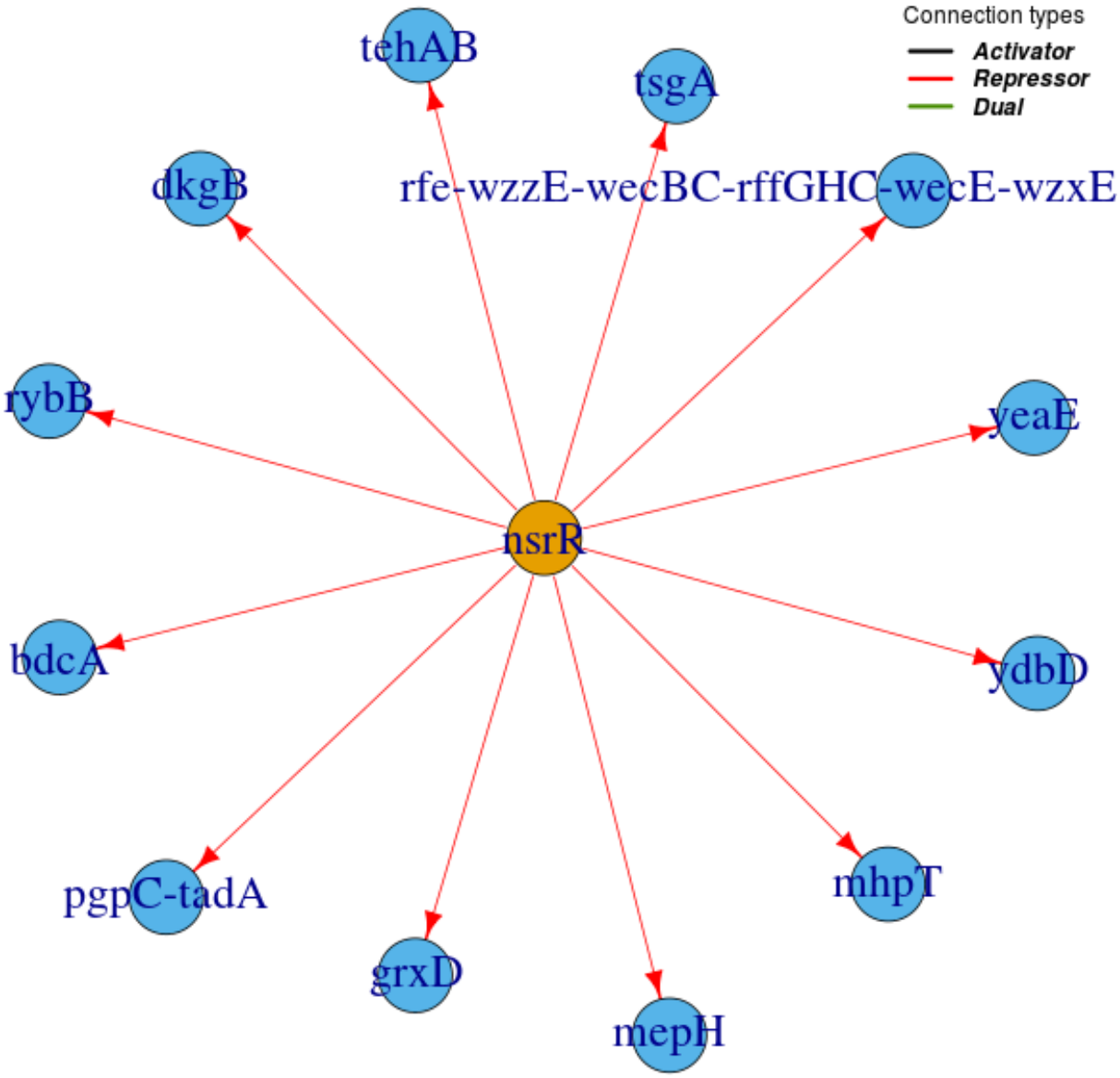

Id = 31

$|n = 1, \ell = 2\rangle$

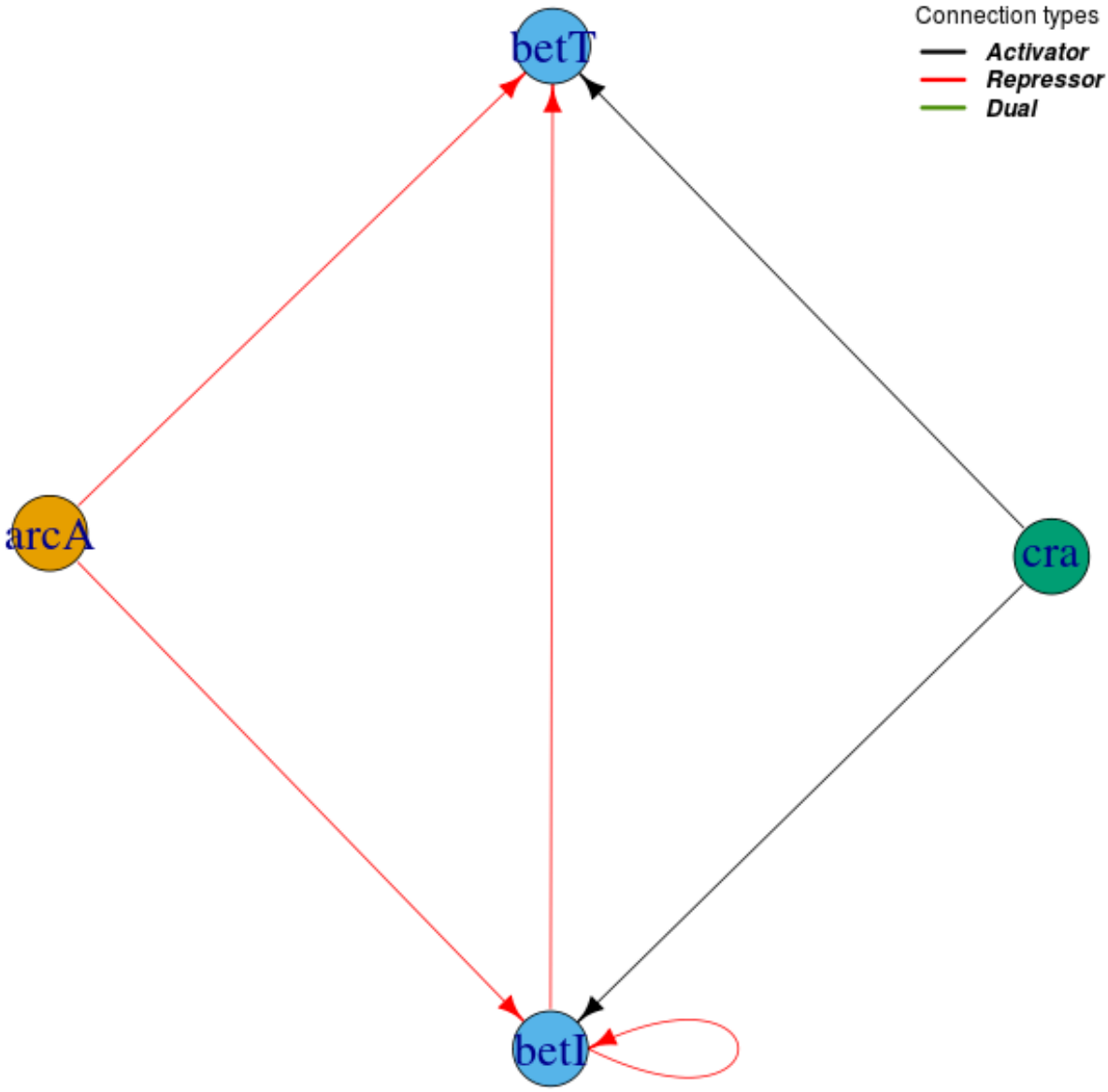

$\mathrm{Id} = 32$

$|n = 0, \ell = 1\rangle$

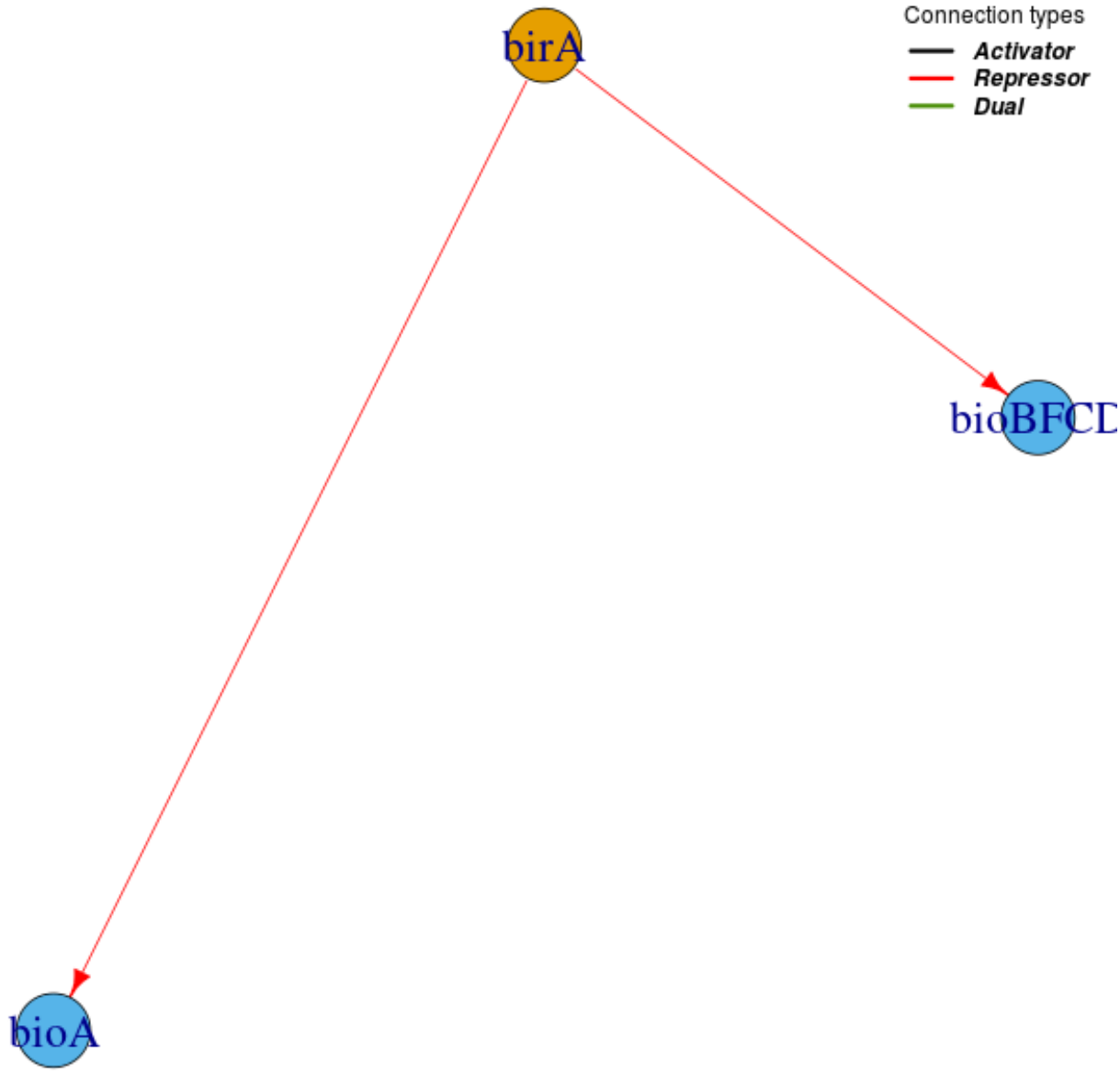

Id = 33

$|n = 0, \ell = 1\rangle$

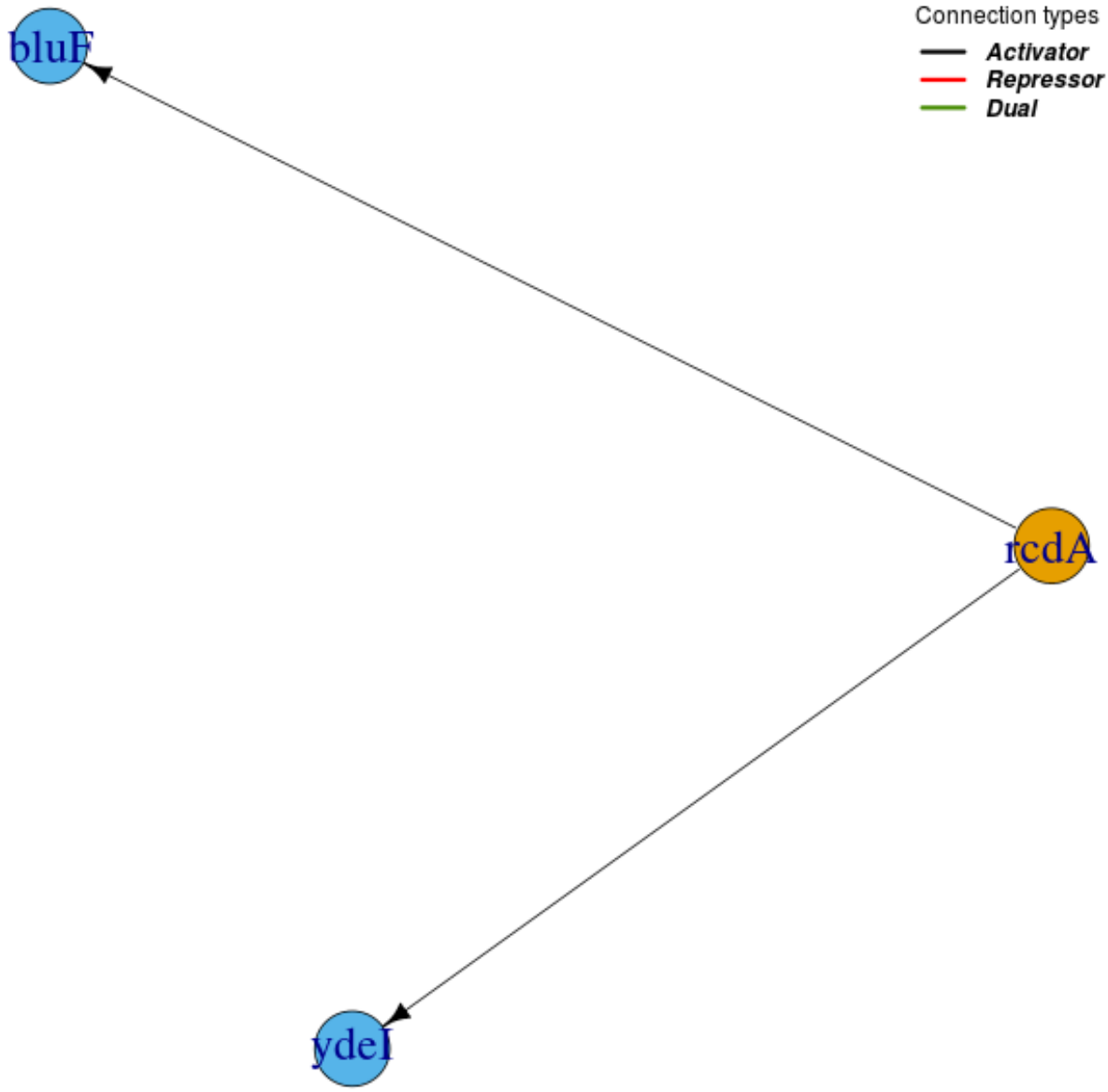

Id = 34

$|n = 0, \ell = 1\rangle$

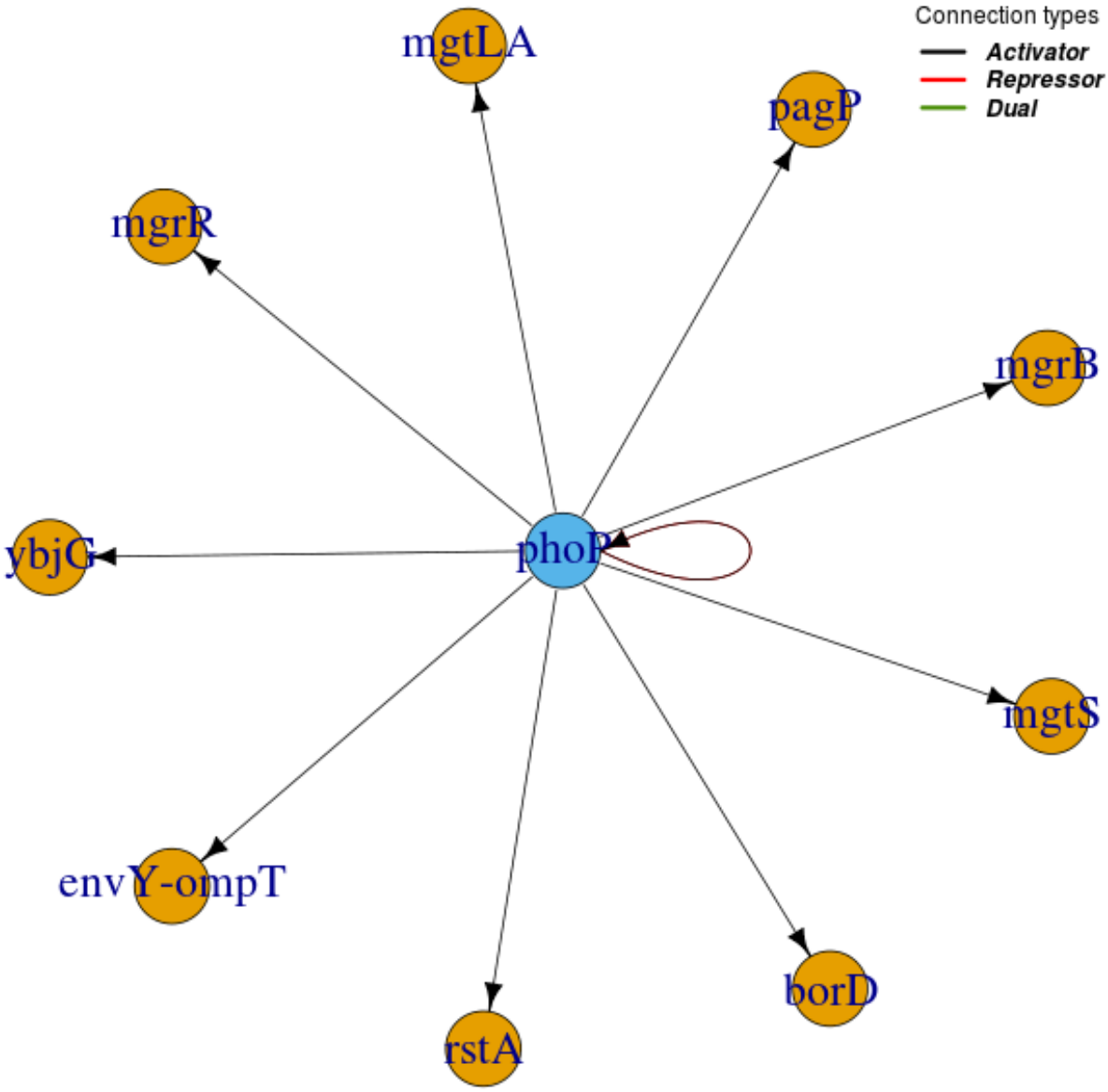

Id = 35

$|n = 0, \ell = 1\rangle$

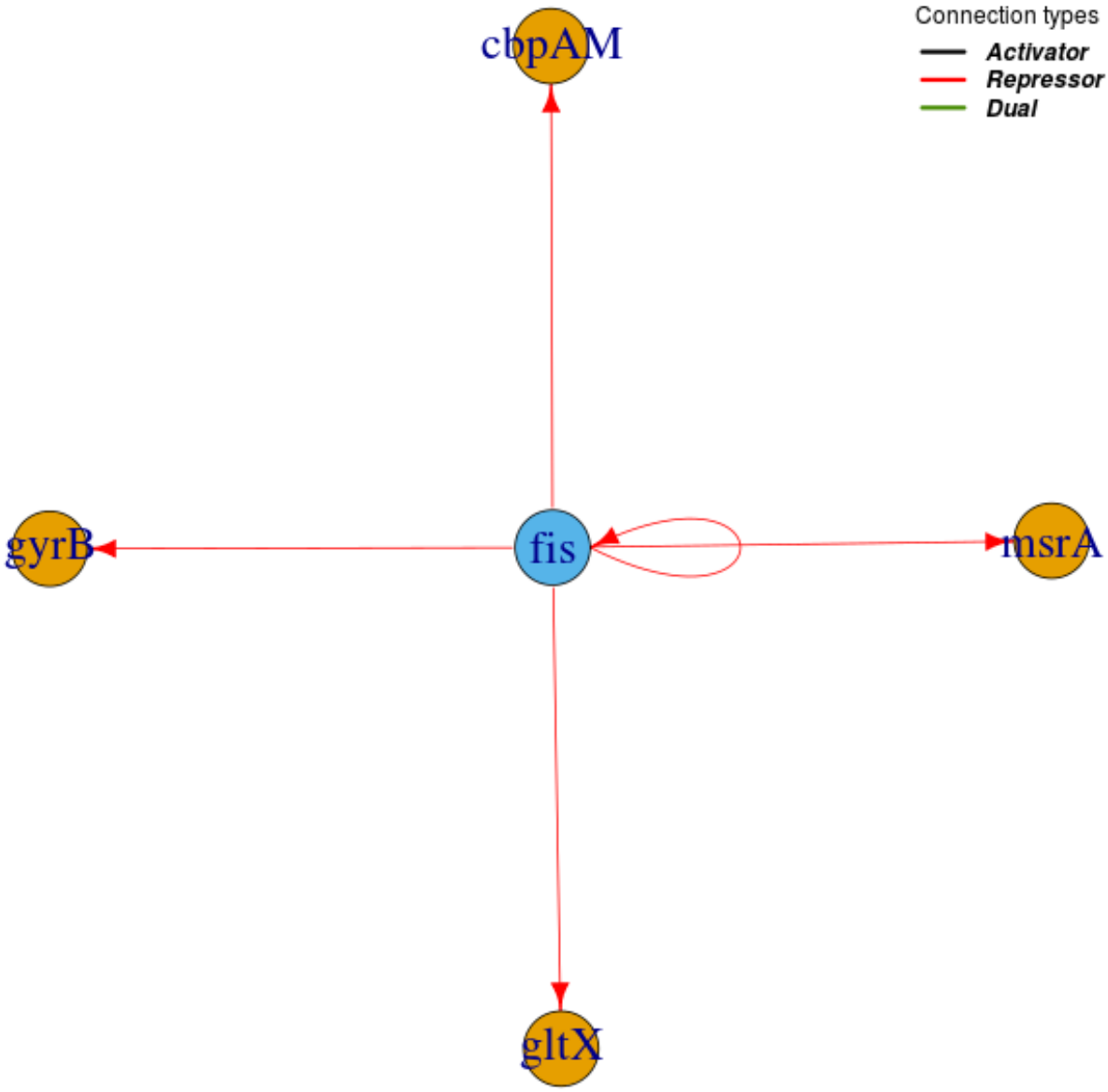

Id = 36

$|n = 1, \ell = 0\rangle$

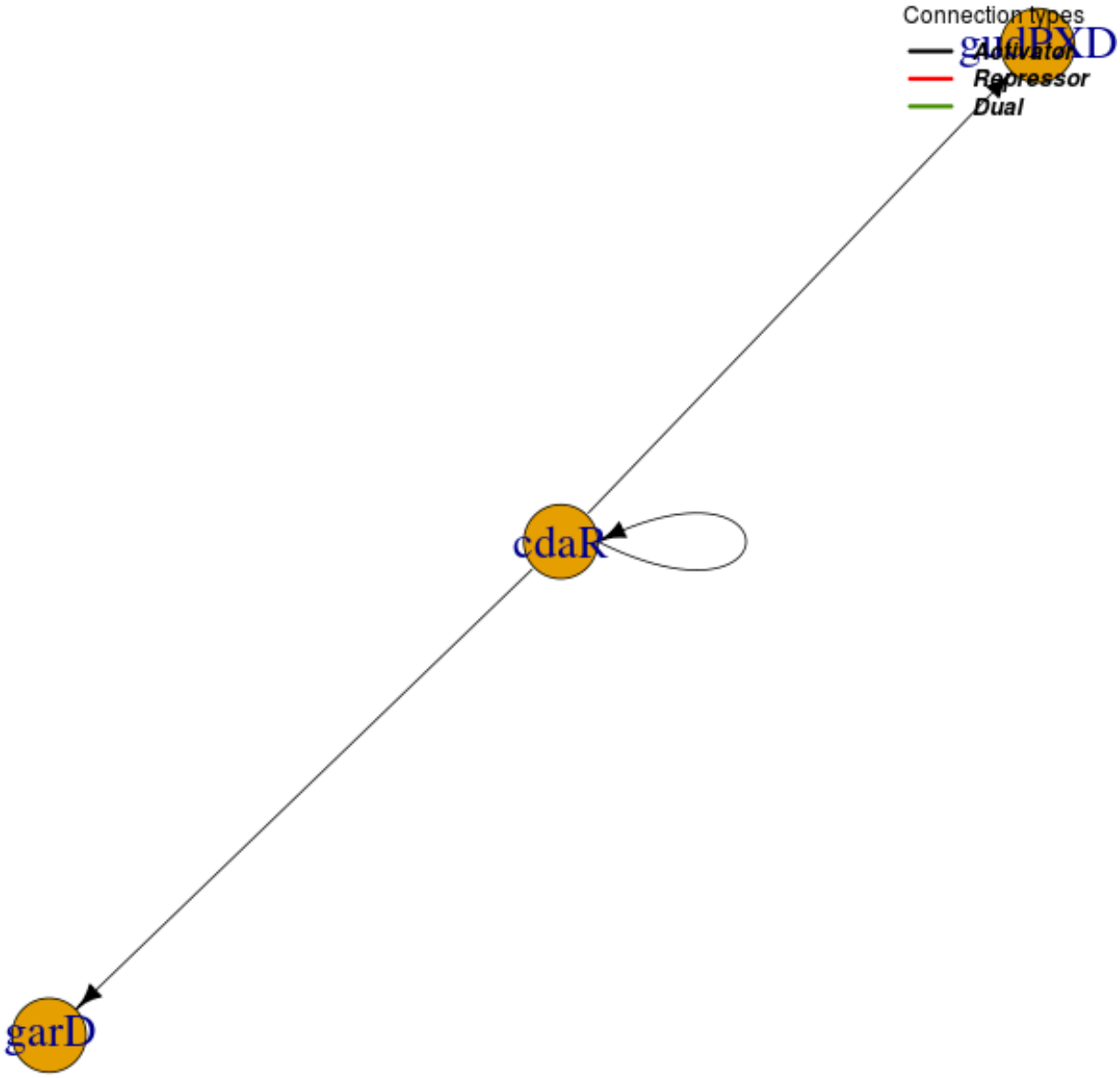

Id = 37

$|n = 1, \ell = 0\rangle$

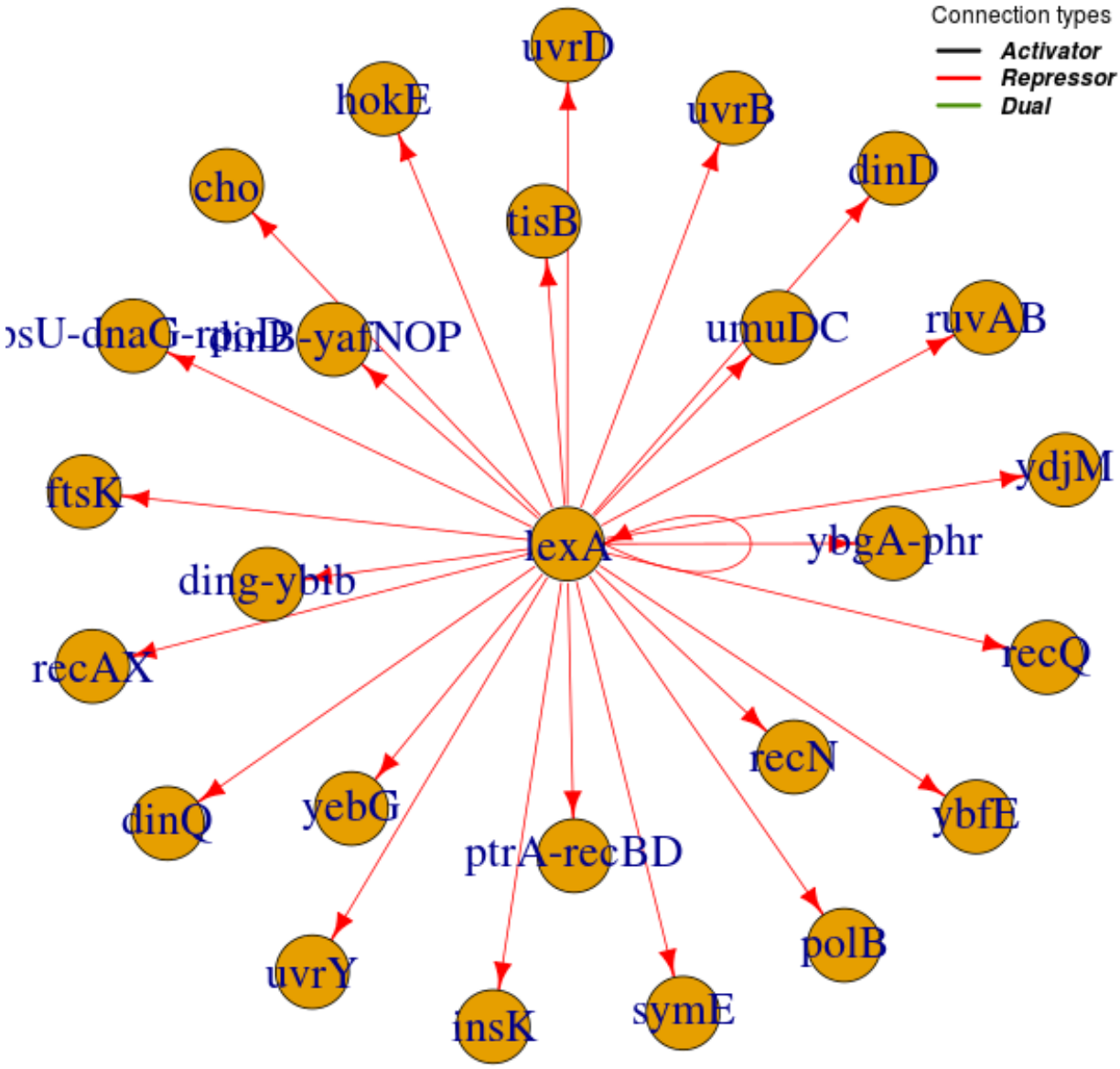

Id = 38

$|n = 0, \ell = 2\rangle$

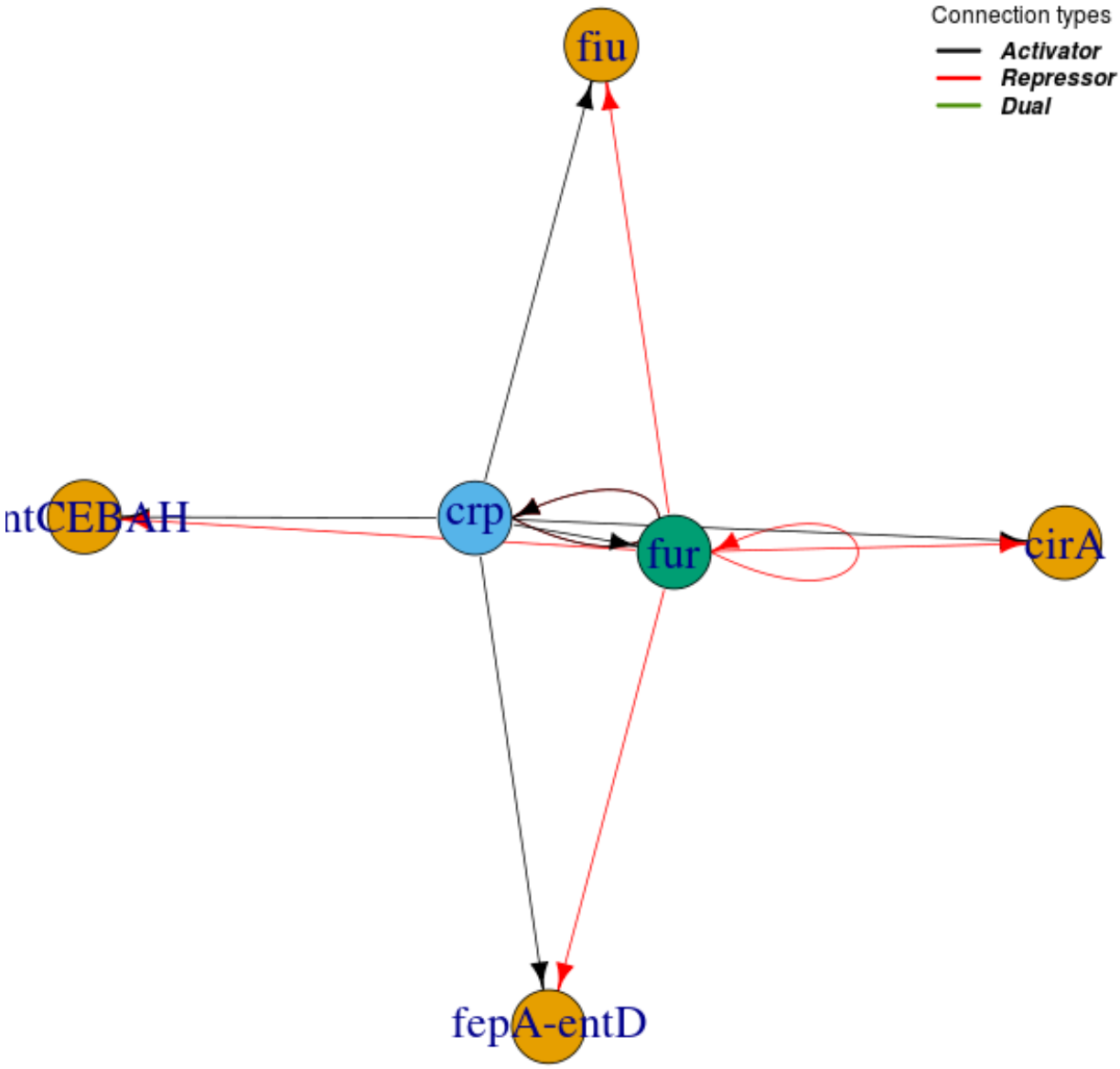

Id = 39

$|n = 0, \ell = 1\rangle$

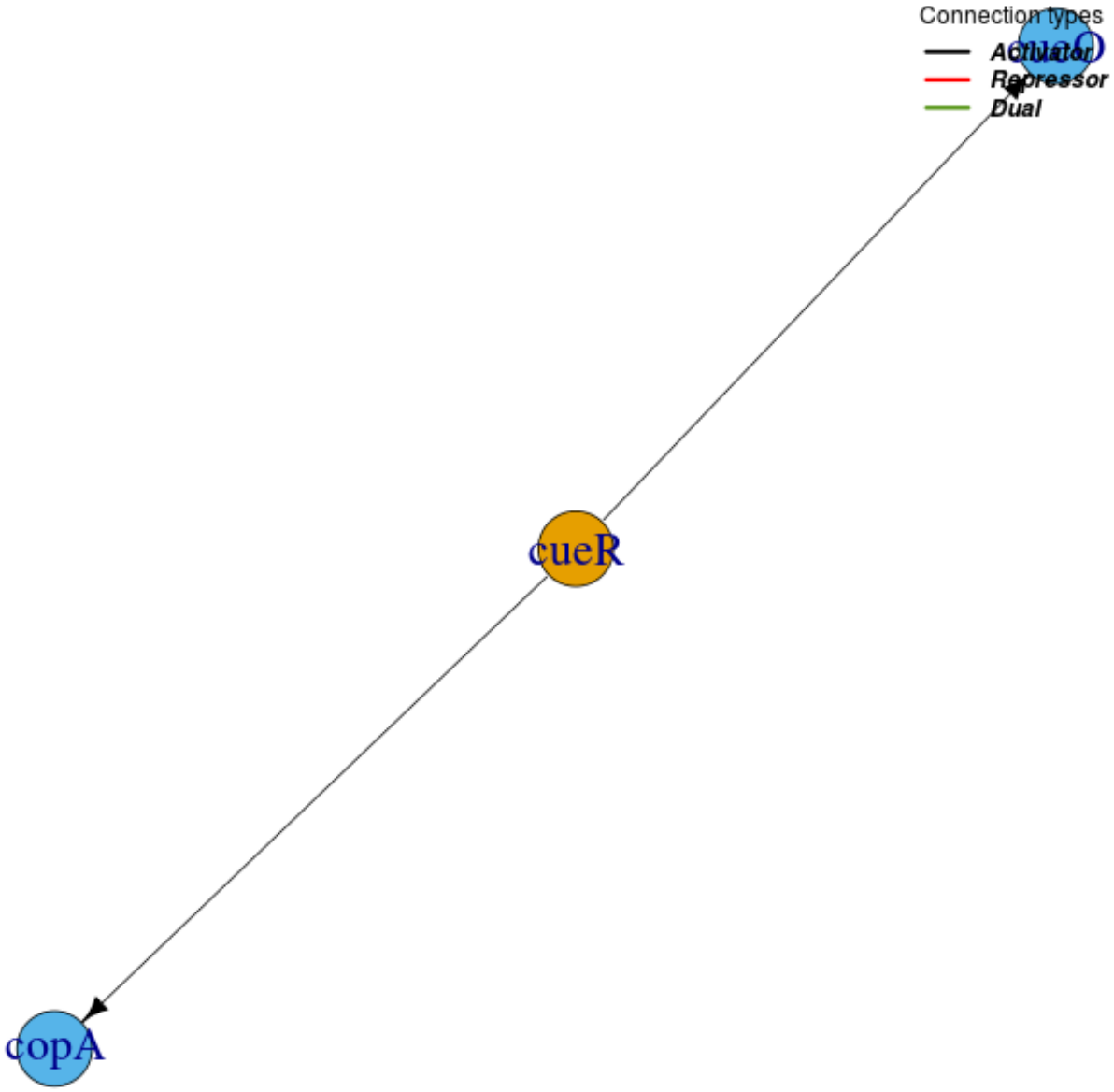

Id = 40

$|n = 0, \ell = 1\rangle$

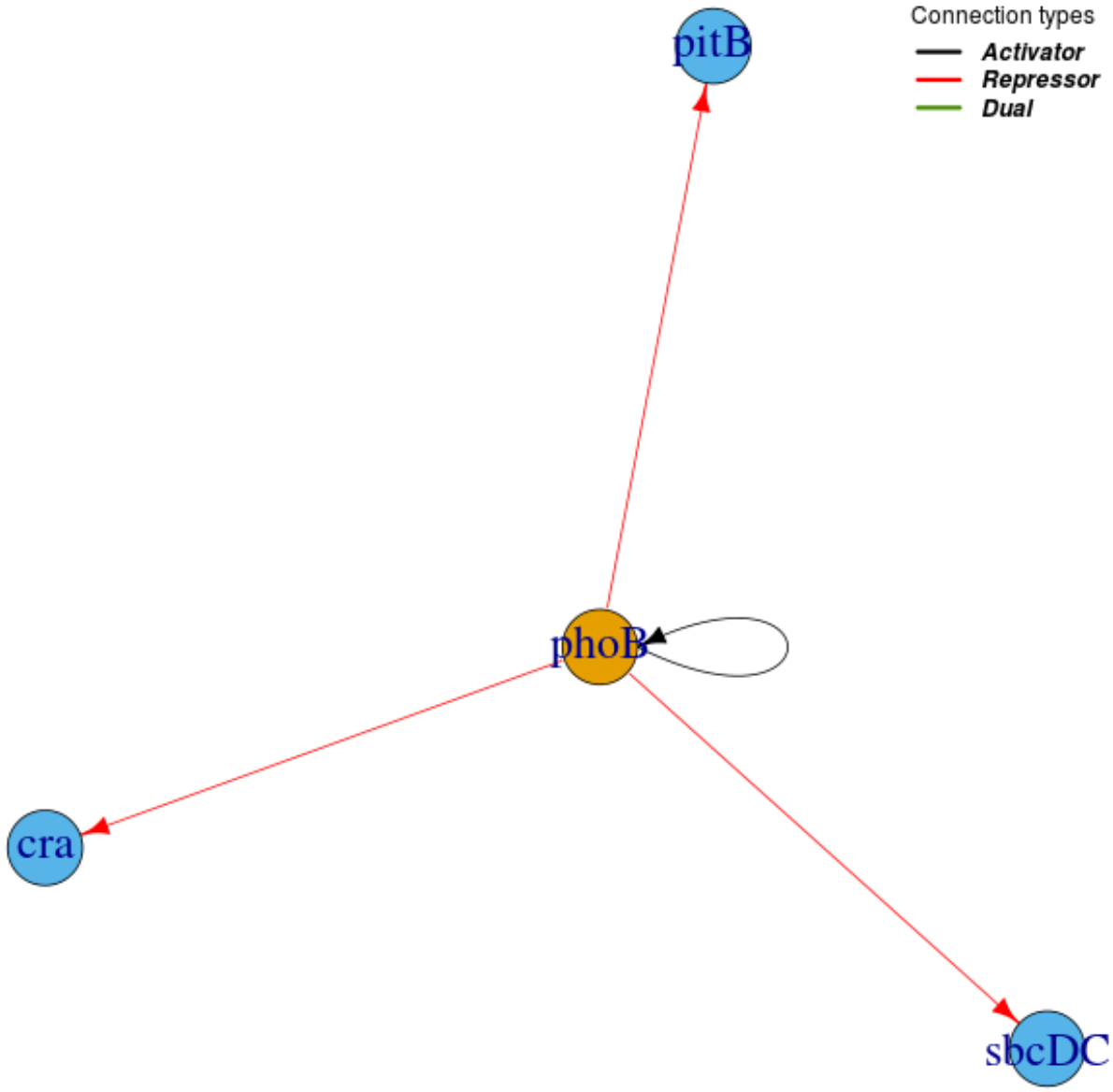

Id = 41

$|n = 0, \ell = 1\rangle$

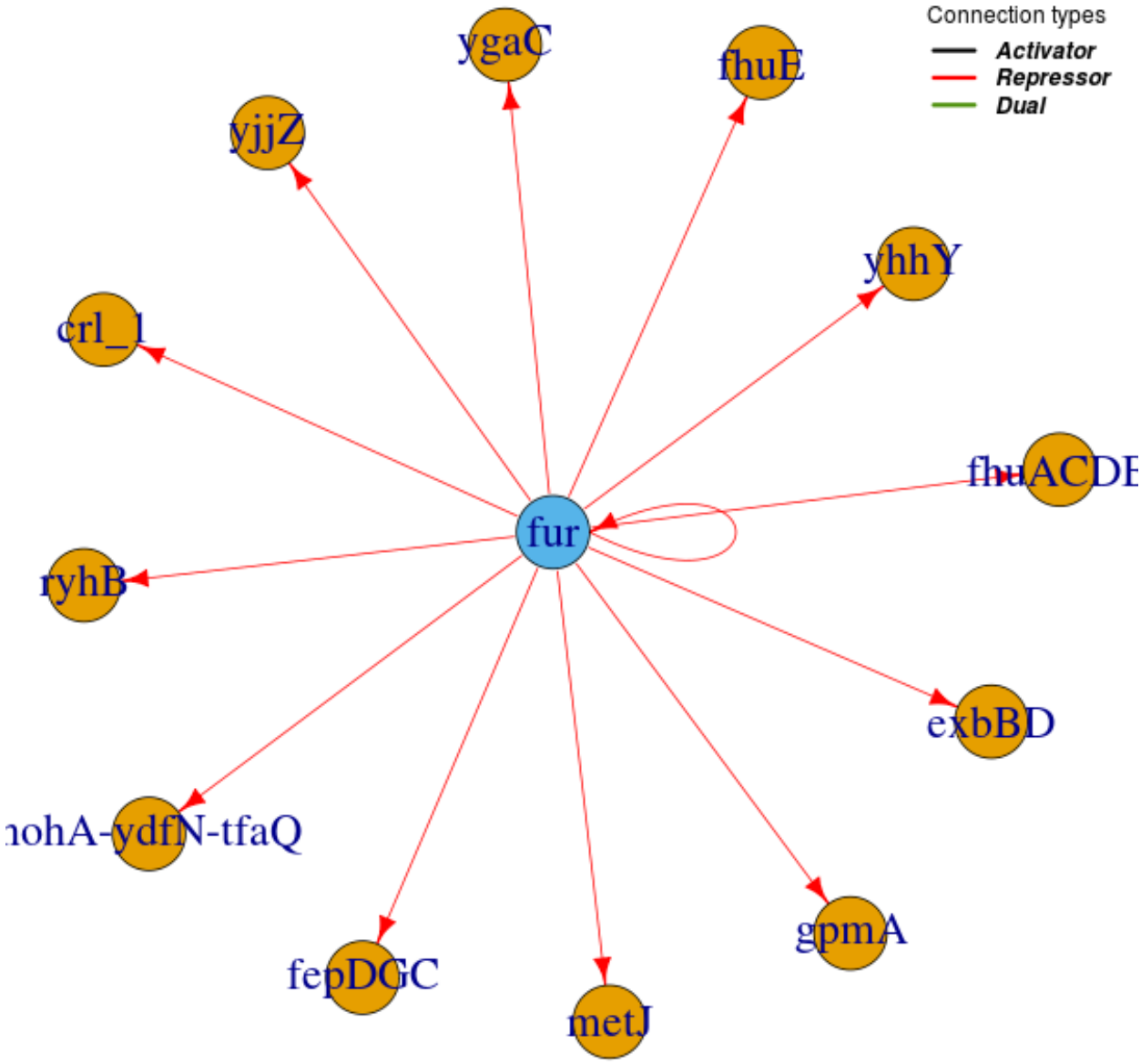

Id = 42

$|n = 1, \ell = 2\rangle$

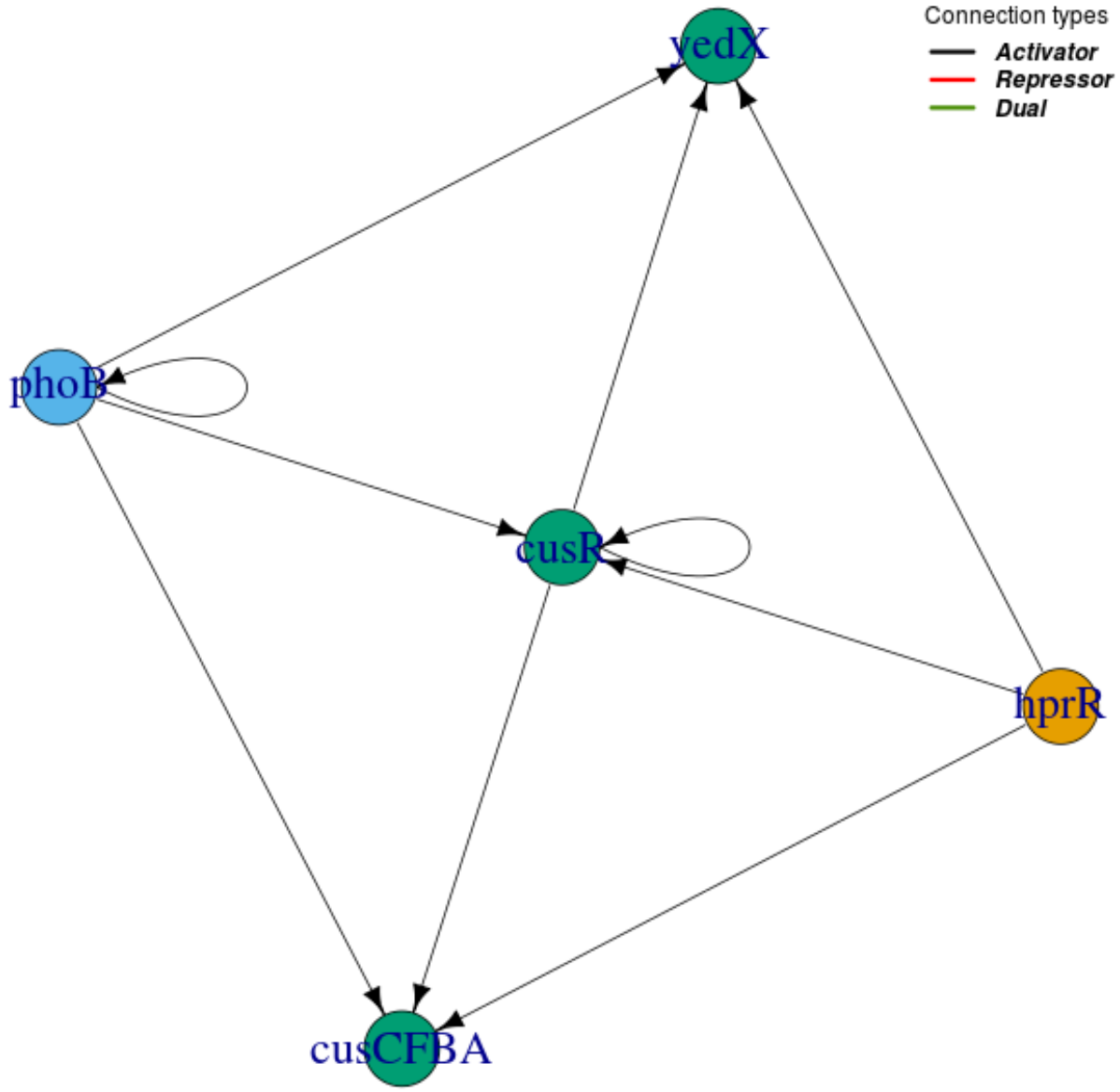

Id = 43

$|n = 0, \ell = 1\rangle$

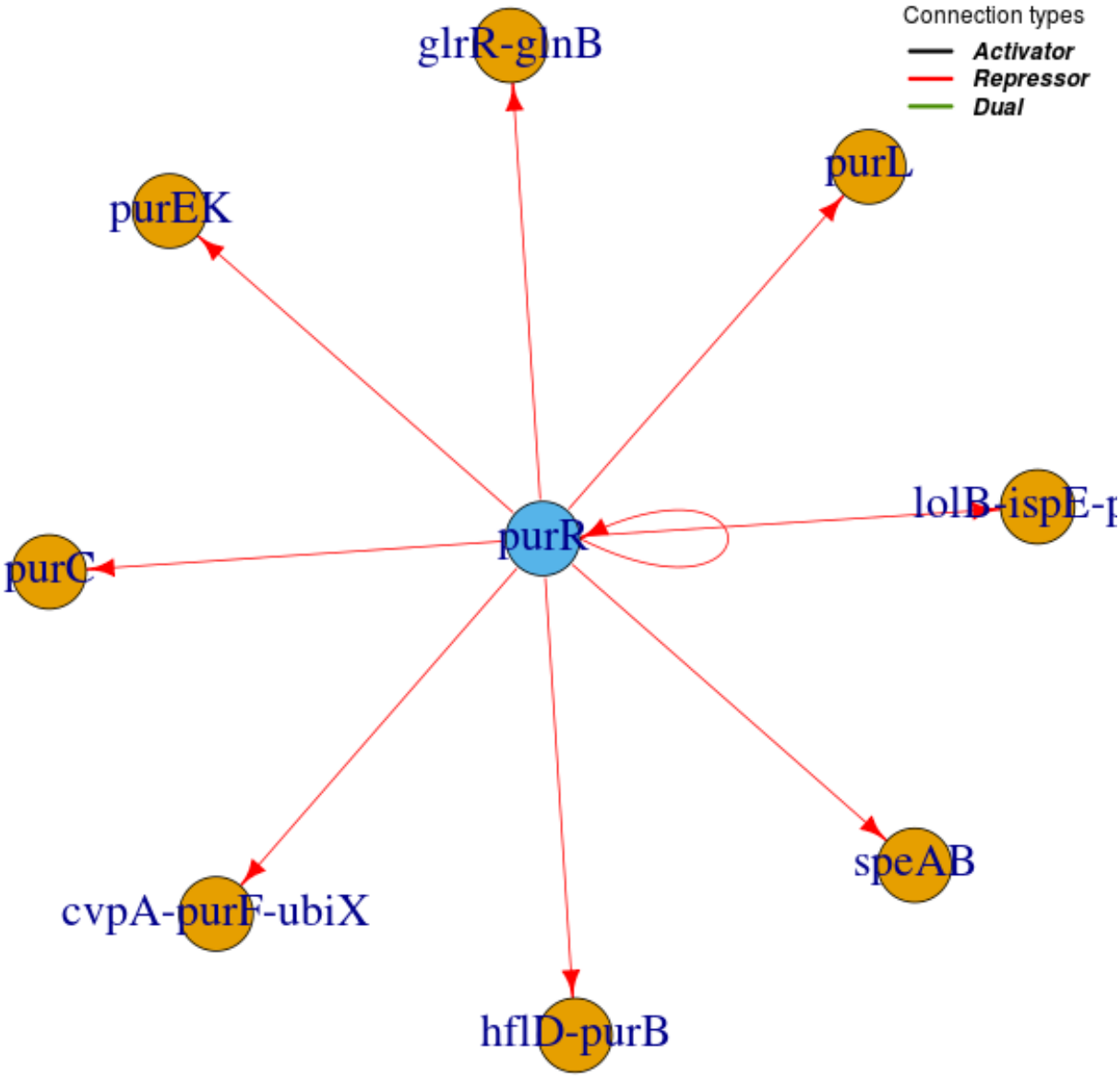

Id = 44

$|n = 0, \ell = 1\rangle$

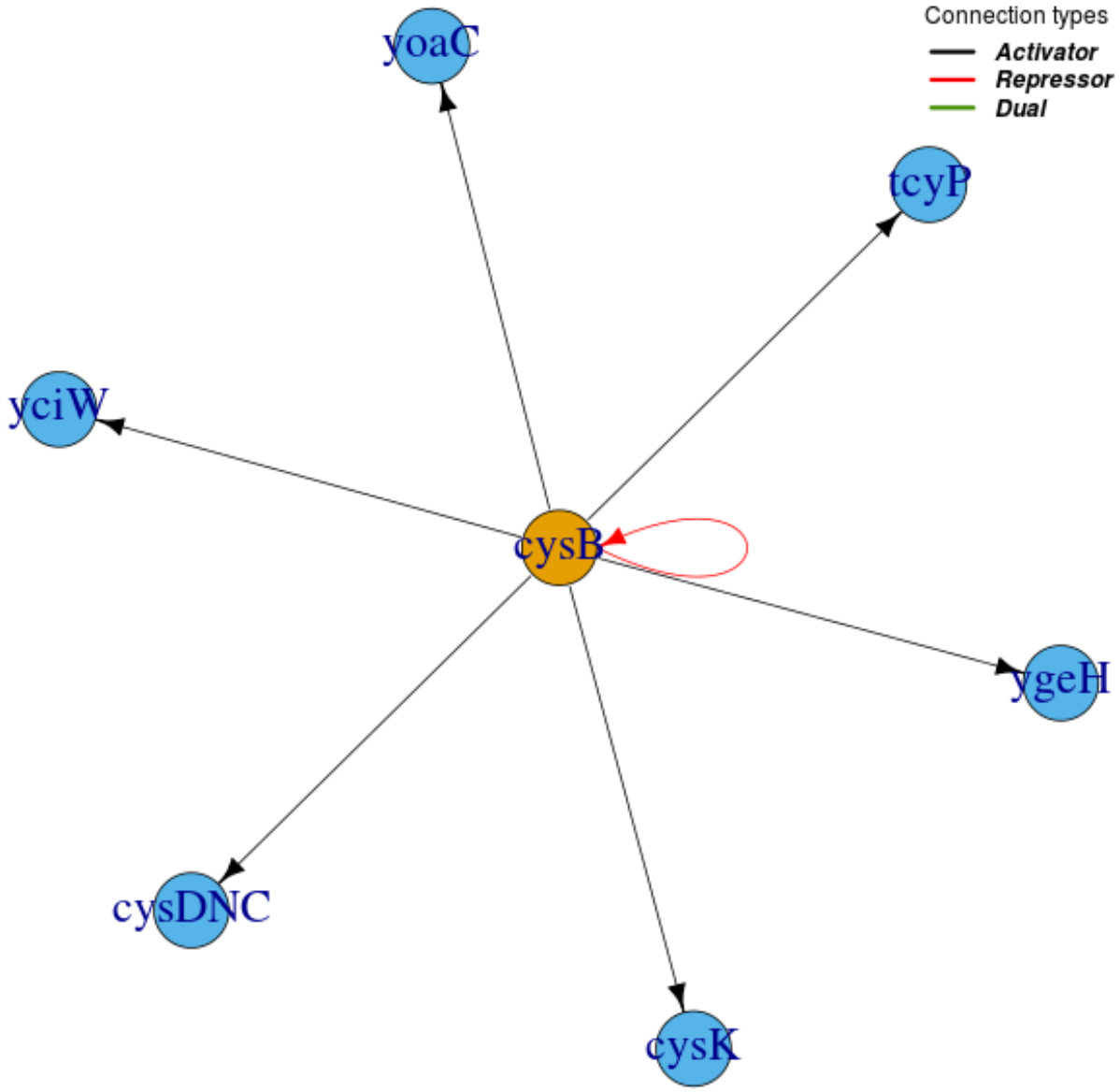

Id = 45

$|n = 1, \ell = 1\rangle$

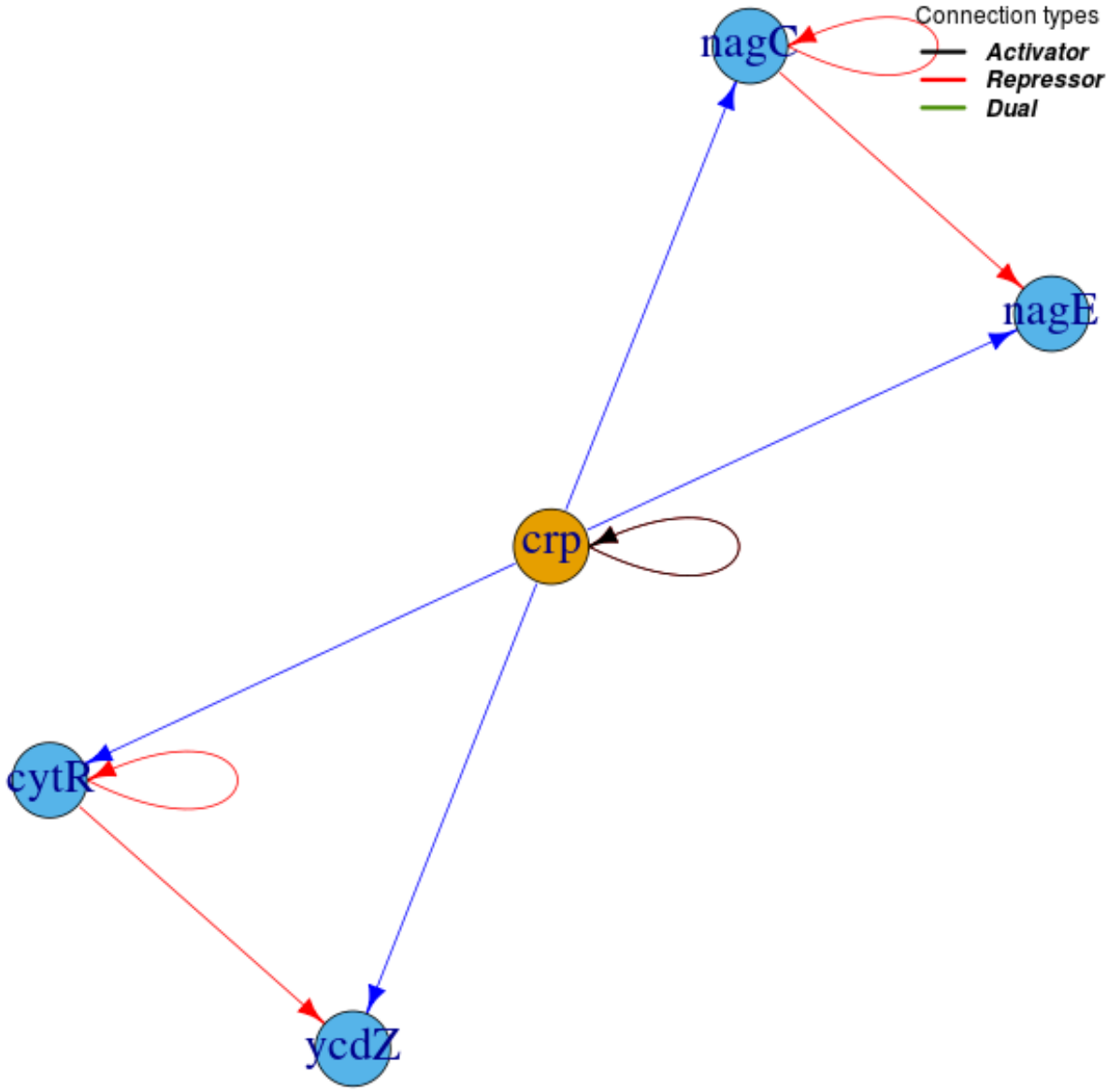

Id = 46

$|n = 0, \ell = 1\rangle$

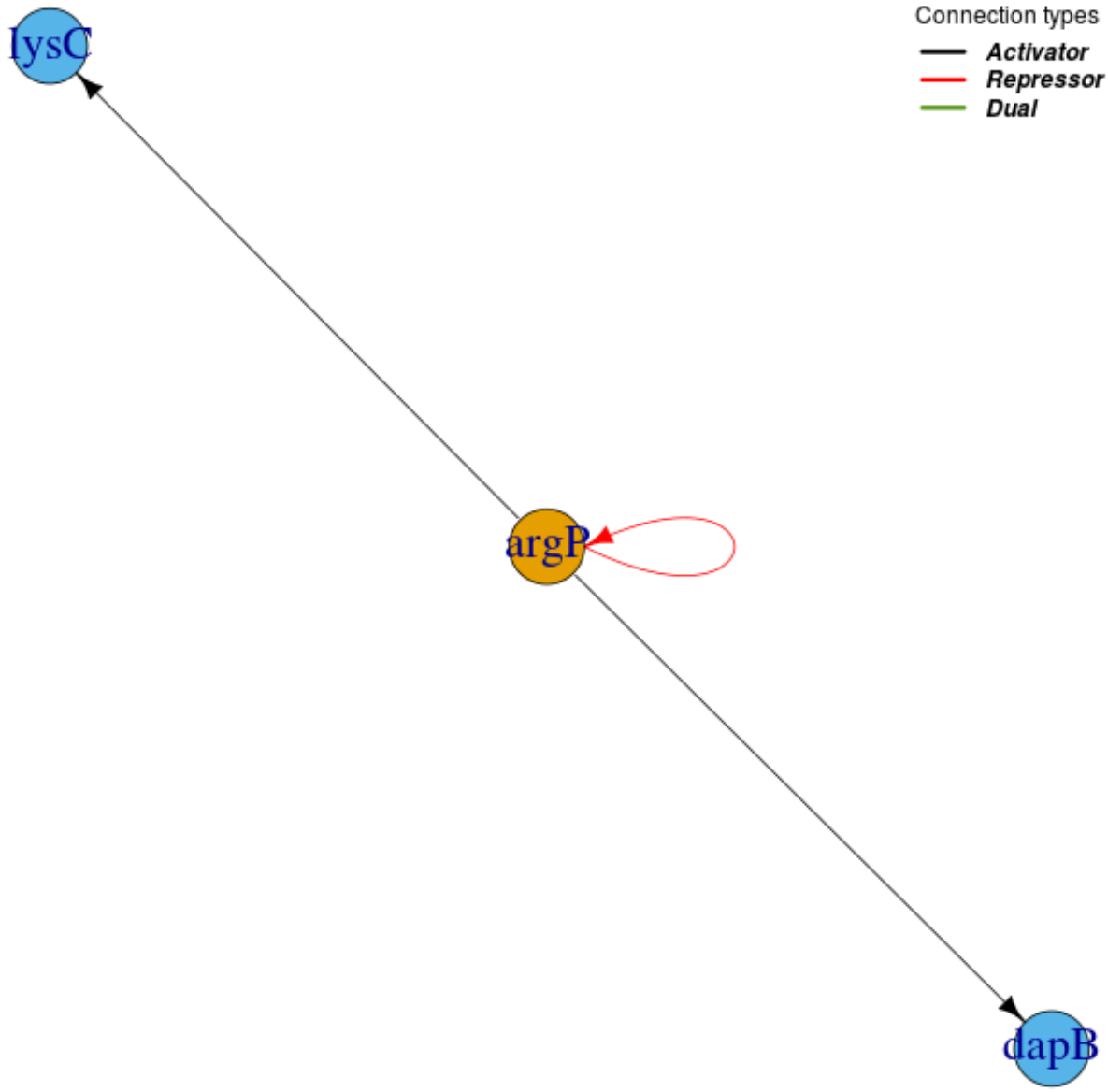

Id = 47

$|n = 0, \ell = 1\rangle$

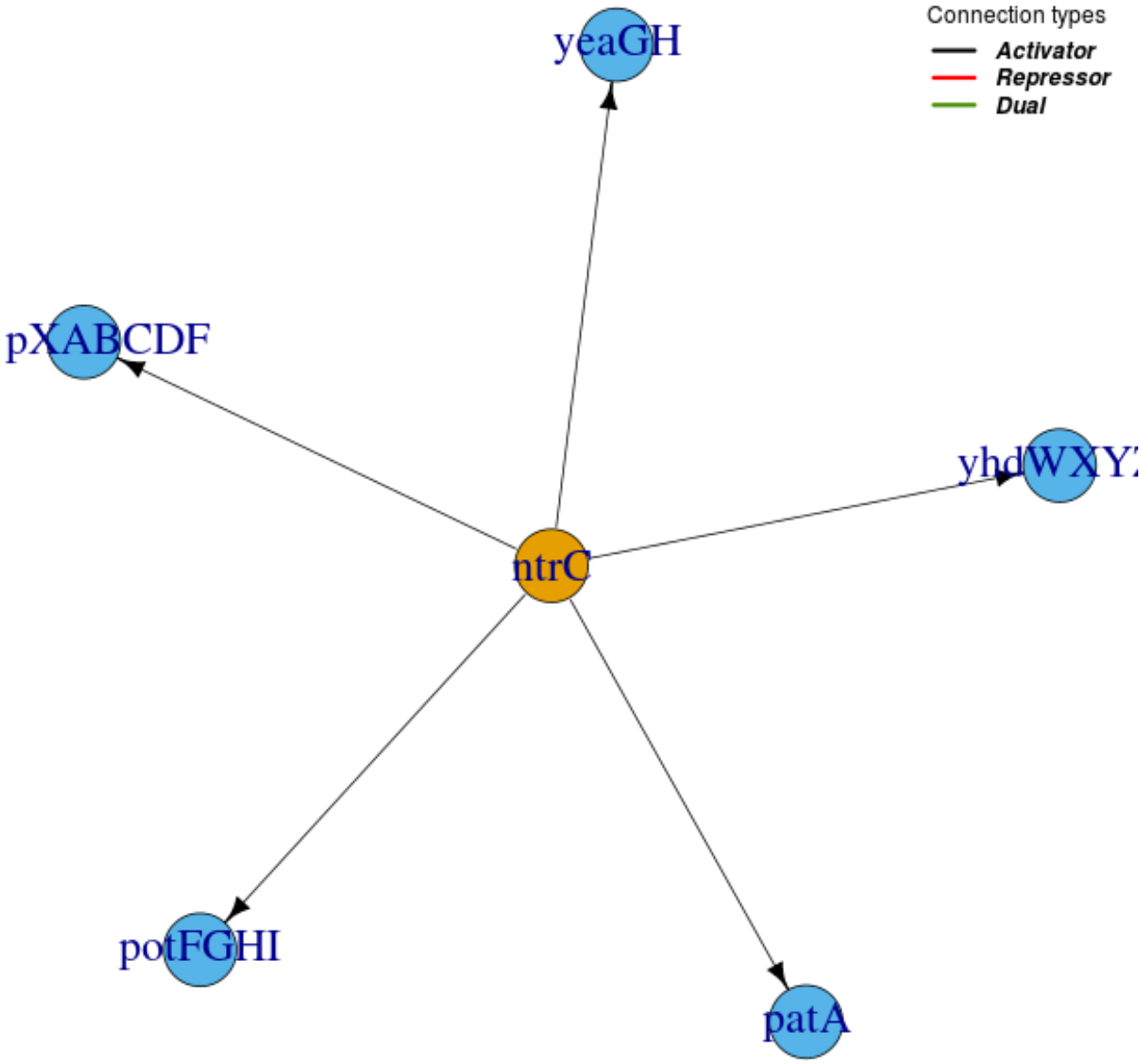

Id = 48

$|n = 0, \ell = 1\rangle$

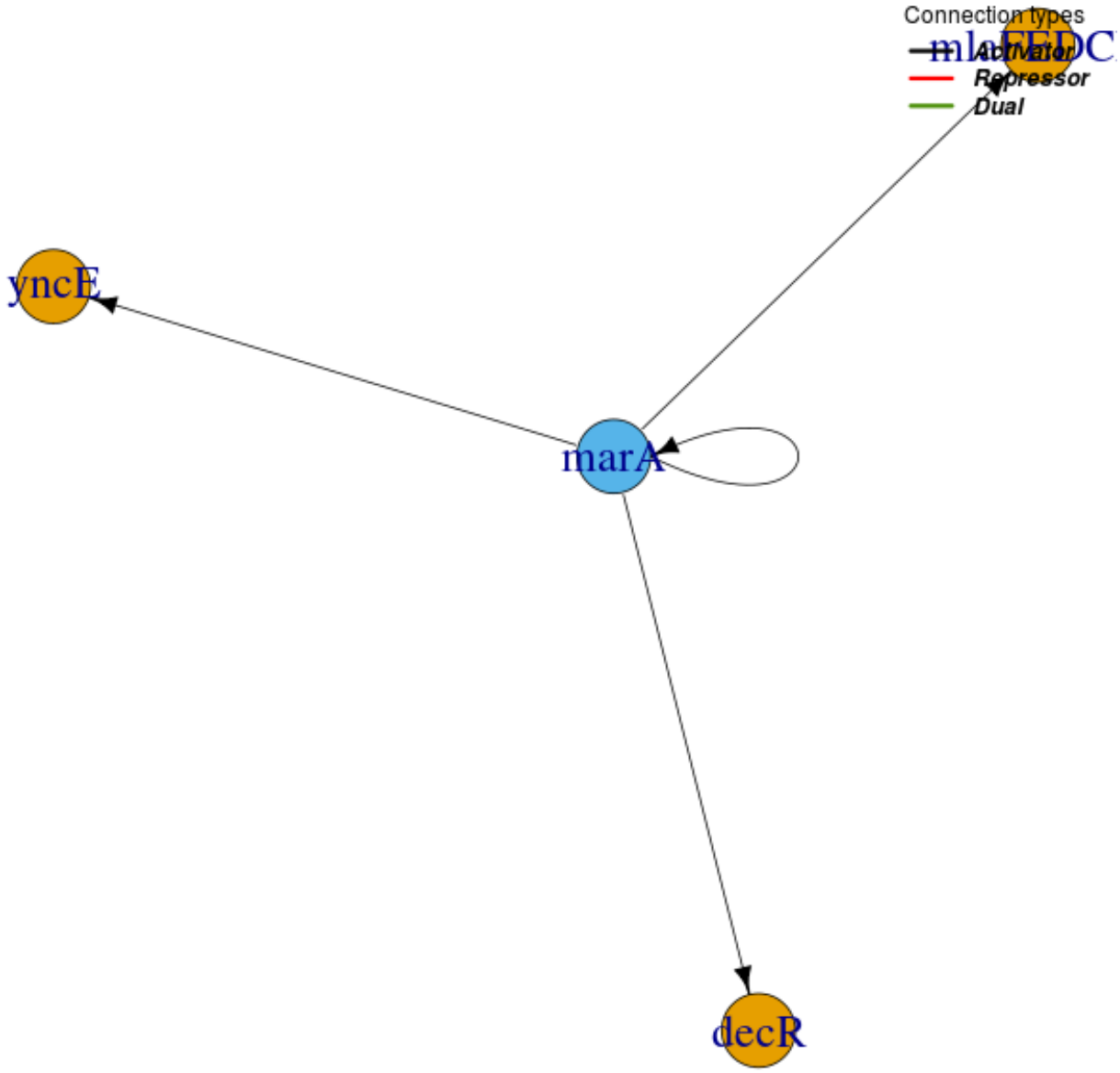

Id = 49

$|n = 0, \ell = 1\rangle$

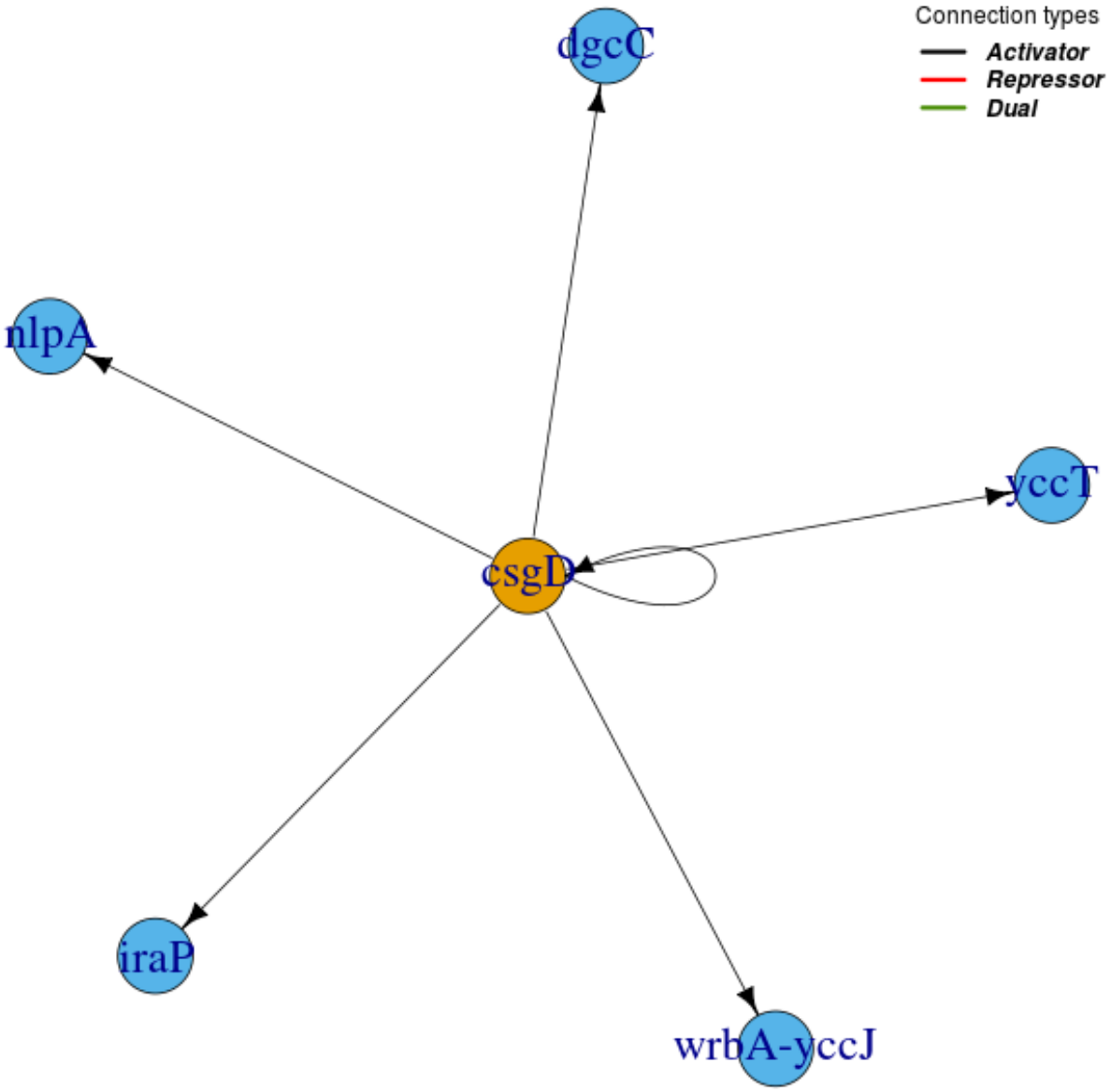

Id = 50

$|n = 0, \ell = 1\rangle$

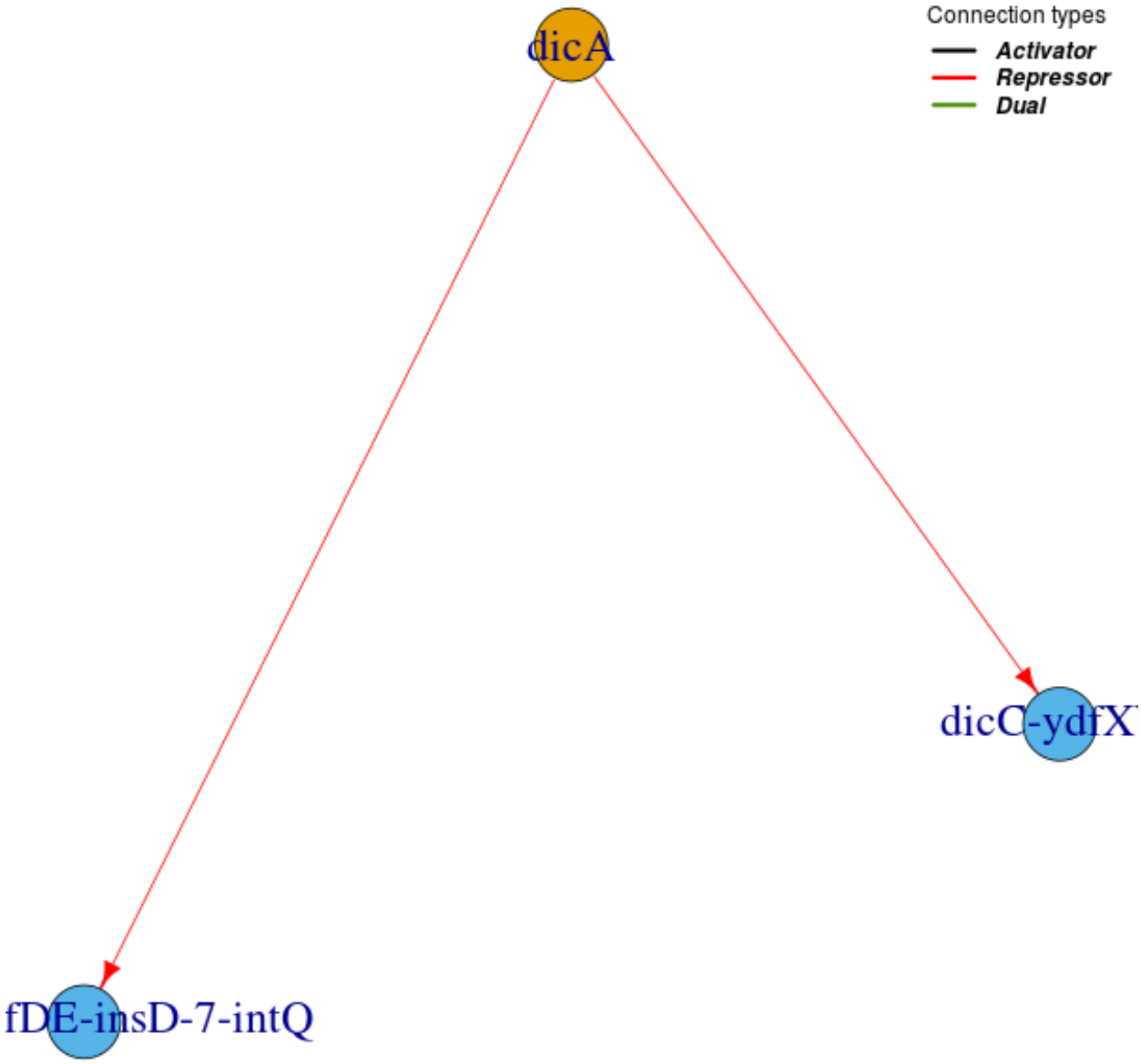

Id = 51

$|n = 1, \ell = 1\rangle$

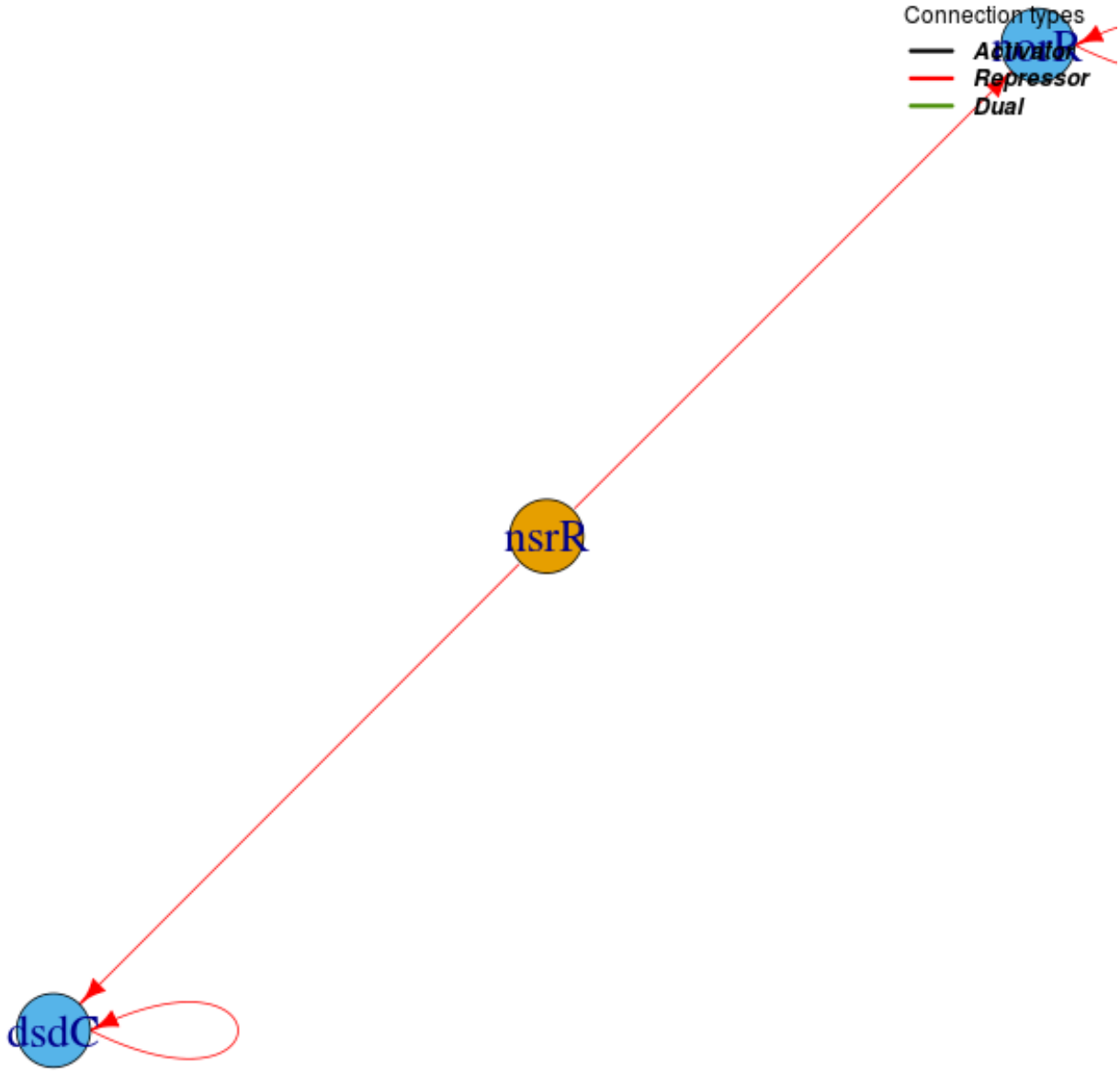

Id = 52

$|n = 0, \ell = 1\rangle$

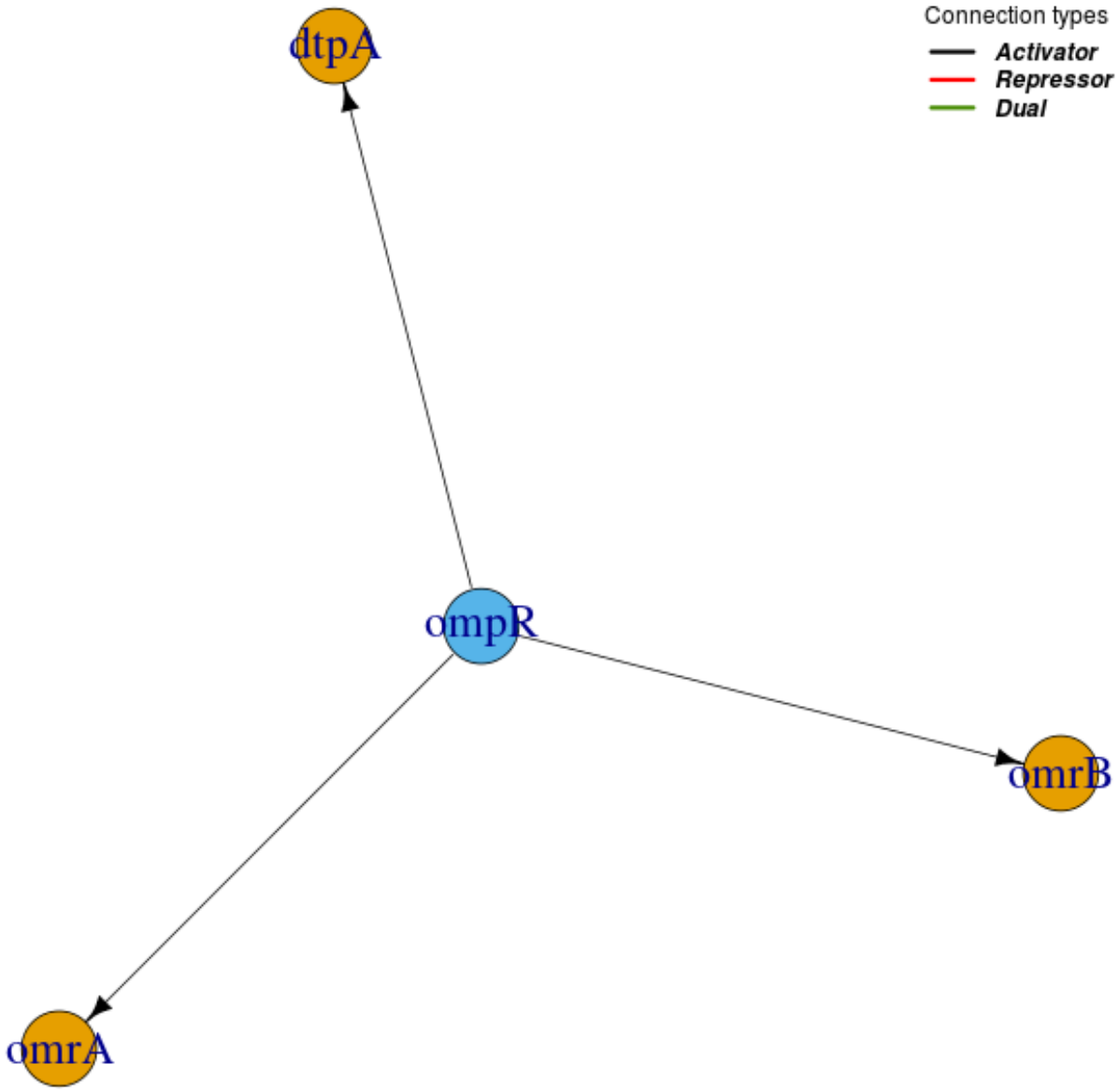

Id = 53

$|n = 0, \ell = 1\rangle$

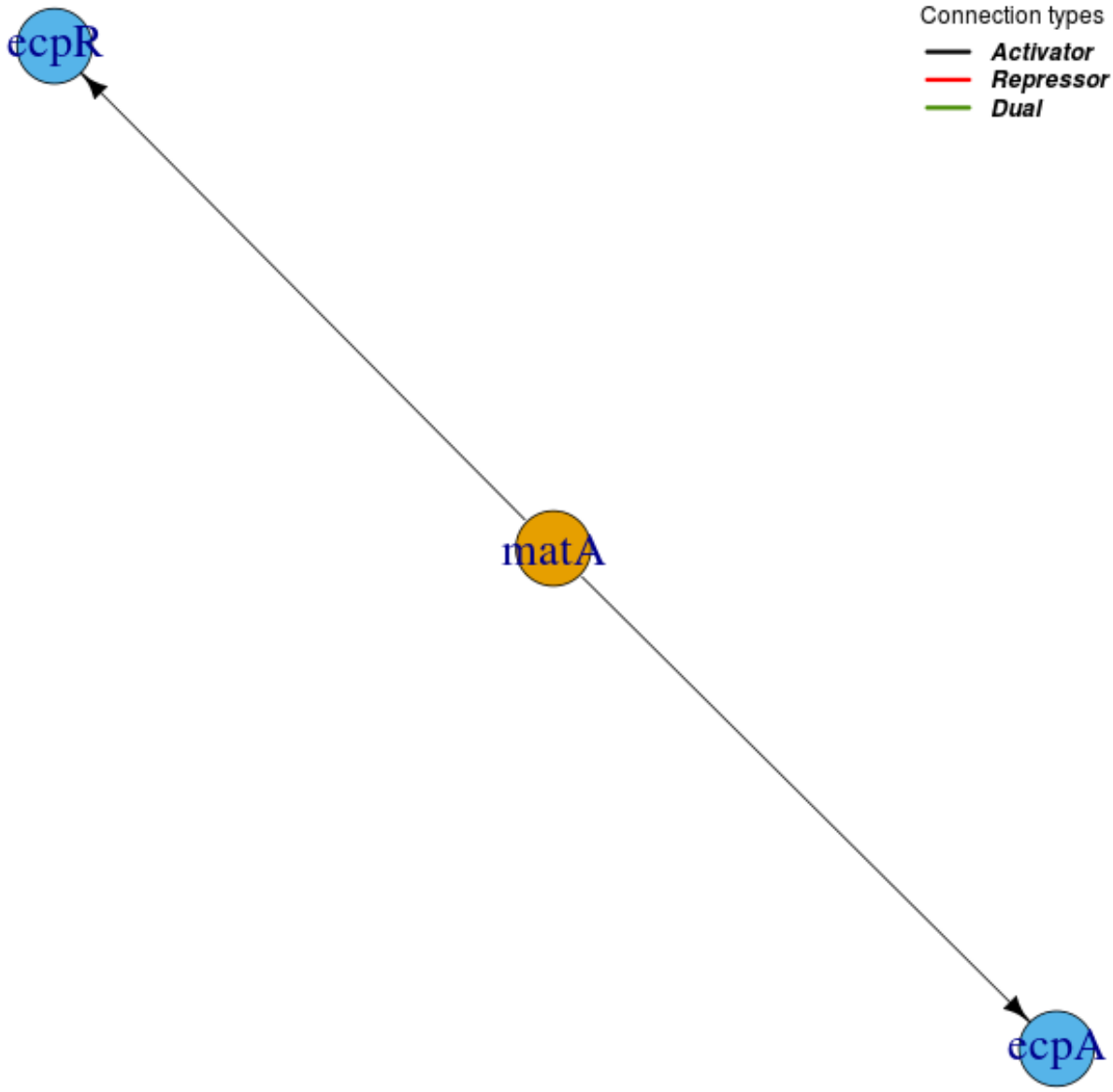

Id = 54

$|n = 0, \ell = 1\rangle$

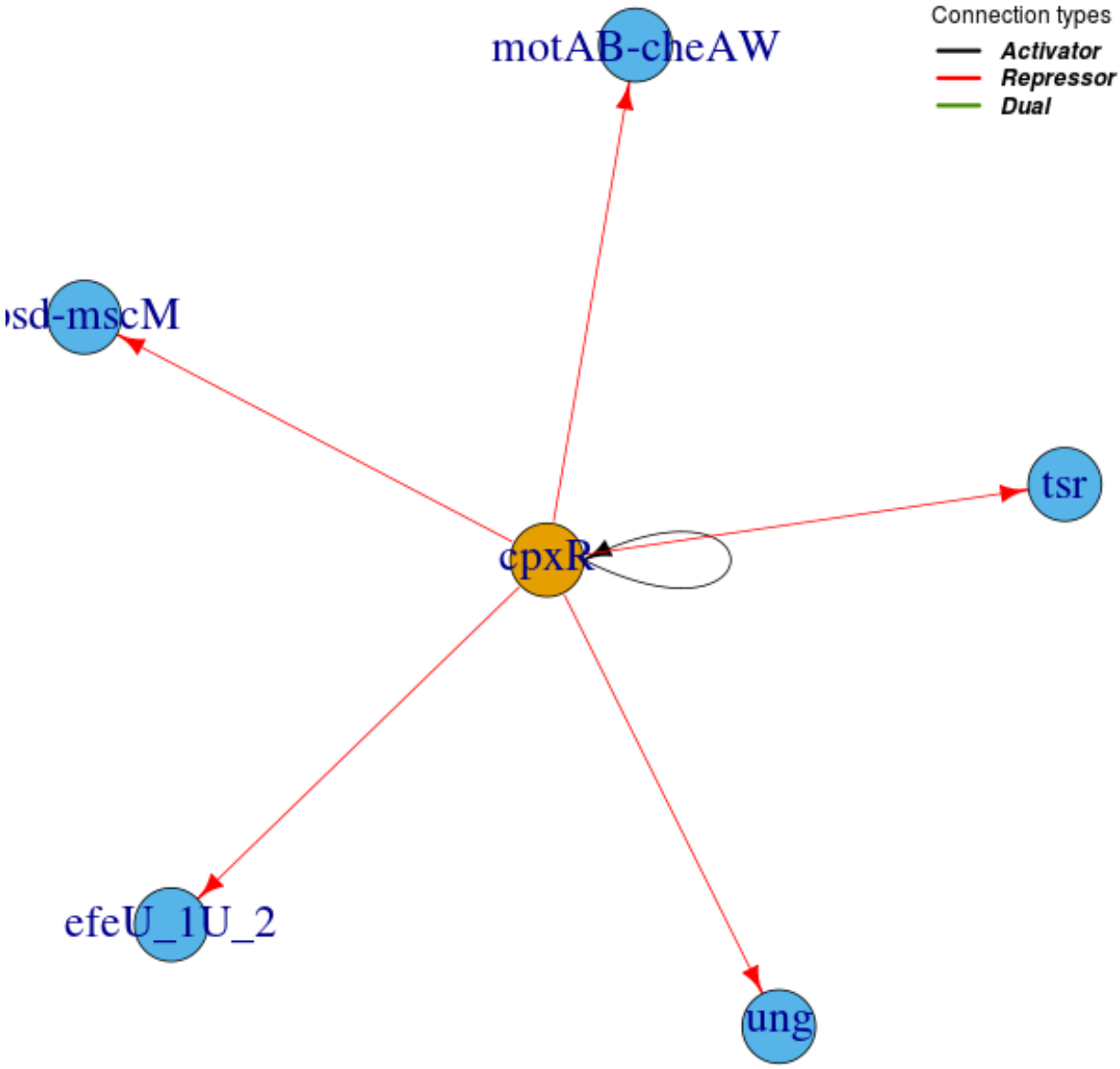

Id = 55

$|n = 0, \ell = 2\rangle$

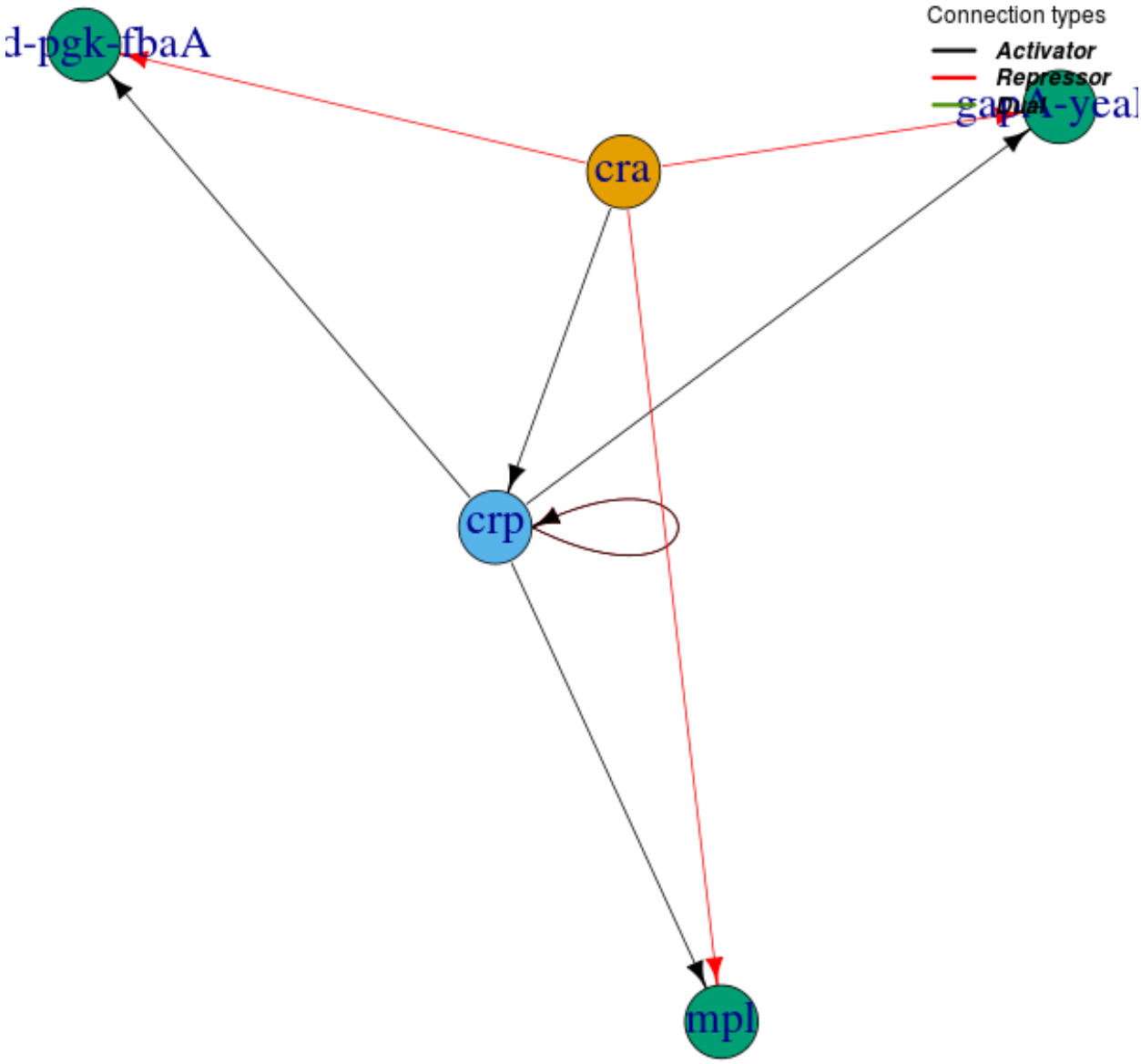

Id = 56

$|n = 1, \ell = 0\rangle$

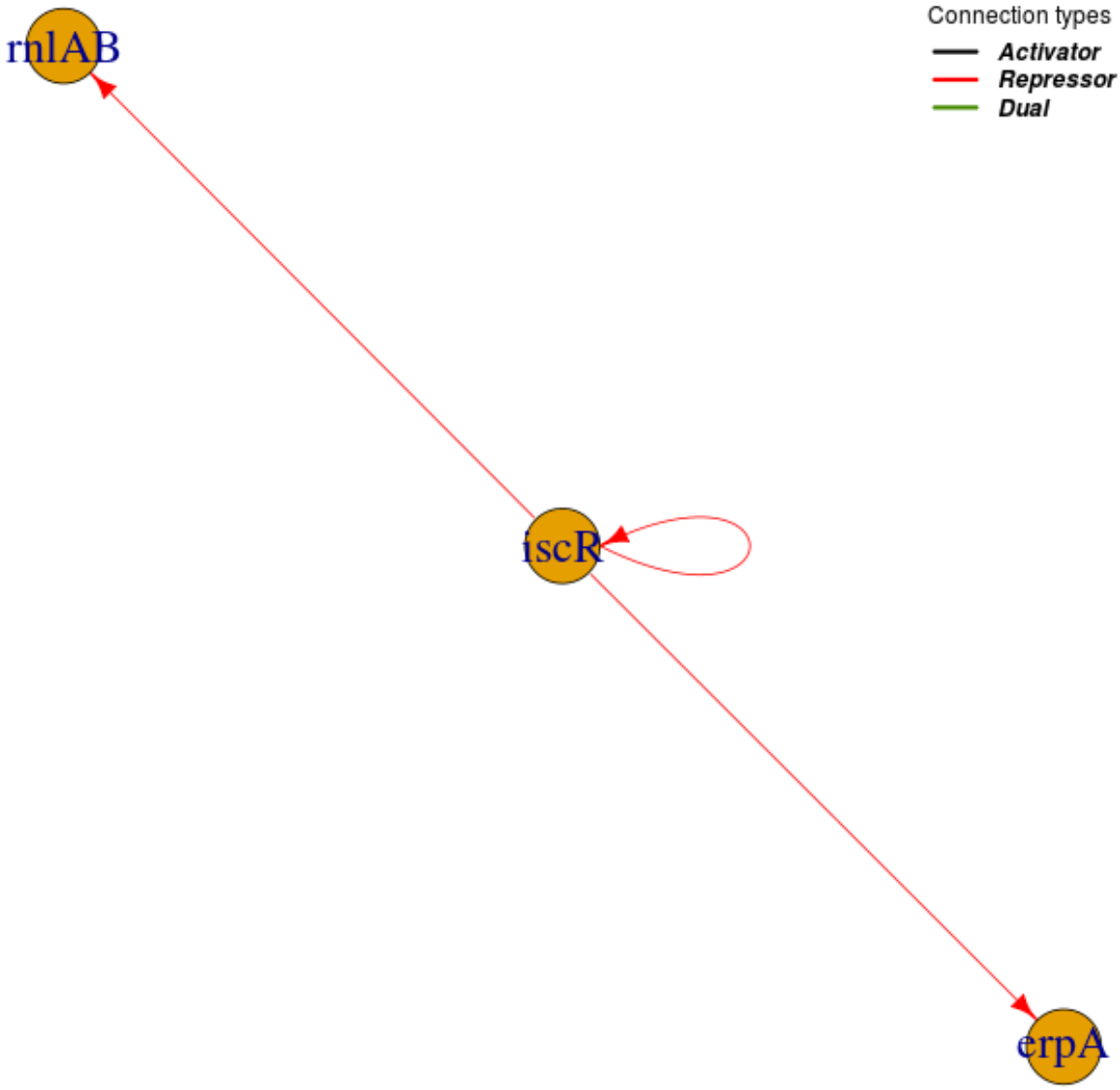

Id = 57

$|\varphi_d = 1.3802..., \ell = 1\rangle$

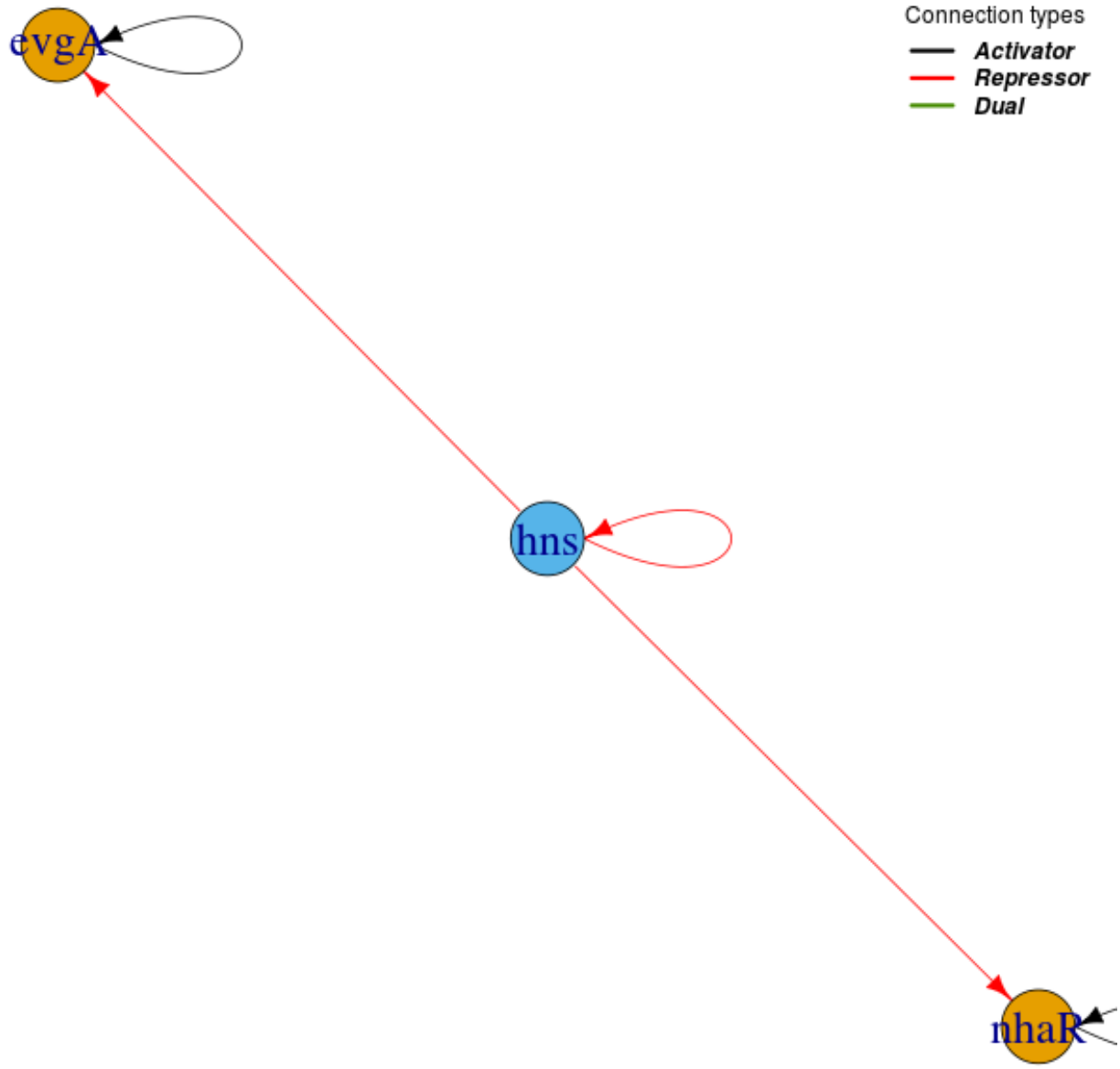

Id = 58

$|n = 0, \ell = 2\rangle$

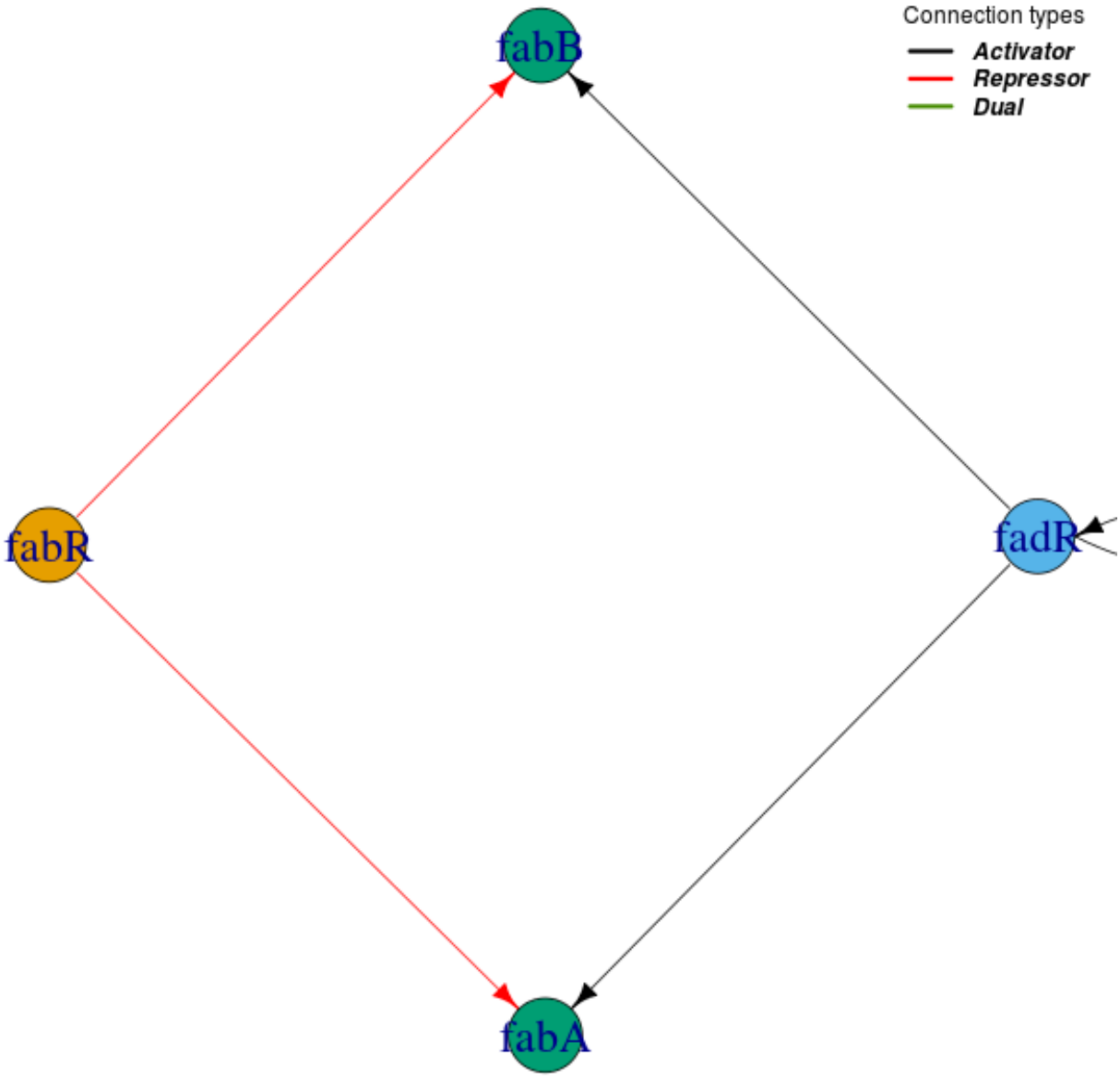

Id = 59

$|n = 0, \ell = 2\rangle$

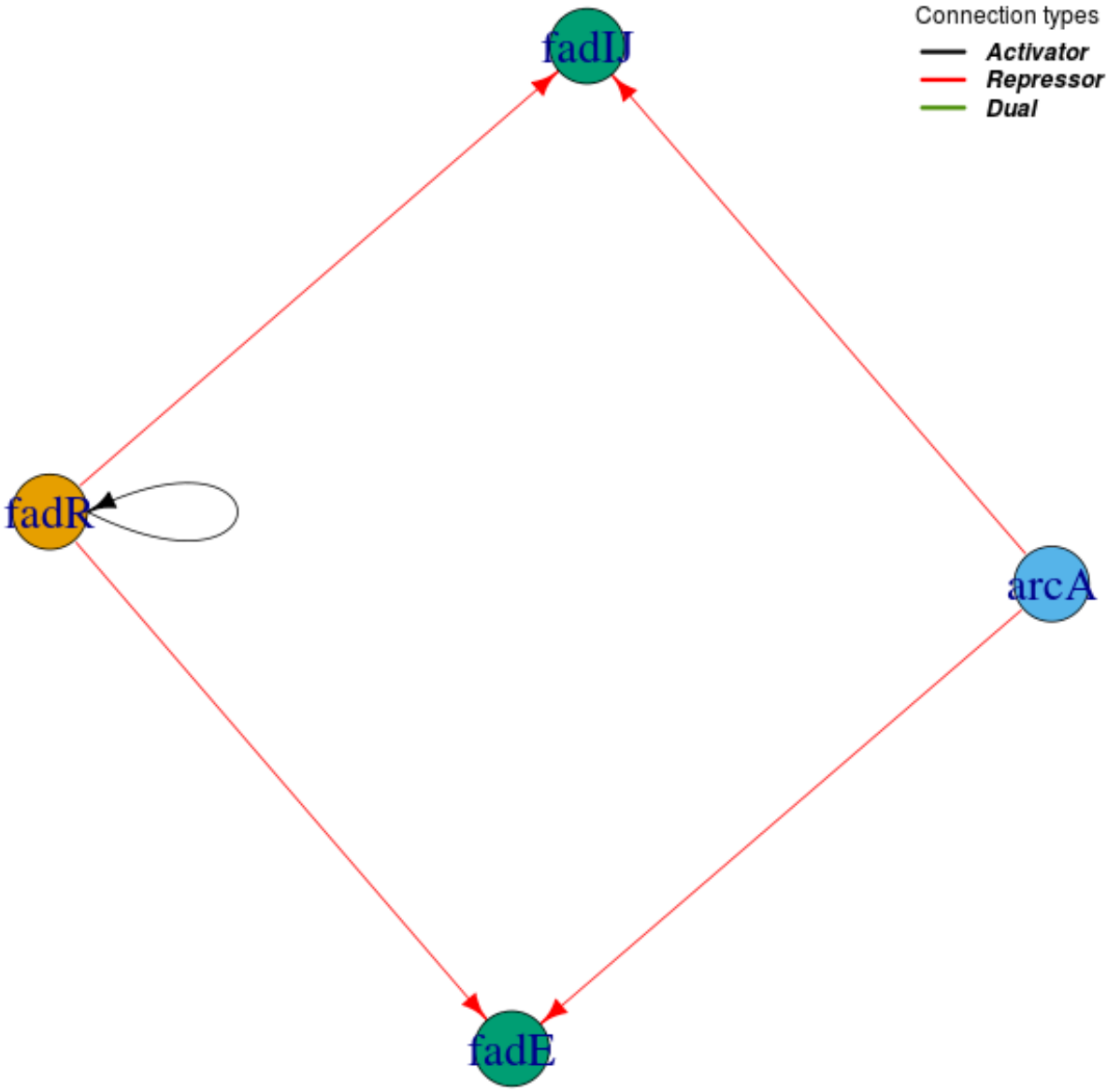

Id = 60

$|n = 0, \ell = 1\rangle$

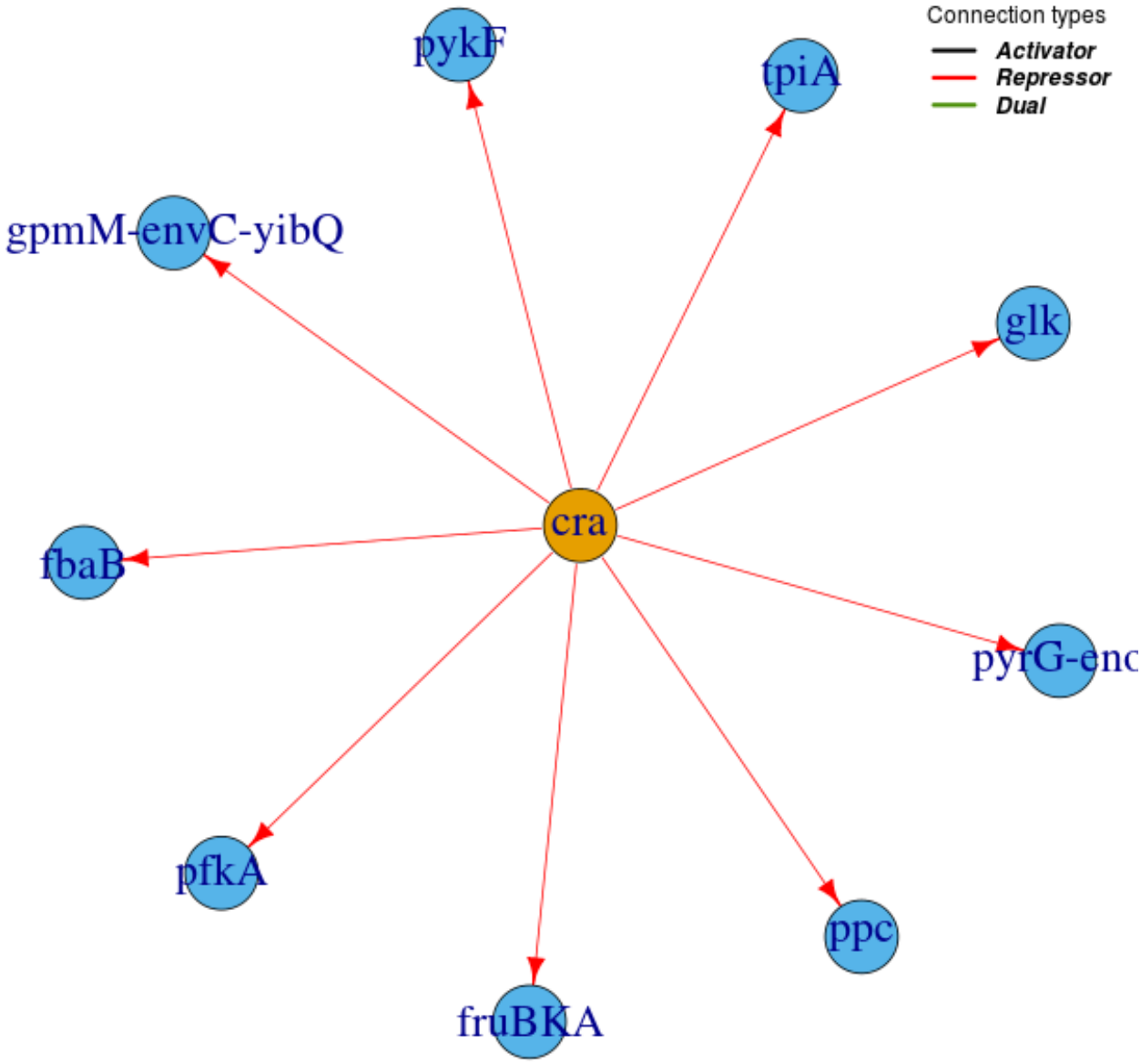

Id = 61

$|n = 0, \ell = 1\rangle$

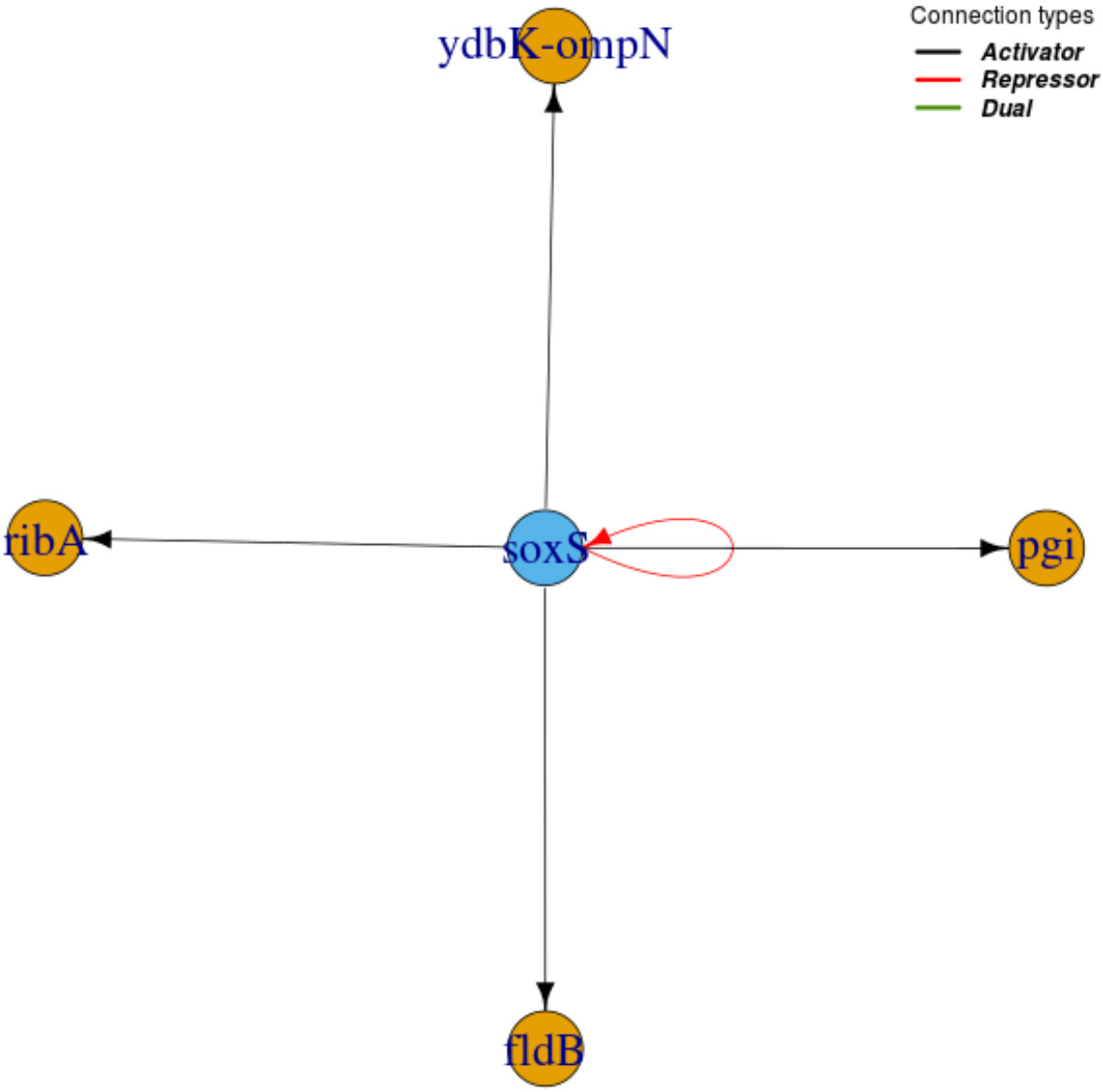

Id = 62

$|n = 0, \ell = 1\rangle$

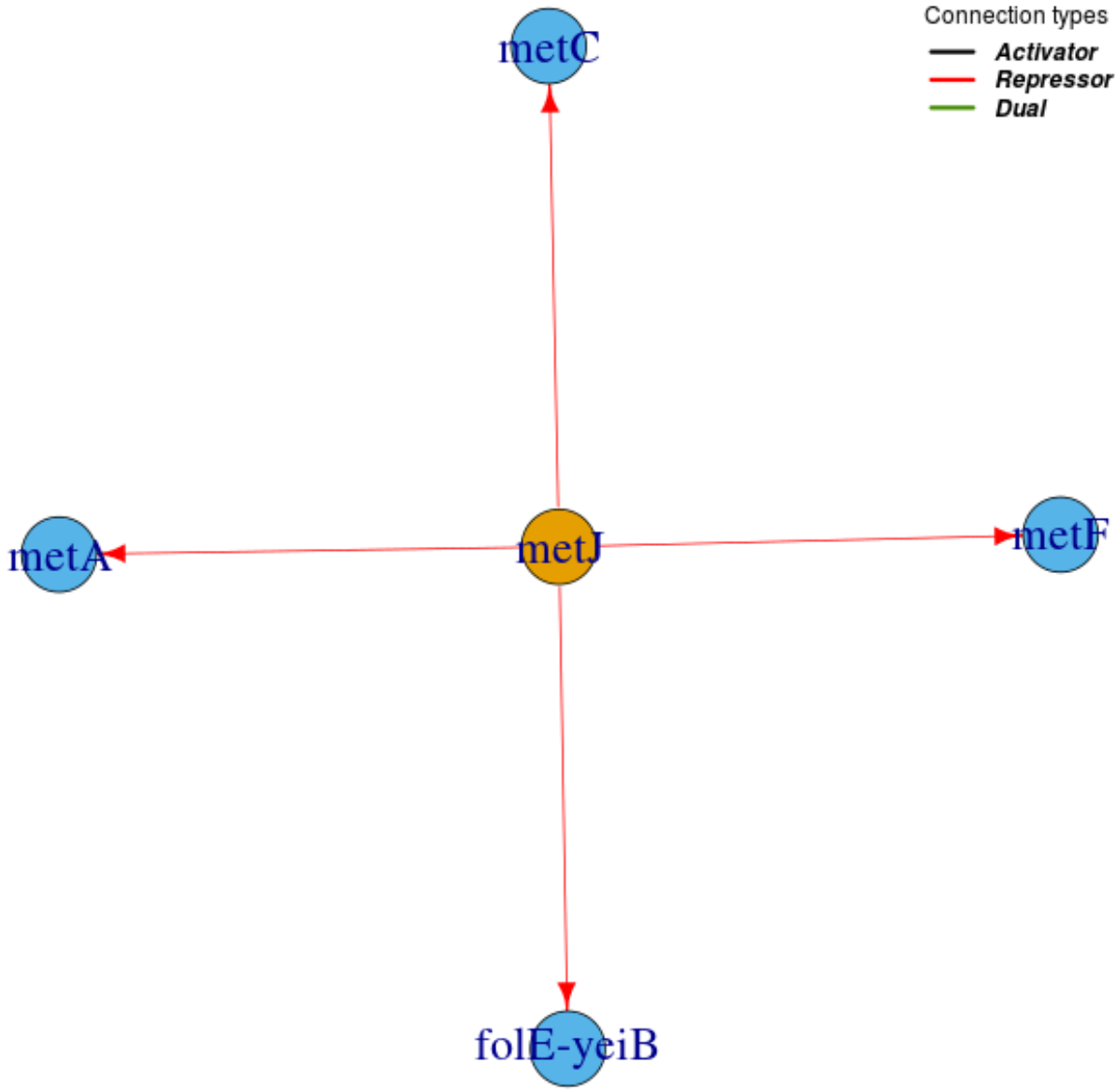

Id = 63

$|n = 0, \ell = 2\rangle$

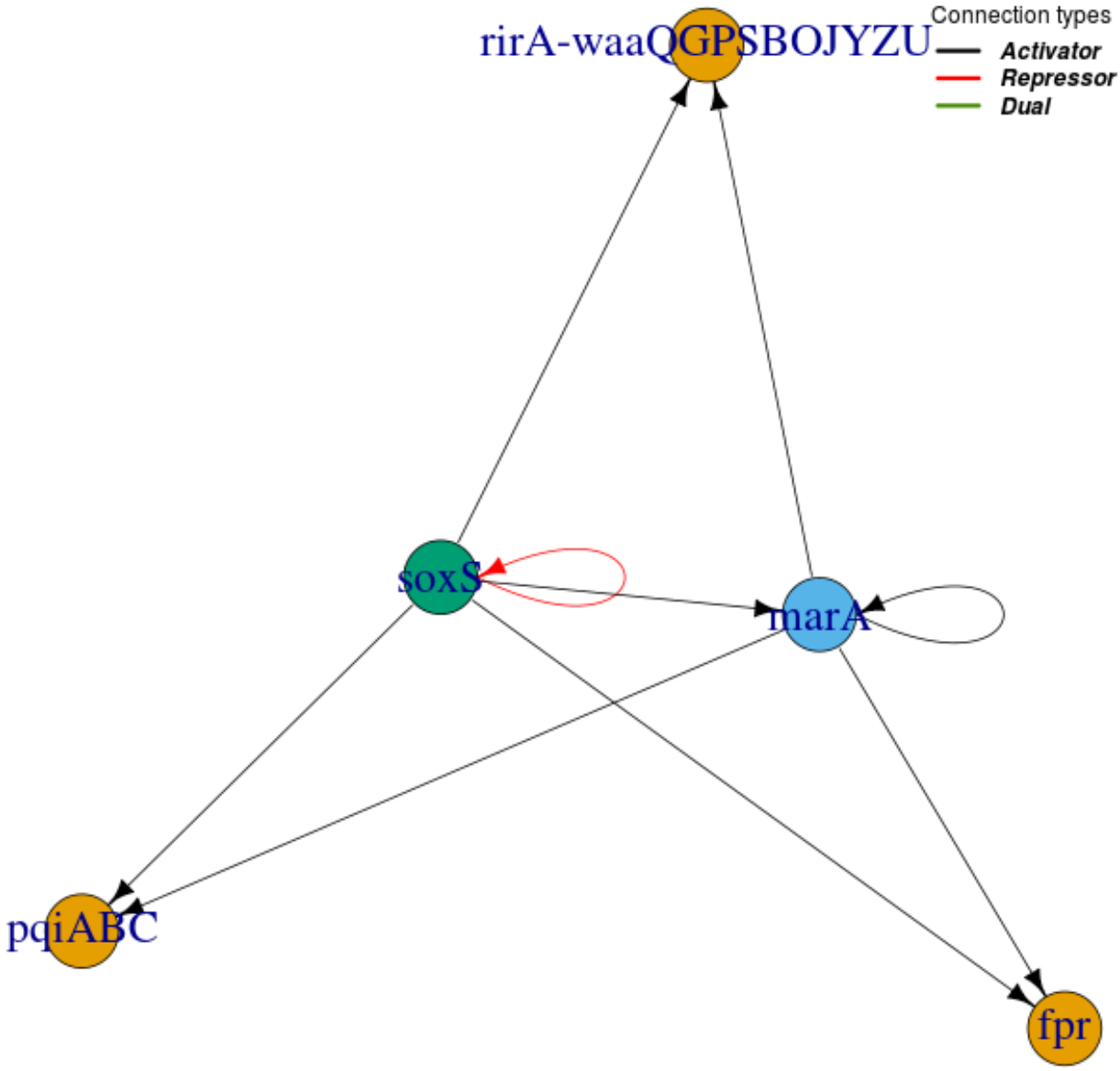

Id = 64

$|n = 1, \ell = 1\rangle$

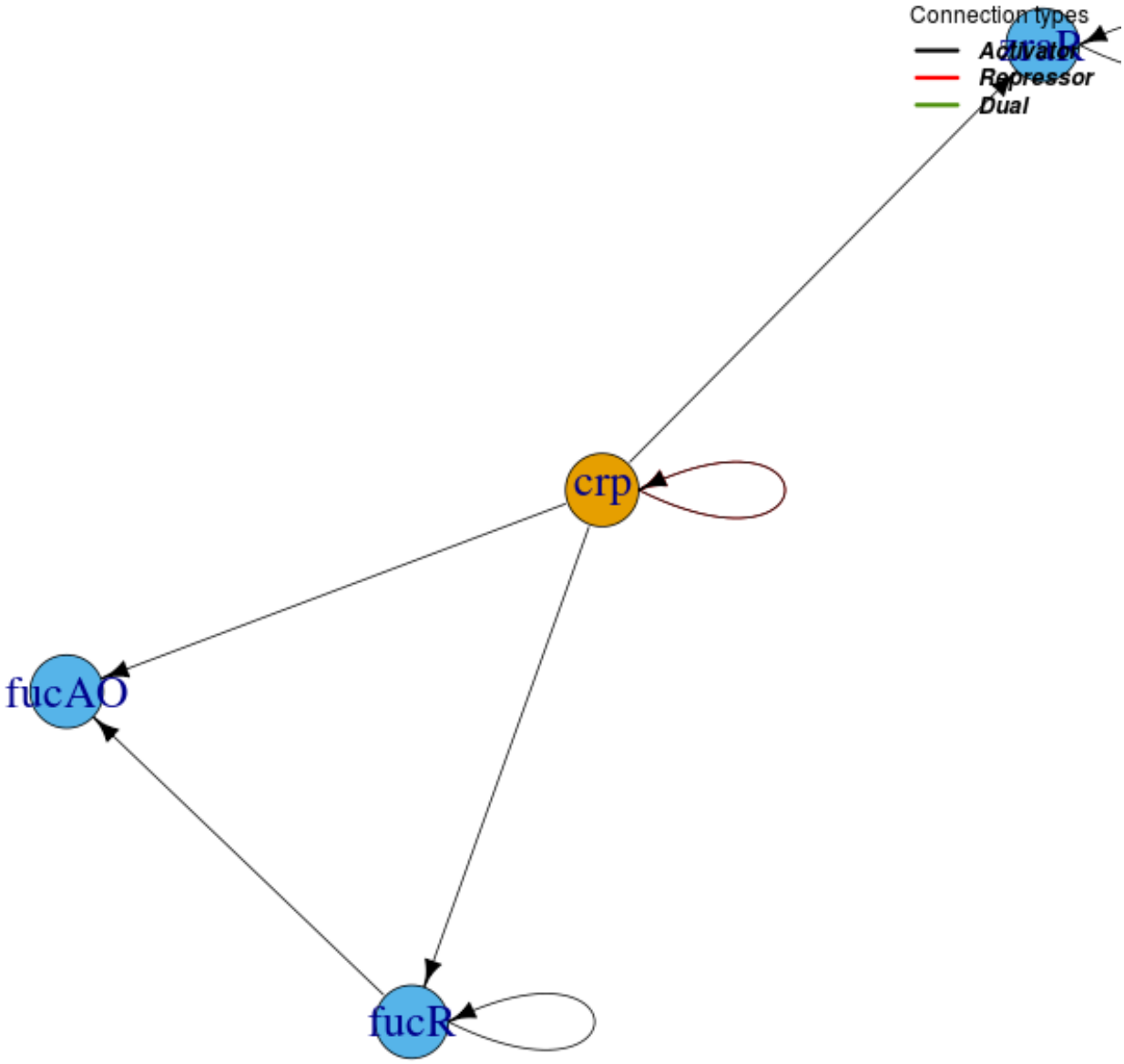

Id = 65

$|n = 0, \ell = 1\rangle$

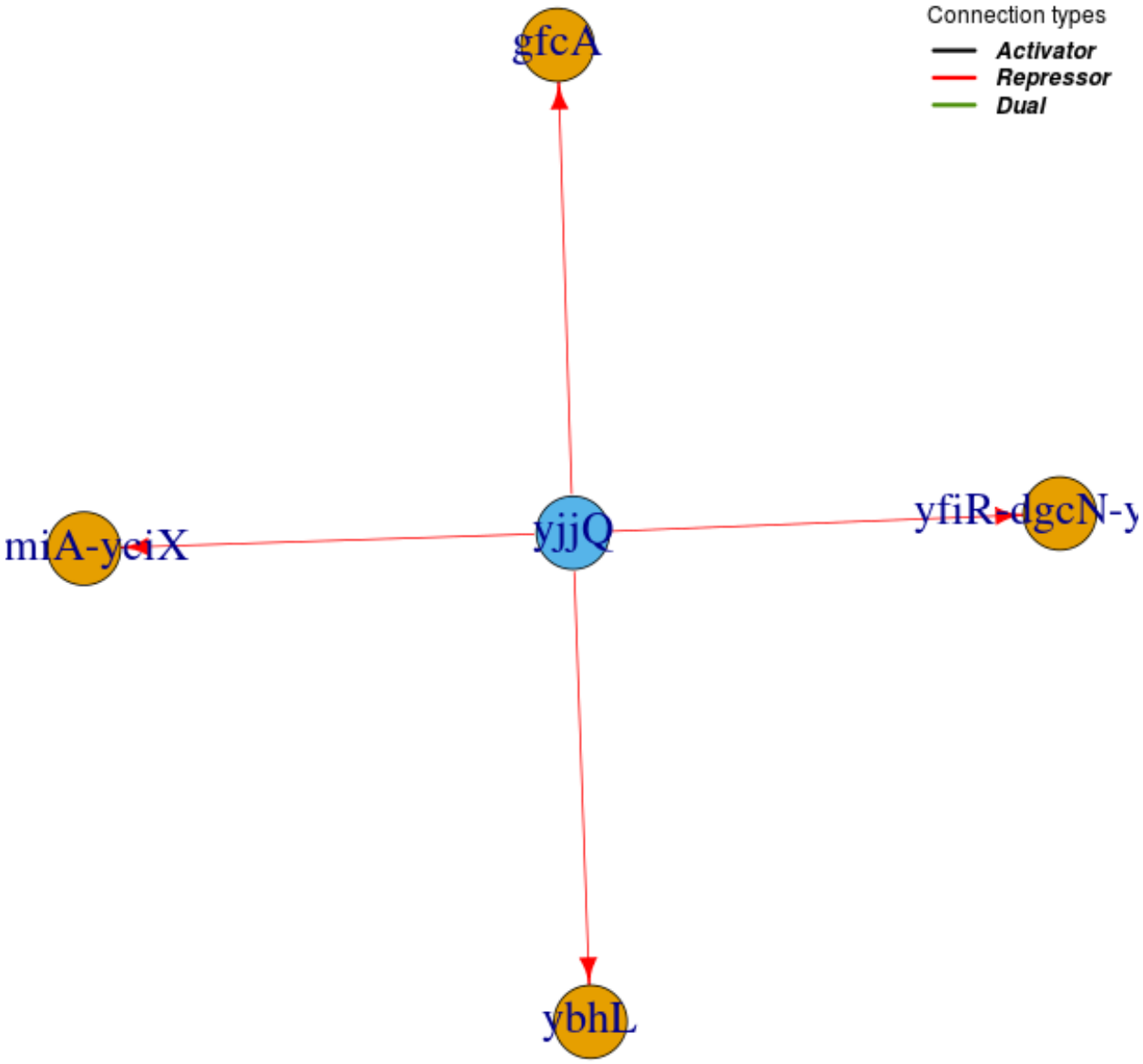

Id = 66

$|n = 0, \ell = 2\rangle$

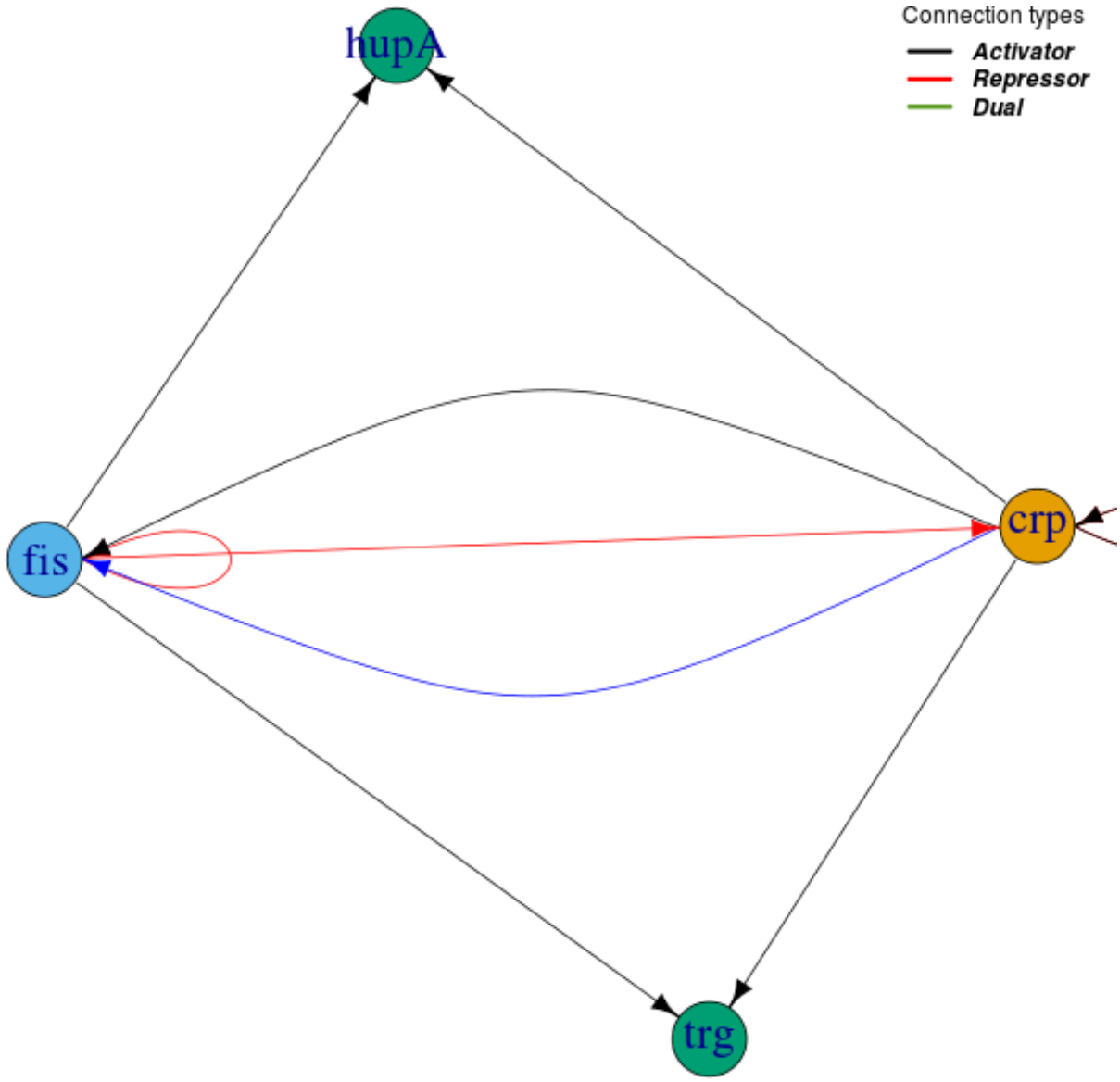

Id = 67

$|n = 0, \ell = 1\rangle$

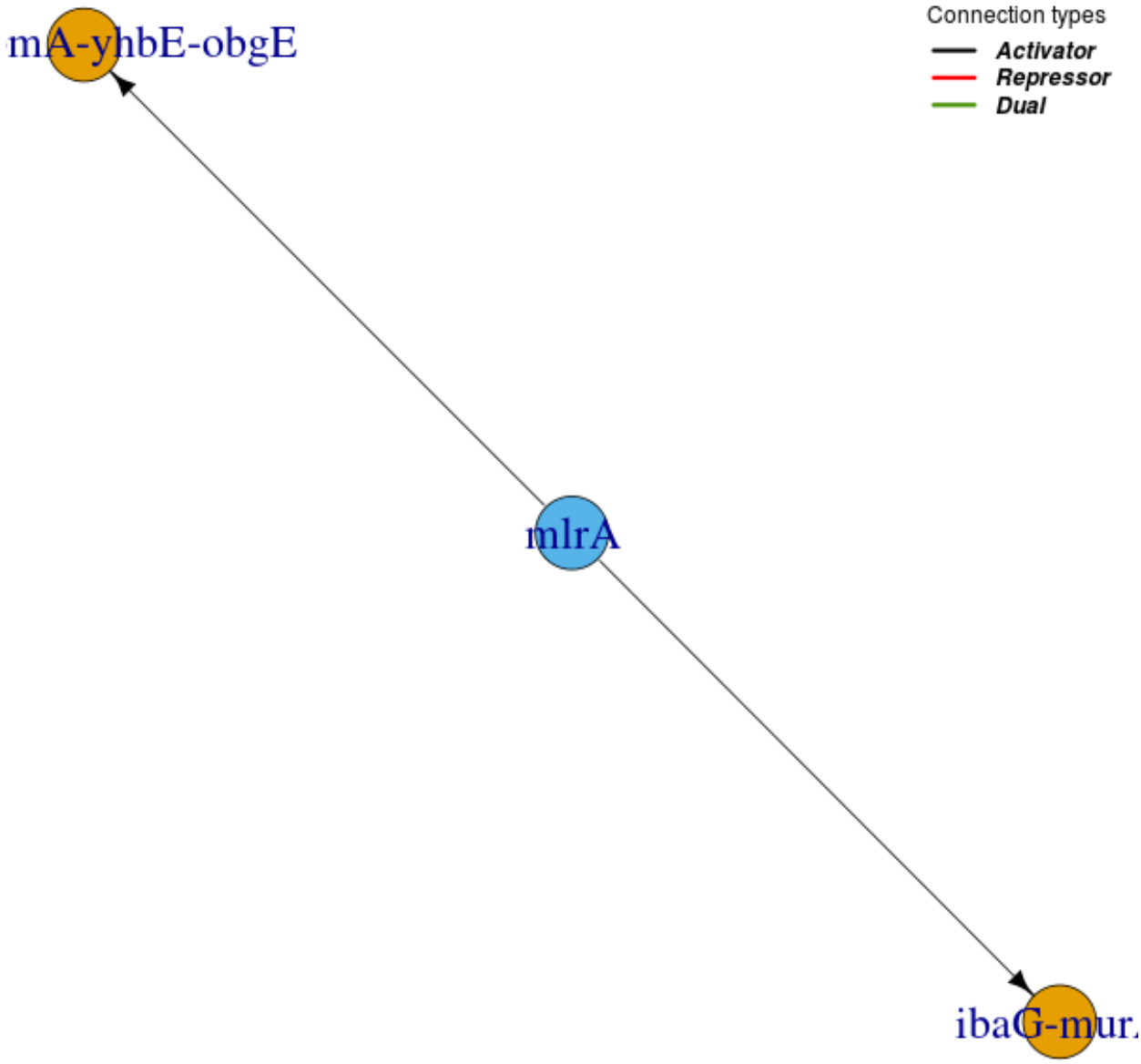

Id = 68

$|n = 0, \ell = 1\rangle$

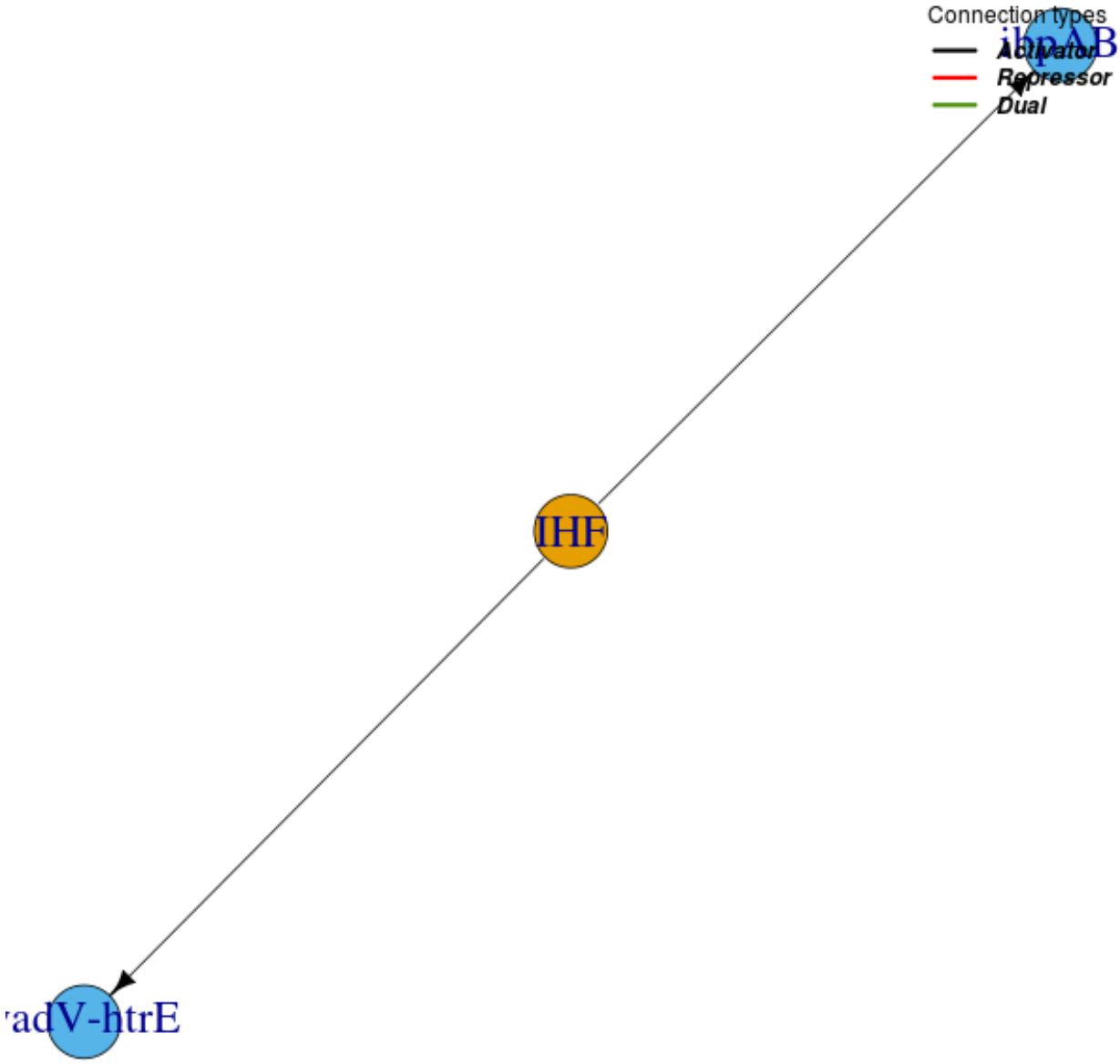

Id = 69

$|n = 1, \ell = 2\rangle$

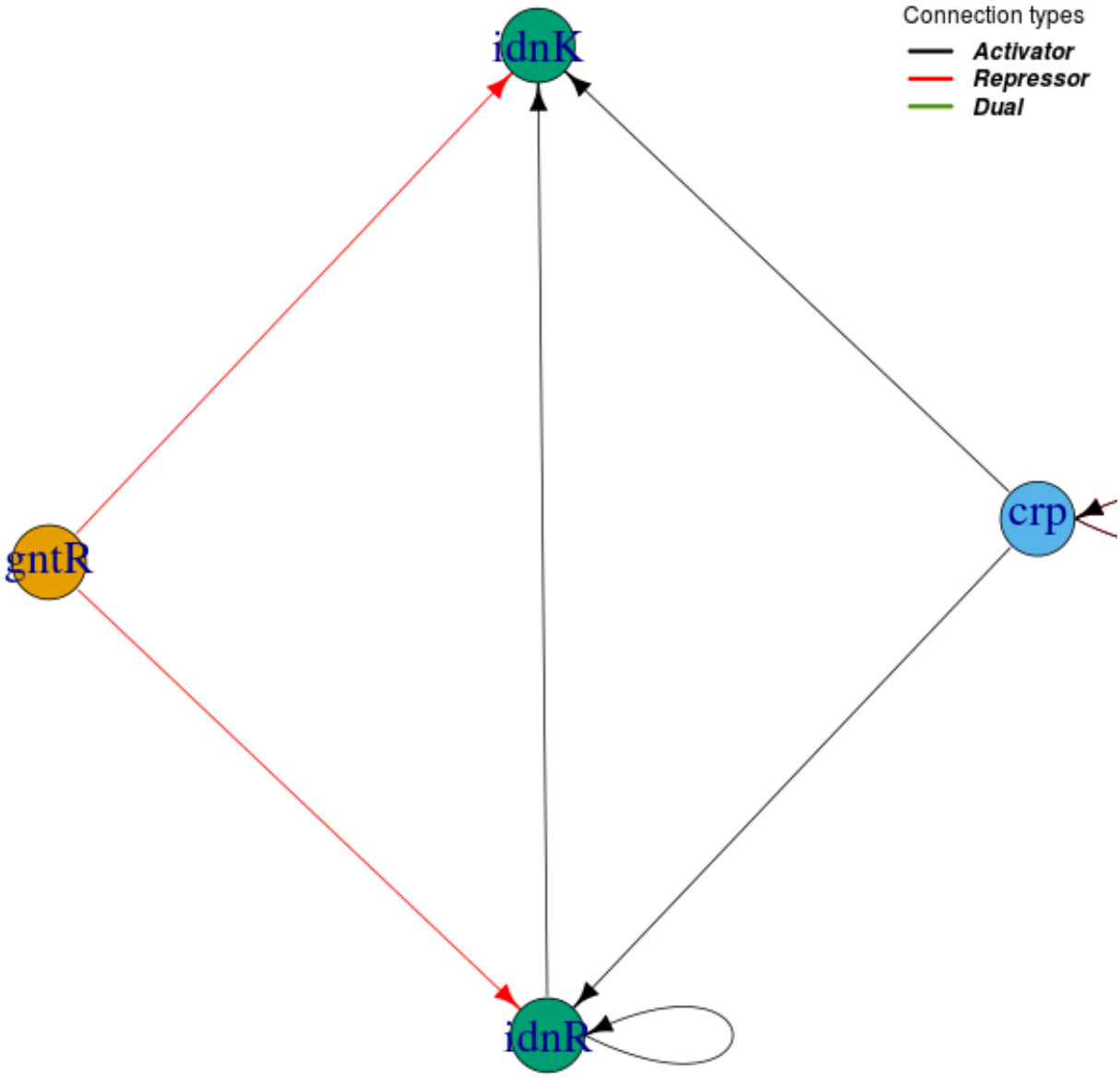

Id = 70

$|n = 0, \ell = 1\rangle$

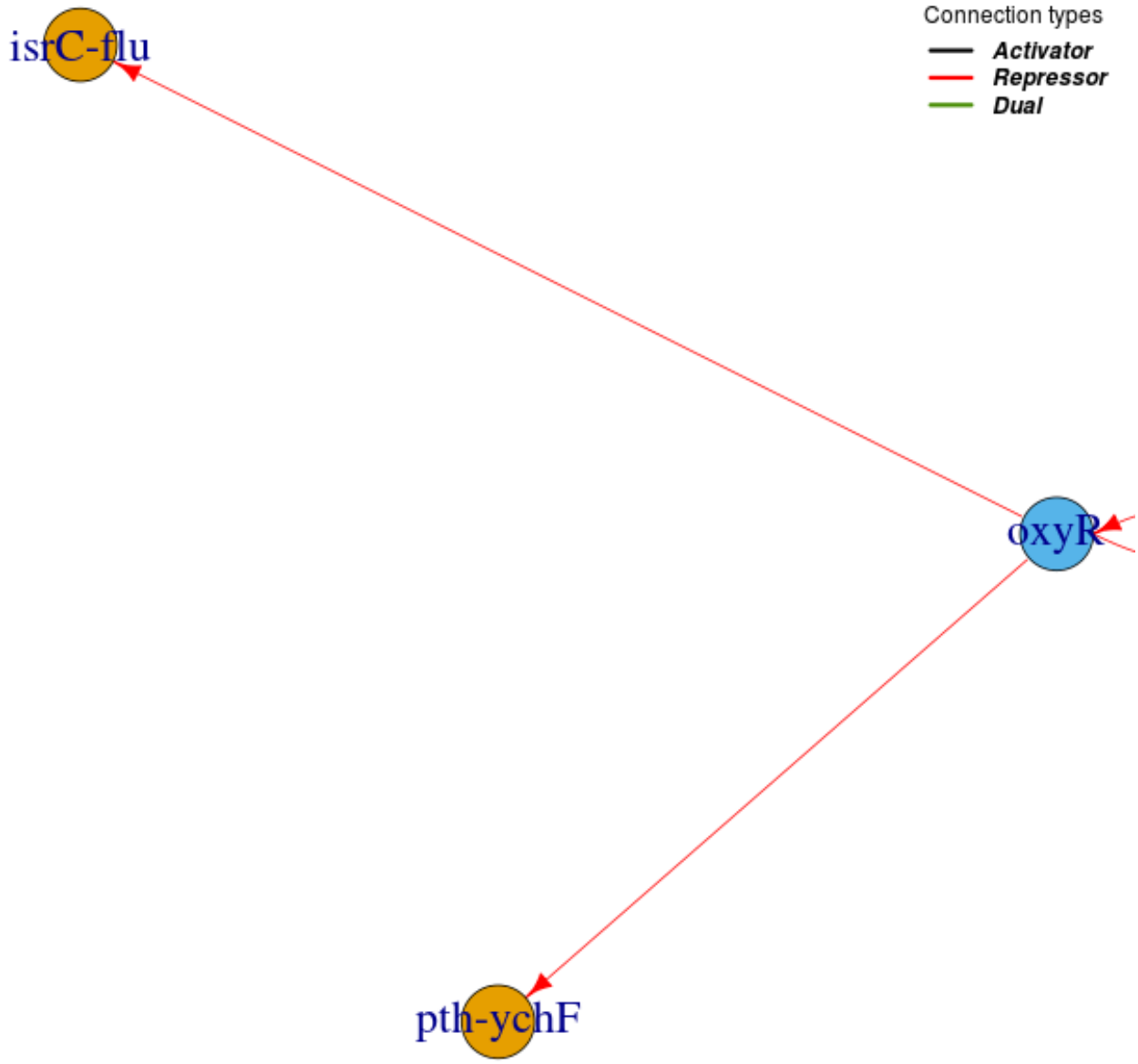

Id = 71

$|\varphi_d = 1.6180..., \ell = 2\rangle$

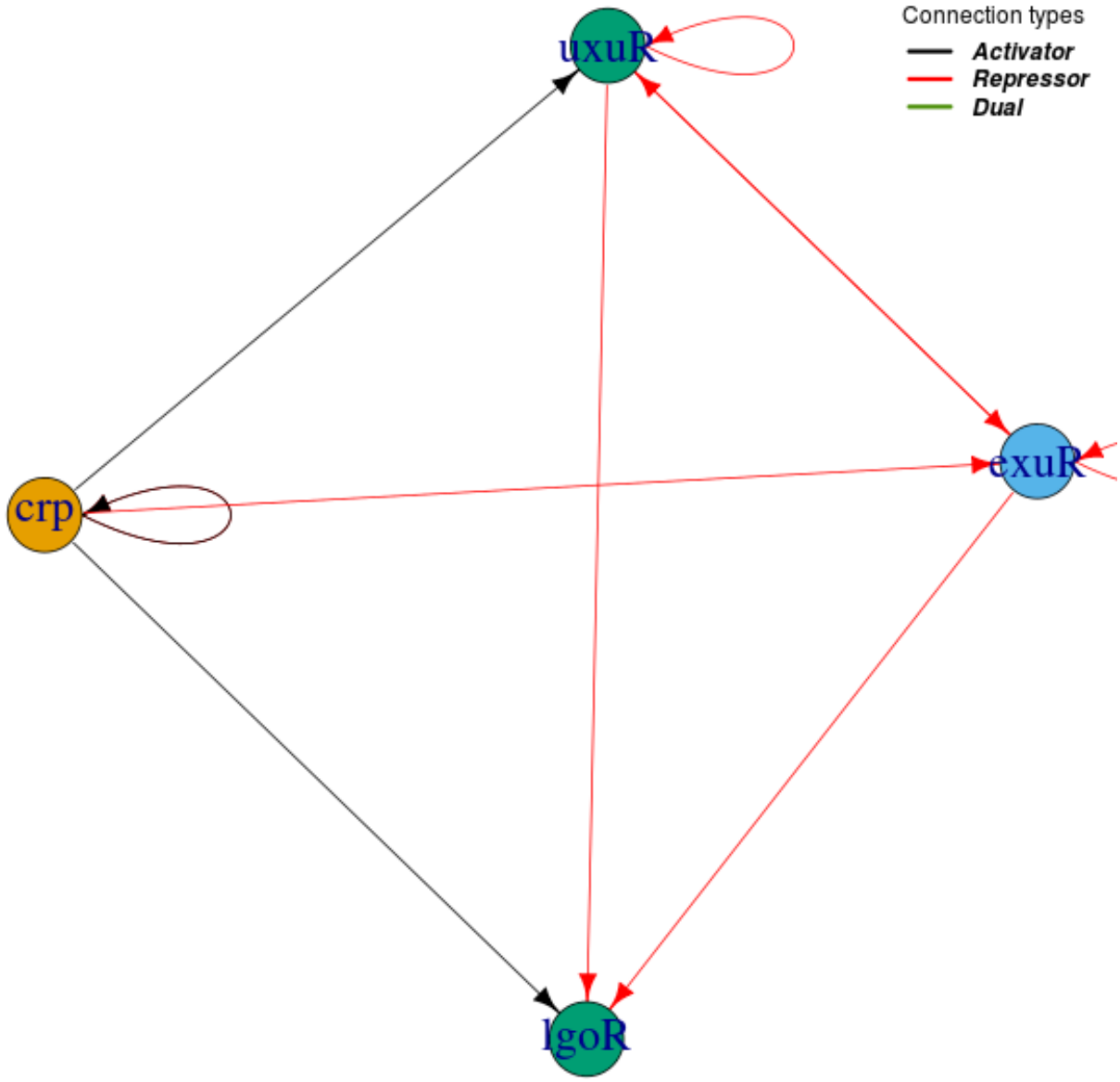

Id = 72

$|n = 0, \ell = 1\rangle$

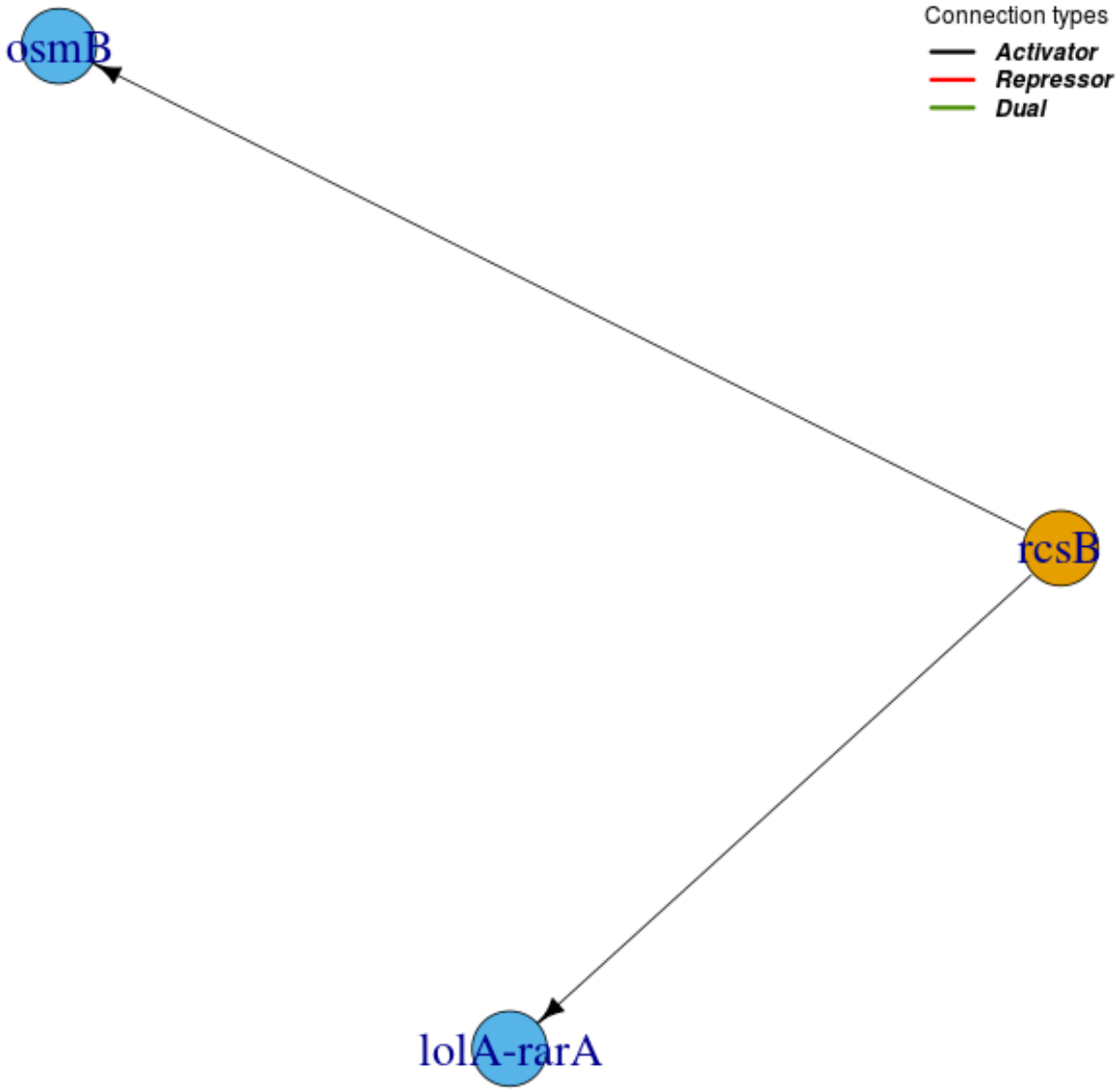

Id = 73

$|n = 1, \ell = 1\rangle$

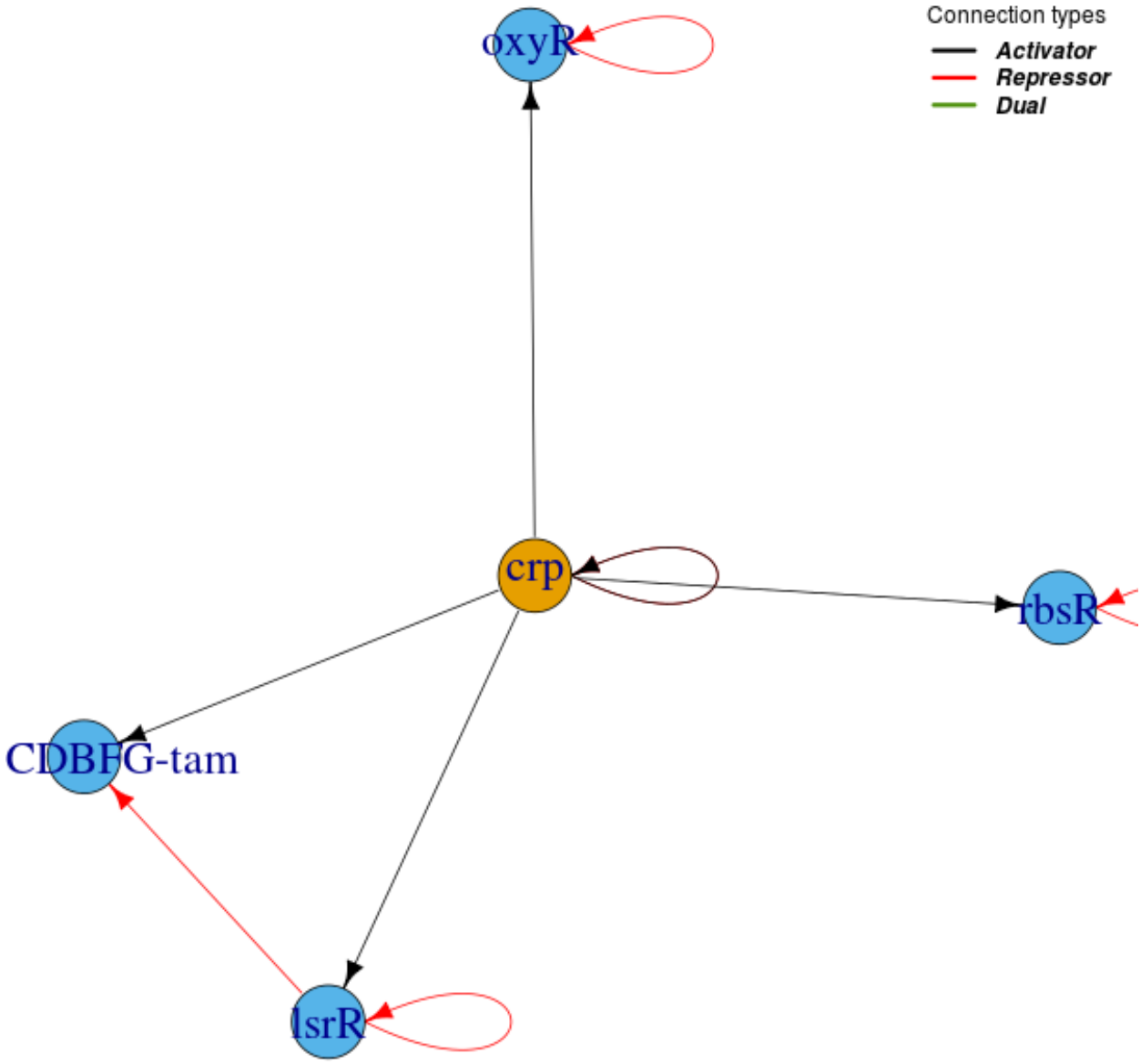

Id = 74

$|n = 1, \ell = 1\rangle$

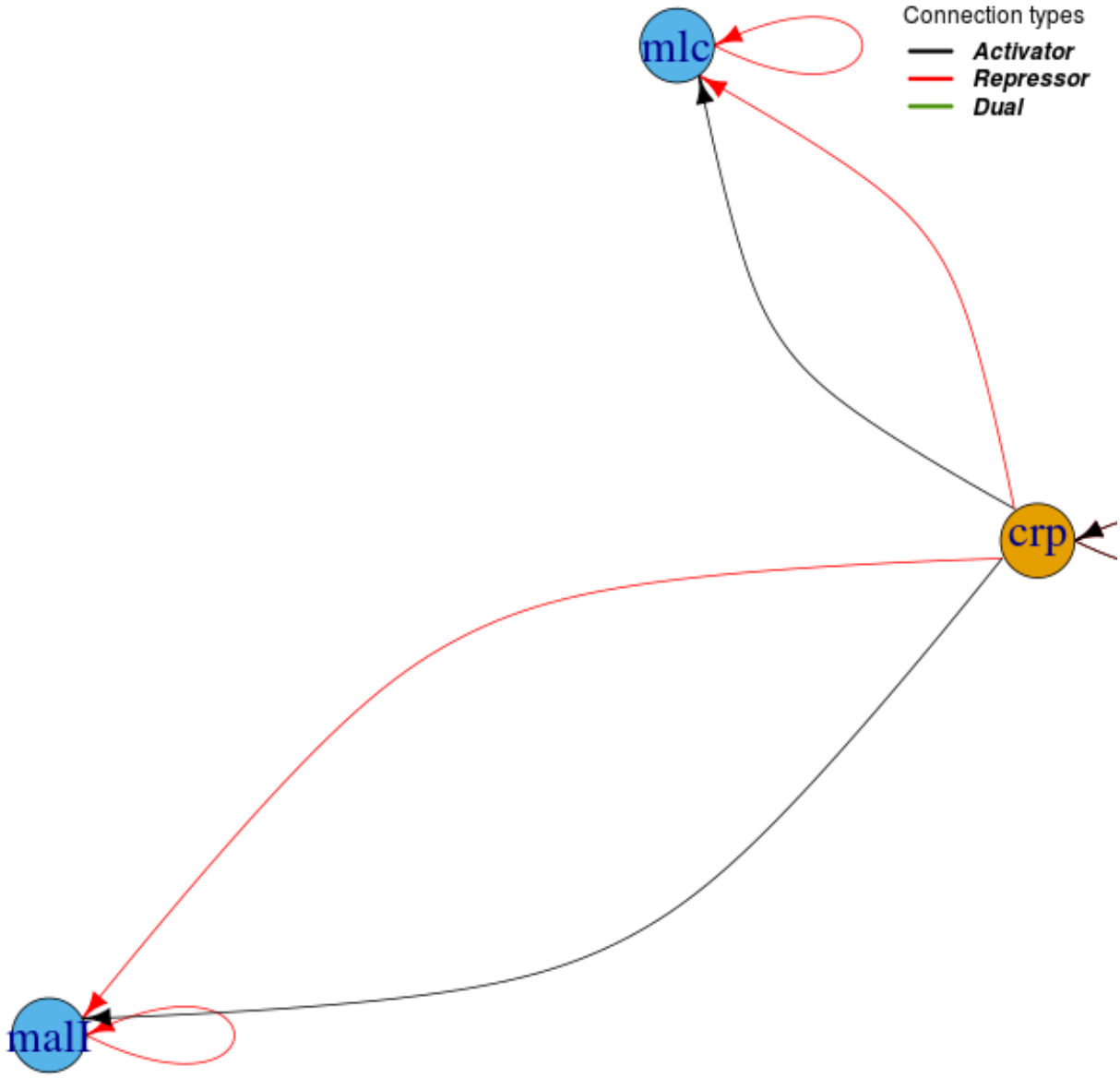

Id = 75

$|n = 0, \ell = 1\rangle$

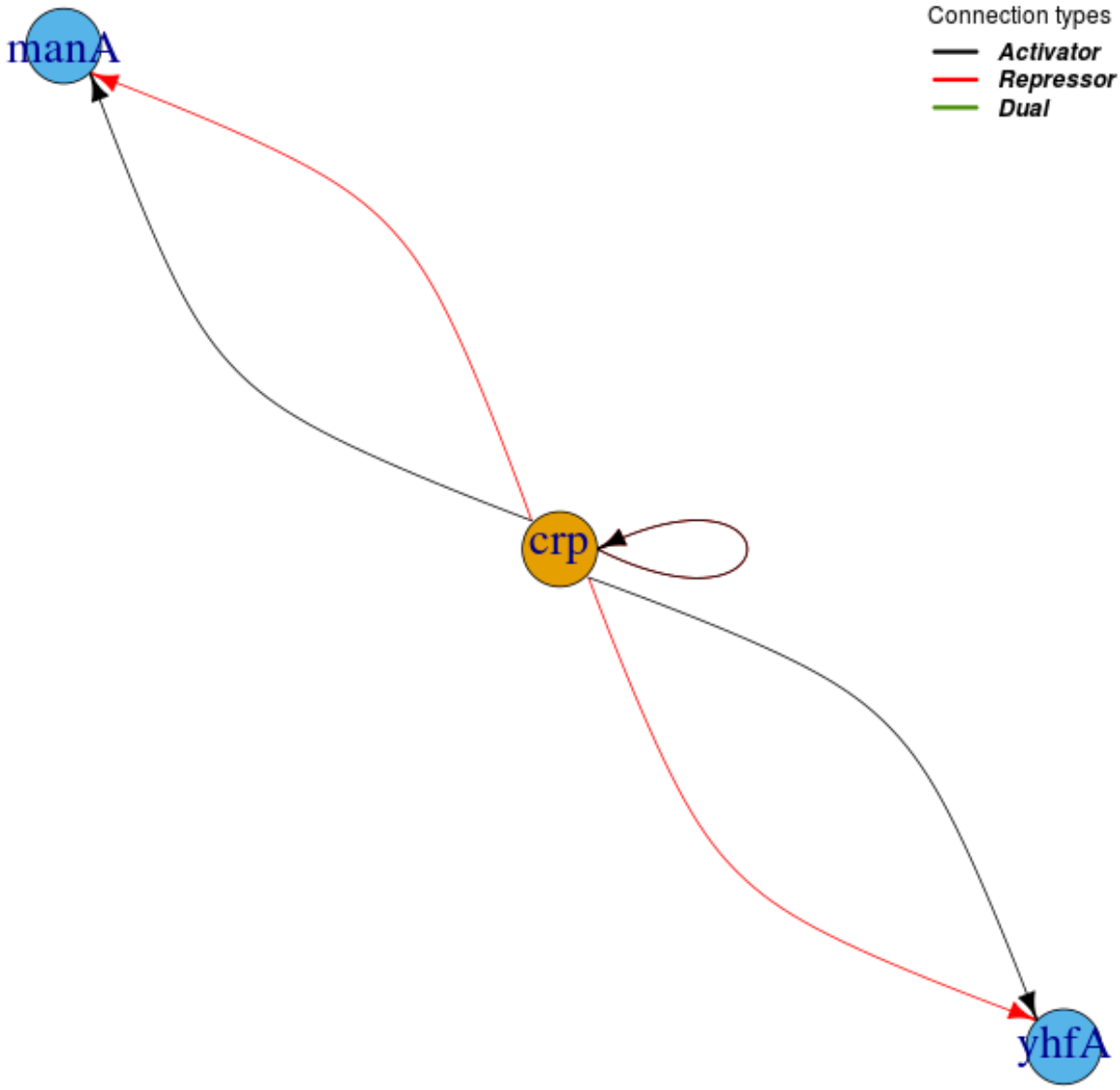

Id = 76

$|n = 1, \ell = 0\rangle$

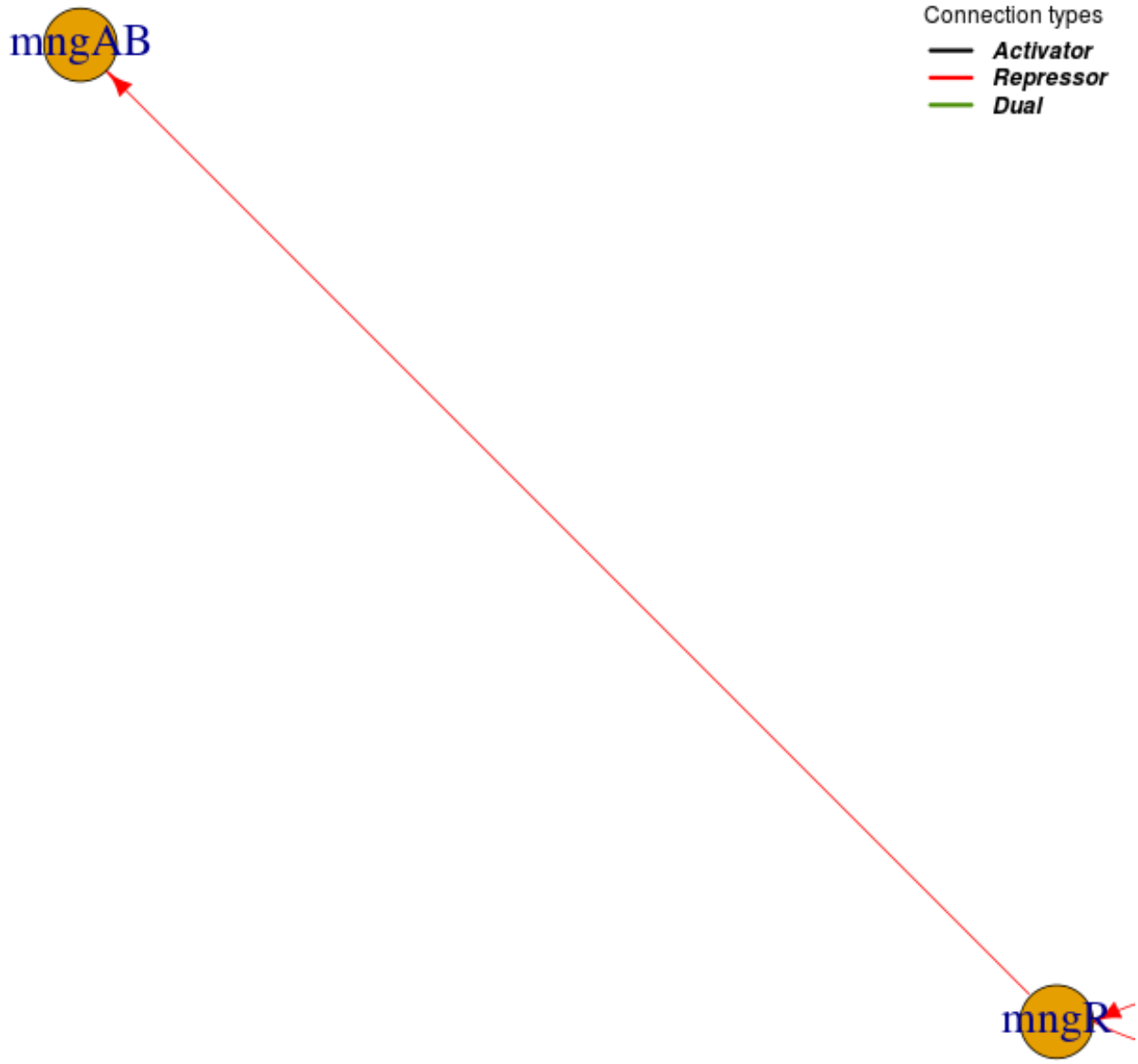

Id = 77

$|n = 0, \ell = 1\rangle$

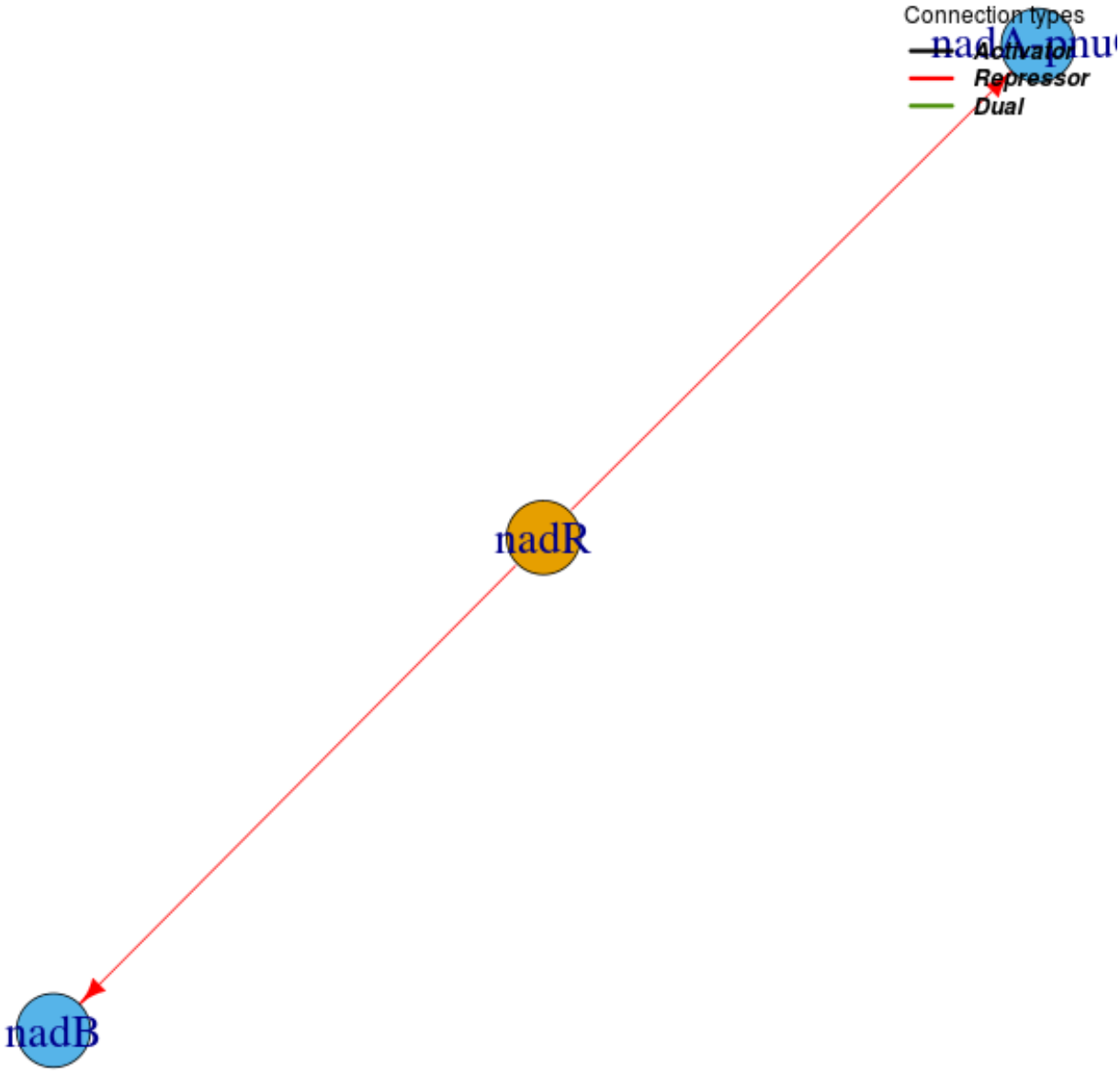

Id = 78

$|n = 1, \ell = 0\rangle$

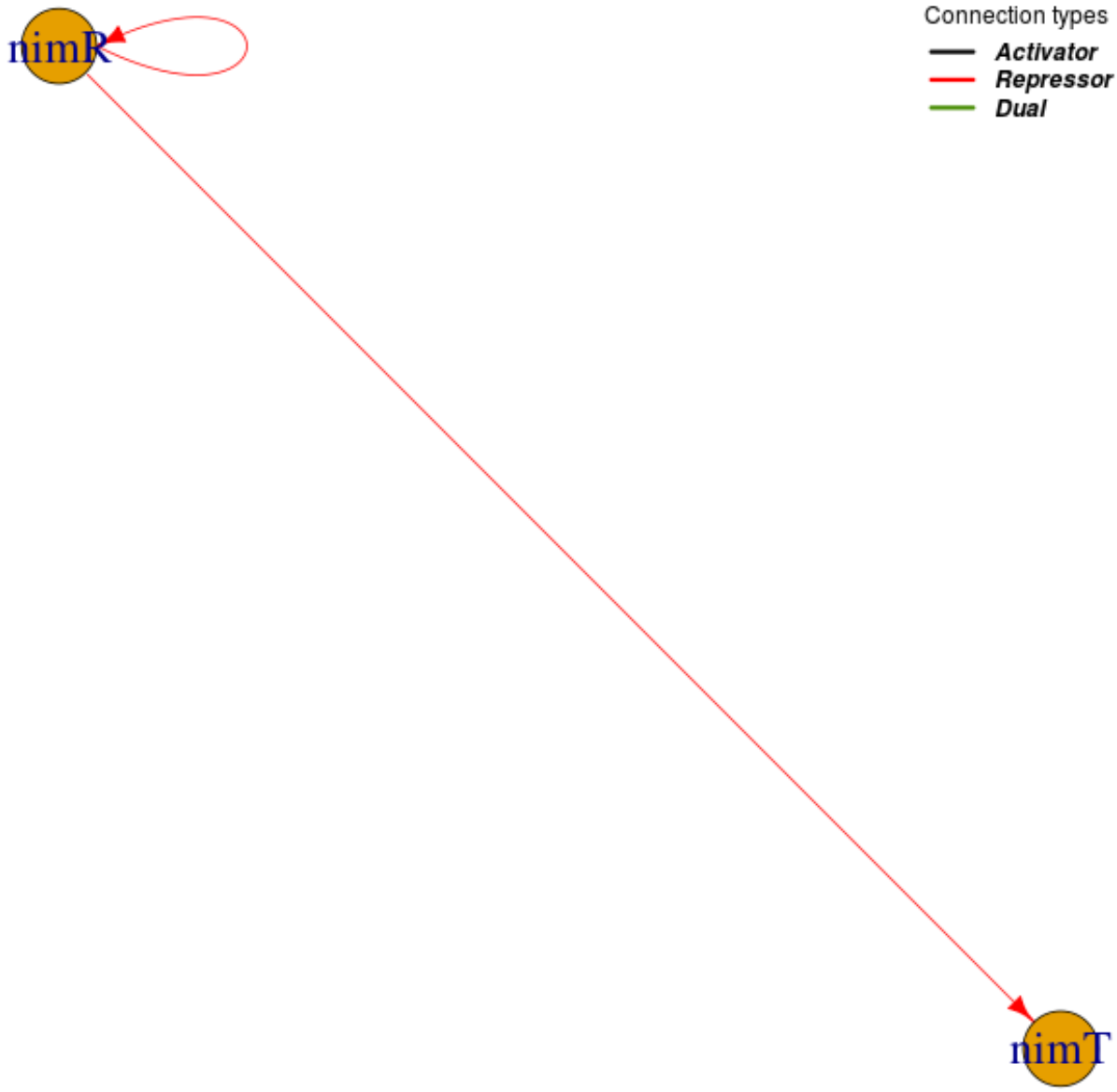

Id = 79

$|n = 0, \ell = 1\rangle$

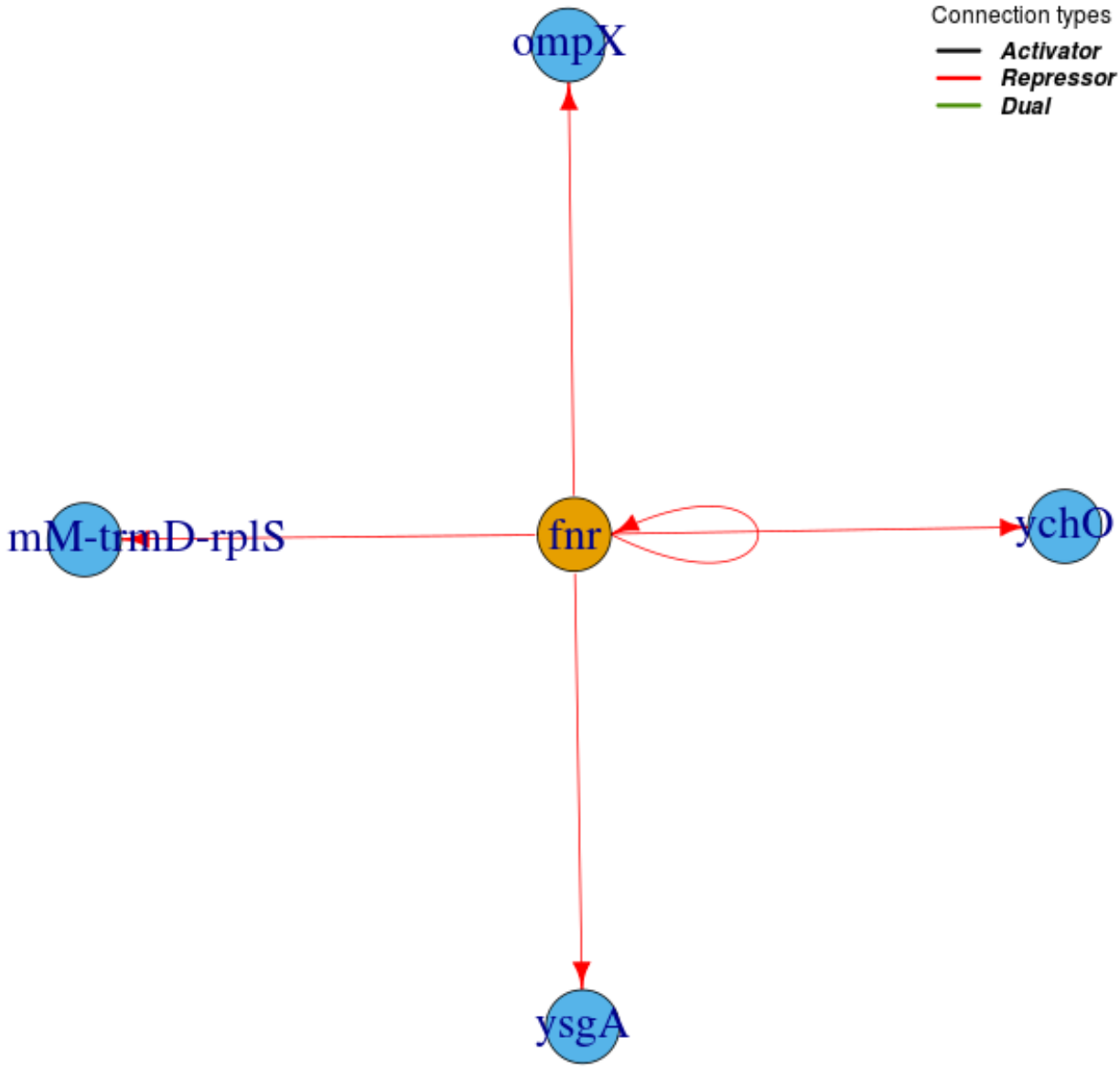

$\mathrm{Id} = 80$

$|n = 0, \ell = 1\rangle$

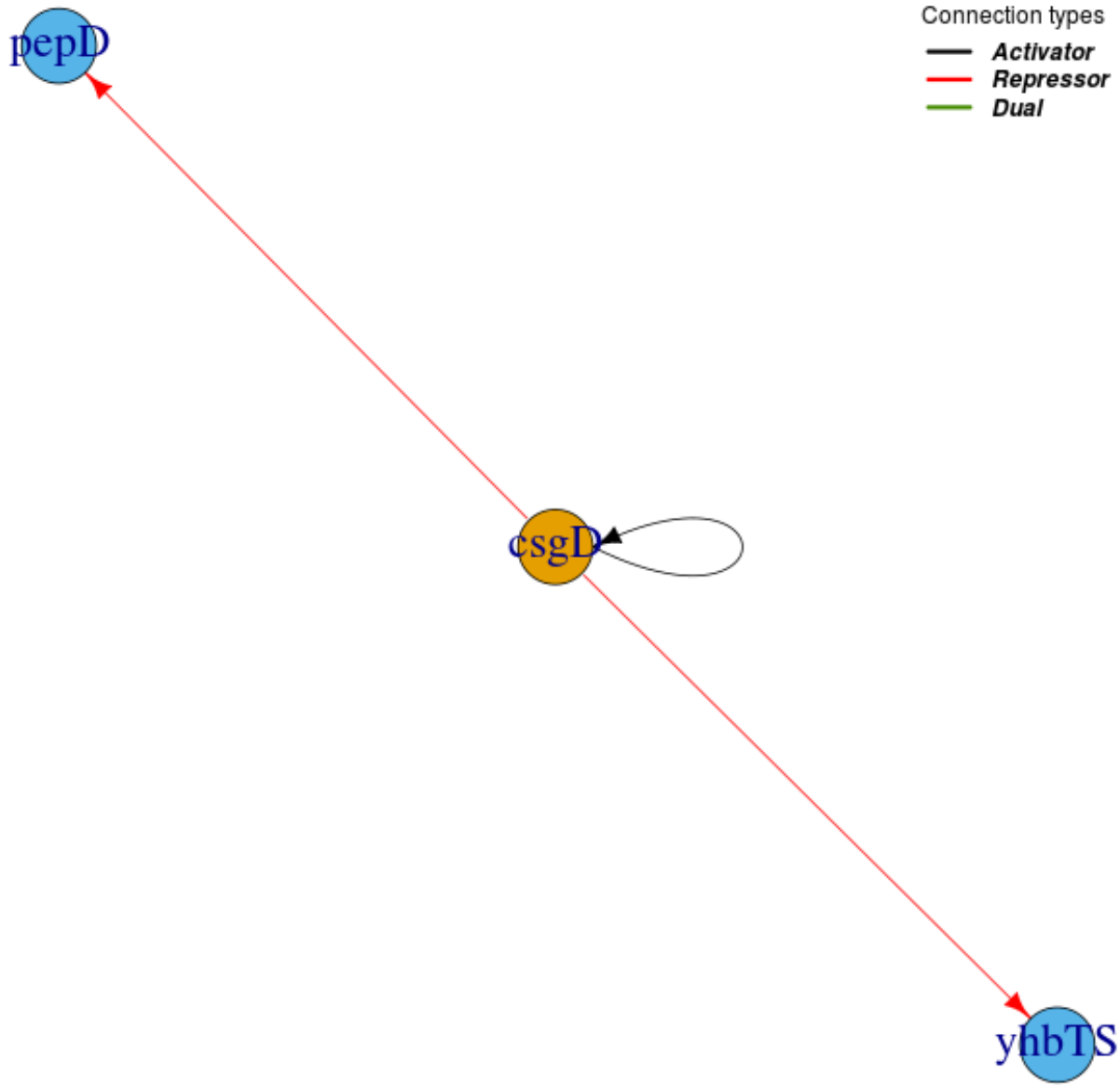

Id = 81

$|n = 2, \ell = 0\rangle$

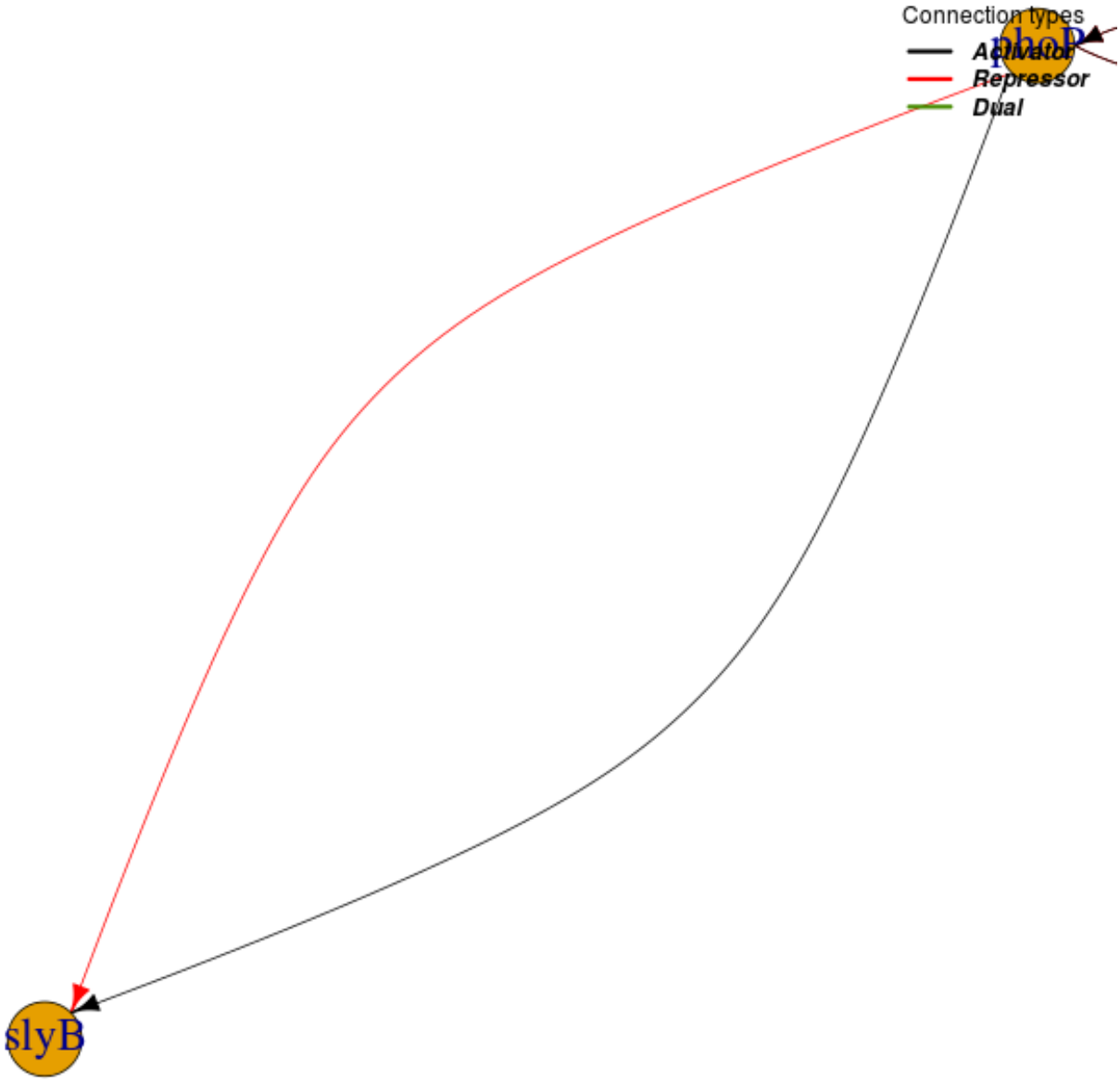

Id = 82

$|n = 0, \ell = 2\rangle$

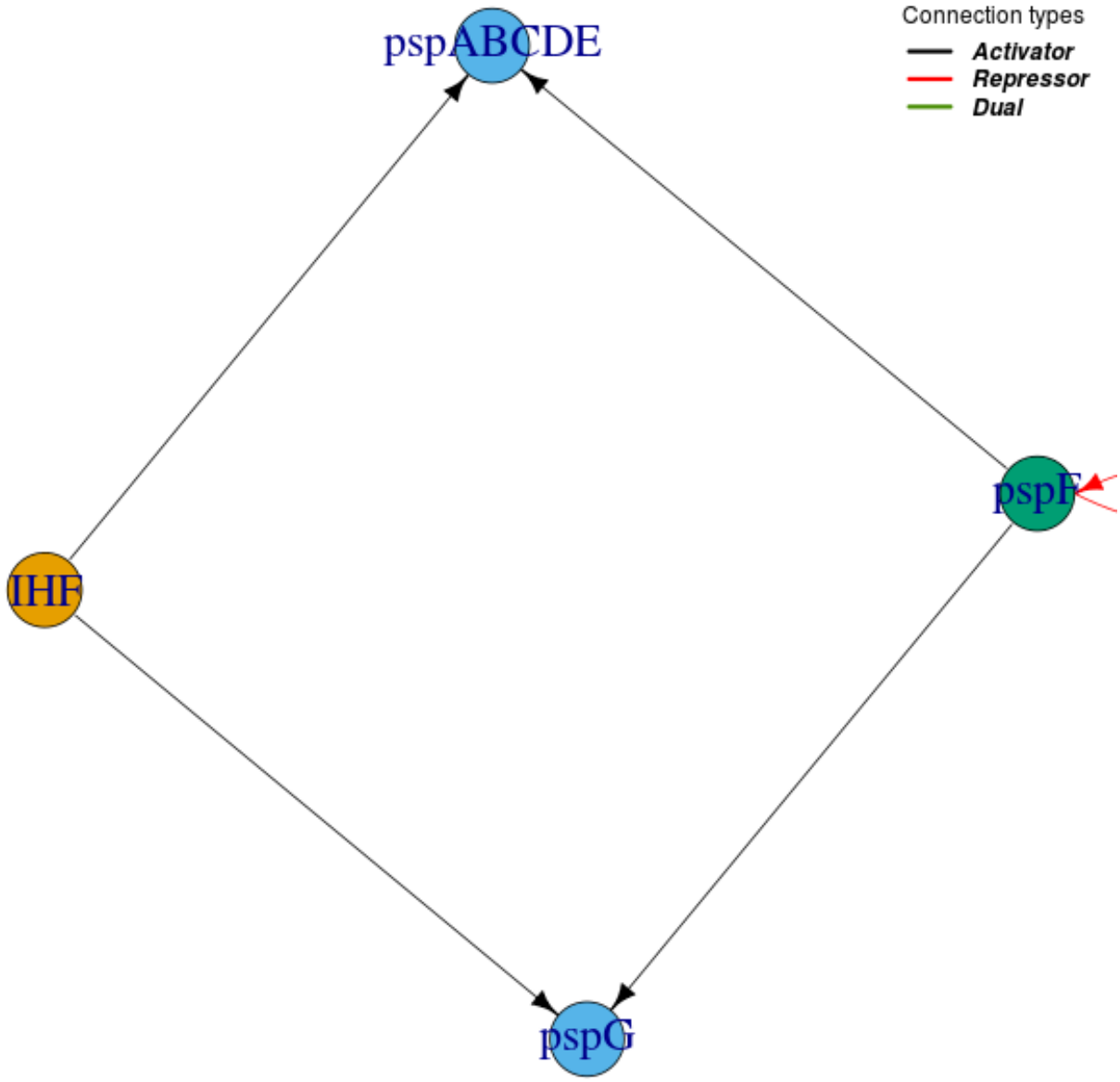

Id = 83

$|n = 1, \ell = 1\rangle$

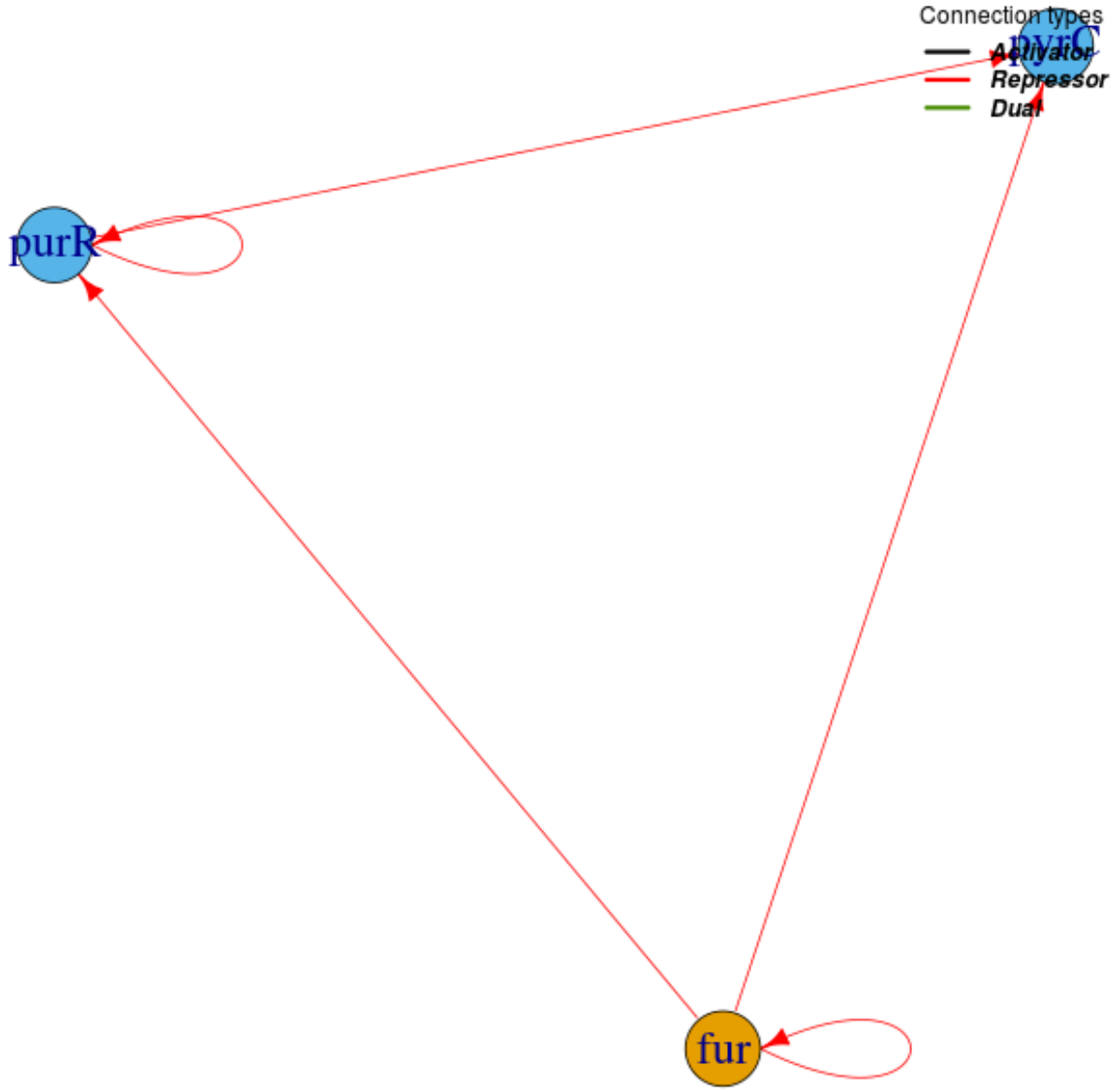

Id = 84

$|n = 2, \ell = 1\rangle$

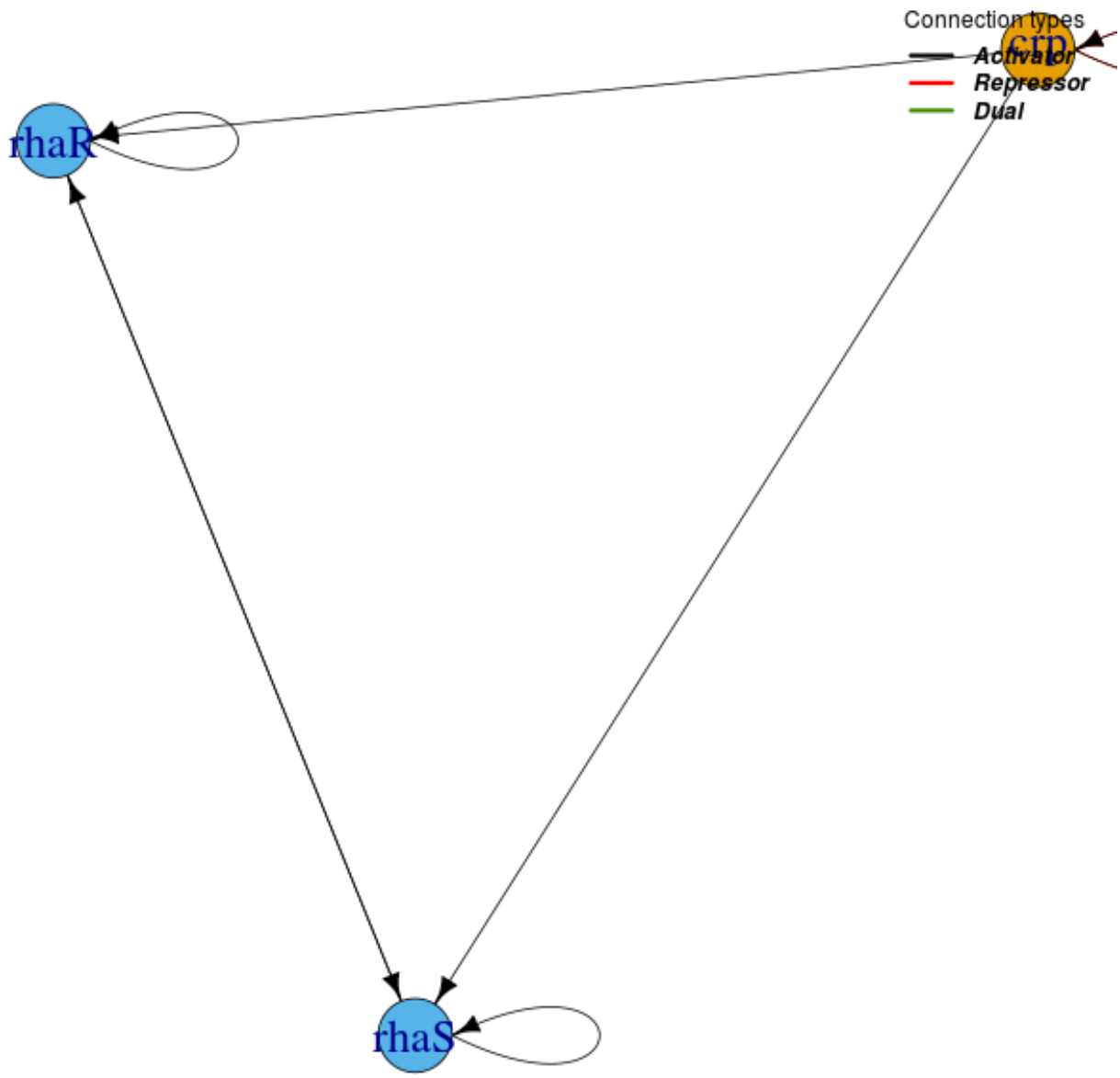

Id = 85

$|n = 0, \ell = 2\rangle$

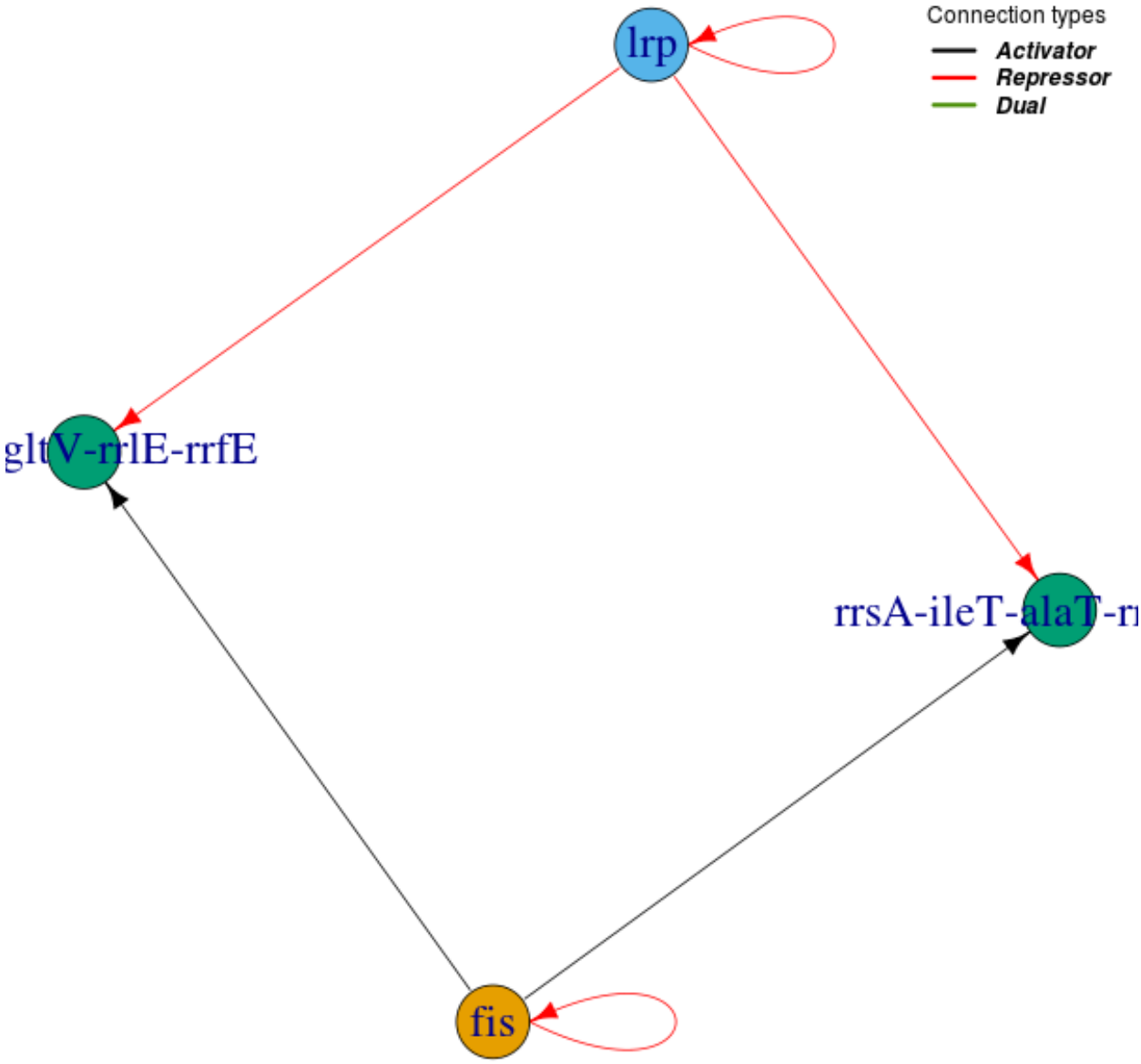

Id = 86

$|n = 0, \ell = 3\rangle$

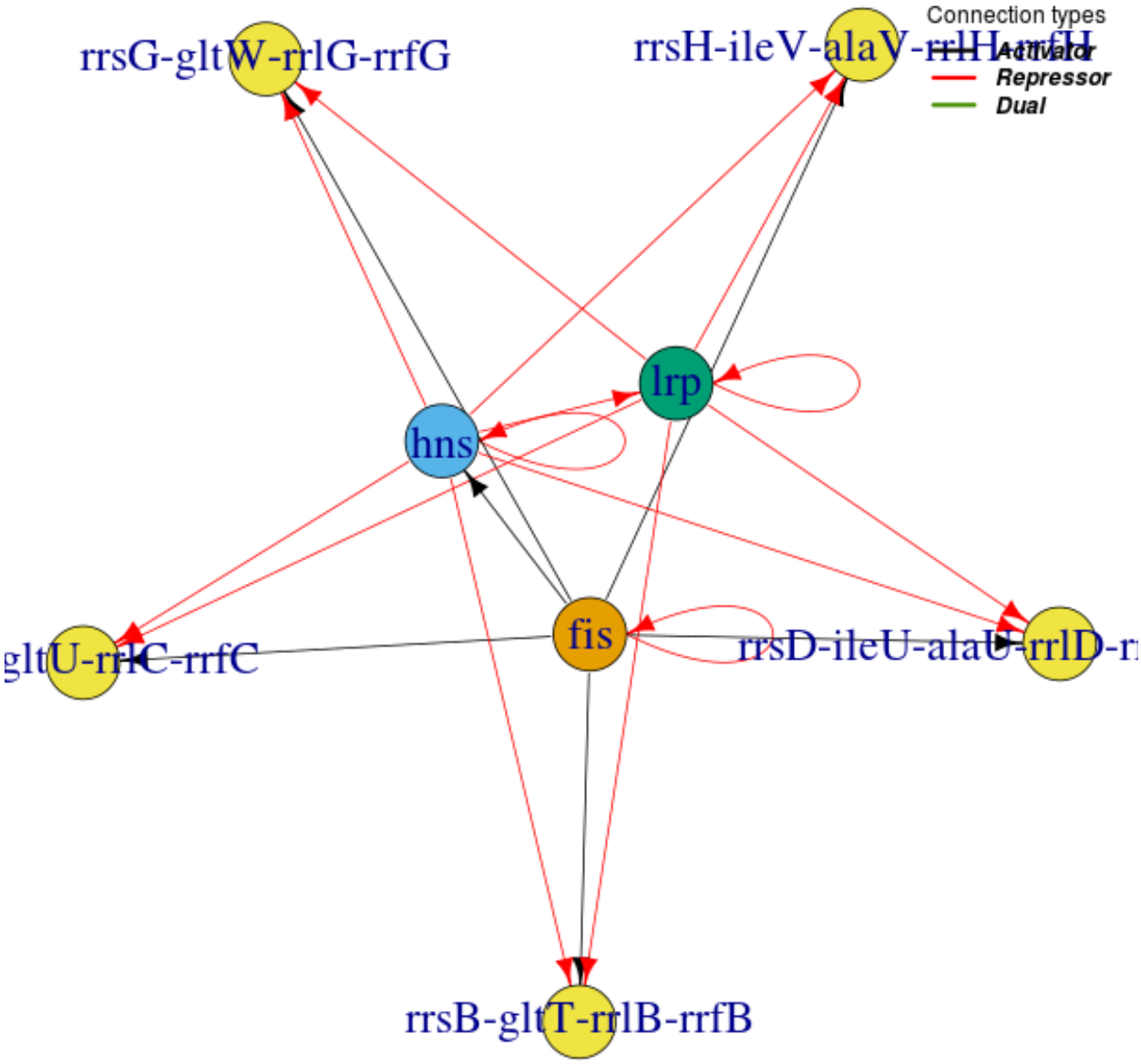

$\mathrm{Id} = 87$

$|n = 0, \ell = 2\rangle$

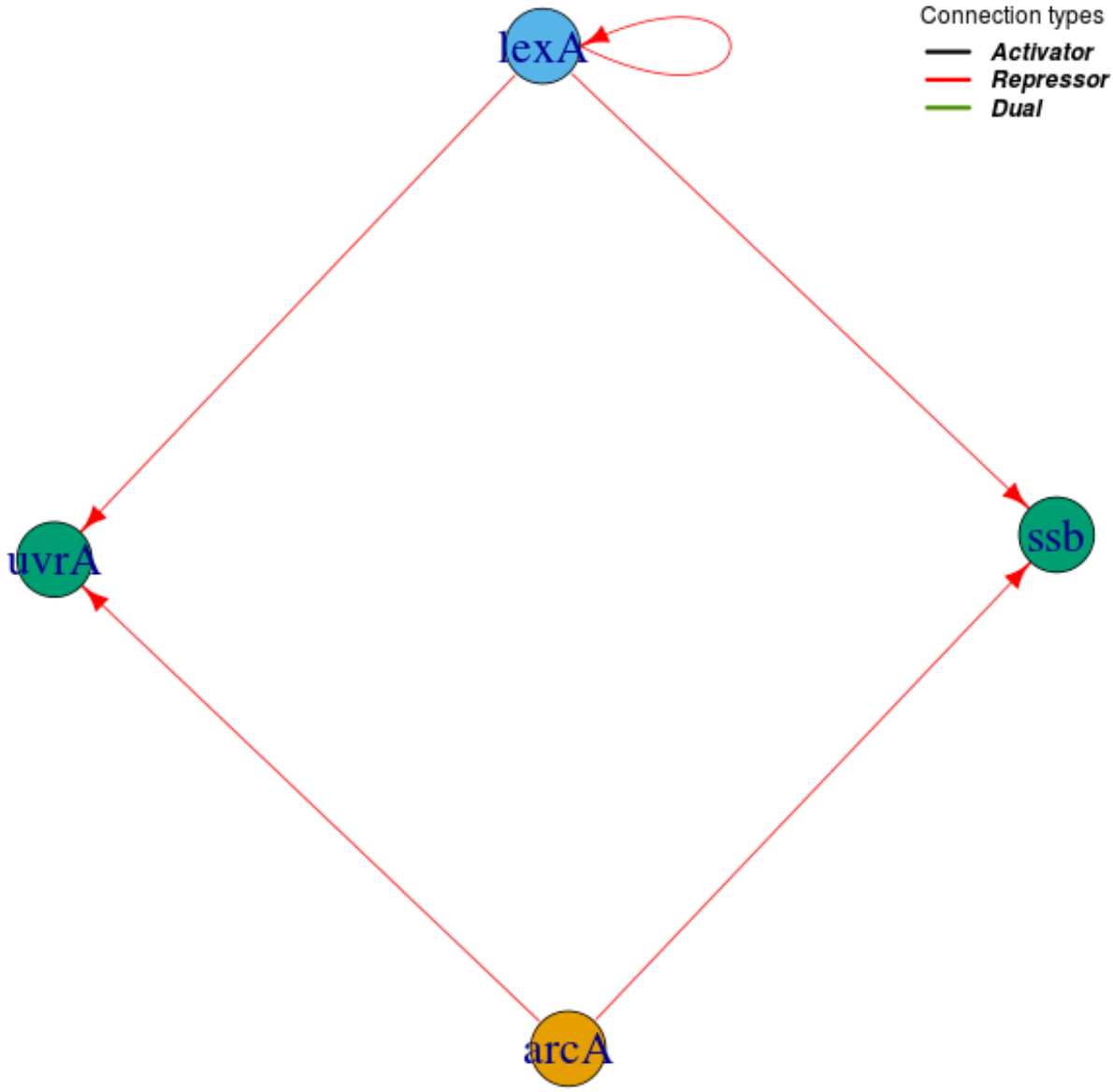

Id = 88

$|n = 1, \ell = 0\rangle$

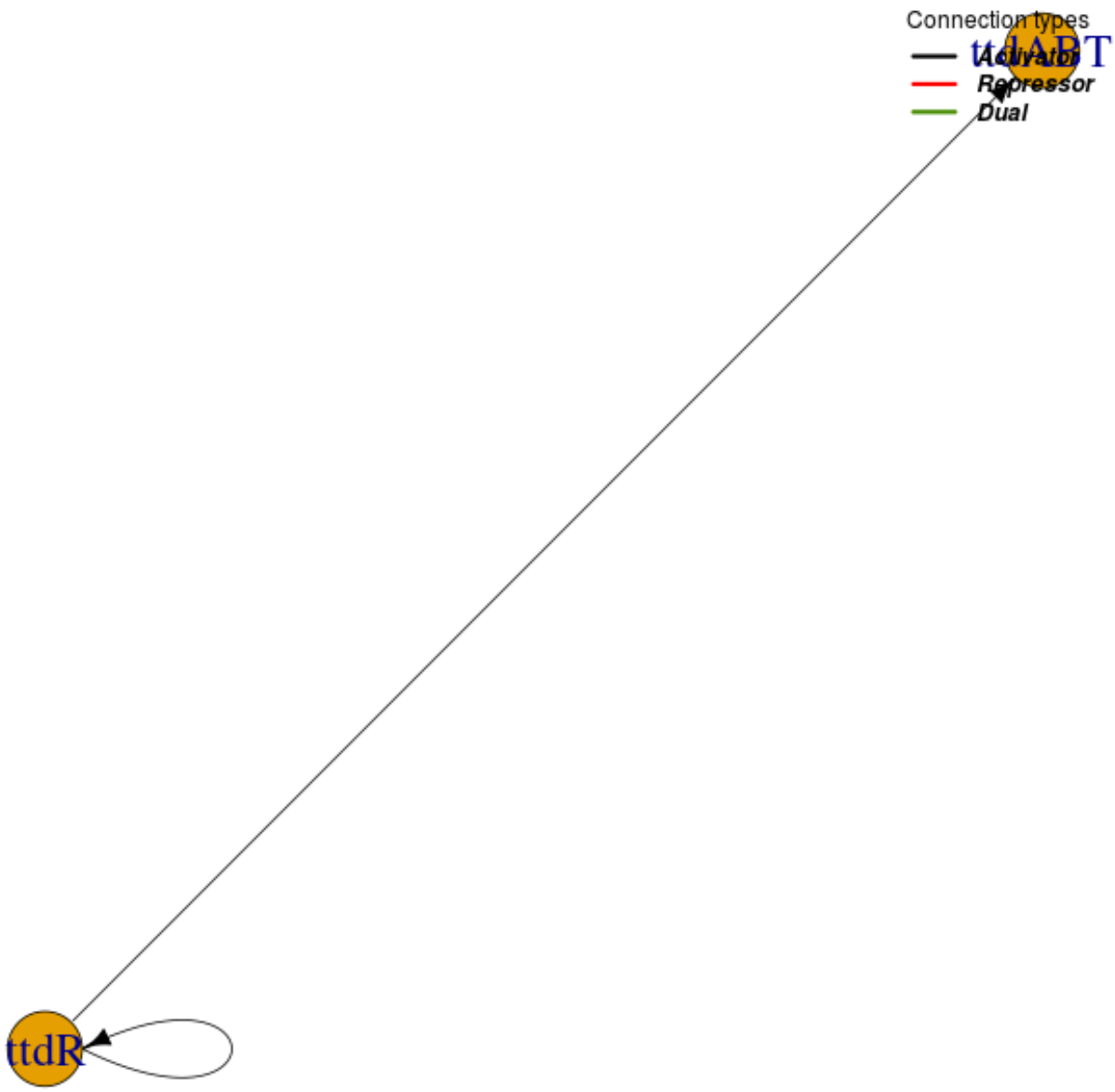

Id = 89

$|n = 0, \ell = 1\rangle$

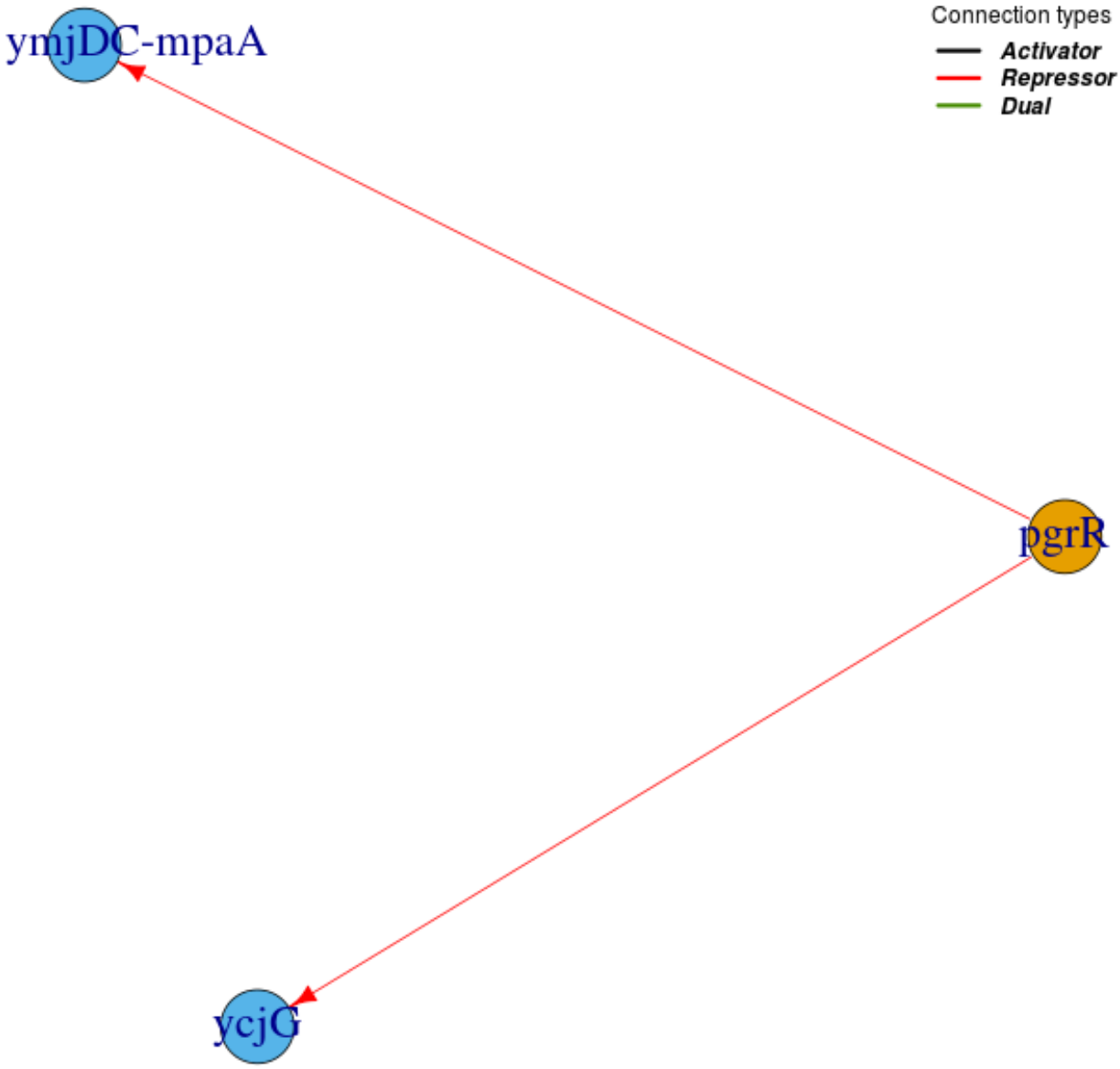

Id = 90

$|n = 0, \ell = 1\rangle$

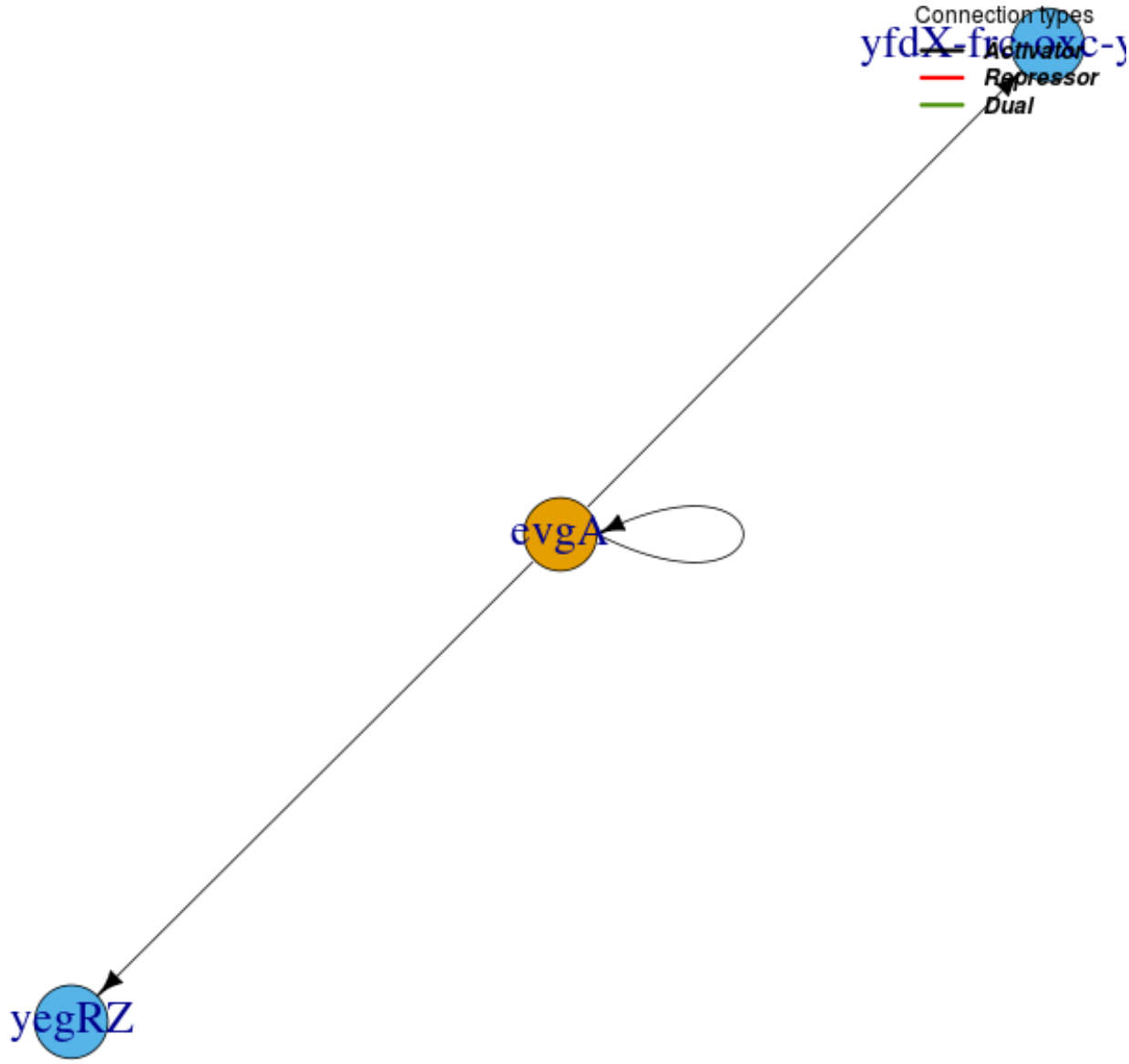

Id = 91

$|n = 0, \ell = 1\rangle$